

TECHNISCHE UNIVERSITÄT MÜNCHEN

TUM School of Engineering and Design

Global Sensitivity Analysis for Models of Active Biomechanical Systems

Sebastian Brandstätter

Vollständiger Abdruck der von der TUM School of Engineering and Design der Technischen Universität München zur Erlangung des akademischen Grades eines

Doktors der Ingenieurwissenschaften (Dr.-Ing.)

genehmigten Dissertation.

Vorsitzender: Prof. Dr. phil. Klaus Bengler

Prüfer der Dissertation:

1. Prof. Dr.-Ing. Christian J. Cyron
2. Assoc. Prof. Alessio Gizzi, Ph.D.
3. Prof. Dr.-Ing. Wolfgang A. Wall

Die Dissertation wurde am 23.06.2021 bei der Technischen Universität München eingereicht und durch die Fakultät für Maschinenwesen am 28.09.2021 angenommen.

*‘Le doute n’est pas une condition agréable, mais
la certitude est absurde.’*

— Voltaire

Abstract

Active biomechanical systems realise many essential functions of the human body, including gastric peristalsis, and growth and remodelling of vascular tissue. Computational models have been tremendously successful in providing insights to both physiological and pathophysiological modes of action of these systems in the past. In the future, these models could also support individualized diagnosis and treatment decisions in everyday clinical practice. To this end, patient-specific predictive simulations are necessary.

Reliable predictive simulations based on models of active biomechanical systems require analysis of the uncertainties involved in the prediction. Models of active biomechanical systems contain many parameters, describing, for example, material properties and reaction rates. Patient-specific measurements of these parameters are difficult to obtain. Thus, a large source of uncertainty in these models results from limited knowledge about model parameters. The standard tool to elucidate the influence of parameters on model output have been local parameter studies, where single parameter values are varied and the resulting change in model output is analysed. This approach is very accessible and interpretation of the results is straightforward, explaining its popularity. However, local parameter studies have two severe shortcomings rendering their application to predictive simulations inadequate. First, interaction phenomena between parameters cannot be identified. Second, input uncertainties are not propagated through the model, which inhibits a rigorous analysis of model output uncertainty.

This thesis proposes variance-based global sensitivity analysis based on Sobol indices as a powerful model analysis framework to overcome these shortcomings for models of active biomechanical systems. Viability and benefits of the approach are demonstrated based on the study of two models. The first model is a novel computational framework for gastric electromechanics proposed as part of the thesis. The second one is a well-established homogenized constrained mixture model for arterial growth and remodelling.

The novel model of gastric electromechanics enabled an efficient, robust description of key phenomena, including entrainment, peristaltic contraction waves, and dysrhythmias. The results of the individual global sensitivity analyses present relevant contributions to the respective fields which are discussed in detail within the thesis. Moreover, the diversity of the examples illustrates the universal capabilities of Sobol's global sensitivity analysis method to investigate important model properties inaccessible by other methods. First, the analyses revealed that significant amounts of parameter interactions can occur in non-linear, multiphysics models of active biomechanical systems. This finding underlines the necessity of global methods for the analysis of these models and demonstrates that previous studies might have underestimated the influence of some parameters. Second, the uncertainty in many parameters was found to have negligible influence on the uncertainty in the output of the models. This result indicates that the complexity of predictions based on these models can be reduced significantly by fixing these uninfluential parameters to their mean values in the future. Third, the uncertainty in the output of the models was frequently found to be dominated by the uncertainty in a few parameters. Hence, reducing the uncertainty in these parameters by acquiring additional knowledge, for example, through high accuracy measurements, will benefit the accuracy of model predictions the most.

In conclusion, global sensitivity analysis can guide both experimental and theoretical future research and should become a fundamental part of development process and predictive use of models of active biomechanical systems.

Zusammenfassung

Aktive biomechanische Systeme sind für viele essentielle Funktionen des menschlichen Körpers, wie beispielsweise die Magenperistaltik oder Wachstums- und Umbauprozesse in vaskulärem Gewebe, verantwortlich. In der Vergangenheit haben Computermodelle mit großem Erfolg Einblicke in die physiologischen und pathophysiologischen Wirkungsweisen dieser Systeme geliefert. Zukünftig könnten diese Modelle auch individualisierte Diagnose- und Behandlungsentscheidungen im klinischen Alltag unterstützen. Hierfür sind patientenspezifische prädiktive Simulationen notwendig.

Zuverlässige prädiktive Simulationen auf der Basis von Modellen aktiver biomechanischer Systeme erfordern die Analyse der mit der Vorhersage verbundenen Unsicherheiten. Modelle aktiver biomechanischer Systeme enthalten viele Parameter, die beispielsweise Materialeigenschaften und Reaktionsraten beschreiben. Patientenspezifische Messungen dieser Parameter sind schwierig. Aus diesem begrenztem Wissen über die Modellparameter resultiert eine große Quelle von Unsicherheiten in diesen Modellen. Das Standardwerkzeug um den Einfluss von Parametern auf den Modellausgang zu untersuchen sind lokale Parameterstudien, bei denen einzelne Parameterwerte variiert und die daraus resultierende Änderung des Modellausgangs analysiert werden. Die Zugänglichkeit und die einfache Interpretation der Ergebnisse dieses Ansatzes erklärt seine Beliebtheit. Lokale Parameterstudien haben jedoch zwei schwerwiegende Einschränkungen, die sie für die Anwendung auf prädiktive Simulationen ungeeignet machen. Erstens können Wechselwirkungsphänomene zwischen den Parametern nicht identifiziert werden. Zweitens werden die Unsicherheiten der Modelleingänge nicht durch das Modell propagiert, was eine rigorose Analyse der Unsicherheit der Modellausgänge verhindert.

In dieser Arbeit wird die varianzbasierte globale Sensitivitätsanalyse auf der Basis von Sobol-Indizes als ein leistungsfähiges Werkzeug zur Modellanalyse vorgestellt, um diese Mängel für Modelle aktiver biomechanischer Systeme zu überwinden. Durchführbarkeit und Vorteile des Ansatzes werden anhand der Untersuchung zweier Modelle demonstriert. Das erste Modell ist ein neuartiges Modell der Elektromechanik des Magens, das im Rahmen dieser Arbeit vorgestellt wird. Das zweite ist ein gut etabliertes homogenisiertes Constrained-Mixture-Modell für arterielle Wachstums- und Umbauprozesse.

Das neuartige Modell der Elektromechanik des Magens ermöglichte eine effiziente, robuste Beschreibung von Schlüsselphänomenen, einschließlich Entrainment, peristaltischen Kontraktionswellen und Dysrhythmie. Die Ergebnisse der einzelnen globalen Sensitivitätsanalysen stellen relevante Beiträge zu den jeweiligen Gebieten dar, die in der Arbeit ausführlich diskutiert werden. Darüber hinaus zeigt die Vielfalt der Beispiele die universellen Fähigkeiten der Methode von Sobol wichtige Modelleigenschaften zu untersuchen, die mit anderen Methoden nicht zugänglich sind. Erstens zeigten die Analysen, dass in nichtlinearen, multiphysikalischen Modellen aktiver biomechanischer Systeme signifikante Mengen an Parameterinteraktionen auftreten können. Diese Erkenntnis unterstreicht die Notwendigkeit globaler Methoden für die Analyse dieser Modelle und zeigt, dass bisherige Studien den Einfluss einiger Parameter unterschätzt haben könnten. Zweitens wurde festgestellt, dass die Unsicherheit in vielen Parametern einen vernachlässigbaren Einfluss auf die Unsicherheit im Modellausgang hat. Dieses Ergebnis deutet darauf hin, dass die Komplexität von Vorhersagen, die auf diesen Modellen basieren, deutlich reduziert werden kann, indem diese weniger einflussreichen Parameter in der Zukunft auf ihre Mittelwerte festgelegt werden. Drittens wurde deutlich, dass die Unsicherheit in der Ausgabe

der Modelle häufig von der Unsicherheit in einigen wenigen Parametern dominiert wird. Daher wird die Reduzierung der Unsicherheit in diesen Parametern durch den Erwerb von zusätzlichem Wissen, z. B. durch präzise Messungen, die Genauigkeit der Modellvorhersagen am meisten verbessern.

Zusammenfassend lässt sich sagen, dass die globale Sensitivitätsanalyse sowohl die experimentelle als auch die theoretische zukünftige Forschung leiten kann und zu einem grundlegenden Bestandteil des Entwicklungsprozesses und der prädiktiven Verwendung von Modellen aktiver biomechanischer Systeme werden sollte.

Danksagung

Ein kritischer Rückblick auf die vergangenen Jahre zeigt, dass viele Menschen im Familien- und Freundeskreis und in der Universität auf verschiedenste Weise zur Erstellung dieser Arbeit beigetragen haben. Mit anderen Worten: Die Fertigstellung meiner Dissertation gibt Anlass Danke zu sagen.

Mein besonderer Dank gilt **Prof. Dr.-Ing. Christian J. Cyron**, meinem Doktorvater, für die exzellente Betreuung dieser Arbeit. Deine visionären Ideen und Deine Begeisterung für Wissenschaft sind immer wieder ansteckend und motivierend. Insbesondere bedanke ich mich für das entgegengebrachte Vertrauen. Nicht zuletzt resultierten daraus die akademischen Freiräume, die es mir ermöglichten ein breites Spektrum an Themen kennenzulernen und zu erkunden. Vielen Dank für Deine Erreichbarkeit, Entscheidungsfreude, sowie die Ermutigung, die unerlässliche Balance zwischen Perfektionismus und Pragmatismus einzugehen.

I express my deepest gratitude to **Prof. Alessio Gizzi**. Thank you for sharing your experience, knowledge, and enthusiasm for electromechanics. Our collaboration was a source of great joy and a big inspiration throughout my PhD studies. It has been a great honour to have you as my second examiner. Lastly and above all, thank you for your continued personal encouragement.

Weiterhin danke ich **Prof. Dr.-Ing. Wolfgang A. Wall** für die bedingungslose Aufnahme in den Lehrstuhl für Numerische Mechanik, an dem diese Arbeit entstanden ist. Vielen Dank, dass ich von diesen exzellenten Rahmenbedingungen profitieren durfte. Ich danke Ihnen für die gute Zusammenarbeit und das bereitwillige Teilen Ihrer Expertise und Ihres Rates. Es hat mich sehr gefreut, Sie als Drittprüfer gewinnen zu können. Für die Übernahme dieser Aufgabe bedanke ich mich herzlich.

Für die Übernahme des Vorsitzes danke ich **Prof. Dr. phil. Klaus Bengler**.

Renata Nagl und **Bettina Schrieber** danke ich für die vertrauensvolle und äußerst kompetente Unterstützung bei allen organisatorischen Angelegenheiten.

Bei meinen **Kolleginnen und Kollegen** am Lehrstuhl für Numerische Mechanik bedanke ich mich für ein angenehmes Miteinander und die außergewöhnliche Hilfsbereitschaft. Ich schätze mich glücklich mit einer Vielfalt an klugen Menschen zusammengearbeitet zu haben, die mir dabei geholfen haben, mich sowohl fachlich als auch persönlich weiterzuentwickeln. Dabei bin ich ausgesprochen dankbar, dass viele von euch zu guten Freunden geworden sind.

Besondere bedanke ich mich bei **Sebastian Fuchs**. Mit keinem anderen habe ich in den vergangenen Jahren enger zusammengearbeitet. Wir haben unzählige Stunden – oft bis spät in die Nacht – mit der Diskussion von Ergebnissen oder dem Verfassen von Artikeln verbracht. Vielen Dank für Deine zielstrebige und unermüdlich positive Art. Danke für Deine Offenheit und Deine freundschaftlichen Anstöße mich immer wieder selbst herauszufordern.

Mein besonderer Dank gilt **Jonas Eichinger**. Von Beginn meiner Promotion an warst Du die entscheidende seelische und moralische Unterstützung am Lehrstuhl. Vielen Dank, dass Du immer ein offenes Ohr für mich hattest und mir mit Rat und Tat zur Seite standest. Danke für Deine stoische Gelassenheit, Deine Vorurteilslosigkeit und Deinen inspirierenden, wohlwollen Blick auf die Welt. Nicht jede unserer zahlreichen Diskussionen war bitterernst. Auch für diesen humorvollen Ausgleich danke ich Dir von Herzen.

Special thanks go to **Luca Berardocco**. I profoundly appreciate our countless, uplifting discussions on science, society and life in general – often with either coffee or beer in hand. Thank you for enriching my life by sharing your amichevole Italian mentality and lifestyle with me.

Johannes Kremheller und **Christoph Schmidt** danke ich für ihre Freundschaft und ihren Beistand der nicht zuletzt aus vielen, unvergesslichen Abenden und Unternehmungen resultierte.

Jonas Biehler danke ich für seine uneingeschränkte Hilfsbereitschaft und für das bereitwillige Teilen seines beeindruckenden Fachwissens. **Karl-Robert Wichmann** danke ich für seine Aufgeschlossenheit, seinen Humor und etliche Pasta-Pesto Abendessen. Bei **Martin Pfaller** bedanke ich mich für seine Frohnatur und seine integrative Persönlichkeit. **Jonas Nitzler** danke ich für die enge und äußerst angenehme Zusammenarbeit, die durch seine offene und fröhliche Art geprägt war. **Barbara Wirthl** danke ich für die erfolgreiche Zusammenarbeit und die Bekräftigung durch unseren ehrlichen – oft auch überfachlichen – Austausch. Bei **Maximilian Rixner** bedanke ich mich für seine Vielzahl an geduldigen Erklärungen in unseren fachlichen Diskussionen. Bei **Patrick Praegla** bedanke ich mich für viele spannende Gespräche und eine ausgezeichnete Büroatmosphäre. **Gil Robalo Rei** danke ich für gewinnbringende fachliche und überfachliche Unterhaltungen mit und über kulinarische Genüsse verschiedenster Art.

Christopher Jelich danke ich für die gemeinsame Begeisterung für Specialty Coffee, der wir bei unseren regelmäßigen Expertentreffen nachgekommen sind. Natürlich ging es nicht immer nur um Kaffee. Unsere langen Gespräche sind immer ein willkommener, weil bestätigender, Ausgleich.

Ich bedanke mich auch bei allen **Studierenden**, die eine studentische Arbeit bei mir geschrieben haben oder als Tutor oder HiWi tätig waren. Ihr wart ein bereichernder Teil meiner Promotion und habt durch Euren Einsatz zum Gelingen beigetragen.

Meinen Freunden danke ich für ihr Verständnis und ihre Treue über diese intensive Zeit hinweg. Vielen Dank an **Bea, Max, Sebi, Marcus, Milo, Michi, Nina und Magdalena** für Eure tatkräftige Unterstützung, Eure guten Ratschläge und dafür, dass ihr immer wieder für den nötigen Ausgleich und wertvolle Erholung gesorgt habt.

Meiner Familie danke ich von ganzem Herzen für ihren bedingungslosen Rückhalt und ihren unermüdlichen Zuspruch. Ohne Euch wäre diese Arbeit nicht möglich gewesen. **Erich und Gisela** danke ich besonders für ihre stets ermutigende Teilhabe und ihre großzügig geteilte Passion für höchste kulinarische Genüsse. **Claudia, Eugen und Anton** danke ich für ihr konstruktives Zuhören und vor allem für ihre verständnisvolle Beharrlichkeit.

Mein größter Dank und Respekt gilt meinen liebevollen Eltern **Gabriele** und **Ullrich**: Danke, dass Ihr mir ein unerschütterliches Fundament bietet auf dem ich mein Leben erfolgreich bauen kann.

Es ist schwer in Worte zu fassen, welche Dankbarkeit ich für die vollkommene Unterstützung meiner Freundin **Valentina** empfinde. Du hast mich auf dem gesamten Weg dieser Promotion durch alle Höhen und Tiefen mit unermesslicher Geduld und Nachsicht begleitet. Vielen Dank für Dein Vertrauen, Deinen Zuspruch, Deinen Rat und den Mut mich manchmal vor mir selbst zu schützen. Kurz: Danke, dass Du immer wieder geduldig das Licht nach mir ausschaltetest.

München, im Februar 2022

Sebastian Brandstätter

Contents

1	Introduction	1
1.1	Motivation	1
1.2	Contributions of this thesis	5
1.3	Outline	9
2	Scientific context	11
2.1	Terminology	11
2.2	On the importance of uncertainty in computational modelling	13
2.3	Continuum modelling of active biomechanical systems	16
2.4	Paper A: Mechanics of the stomach: A review of an emerging field of biomechanics	17
2.5	Importance of growth and remodelling for the cardiovascular system	19
3	Global sensitivity analysis	21
3.1	Literature review	21
3.2	A brief introduction to sensitivity analysis	22
3.2.1	Objectives of sensitivity analysis	22
3.2.2	Overview of existing methods	23
3.3	Sobol indices: a variance-based approach to global sensitivity analysis	28
3.3.1	Definition	28
3.3.2	Interpretation	30
3.3.3	Computation	33
3.3.4	Use cases	33
4	Results I: gastric electromechanics	35
4.1	Paper B: Computational model of gastric motility with active-strain electromechanics	35
4.2	Global sensitivity analysis of an active-strain electromechanics model for gastric peristalsis	37
4.2.1	Idealized model of gastric peristalsis	37
4.2.2	Probability distributions of parameters	38
4.2.3	Quantities of interest	47
4.2.4	Results	49
5	Results II: arterial growth and remodelling	53
5.1	Paper C: Global sensitivity analysis of a homogenized constrained mixture model of arterial growth and remodeling	53

6	Discussion	57
6.1	Gastric electromechanics	57
6.1.1	Computational model of gastric motility	57
6.1.2	Global sensitivity analysis for the model of gastric motility	58
6.2	Arterial growth and remodelling	60
6.3	The big picture	62
7	Conclusion and outlook	65
7.1	Future Perspectives for global sensitivity analysis of models of active biomechanical systems	66
	Bibliography	69
	Appended publications	91
	Paper A Mechanics of the stomach: A review of an emerging field of biomechanics	93
	Paper B Computational model of gastric motility with active-strain electromechanics	113
	Paper C Global sensitivity analysis of a homogenized constrained mixture model of arterial growth and remodeling	137

Acronyms

AAA	abdominal aortic aneurysm
ANOVA	analysis of variance
BACI	Bavarian Advanced Computational Initiative
CV	coefficient of variation
FEM	finite element method
HDMR	high-dimensional model representation
ICC	interstitial cell of Cajal
KDE	kernel density estimation
MEF	mechano electric feedback
MRI	magnetic resonance imaging
ODE	ordinary differential equation
PDF	probability density function
SMC	smooth muscle cell
VDCC	voltage-dependent calcium channel
WHO	World Health Organization

1 Introduction

1.1 Motivation

Active biomechanical systems are fundamental for life. From the beating of the heart to locomotion, they realise many essential body functions. Thus, understanding physiological and pathophysiological processes within these systems is crucial.

Computational modelling of active biomechanical systems has been tremendously successful in providing valuable insights to these systems in the past. In the future, models of active biomechanical systems could also support individualized diagnosis and treatment decisions in personalized medicine. For this reason, the field has received growing attention from researchers over the last decades. To name but a few success stories of recent years, computational models of active biomechanical systems have helped to unravel the complex electromechanical processes underlying the functions of the human heart [1–4]. They improved the understanding of the tight coupling between mechanics and cell biology during growth and remodelling of soft tissue [5–7], and revealed fundamental principles of voluntary force generation in the musculoskeletal system essential for human motion [8, 9]. However, despite great accomplishments, there remain many open questions in this field.

An evident concern is that some areas have received considerable research attention while others remain barely explored. For example, the cardiovascular system has been studied extensively in the past; this might be explained by its literally vital significance for the human body. In 2020, the World Health Organization (WHO) elucidated vividly: ‘The world’s biggest killer is ischaemic heart disease, responsible for 16% of the world’s total deaths’ [10]. Notwithstanding, cardiovascular diseases are also repeatedly listed among the top preventable causes of death due to their avoidable risk factors. In tackling the global epidemic of cardiovascular diseases, it seems therefore imperative to focus not only on the directly affected circulatory system but also on the risk factors.

One of the widest spread avoidable risk factors is obesity. In fact, obesity increases the risk for many of the leading causes of death, including heart disease, stroke, certain types of cancer, respiratory diseases, and diabetes [11–13]. Fundamentally, obesity is caused by an imbalance between energy consumption and expansion. From a biomechanical point of view, it is, however, primarily linked to the gastrointestinal system. Thus, the gastrointestinal system also deserves recognition by the biomechanical community. Comparing the research efforts spent on the cardiovascular and gastrointestinal systems reveals that the latter lags about 20 years behind [14]. Certainly, the fact that some fields seem to lag behind does by no means diminish the importance of the progress made in others. On the contrary, it is but one line of argument to motivate the exploration of new territory and to continue the success story of biomechanics in other parts of the human body. It is this prospect precisely that drove the research on the mechanics of the human stomach presented in this thesis. In the first part of this thesis, a novel computational

electromechanical model of the human stomach is presented, which is capable of describing, for the first time, peristaltic contraction waves in health and disease.

A more general concern with current models of active biomechanical systems is related to their predictive capabilities. If these models shall be used in everyday clinical practice, for example, for individualised diagnosis, decisions on treatment options or planning of surgical interventions, they will inevitably be used as predictive models. Model prediction describes the calculation and use of model outputs without their physical measurement or observation. In other words, predictive use of a model means to employ a model that has been validated and verified in one situation to make a prognosis about a new, unknown situation. Typical generic examples of computational model predictions include [15]

- the simulation of an experiment before it is performed,
- the study of phenomena that cannot be studied experimentally, and
- the extrapolation from the current level of knowledge to uncharted areas.

Many of the applications envisioned for computational models in personalized medicine can readily be associated with one of these categories. This is illustrated by the fact that any potential future patient is a unique human being who will differ from previous patients due to the ‘individual variability and inherent complexity of human biological systems’ [16]. By measuring and adapting the computational domain, boundary conditions and parameters, the model could in part be personalized. However, there will always remain uncertainty in the model, for example, due to measurement errors or inaccessibility of information [17]. For instance, some model parameters might be immeasurable, because there are no experimental setups to measure them *in-vivo* or because of cost limitations. In both cases, patient-specific values are inaccessible and often the best one can hope for are population-based values. Ultimately, uncertainty remains an inevitable part of model prediction. Therefore, model predictions are only useful if they contain information about the potential error or the amount of uncertainty that persists in the proposed solution. Certainly, this is true for any model but maybe even more so for models of active biomechanical systems in clinical applications. On the one hand, these models have to consider the large variability associated with the underlying biological systems. Indeed, the biological variability is not limited to fluctuations between patients but also shows within a patient [18–20]. On the other hand, the risk of model predictions is high since false predictions can have disastrous consequences for the patient [21]. All in all, the reliability and therefore usefulness of models of active biomechanical systems depend crucially on a proper treatment of the involved uncertainties. More specifically, a first goal is to quantify model output uncertainties resulting from uncertainties inherent to the model, its inputs, and its parameters. This is precisely the focus of the field of uncertainty quantification. In a next step, it is crucial to identify the sources of input uncertainty that are most dominant and the ones that could potentially be neglected. Generally, these questions are related to the quantification of the amount of model output variability that can be attributed to the individual input uncertainties, a task known as global sensitivity analysis. Global sensitivity analysis can help to save resources by reducing the overall problem complexity and by focusing any attempts of uncertainty reduction on the most rewarding sources.

The necessity for uncertainty quantification and global sensitivity analysis appears to be largely undebated in the biomechanical community, yet, only few studies present a proper uncertainty

analysis of their results [17, 22, 23]. In part, this might be explained by a lack of awareness of the methods that have been developed, extensively studied and successfully applied in other fields [24–26]. Certainly, the high computational cost associated with uncertainty quantification and global sensitivity analysis methods is also a limiting factor considering the already high costs of the models alone. However, two factors begin to mitigate this limitation. First, high-performance computing platforms become cheaper and more accessible and second, methodological advances in the field improve the efficiency of the algorithms [19, 21, 27, 28].

A major part of this thesis is concerned with global sensitivity analysis. The main goal is the adaptation and application of state-of-the-art global sensitivity analysis methods to cutting-edge, non-linear, and multi-physics models of active biomechanical systems. This thesis focuses on variance-based, global sensitivity measures called Sobol indices. The two biggest advantages of Sobol indices are their global nature and their easy and conclusive interpretability. Here, ‘global’ refers to the fact that the complete input space is explored making it possible to identify interaction phenomena – an essential property when studying non-linear models. Sobol indices rely on the additive decomposition of the output variance. Each summand can be identified as the variance contribution of a specific input or a combination of inputs. The indices can then be understood as the fractions of the total output variability caused by the uncertainty in the inputs and their combinations. This reveals a related advantage of the method: if done properly, the method inherently includes an uncertainty quantification provided that variance is accepted as the proper measure for uncertainty. In many cases, it is deemed essential to conduct uncertainty analysis prior to sensitivity analysis [23, 26]. This best-practice recommendation is based on the rational that the actual significance of the relative importance of an input depends heavily on the absolute, overall variability of the output. Last but not least, Sobol indices are non-intrusive in the sense that they rely on black-box evaluations of the model only. This makes them a versatile tool for tackling some of the challenges associated with uncertainties inherent to any mathematical model. Naturally, the method also has some drawbacks, here, above all, the extreme computational expense should be mentioned.

This thesis shows that global sensitivity analysis is an accessible tool of great value for models of active biomechanical systems. It does so by applying the method to two models at different development stages and from different biological backgrounds.

First, a global sensitivity analysis for the novel gastric electromechanics model developed in the first part of the thesis is performed. The benefit of conducting a global sensitivity analysis early during model development are manifold. Imagine the model output is found to depend heavily on an input previously believed to be insignificant. This could have various reasons. It might point to a mistake in the implementation or a bug in the code, but it could also be a conceptual error in the model formulation. Yet, this finding could also point to an unknown feature of the system. In general, global sensitivity analysis can be a great, structured way to uncover the processes within and interactions between subsystems of a model, thereby gaining valuable system knowledge that is inaccessible otherwise.

Next, global sensitivity analysis is applied to a homogenized constrained mixture model of growth and remodelling in arterial tissue. Growth and remodelling of soft load-bearing tissue, such as arterial tissue, have been studied extensively over the last decade. The development of mathematical models underpinned by theoretical and computational studies has helped to unravel the complex mechanobiological mechanisms involved in these processes. With the help of sophisticated mechanistic models, such as the homogenized constrained mixture model, growth

and remodelling have been identified to play a major role in diseases such as aneurysms [29–33]. Aneurysms are local, pathological dilatations of blood vessels that often continue to grow until rupture. A ruptured aneurysm is a serious medical condition that often ends fatally. Therefore, predicting disease progression based on the current state is a desirable goal for clinical practitioners. Based on such a prediction, decisions on therapeutic options could be made and, for example, surgical interventions could be planned. Many academic studies have proven that constrained mixture models are conceptually capable of predicting aneurysm growth [7, 30–32, 34–50]. The next logical advancement is to enhance the reliability of these predictions in preparation for clinical application. So far, studies have relied on rough estimates of parameter values often these are population-averaged values. The determination of patient-specific model parameter values is, however, essential for individualized predictions. For many of the model parameters it is currently either impossible or very difficult to derive patient-specific values, especially within a clinical workflow. Global sensitivity analysis will help understand which of the parameters have the largest influence on aneurysm growth predictions. This knowledge can guide future research on patient-specific parameter measurements to focus on the most rewarding parameters. In this way, this thesis brings homogenized constrained mixture models in particular, and models of active biomechanical systems in general, closer to the clinical application they are destined for.

1.2 Contributions of this thesis

Computational models have become essential tools for unravelling fundamental principles of active biomechanical systems. Yet, their broad predictive application, for example, in clinical practice, remains pending. In this context, three major challenges were identified:

(C1) The research effort is unequally distributed between subfields:

Some systems, such as the cardiovascular system, have been studied extensively in the past. Others, like the gastrointestinal system, lag behind significantly. The lack of models capturing the complex multiphysics of the stomach hinders both scientific and medical progress.

(C2) Models of active biomechanical systems could contain non-linear, non-monotonic interactions between parameters:

Active biomechanical systems involve non-linear couplings between multiple physical fields and spatiotemporal scales. Models describing these systems have to reflect this complexity and non-linear, non-monotonic interactions between model parameters cannot be ruled out. The standard tool for the analysis of the influence of parameters on the model output have been local parameter studies. However, this approach is incapable of detecting parameter interactions. Thus, a comprehensive investigation requires more sophisticated methods.

(C3) The large variability of biological systems requires a rigorous analysis of uncertainties:

Reliable model predictions based on models of active biomechanical systems demand an analysis of the uncertainties involved in the process. Multiple sources of uncertainty exist, but a major source of epistemic uncertainty results from limited data on the model parameters. Most existing modelling studies tend to completely neglect the existence of parameter uncertainties because comprehensive, yet accessible analysis frameworks remain scarce. Hence, there is a clear need for such an analysis framework in the field of computational modelling of active biomechanical systems.

The three papers and the original results presented in this thesis constitute the following major contributions to meet challenges (C1), (C2) and (C3). Figure 1.1 graphically illustrates the contributions and relations between them.

Contributions to challenge (C1):

(I) A comprehensive review describing state of the art and future perspectives of computational modelling of the human stomach was presented (Paper A):

Computational models of the stomach were found to be urgently needed in light of its critical importance for human health. Anatomy and (patho-)physiology of the human stomach indicate that its functionality relies on a complex coupling between various physical phenomena on multiple spatiotemporal scales. An extensive literature review of the modelling of gastric mechanics revealed that, despite its importance, it has received far less attention compared to other fields of biomechanics. Thus, there is a vast discrepancy between the

complexity of the problem and existing modelling approaches. Most models do not reflect the multiphysical nature of the problem. Hence, a computational multiphysics model combining electrophysiology, wall mechanics, and fluid mechanics is clearly needed.

(II) An efficient and robust multiphysics computational framework for gastric electromechanics in health and disease was developed (Paper B):

The framework combines a robust gastric electrophysiology model with an active-strain, finite elasticity model of a membranous wall. The phenomenological nature of the electrophysiology model enables an efficient, yet general description with only four state variables. In contrast to previous models, the model remained stable for arbitrary simulation times. This allowed to simulate key phenomena like entrainment and normal, ring shaped contraction waves on an idealized stomach geometry. The multiphysics nature of the model allowed, for the first time, to study the link between gastric electrophysiology and mechanics in pathological conditions, like spiral-shaped gastric dysrhythmia.

Contribution to challenges (C2) and (C3):

(IV) Variance-based global sensitivity analysis of the novel model for gastric electromechanics was performed (Section 4.2):

Overall 20 uncertain parameters and four different quantities of interest – uncontracted state, amplitude, width, and propagation speed of normal peristaltic contraction waves – were studied. The analysis showed that interactions between the parameters can result in physiologically infeasible model behaviour. Therefore, a physiologically admissible parameter space was derived. From these 20 free parameters, only six influenced at least one of the quantities of interest. Except for the amplitude, each quantity of interest was dominated by the influence of a single parameter. The active part of the contractions – amplitude, width, and propagation speed – were found to be independent from the elastic properties of the stomach tissue. Overall, the diffusion coefficient of the electric potentials of interstitial cells of Cajal (ICCs) was the most important parameter. Interactions between the parameters played a role in both amplitude and propagation speed of the contraction waves but a negligible role in their width and the uncontracted state. Finally, these findings were used to indicate promising research directions for the enhancement of the model formulation as well as the models predictive capabilities.

(V) Variance-based global sensitivity analysis of a homogenized constrained mixture model for arterial growth and remodelling was performed (Paper C):

In two application cases, a hypertensive aorta and an abdominal aortic aneurysm (AAA) the importance of, respectively, 9 and 10 uncertain parameters for the development of the maximum diameter of the vessel was studied over a period of 10 years. In the hypertension case interactions between the parameters played a lesser role in defining output variance. However, they played a significant role in the AAA case. In both cases, the same three parameters – stress-dependent collagen production, collagen half-life time, and strain-stiffening of collagen fibres – were identified as the most important ones for the inelastic growth and remodelling response of the model. The findings were shown to have important implications for future research. For similar computational studies in the future, it

can be acceptable to use available population-average values for the uninfluential parameters. Measurements or estimation of stress-dependent collagen production and collagen half-life time would allow significant improvement of predictions of AAA enlargement.

(VI) Variance-based global sensitivity analysis based on Sobol indices was identified as a powerful tool necessary for comprehensive studies of models of active biomechanical systems (7):

An efficient implementation of the method in a scalable computing framework allowed the direct application of variance-based global sensitivity analysis based on Sobol indices to models of unprecedented complexity. The diversity of the performed analyses demonstrated the universal capabilities of Sobol's method to reveal important model properties inaccessible by current standard methods.

The analyses revealed that, in models of active biomechanical systems,

- **significant amounts of parameter interactions can occur.**
This finding underlines the necessity of global methods for their analysis and implies that previous studies with local methods might have underestimated the influence of some parameters.
- **the uncertainty in many parameters has negligible influence on the uncertainty in the output of the model.**
This result indicates that, in the future, the complexity of predictions based on models of active biomechanical systems can be reduced significantly by identifying and fixing these uninfluential parameters to their mean values.
- **the uncertainty in the output of the models is frequently dominated by the uncertainty in a few parameters.**
The method suggests that reducing the uncertainty in the most important parameters will benefit the accuracy of model predictions the most.

These findings can have important implications for both computational and experimental studies of active biomechanical systems in the future. Overall, global sensitivity analysis should become an essential part of the development and analysis process of models of active biomechanical systems.

As indicated above, the following three publications together with the original results of Section 4.2 constitute the core of this thesis (see also Figure 1.1). The list is in order of presentation of the papers in the thesis:

- **Paper A [14]:** S. Brandstaeter, S. L. Fuchs, R. C. Aydin, and C. J. Cyron, 'Mechanics of the stomach: A review of an emerging field of biomechanics', *GAMM-Mitteilungen*, vol. 42, no. 3, e201900001, 2019. DOI: [10.1002/gamm.201900001](https://doi.org/10.1002/gamm.201900001)
- **Paper B [51]:** S. Brandstaeter, A. Gizzi, S. L. Fuchs, A. M. Gebauer, R. C. Aydin, and C. J. Cyron, 'Computational model of gastric motility with active-strain electromechanics', *ZAMM - Journal of Applied Mathematics and Mechanics / Zeitschrift für Angewandte Mathematik und Mechanik*, vol. 98, no. 12, pp. 2177–2197, 2018. DOI: [10.1002/zamm.201800166](https://doi.org/10.1002/zamm.201800166)

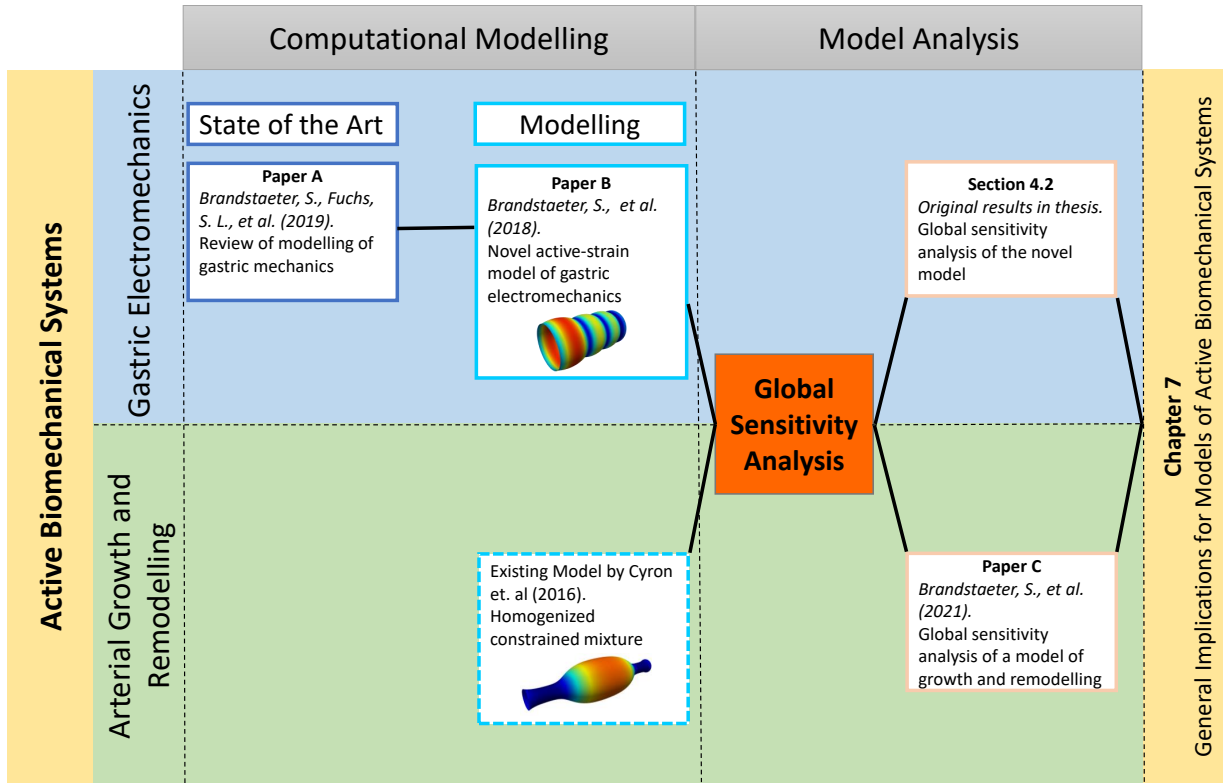


Figure 1.1: Graphical overview of the contributions of this thesis and relations between them (Paper A, [14]; Paper B, [51]; Paper C, [52]; Section 4.2.1; Chapter 7).

- **Paper C [52]:** S. Brandstaeter, S. L. Fuchs, J. Biehler, R. C. Aydin, W. A. Wall, and C. J. Cyron, ‘Global Sensitivity Analysis of a Homogenized Constrained Mixture Model of Arterial Growth and Remodeling’, *Journal of Elasticity*, vol. 145, pp. 191–221, 2021. DOI: [10.1007/s10659-021-09833-9](https://doi.org/10.1007/s10659-021-09833-9)

All computational models of active biomechanical systems have been implemented in the in-house finite element code Bavarian Advanced Computational Initiative (BACI) [53]. Existing functionality of BACI was reused where possible. To this end, the dissertations of Vuong [54], Farah [55], and Bräu [56] were of particular importance. The global sensitivity analysis framework was implemented in the QUEENS code project [57]. QUEENS is a general purpose framework for large scale uncertainty quantification, physics-informed machine learning, bayesian optimization, inverse problems and simulation analytics. Within QUEENS, the implementation of Sobol indices has been adapted from the open-source project SALib [58]. QUEENS was provided by courtesy of AdCo EngineeringGW GmbH, which is gratefully acknowledged.

1.3 Outline

The remainder of this thesis is structured as follows.

Chapter 2 details fundamental principles and basic knowledge of the topics covered in the thesis. First, terminology and definitions essential for this thesis are presented in Section 2.1. Second, an overview on different sources of uncertainties in computational modelling is given in Section 2.2. Third, Section 2.3 specifies reference literature that provides the basic knowledge required to follow the presentation of the models of active biomechanical systems of later chapters. Fourth, Section 2.4 summarizes Paper A, which presents the necessary biological background on anatomy and physiology of the human stomach. In addition, it presents a thorough review of the state of the art of computational modelling of the stomach, identifies limitations and challenges, and provides future perspectives and promising fields of application. Finally, the biological background and relevance of growth and remodelling for the cardiovascular system together with a definition of these terms are briefly outlined in Section 2.5.

Chapter 3 provides an introduction to global sensitivity analysis. The chapter begins with a literature review in Section 3.1. Section 3.2 continues with a brief but general introduction to sensitivity analysis, including possible objectives and an overview of existing methods. Section 3.3 presents a comprehensive derivation of Sobol indices for variance-based global sensitivity analysis, the core method of this thesis.

Chapter 4 presents results for the first field of application: gastric electromechanics. In Section 4.1, a novel computational framework for gastric electromechanics is presented in the form of a summary of Paper B. Thereafter, Section 4.2 displays a global sensitivity analysis of this model.

Chapter 5 details the global sensitivity analysis results of a homogenized constrained mixture model for arterial growth and remodelling, the second field of application covered in this thesis. The results are presented in the form of a summary of Paper C.

Chapter 6 discusses the main results of both applications separately and, on a larger scale, of global sensitivity analysis of models of active biomechanical systems in general.

Chapter 7 concludes the thesis by providing a summary of the general findings and promising future perspectives.

The Appendix contains unchanged reprints of the three embedded publications.

2 Scientific context

This chapter outlines the scientific context of this thesis. It presents required basic knowledge and terminology of the covered topics. The chapter begins by introducing core terms and definitions. The next section elucidates the importance of uncertainties in computational modelling and presents an overview on different sources of model uncertainties. Next, a brief literature review presents references to textbooks containing the basic knowledge required to follow the presentation of the models of active biomechanical systems of later chapters. Thereafter, Paper A is summarized. The paper provides the necessary biological background on anatomy and physiology of the human stomach. Additionally, it presents a thorough review of the state of the art of mathematical modelling of the human stomach and identifies limitations and challenges. It also provides future perspectives and promising fields of application for computational models of gastric mechanics. Finally, the mechanobiological background of growth and remodelling processes in the cardiovascular system and definitions of important terms of the field are briefly outlined.

2.1 Terminology

This section establishes the essential terminology and necessary definitions for one of the core topics of this thesis: global sensitivity analysis. In a very general way, *Sensitivity analysis* can be defined as:

Definition 2.1: Sensitivity analysis

Sensitivity analysis is the quantification of the relative contributions of inputs to the output of a model by determining how variations in the inputs affect the observed output.

In order to be useful, Definition 2.1 necessitates the clarification of the three terms: *model*, *input*, and *output*. The following definitions of these terms are adapted from [59, Chapter 2], [23, 60, 61].

Definition 2.2: Model, output, and input

A model is a simplified, instructive representation of a system.

A model output is any response, data or information that has been produced by a model.

A model input is anything that can prompt a variation in the model output.

This definition of model covers, for example, physical models, like experiments and product prototypes, but also abstract ones like mathematical equations and computer codes. Examples for model outputs include the measured quantities of an experiment like the Young's modulus of

a material in classic, linear tensile testing or, for mathematical models, any objective function of the model response like the cost of a product, or the complete spatio-temporal displacement field of a stomach during peristalsis. In principle, a model can have many outputs. For a meaningful sensitivity analysis, it is therefore paramount to determine which outputs should be investigated [26, 62]. Naturally, this choice depends on the context and the objective of the analysis (see Section 3.2.1). Many decisions have to be made during model setup including the type and structure of the model, the parameters, the boundary and initial conditions, the resolution, the discretization method and many more [23]. All of these choices are associated with some uncertainty, are therefore assumptions and can in general be considered inputs of the model that if varied result in a different output value. A sensitivity analysis can however only analyse a subset of all inputs. The inputs in this subset of interest are usually referred to as *(input) factors* in the sensitivity analysis community [26]. Again, the decision which input factors should be considered in a specific analysis depends strongly on the objective of the analysis. This thesis focuses on *model parameters* as model inputs and refrains from the rigorous distinction between model inputs and model factors. Therefore, the terms parameter, input, and factor are used interchangeably. In part, this simplified terminology is justified by the fact that many inputs of the mathematical models investigated herein can indeed be parameterized. It is, however, stressed once again that, in general, sensitivity analysis is not restricted to parameters of mathematical models but can also be understood in a broader sense (see, for example, [26]).

A very important classification of sensitivity analysis methods involves the distinction between local and global methods.

Definition 2.3: Local sensitivity analysis

Local sensitivity analysis focuses on the change in the model output when the inputs are perturbed about a nominal value [63, Chapter 14].

Local sensitivity analysis is often carried out by analysing the derivative of the output with respect to individual inputs. In this way, local sensitivity analysis is regularly found in the context of optimization, adjoint methods and deterministic model calibration. For many investigators, including many engineers, local sensitivity analysis remains the standard technique and synonymous to sensitivity analysis in general [23, 63]. This approach has, however, severe limitations regarding the treatment of non-linear models. Therefore, non-linear models require a global perspective. While local sensitivity analysis restricts the analysis to a single point of interest in the model input space, global methods cover the entire input space. One attempt is to conduct a local analysis for multiple points of the input space, for example, for all critical points – like equilibrium or bifurcation points – of the model [63]. These approaches are also called hybrid local-global methods [64]. Another, more general approach is statistical in nature and tries to relate input and output model uncertainties. This thesis follows this approach and defines global sensitivity analysis according to [61] as:

Definition 2.4: Global sensitivity analysis

Global sensitivity analysis is the study of how uncertainty in the model output can be apportioned to contributions from the uncertainties in the model inputs.

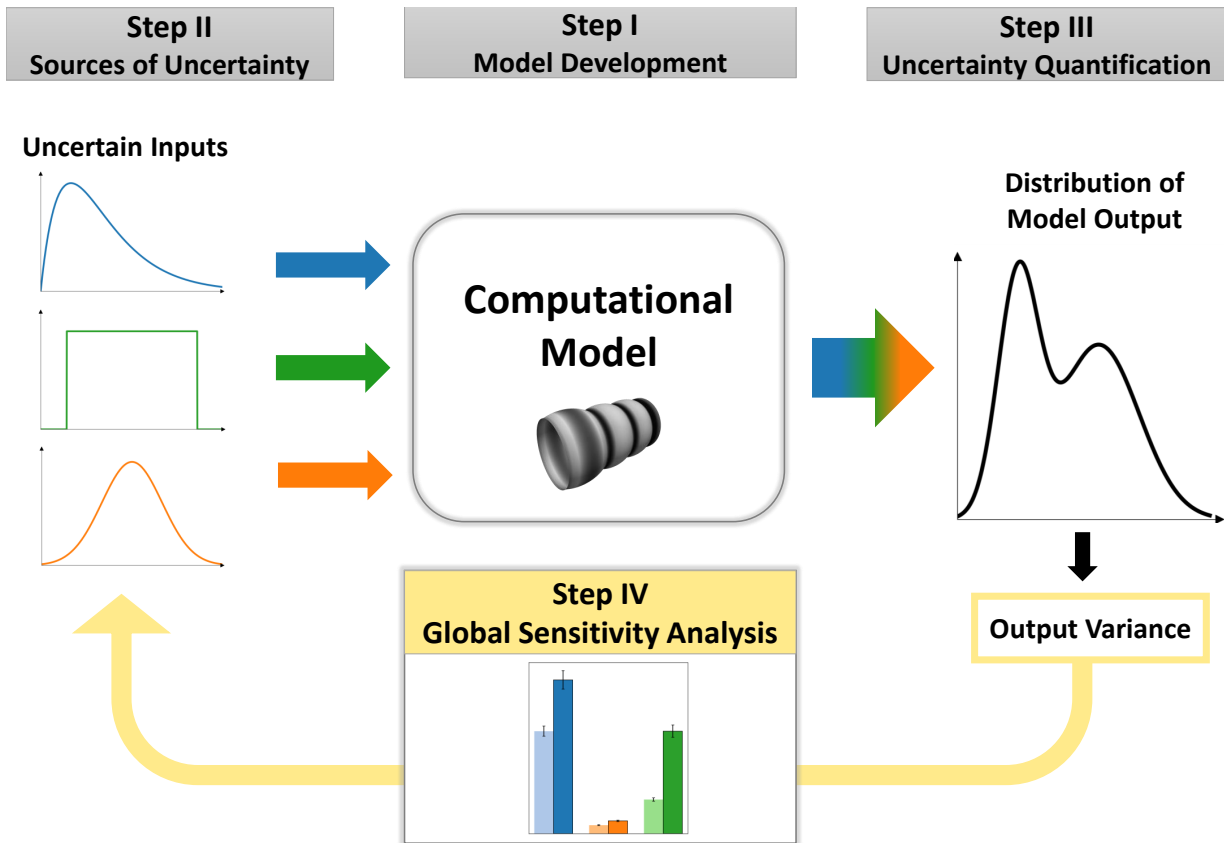


Figure 2.1: Schematic representation of a global sensitivity analysis of a computational model (see Definition 2.4). (figure based on [23, 66]).

In this form, global sensitivity analysis complements uncertainty quantification, which is concerned with the quantification of the model output uncertainty based on model input uncertainties. Global sensitivity analysis then closes the loop by attributing amounts of model output uncertainty to the respective input uncertainties. Figure 2.1 illustrates global sensitivity analysis of a computational model and shows its relation to model development and uncertainty quantification. In conclusion, local sensitivity analysis can only be instructive in a deterministic setting while global sensitivity analysis embraces uncertainties [65].

2.2 On the importance of uncertainty in computational modelling

‘All models are wrong, but some are useful’

— George E. P. Box

This famous aphorism expresses that any model fails to capture the true complexity of reality. At the same time, it asserts the positive message that the inevitable approximation error does not necessarily result in futility [67, 68]. Thereby, Box’s aphorism immediately poses a central

question: ‘How much imperfection is acceptable in a model before it becomes useless?’ Finding a definitive answer to this question is extremely difficult – if possible at all. However, a first step is to embrace the certain approximative nature of mathematical models and therefore understand any modelling endeavour as a journey under uncertainty. The attempt to evade this truth can be misleading: in hope of sufficiently increasing model accuracy simply by developing more complex models which include more phenomena in greater detail is an inherently flawed strategy. At some point, it will always become necessary to analyze the remaining uncertainties. In order to do so, it is enlightening to look at possible sources of uncertainty. For this purpose, this section introduces a taxonomy of uncertainty in computational models based on [21, 69, 70].

Two basic types of uncertainties can be distinguished. On the one hand, *aleatoric uncertainties* result from ‘true’ randomness or variability inherent to the system. On the other hand, *epistemic uncertainties* describe uncertainties that result from a lack of knowledge. The distinction becomes important in the context of modelling because only epistemic uncertainties can be reduced by collecting additional information while aleatoric uncertainties will prevail no matter how much knowledge is gained. In other words, any potential for uncertainty reduction in a model is fully determined by the epistemic uncertainty of the model. When looking at the output uncertainty of computational models, the following sources of uncertainty can be identified:

- **Input uncertainty:** Typically not all model inputs are known precisely. The uncertainty in the model inputs propagates through the model and results in output uncertainty. Often uncertain inputs can be understood as unknown model parameters (see Section 2.1). Therefore input uncertainty is sometimes also directly referred to as parameter uncertainty. Indeed, incomplete knowledge of precise values of the model parameters is a very common source of input uncertainty. For example, even if the value of a parameter can be measured with high precision, there will always remain some measurement error and therefore uncertainty about the true value. This thesis will mostly look at input uncertainty resulting from unknown values of physical parameters like material stiffnesses, diffusion coefficients or mass gain factors. Other examples for input uncertainty in the context of computational models of active biomechanical systems include uncertainty in the boundary conditions – like mean blood pressure or the properties of surrounding tissue – and uncertainty in the model domain resulting for example from errors in the reconstruction process from medical images.
- **Model inadequacy:** By definition, models are only approximations of real-world processes (see Section 2.1). Therefore, even if every model input was known precisely, that is, even if there is no input uncertainty, there will always remain a certain discrepancy between the model prediction and the real-world. This discrepancy is called model inadequacy. Model inadequacy is epistemic in nature: it can be reduced – albeit never fully extinguished in practice – by improving the model, for example, by incorporation of additional, previously neglected phenomena.
- **Residual variability:** Based on the conditions implied by a complete set of inputs, a model is assumed to predict the value of some real-world process. If the process is repeated under the same conditions, the same outcome is expected. It is sometimes possible to prove this repeatability for models. In case of mathematical models it is, for example, closely related to the proof of the uniqueness of a solution. However, this is not necessarily true for the

real-world process: if the process is repeated under the same conditions its outcome might still vary. The variation of the process even if its conditions are specified is referred to as residual variability. At first sight residual variability might look like the prime example of aleatoric uncertainty. But in reality, one never knows whether one truly specified the complete real-world conditions. It might very well be that if only additional, unknown or unrecognized conditions were specified, the residual variability could be reduced. This would render it epistemic in nature. Then, residual variability could essentially be considered a special type of model inadequacy. To make the definition clear, this thesis considers only the aleatoric part as true residual variability. Therefore in this thesis, residual variability is the variation in a process's output that remains even if its conditions are fully specified.

Distinguishing between the different sources of uncertainty is very difficult in practice. Consider for example that one observes a mismatch between a model prediction and the real-world. It seems impossible to determine whether this mismatch stems from model inadequacy or residual variability. It boils down to the fact that one never really knows whether the process's conditions are fully-specified and one deals with (aleatoric) residual variability or whether the model assumptions are inappropriate or incomplete and one deals with (epistemic) model inadequacy. Therefore the distinction remains rather theoretical. Essentially, model inadequacy can be considered a property of the model and residual variability a property of the real-world process.

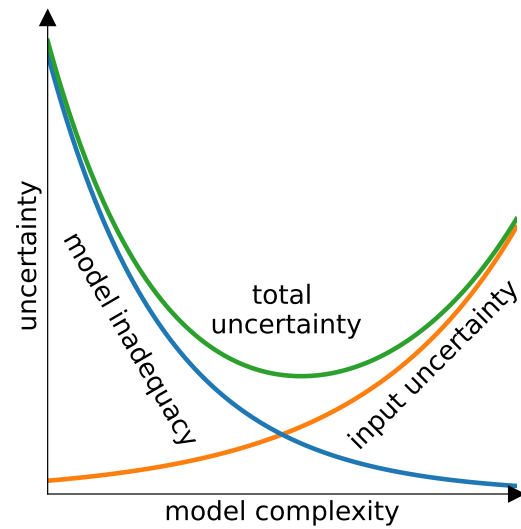
This thesis assumes that the systems investigated have very little – if any – residual variability at the scale of interest and it can therefore be neglected. All the remaining uncertainties are epistemic in nature and can therefore be reduced by gaining system knowledge. Here, this thesis focuses on the treatment of two types of epistemic model uncertainties: model inadequacy and parameter uncertainty.

The uncertainty due to model inadequacy can be reduced by increasing model complexity. For example, the incorporation of additional physiological processes and the consideration of a more detailed model domain both increase model accuracy but also complexity. This is the reasoning behind many modelling studies including the first part of this thesis which presents a novel, computational model of gastric electromechanics. However, this approach alone cannot lead to success in the sense that it does not necessarily result in the most useful model predictions. George E. P. Box outlines this perfectly:

Since all models are wrong the scientist cannot obtain a 'correct' one by excessive elaboration. On the contrary following William of Occam he should seek an economical description of natural phenomena. Just as the ability to devise simple but evocative models is the signature of the great scientist so overelaboration and overparameterization is often the mark of mediocrity. [71, p. 792]

The framework of model uncertainty allows for an illustrative rationale of the law of parsimony, which Box passionately argues for. While increasing model complexity reduces model inadequacy, it simultaneously inflates input uncertainty. More complex models require more inputs, which can only ever be measured up to a limited precision. Therefore, finding the optimal model complexity that results in the minimal total uncertainty requires a compromise between model inadequacy and input uncertainty (see Fig. 2.2) [17]. Uncertainty quantification and sensitivity analysis are essential tools for dealing with this challenge (see Figure 2.1). First, uncertainty quantification enables the quantification of model output uncertainty caused by uncertain

Figure 2.2: Idealized representation of the total uncertainty in a model. The total uncertainty results from the superposition of model inadequacy and input uncertainty. While model inadequacy reduces with increasing model complexity, input uncertainty increases with model complexity. Therefore, finding the minimal total uncertainty requires a compromise between model inadequacy and input uncertainty. (figure based on [72])



inputs. Second, sensitivity analysis can help manage model complexity. Identifying inputs that have little influence on the output variability allows to reduce model complexity by fixing these inputs at a certain value, often the mean value. At the same time, identifying the most influential parameters allows to focus accurate but expensive measurements on the most beneficial parameters. Ultimately, the treatment of model uncertainty presents the unifying framework of this thesis and the fundamental role of model uncertainty inspired the investigation of global sensitivity analysis for complex models of active biomechanical systems.

2.3 Continuum modelling of active biomechanical systems

Biomechanics is a broad field where many different modelling techniques have been used successfully. Available methods span from experimental techniques for *in-vitro* or *in-vivo* measurements to a myriad of mathematical and computational modelling frameworks. Naturally, the appropriate model description depends critically on the question it shall help answer.

Herein, mathematical models based on the powerful non-linear continuum mechanics framework are studied. Detailed presentations of the specific model formulations for the active biomechanical systems studied herein are contained in the embedded articles. For an overview of models for gastric mechanics refer to Section 2.4. A novel modelling framework for gastric motility can be found in Section 4.1. A homogenized constrained mixture formulation for arterial growth and remodelling is contained in Section 5.1. Following these specialised and concise descriptions requires a sound knowledge of the basic concepts of non-linear continuum mechanics. Interested readers are referred to one of the excellent textbooks that exist in the literature. The book by Holzapfel [73] is highly recommended as an exhaustive and accessible starting point. Of course, the classic text by Truesdell and Noll [74] should also be mentioned as an additional reference here. Readers who simply seek a short refresher are referred to the summaries provided in [75] or [21].

Gastric electromechanics additionally requires a mathematical description for bioelectric activity. Bioelectric activity on the tissue level is an inherently multi-scale phenomenon. One needs to take into consideration the interaction between processes on the cellular scale and the tissue scale. This is formalized in special, homogenized reaction-diffusion systems based on Fick's law. An in-depth introduction to the mathematical modelling of electrophysiology on different scales and their homogenization can be found in the books by Keener and Sneyd [76, 77] and Franzone et al. [78] for comprehensive reference works.

The above mentioned modelling frameworks result in systems of partial differential equations that, in general, need to be solved numerically. This thesis uses the finite element method (FEM) for the numerical solution of the model equations. An extensive introduction can, for example, be found in [79, 80].

2.4 Paper A: Mechanics of the stomach: A review of an emerging field of biomechanics

Sebastian Brandstaeter*, Sebastian L. Fuchs*, Roland C. Aydin, Christian J. Cyron

* these authors contributed equally to this work.

published in

GAMM - Mitteilungen, vol. 42, no. 3, e201900001, 2019. DOI: [10.1002/gamm.201900001](https://doi.org/10.1002/gamm.201900001).

Summary

Energy intake is an essential process for any living organism. For humans, digestion of food constitutes the only source of energy. Unsurprisingly, health is strongly tied to a normal functioning digestive system and diseases linked to the stomach are significant sources of morbidity in industrialized countries. One of the main risk factors for many leading causes of death is obesity. The costs for treating obesity has steadily increased from \$79 billion in 1998 to \$147 billion in 2008 and the estimated prevalence was 36 % in the United States in 2010. Furthermore, 10–45 % of the general population suffer from some form of dyspepsia, also called indigestion. Dyspepsia does significantly diminish individual well-being which also negatively influences economic productivity of patients. These are just two examples of highly prevalent health problems that are closely related to the mechanics of the stomach: for instance, one of the few permanent treatment options for obesity, bariatric surgery, involves the irreversible adjustment of gastric geometry and thereby mechanics. Further, dyspepsia is often associated with impaired control of gastric smooth muscle contractions.

This demonstrates that gastric mechanics is of enormous relevance. A fact that is, however, not at all reflected by current research efforts. A comparison with the field of cardiovascular mechanics reveals that modelling of the stomach lags behind around 20 years. In part this might be explained by the fact that gastric mechanics inherently involves multiple complex and tightly coupled physical fields: the gastric electrophysiological system coordinates the intricate

contraction patterns of the stomach wall known as gastric motility. Gastric motility serves to accommodate food intake, and to mix and grind digesta. In addition to being coupled physically, all these processes are also controlled by a sophisticated neural and hormonal system. The biological and physiological basis of these systems and their complex interactions have not been fully understood yet. However, recent progress in these fields finally allows to address one of the big open topics in biomechanics: the development of mathematical and computational multiphysics models of the stomach. The resulting models will, in turn, give previously inaccessible insights into the gastric system.

To this end, the paper begins with an overview of the anatomy and physiology of the human stomach. The core contribution is presented by an exhaustive review of existing approaches to mathematical and computational modelling of gastric mechanics. It is revealed that, on the one hand, some phenomena like gastric electrophysiology and fluid mechanics of digesta have received isolated research attention. This is exemplified by the presentation of three gastric electrophysiology models describing the propagation of electric signals through the stomach wall with increasing detail: the monodomain, bidomain and extended bidomain models. On the other hand, mathematical modelling of the solid mechanics of the gastric wall is identified to fall short of state-of-the-art soft tissue models that have been applied with great success to other biological soft tissues as, for example, arterial tissue. The paper delineates the biggest challenges, possible solutions and the potential impact of a comprehensive computational model of the mechanics of the human stomach.

Most importantly, the multiphysics nature of the organ needs to be embraced in future models. The integrated system behaviour can only be captured and understood by incorporating several tightly coupled, complex phenomena at once: gastric electrophysiology, solid mechanics of gastric tissue and fluid mechanics of digesta. Such a coupled multiphysics model will allow thorough, *in-silico* analyses of digestion in health and disease. Ultimately, it will also offer unprecedented opportunities in many other fields such as computer-aided medicine and food design.

Author contributions

C.J.C. conceived and directed the review. **All authors** wrote the manuscript. In detail, **S.B.** was primarily responsible for writing major parts of Section 2.3, Section 3.2, as well as Section 3.3. **All authors** discussed the content and commented on the manuscript. **S.B.** and S.L.F. contributed equally to this work.

2.5 Importance of growth and remodelling for the cardiovascular system

The field of *mechanobiology* studies the processes that allow living soft tissues to react to and influence mechanical quantities – such as forces. A key concept of mechanobiology is tensional [81] or *mechanical homeostasis* [6, 82–84]. It postulates that cells within living tissues continuously strive to remain in, or return to a preferred mechanical tissue state, often referred to as *homeostatic target*. Cells do so by means of growth and remodelling, two essential mechanisms for tissue adaptation.

Growth describes the cell-mediated deposition or degradation of mass increments resulting in a change of geometry. This thesis considers only volumetric growth and assumes that the change of mass of the whole tissue results in a change of the overall volume while the mass density remains constant everywhere over time.

Remodelling refers to an adaptation of the microstructure of tissues. Cells within tissues are constantly degrading and reintegrating collagen fibres as well as adjusting inter-fibre connections of the extracellular matrix.

In this way, the mechanobiological processes of growth and remodelling form an integral part of cardiovascular (patho-)physiology. Indeed, many cardiovascular diseases have been shown to be associated with altered mechanical conditions. Prominent examples include hypertension [46, 85, 86] and aneurysms [31, 46, 82, 84]. Aneurysms are local dilatations of blood vessels that often continue to grow over years until rupture and constitute a substantial source of morbidity in industrialized countries [87].

3 Global sensitivity analysis

This chapter offers a brief summary of the fundamentals of sensitivity analysis including a short overview of existing methods. Its purpose is to lay out the reasoning behind global methods. In the next step, a detailed derivation of the variance-based, global sensitivity analysis method called Sobol indices is presented. The chapter continues by presenting a computational scheme for efficient calculation of the indices and concludes with a short guide on how Sobol indices can be interpreted and used.

3.1 Literature review

Many authors have written introductory texts on sensitivity analysis of varying level of detail and with different focus. Today, there exists an extensive list of reference texts on sensitivity analysis methods in theory and in application. The following paragraphs give an overview on texts that might be helpful in studying the field.

First, a list of excellent textbooks is presented. Local and hybrid local-global methods have been discussed in great detail in the two-volume monograph of Cacuci et al. [88, 89]. Certainly, the book by Saltelli et al. [61] constitutes the standard textbook on global sensitivity analysis. A short, concise and very accessible introduction to local and global methods can be found in Chapter 14 and 15, respectively, of the book by Smith [63]. Similarly, Part IV of the very extensive ‘Handbook of Uncertainty Quantification’ by Ghanem et al. [25] offers a recent overview of well-established local and global sensitivity analysis approaches. Iooss and Lemaître [90] focus on global methods and provide a classification and decision diagram which can help to find an appropriate method based on the objective of the study and the properties of the model. A mathematically thorough introduction to uncertainty quantification and sensitivity analysis can be found in the book of Sullivan [24]. And finally, Chapter 7 in Santner et al. [91] presents sensitivity analysis in the context of design and analysis of computer experiments.

Second, there are also many very good review articles covering sensitivity analysis. In [65], Borgonovo and Plischke present a review of local and global sensitivity analysis in the context of operational research. Wentworth et al. [92] show, in a structured and accessible way, how global sensitivity analysis methods can be used for parameter selection in biological and physical models exemplified for a dynamic HIV model. Similarly, Eck et al. [17] offer an exceptionally well written and detailed ‘guide to uncertainty quantification and sensitivity analysis in cardiovascular applications’. A systematic review of sensitivity analysis methods including an informative classification is presented by Pianosi et al. in [62]. A recent overview of available software packages is offered by Douglas-Smith et al. in [93]. Qian and Mahdi wrote a comprehensive but concise review of sensitivity analysis methods laying out their importance for biomedical sciences [64]. Most recently, Razavi et al. [26] presented a must read manifesto for global sensitivity analysis as ‘an essential discipline for systems modeling’. The authors – including many

of the pioneers in the field – offer not only an excellent overview of the state of the art but also future perspectives.

3.2 A brief introduction to sensitivity analysis

As described in the previous section, a great number of excellent texts introduces the basic concepts of sensitivity analysis. Content and structure are quite similar in most texts, which might be explained by the fact that there is only a limited number of different approaches one can take to introduce the fundamental concepts and essential quantities in a coherent way. For this reason, a structure similar to the one in Smith's book [63] and in [62, 64] is followed. The content of the section is, however, compiled from many of the texts presented in Section 3.1. Therefore, references to the respective, specialized texts are supplied in place.

3.2.1 Objectives of sensitivity analysis

Reasons for conducting sensitivity analysis are diverse. As for any study, it is essential to establish a clear understanding of the insights that one wishes to obtain by conducting a sensitivity analysis [65]. In other words, sensitivity analysis should always serve to answer a question, not least because the objective of the analysis influences the choice of an appropriate method. Objectives of a sensitivity analysis may include [26, 61, 63, 94, 95]:

- **Model insight:** Sensitivity analysis can ascertain whether the model output is robust or vulnerable with regards to perturbations in the inputs. It can also help explore causalities: how do combinations of and interactions between, for example, competing hypotheses, different scales, or various input parameters influence a model? This way, sensitivity analysis can provide valuable model insights and illuminating scientific discoveries.
- **Decision making:** The quantification of the sensitivity of an outcome on different decision options, hypotheses, constraints, and assumptions and their associated uncertainties can support the decision making process under uncertainty.
- **Parameter fixing:** Variations of uninfluential parameters do not result in large variations of the output. The identification of uninfluential model parameters allows to fix them at any nominal value within their range of variability without significant reduction in output uncertainty. For simplicity, the mean value is often chosen as said nominal value. By removing these parameters from any subsequent uncertainty analyses, the problem size can effectively be reduced. Parameter fixing is often also referred to as the *factor fixing setting*, *parameter selection*, or *parameter screening*.
- **Parameter prioritization:** A priority analysis is in some ways the opposite to parameter fixing. It aims at identifying the most important parameters. These are the ones that if they were fixed, would result in a significant reduction of output uncertainty. Therefore, focusing future efforts on reducing the uncertainties in these influential parameters can be considered the most efficient and rewarding use of resources. For example, parameter prioritization provides a rationale to experimental researchers to concentrate on the development or improvement of measurement protocols for specific, important parameters.

Priority analysis is often also referred to as the *factor prioritization setting* or *parameter ranking*.

- **Parameter mapping:** There might be a region of particular interest in the output space. One might then be interested in knowing whether there are inputs or combinations of inputs that are responsible for outputs in this special domain of interest. For example, which domain in the parameter space produces output values above a certain threshold. This setting is called parameter mapping and plays an important role, for example, in system reliability.
- **Variance cutting:** For certain model applications there are predefined threshold values for the output uncertainty. The reduction of the initial level of output uncertainty below this threshold is the goal of variance cutting.
- **Model calibration:** In preparation of model calibration, also called parameter estimation or identification, sensitivity analysis can help identify which model output is sensitive to the parameters that should be estimated. If data is only available for an insensitive output, a reliable estimation of parameter values can be expected to be difficult. One can also apply sensitivity analysis methods directly to the objective function or likelihood of the calibration task. In this way, sensitivity analysis can be a practical tool in handling the non-identifiability issues frequently encountered during model calibration.

While the above list does not claim to be exhaustive, it gives an idea on the kind of interesting questions sensitivity analysis can answer.

3.2.2 Overview of existing methods

There exists a myriad of sensitivity analysis methods and not every method is equally suitable for each of the objectives presented in the previous section. This section presents an overview of well-established classes of methods. Therefore, only the conceptual idea of the methods, their advantages and limitations will be laid out without any mathematical details. For a comprehensive overview the interested reader is referred to [25, 26, 62, 64, 65, 90].

Remark 1 *The following presentation assumes a model is a function that takes a vector of inputs and returns a single, scalar-valued output. A mathematical definition of this setting can be found in Section 3.3.1. Many methods for sensitivity analysis rely on this assumption. In practice, the assumption often does, however, not hold (directly) for many models of interest. For example, any model based on differential equations per definition returns a function as an output. Still, the methods can be applied successfully. On the one hand, they can often be applied given some minor additional modelling assumptions (see Section 5.1) and, on the other hand, research in lifting the restriction is very active (see Section 7.1).*

Local approaches

One-at-a-time approach Perhaps the most straightforward way to investigate model output sensitivity is to vary one input after another and observe the change in the output. The approach is intuitive and formally described by holding all inputs at their nominal value except for one which is changed by a fraction of its nominal value [64]. The resulting fractional change in the output can be used to ascertain the sensitivity of the output to the single varied input. Quantitative sensitivity measures based on this approach provide both the direction and magnitude of change which can, in turn, be used to rank the parameters according to their impact [65]. Sometimes the method is used for qualitative evaluation only, for example, by plotting the model output for the nominal value in comparison with the varied one. At its core, the method is very closely related to what is referred to as parameter studies in computational modelling. The simplicity of the method is a big advantage but its local nature, that is, the reference to a nominal value, is a severely limiting factor. By changing but one parameter at a time, it is impossible to detect interactions between the parameters, which is why one-at-a-time methods are suitable only for linear models. A natural way of extending the approach might be to repeat the process for different fractional changes. While this certainly increases the information content, it does not help to overcome its restriction to linear models.

Derivative-based approach The archetype of a local sensitivity measure is the first partial derivative of the output with respect to one of its inputs evaluated at a nominal value of interest. Per definition, partial derivatives give notion to the amount of change in the output due to a small (infinitesimal) change in one input while the others are held constant. A large value implies that a small perturbation of the input from its nominal value results in a large change of the output and the output can be considered sensitive to said input. Many investigators are familiar with this notion of sensitivity. Applications of the method are manifold, for example, reliability analysis and risk assessment traditionally rely heavily on it. It also has strong ties to (deterministic) model calibration, data assimilation, and, in general, optimization. The challenge in applying the method lies in the computation of the derivatives especially in case of a large system size with many inputs. In general, there are multiple ways of approaching this issue. If framed correctly, the one-at-a-time approaches described above can be considered a naive approach to this [96]. A more refined approach would be the use of numerical approximations schemes like finite differences. While this approach is straightforward, its computational cost is often prohibitive. If the code base allows for it, automatic differentiation can help here [97]. A completely different but elegant way, in particular for very large-dimensional cases, is to resort to adjoint methods [88].

Certainly, the sound mathematical basis and easy interpretability are big advantages of the method. It suffers, however, from two notable deficiencies [23]. First, if the model is non-linear with respect to a parameter, the partial derivative with respect to this parameter will change depending on where in the parameter's range it is evaluated. Second, if the model parameters are involved in interactions between each other, the value of the partial derivative with respect to one parameter will change depending on the values of the remaining ones. These points illustrate the local nature of the method. In summary, first partial derivatives are unrestrictedly valid only in case of linear models.

Global approaches

Global approaches are almost exclusively sample based. They require an input-output sample where each sample point consists of a set of input values together with the corresponding output value. As with any sample based approach, the information value of the sample critically determines success. Since a global perspective is of interest, the sample points should sufficiently cover the complete input space. Many different sampling strategies exist that attempt to fulfil this requirement in some optimal sense. A very general and therefore popular sampling strategy is the Monte Carlo method [98]. However, approaches like Latin-Hypercube design of experiments [99–101] and quasi-random, low-discrepancy sequences like Sobol sequences [102–105] have repeatedly been shown to outperform crude Monte Carlo methods in sensitivity analysis applications [106, 107].

Visual methods Graphical tools are basic but essential methods for global sensitivity analysis. Based on any given input-output sample, visual methods can be readily applied. In the following, the two most common methods are presented. Refer to [62, 64] for more examples and visualization ideas.

A collection of scatterplots between the model output and each input can help to determine the nature of the input-output relations, for example, whether the output depends linearly or non-linearly on an input [95]. Scatterplots can also serve to distinguish qualitatively between influential and unimportant parameters (see [63, Example 15.1]). Plain marginal scatterplots can, however, not detect interactions between the inputs [91]. To this end, parallel coordinates plots can be used [90, 95]. In these plots, each input is represented by a vertical axis depicted together with an additional vertical axis for the output. Hence, for each input and the output there exists a parallel, vertical coordinate axis resulting in the name-giving layout. A sample point is represented by a line connecting its input values to the corresponding output value. Restricting the output axis, for example, to the small values shows which combination of input values is responsible for this output region revealing potential interactions effects. For an example of a parallel coordinates plot see Fig. 7 in Paper C. Parallel coordinates plots are sometimes also referred to as cobweb plots but they should not be confused with cobweb plots known from dynamic systems analysis.

Certainly, the biggest advantage of visual methods is that their application is often straightforward and does not require little prior knowledge. They are suitable for both linear and non-linear models and relatively cheap in particular if an existing input-output sample can be leveraged. The drawback of visual methods is their purely qualitative nature. The amount of information can be overwhelming in particular for large numbers of inputs. For this reason, visual methods require experience in interpretation [91]. The ability to dynamically adjust the representation, for example, the arrangement of coordinates in a parallel coordinates plot, can help tremendously in this regard. For an example refer to the supplementary material of Paper C, [52] available online.

Screening methods Screening methods have been developed to achieve efficient parameter fixing (see Section 3.2.1) in a global setting with a large number of inputs. The rationale behind these approaches is that practice has shown that often the output is sensitive only to a small number of inputs. The goal of screening methods is to efficiently separate the influential from the unimportant parameters. In this context, efficiency refers to the number of necessary

model evaluations in balance with realistic assumptions of model complexity, that is, number of inputs investigated. In a next step, more detailed and expensive methods can then be applied for an in-depth analysis of the remaining, influential parameters [90].

Many different screening methods exist each for a particular use case. Refer to [108] and [90] for detailed overviews. The method of Morris [109, 110] is a very common method. Morris screening allows to distinguish between three classes of inputs: The first group are uninfluential inputs with negligible effects, the second group contains inputs that have large linear effects but are not involved in any interactions, and the third group are influential inputs that have large non-linear effects both with and without interaction effects. The ranking is based on averaging coarse difference measures called elementary effects. Elementary effects are nothing else than crude finite difference approximations of the derivatives. Morris derived two sensitivity measures for each parameter from them. First, the mean of the absolute value of the elementary effects is a measure for overall influence: the larger the mean the higher the influence. Second, the standard deviation of the elementary effects is a measure for non-linearity or interaction effects: the higher the standard deviation is, the less likely the linearity hypothesis is true. The efficiency of the method results from the smart evaluation of the individual elementary effects. The global nature results from the random distribution of the evaluation points in the input space and the subsequent averaging.

The method of Morris for parameter screening is a popular method because it presents a computationally efficient way of globally ranking the importance of parameters for large, non-linear models. Generally, the method returns semi-quantitative sensitivity measures as their absolute values are hard to interpret. Therefore, the ranking of parameters can be difficult: the threshold that separates influential from uninfluential parameters remains problem dependent. Nevertheless, one can often find a clear line of demarcation in practice, especially for large models [64]. Naturally, the method also has some disadvantages. For very expensive models with solution times of multiple hours to days, it might be too expensive. More importantly, the method has difficulties in treating interactions and non-linearity in detail. While Morris screening is able to detect the presence of non-linearity and interactions, it is impossible to distinguish between the two. Consequently, if interactions are present, it is not possible to detect which parameters are involved in them [64].

Variance-based methods Assuming that the inputs are random variables with probability distributions, the model output is then also a random variable whose distribution results from propagating the input distributions through the model. Methods that analyse the properties of the output distribution to conduct sensitivity studies are called distribution-based methods in general. A special class are variance-based sensitivity analysis methods which are based on the analysis of the variance of the output distribution in particular. They quantify how the individual inputs and their interactions contribute to the resulting variance [26]. The most common method, Sobol's method, can be understood by the functional analysis of variance (ANOVA) decomposition [111–113] (see Section 3.3). This decomposition of the output variance ensues a sum where each summand can be directly linked to individual and combinations of inputs. The sensitivity measures, called Sobol indices, are then understood as the fractions of the total output variance invoked by the inputs or their interactions. Therefore, the indices are bound between zero and one which immediately gives rise to their notion of importance. Values close to one

indicate high influence whereas values close to zero characterize uninfluential – combinations of – parameters. In this way, Sobol indices allow for a rigorous, quantitative comparison of the global influence of specific parameters and all possible combinations.

Sobol indices have compelling properties. Perhaps the two biggest advantages are their truly global nature, and the easy and conclusive interpretability. It is the only method presented so far that is suitable for both parameter fixation and parameter prioritization for non-linear, non-monotonic models. A related advantage stems from the fact that the method naturally supplies an estimate for the output distribution. Therefore, if done properly, the method inherently includes an uncertainty quantification, provided variance is accepted as the proper measure for uncertainty. The basic version of the method relies on the assumption that the inputs are statistically independent. Clearly, this is a limitation since in reality many input parameters can be expected to be dependent. While the definition of the indices themselves stays valid, the interpretability is lost in case of dependent inputs reducing their information value significantly. Additionally, the amount of detailed information contained in Sobol indices does not come without a price. The computational burden of the method is extreme if brute-force realisation is attempted. In practice, more sensible approaches balancing computational cost and informational content have been developed (see Section 3.3.1 for details). Nevertheless, application to complex, expensive models remains a challenging task and requires sophisticated software implementations and efficient use of computing resources (see, Section 1.2), surrogate modelling approaches, or both. For a detailed discussion of challenges and potential remedies see Section 7.1.

Moment-independent methods Sometimes, the uncertainty in the output distribution is inadequately described by the variance [90]. This is for example the case in the factor mapping setting (see Section 3.2.1), where a specific region of the output space is of particular interest. For this purpose, there exist distribution-based methods that refrain from focusing on specific moments – like variance, skewness, or kurtosis – of the output distribution. These methods are called moment-independent. Generally, they measure the difference between variants of output distributions with reference to the unconditional output distribution. It is compared to the conditional output distributions that result from fixing one or more inputs [26]. The most common method is Regional Sensitivity Analysis or Monte Carlo filtering [114–118]. Other variants are based on the area enclosed between the two distributions [119], entropy or the principle of mutual information [120–122], statistical tests [123] or generic input-output samples [124].

Other methods The above presented methods represent but a small fraction of the overall available methods for sensitivity analysis. For an in-depth overview, the interested reader is referred to the literature presented in Section 3.1. Nevertheless, the list above is appended with some of the most prominent alternative global methods: regression-based methods, like the Pearson and Spearman correlation coefficients or Standard Regression Coefficients (see [90]) rely on fitting a linear model through the input-output sample. Derivative-based global sensitivity measures present an efficient method with a link to Morris screening and Sobol indices [125, 126]. Recently, a new class of methods called variogram-based methods have been proposed by Razavi and Gupta [127–129] to ‘bridge between derivative and distribution-based methods’ [26]. Lastly, Shapley effects are based on game theory and have been suggested as generalizations of Sobol indices to models with dependent inputs [94, 130–132].

3.3 Sobol indices: a variance-based approach to global sensitivity analysis

This section is based on an early, unabridged version of Section 2 of Paper C. It has been expanded further such that it contains a detailed, comprehensive presentation of the method that can be followed with minimal prior knowledge.

To date, many parameter sensitivity studies in computational mechanics still rely on local methods where the value of one parameter is changed after another and the resulting change in model output is analysed. As pointed out in Section 2.1, this approach is, however, inadequate for non-linear models investigated under uncertainty. Local methods grossly underestimate the parameter space due to the ‘curse of dimensionality’ [23, 133] and fail to detect potentially crucial interactions between the parameters. Variance-based global sensitivity analysis does not suffer from these limitations. It samples the complete input space and quantifies the global influence of parameters on the model output by attributing the amount of output uncertainty to individual parameters and their combinations.

This section presents the most popular variance-based sensitivity analysis framework referred to as the method of Sobol or simply Sobol indices. The method has originally been developed by Russian mathematician Ilya M. Sobol in 1990 [111, 112]. Since then it has received considerable attention which resulted in major methodological advancements [94, 113, 126, 134] as well as in the development of efficient computational evaluation schemes [27, 135, 136]. Sobol’s method is very general and potential fields of application are diverse but environmental science [62] and risk assessment [137] were among the early adopters.

3.3.1 Definition

In this section Sobol indices [61, 92, 112, 113, 133, 138] as variance-based, global sensitivity measures for generic, non-linear models are derived. It begins by laying out some essential notations and concepts. No distinction will be made between random variables and their realizations in the following so that the notation stays accessible. It is trusted that the difference becomes clear from the context.

Let $\mathbf{x} = \{x_1, x_2, \dots, x_n\} \in \Omega \subseteq \mathbb{R}^n$ denote a continuous random vector composed of n real-valued random variables x_i . Then, $\mathbf{x}_{\sim i}$ shall stand for the random vector derived from \mathbf{x} by removing component x_i . Thus,

$$\mathbf{x}_{\sim i} = \{x_1, x_2, \dots, x_{i-1}, x_{i+1}, \dots, x_n\}. \quad (3.1)$$

The value of a scalar-valued function f of \mathbf{x} is again a random variable. The expected value of this random variable is denoted by

$$\mathbb{E}_{\mathbf{x}} [f(\mathbf{x})] = \int_{\Omega} f(\mathbf{x}) p_{\mathbf{x}}(\mathbf{x}) d\mathbf{x}, \quad (3.2)$$

where $p_{\mathbf{x}}(\mathbf{x})$ is the probability density function of \mathbf{x} . The variance of $f(\mathbf{x})$ is defined as

$$\mathbb{V}_{\mathbf{x}} [f(\mathbf{x})] = \mathbb{E}_{\mathbf{x}} [(f(\mathbf{x}) - \mathbb{E}_{\mathbf{x}} [f(\mathbf{x})])^2] = \int_{\Omega} (f(\mathbf{x}) - \mathbb{E}_{\mathbf{x}} [f(\mathbf{x})])^2 p_{\mathbf{x}}(\mathbf{x}) d\mathbf{x}. \quad (3.3)$$

A square-integrable function f shall describe the generic, non-linear model of interest. f has n independent inputs $\mathbf{x} = \{x_1, x_2, \dots, x_n\}$ and a scalar output y such that

$$f : K^n = [0, 1]^n \rightarrow \mathbb{R}, \quad \mathbf{x} \mapsto y = f(\mathbf{x}). \quad (3.4)$$

The inputs \mathbf{x} are assumed to be distributed uniformly within the n -dimensional unit hypercube $K^n \subset \mathbb{R}^n$ without loss of generality (see [133] or Chapter 15 in [63]).

$$x_i \sim U(0, 1), \quad (3.5)$$

where $U(0, 1)$ denotes the continuous uniform probability distribution on the interval $[0, 1]$. The joint probability density function can be given to

$$p_{\mathbf{x}}(\mathbf{x}) = \prod_{i=1}^n p_{x_i}(x_i) = 1, \quad (3.6)$$

because of the independence of the inputs x_i . Based on these assumptions, the following global sensitivity measures is introduced as originally proposed by [112, 113, 133, 138].

Definition 3.1: First order Sobol sensitivity index

The first order Sobol sensitivity index (also called main effect) S_i of parameter x_i is defined as

$$S_i = \frac{\mathbb{V}_{x_i} [\mathbb{E}_{\mathbf{x}_{\sim i}} [y|x_i]]}{\mathbb{V}_{\mathbf{x}} [y]} \quad (3.7)$$

where $\mathbb{V}_{\mathbf{x}} [y] > 0$ is the total, unconditional variance of y over all input parameters and $\mathbb{E}_{\mathbf{x}_{\sim i}} [y|x_i]$ is the conditional expected value of y given the value of parameter x_i . The first order Sobol index is also called the main effect of x_i .

The first order index S_i describes the fraction of the variance of y due to the uncertainty in parameter x_i alone. In other words, it represents the amount by which the variance of y could be decreased if the precise value of x_i was known.

Definition 3.2: Total Sobol sensitivity index

The total Sobol sensitivity index S_i^T of parameter x_i is defined as

$$S_i^T = 1 - \frac{\mathbb{V}_{\mathbf{x}_{\sim i}} [\mathbb{E}_{x_i} [y|\mathbf{x}_{\sim i}]]}{\mathbb{V}_{\mathbf{x}} [y]} = \frac{\mathbb{E}_{\mathbf{x}_{\sim i}} [\mathbb{V}_{x_i} [y|\mathbf{x}_{\sim i}]]}{\mathbb{V}_{\mathbf{x}} [y]}. \quad (3.8)$$

where $\mathbb{V}_{\mathbf{x}} [y] > 0$ is the total, unconditional variance of y over all input parameters. $\mathbb{E}_{x_i} [y|\mathbf{x}_{\sim i}]$ is the conditional expected value and $\mathbb{V}_{x_i} [y|\mathbf{x}_{\sim i}]$ the conditional variance of y given the values of all parameters except for x_i . The total Sobol index is also referred to as the total effect.

The total Sobol index presents the mean amount of output variance remaining if the precise value of every parameters but x_i was known. In other words, it gives a measure for the overall

importance of parameter x_i for the variance of the output y , that is, the importance of x_i – its first order index – in addition to every higher order interaction of x_i .

In summary, the first order Sobol indices S_i quantify the sensitivity of the output to each parameter alone and the total Sobol indices S_i^T quantify additionally the sensitivity of the output to all the interactions that each parameter is involved in. There are also higher order indices that quantify the influence of specific interaction terms (see Definition 3.4) but these are rarely used in practice. Computing the above two types of indices presents a good balance between computational cost (see Section 3.3.3) and insights gained (see Section 3.3.4).

3.3.2 Interpretation

An instructive interpretation of Sobol indices can be achieved based on the additive decomposition of the model function f called ANOVA representation of f [112, 138].

In the following, arbitrary subsets of $\mathbf{x} = \{x_1, x_2, \dots, x_n\}$ for $n \in \mathbb{N}^+$ will be selected. The selected parameters are denoted by $\mathbf{x}_{i_1 i_2 \dots i_s} = \{x_{i_1}, x_{i_2}, \dots, x_{i_s}\}$, where an ordered index set $I = \{i_1, i_2, \dots, i_s\}$ of cardinality $s \leq n$ with $1 \leq i_1 < i_2 < \dots < i_s \leq n$ was introduced. The index set I is a subset of all n indices such that $I \subseteq \{1, 2, \dots, n\}$. Three special classes of I with cardinality 1, 2, and 3 are the index sets $I = \{i\}$, $I = \{i, j\}$, and $I = \{i, j, k\}$, respectively. An example for $n = 4$ and $s = 3$ is the set $\{1, 3, 4\}$ which results in $\mathbf{x}_{134} = \{x_1, x_3, x_4\}$. With this notation, the ANOVA representation of f can be defined.

Definition 3.3: Analysis of variance (ANOVA) representation of f

A representation of a function f as

$$f(x_1, x_2, \dots, x_n) = f_0 + \sum_{i=1}^n f_i(x_i) + \sum_{i=1}^{n-1} \sum_{j>i}^n f_{ij}(x_i, x_j) + \sum_{i=1}^{n-2} \sum_{j>i}^{n-1} \sum_{k>j}^n f_{ijk}(x_i, x_j, x_k) + \dots + f_{12\dots n} \quad (3.9)$$

is called analysis of variance (ANOVA) representation or high-dimensional model representation (HDMR), if

$$f_0 = \text{const.} \quad (3.10)$$

and

$$\int_0^1 f_{i_1 i_2 \dots i_s}(x_{i_1}, x_{i_2}, \dots, x_{i_s}) dx_{i_k} = 0, \quad \forall i_k \in \{i_1, i_2, \dots, i_s\}, \quad (3.11)$$

where $f_{i_1 i_2 \dots i_s}(x_{i_1}, x_{i_2}, \dots, x_{i_s})$ is an arbitrary summand of the right hand side of Eq. (3.9) other than f_0 .

Eq. (3.11) states that for each summand in Eq. (3.9) integrals with respect to any of its variables vanish. Recall that the model f was required to be square-integrable over the unit hypercube K^n . In that case one can prove that Eq. (3.9) exists and is unique [112]. In the following, both the independence assumption of the parameters and the assumption of uniformly distributed

parameters within the unit hypercube are exploited. These assumptions allow to avoid the explicit statement of the probability density functions $p_{x_i}(x_i) = 1$ in many of the integrals below. One may, for example, write $\int_0^1 f(x_i)p_{x_i}(x_i)dx_i = \int_0^1 f(x_i)dx_i$.

Two important properties follow from Definition 3.3. First, f_0 can be identified as the expected value of the model output $y = f(\mathbf{x})$

$$f_0 = \int_{K^n} f(\mathbf{x})d\mathbf{x} = \mathbb{E}_{\mathbf{x}}[y]. \quad (3.12)$$

Second, any two different summands of Eq. (3.9) are orthogonal, such that

$$\int_{K^n} f_{i_1 i_2 \dots i_s}(x_{i_1}, x_{i_2}, \dots, x_{i_s}) f_{j_1 j_2 \dots j_l}(x_{j_1}, x_{j_2}, \dots, x_{j_l}) d\mathbf{x} = 0 \quad (3.13)$$

with ordered index sets $I = \{i_1, i_2, \dots, i_s\}$, $J = \{j_1, j_2, \dots, j_l\}$, $s, l \leq n$ and $I \neq J$.

While the terms in Eq. (3.9) can in theory be derived, in practice one does not need to compute the summands to use indices Eq. (3.7) and Eq. (3.8). Indeed one does not even have to know the form of $f(\mathbf{x})$. It suffices to be able to evaluate it point wise [113]. Nevertheless, it is very instructive to look at the computation of the individual summands. For the sake of conciseness, a shortening in notation by making use of $f_{i_1 i_2 \dots i_s}(x_{i_1}, x_{i_2}, \dots, x_{i_s}) = f_{i_1 i_2 \dots i_s}$ and $dx_{j_1} dx_{j_2} \dots dx_{j_{n-s}} = d\mathbf{x}_{\sim i_1 i_2 \dots i_s}$ is introduced. Here, the ordered index sets $I = \{i_1, i_2, \dots, i_s\}$ with $1 \leq i_1 < i_2 < \dots < i_s \leq n$ and $J = \{j_1, j_2, \dots, j_{n-s}\}$ with $1 \leq j_1 < j_2 < \dots < j_{n-s} \leq n$ are disjunct such that $I \cap J = \emptyset$ and $I \cup J = \{1, 2, \dots, n\}$. Then one can compute the individual summands in Eq. (3.9) by the following recursive scheme:

$$\begin{aligned} \int_{K^n} f(\mathbf{x})d\mathbf{x} &= f_0 = \mathbb{E}_{\mathbf{x}}[y] \\ \int_{K^{n-1}} f(\mathbf{x})d\mathbf{x}_{\sim i_1} &= f_0 + f_{i_1} \\ \int_{K^{n-2}} f(\mathbf{x})d\mathbf{x}_{\sim i_1 i_2} &= f_0 + f_{i_1} + f_{i_2} + f_{i_1 i_2} \\ &\vdots \\ \int_{K^{n-s}} f(\mathbf{x})d\mathbf{x}_{\sim i_1 i_2 \dots i_s} &= f_0 + \sum_{i=i_1}^{i_s} f_i + \sum_{i=i_1}^{i_s-1} \sum_{j>i}^{i_s} f_{ij} + \sum_{i=i_1}^{i_s-2} \sum_{j>i}^{i_s-1} \sum_{k>j}^{i_s} f_{ijk} + \dots + f_{i_1 i_2 \dots i_s} \\ &\vdots \\ f(\mathbf{x}) &= f_0 + \sum_{i=1}^n f_i + \sum_{i=1}^{n-1} \sum_{j>i}^n f_{ij} + \sum_{i=1}^{n-2} \sum_{j>i}^{n-1} \sum_{k>j}^n f_{ijk} + \dots + f_{12 \dots n} \end{aligned} \quad (3.14)$$

Solving each line in Eq. (3.14) for the highest summand

$$f_{i_1 i_2 \dots i_s} = \int_{K^{n-s}} f(\mathbf{x})d\mathbf{x}_{\sim i_1 i_2 \dots i_s} - f_0 - \sum_{i=i_1}^{i_s} f_i - \sum_{i=i_1}^{i_s-1} \sum_{j>i}^{i_s} f_{ij} - \sum_{i=i_1}^{i_s-2} \sum_{j>i}^{i_s-1} \sum_{k>j}^{i_s} f_{ijk} - \dots \quad (3.15)$$

leads to the desired instructive interpretation. $f_{i_1 i_2 \dots i_s}$ is the part of $f(\mathbf{x})$ that depends solely on interaction terms between the $\{x_{i_1}, x_{i_2}, \dots, x_{i_s}\}$. All remaining variables are integrated out and lower order terms are subtracted.

The ANOVA representation Eq. (3.9) can be used to decompose the variance of $f(\mathbf{x})$

$$\mathbb{V}_{\mathbf{x}}[f(\mathbf{x})] = \int_{K^n} f^2(\mathbf{x}) d\mathbf{x} - (\mathbb{E}_{\mathbf{x}}[f(\mathbf{x})])^2 = \int_{K^n} f^2(\mathbf{x}) d\mathbf{x} - f_0^2. \quad (3.16)$$

Plugging Eq. (3.9) together with the orthogonality property Eq. (3.13) into Eq. (3.16) results in the core variance decomposition formulation

$$\mathbb{V}_{\mathbf{x}}[f(\mathbf{x})] = \sum_{i=1}^n \mathbb{V}_{x_i}[f_i] + \sum_{i=1}^{n-1} \sum_{j>i}^n \mathbb{V}_{x_i x_j}[f_{ij}] + \sum_{i=1}^{n-2} \sum_{j>i}^{n-1} \sum_{k>j}^n \mathbb{V}_{x_i x_j x_k}[f_{ijk}] + \dots + \mathbb{V}_{\mathbf{x}}[f_{12\dots n}] \quad (3.17)$$

where the individual summands in Eq. (3.17)

$$\mathbb{V}_{x_{i_1} x_{i_2} \dots x_{i_s}}[f_{i_1 i_2 \dots i_s}] = \int_{K^{n-s}} f_{i_1 i_2 \dots i_s}^2 dx_{i_1} dx_{i_2} \dots dx_{i_s} \quad (3.18)$$

can be identified as the variances of the summands in Eq. (3.9). Recalling the interpretation of $f_{i_1 i_2 \dots i_s}$ above, this means that $\mathbb{V}_{x_{i_1} x_{i_2} \dots x_{i_s}}[f_{i_1 i_2 \dots i_s}]$ describes the variance contribution attributed solely to the interaction between $\{x_{i_1}, x_{i_2}, \dots, x_{i_s}\}$. Due to Eq. (3.11), the expected value of $f_{i_1 i_2 \dots i_s}$ is 0. Finally, Eq. (3.17) suggests the definition of the following general sensitivity indices:

Definition 3.4: Sobol sensitivity index of order s

The s -th order Sobol sensitivity index of the function f , given by Eq. (3.4), is defined as

$$S_{i_1 i_2 \dots i_s} = \frac{\mathbb{V}_{x_{i_1} x_{i_2} \dots x_{i_s}}[f_{i_1 i_2 \dots i_s}]}{\mathbb{V}_{\mathbf{x}}[f(\mathbf{x})]}, \quad (3.19)$$

where the $\mathbb{V}_{\mathbf{x}}[f(\mathbf{x})] > 0$ is the total, unconditional variance of $y = f(\mathbf{x})$ over all input parameters and $\mathbb{V}_{x_{i_1} x_{i_2} \dots x_{i_s}}[f_{i_1 i_2 \dots i_s}]$ is the variance contribution attributed solely to the interaction between $\{x_{i_1}, x_{i_2}, \dots, x_{i_s}\}$.

The s -th order Sobol sensitivity index $S_{i_1 i_2 \dots i_s}$ quantifies the amount of output variance caused by the interactions between the s parameters $\{x_{i_1}, x_{i_2}, \dots, x_{i_s}\}$ excluding any potential lower order interactions between these parameters.

Due to Eq. (3.17) the following essential property holds

$$\sum_{i=1}^n S_i + \sum_{i=1}^{n-1} \sum_{j>i}^n S_{ij} + \sum_{i=1}^{n-2} \sum_{j>i}^{n-1} \sum_{k>j}^n S_{ijk} + \dots + S_{12\dots n} = 1 \quad (3.20)$$

The total sensitivity index S_i^T as defined in Definition 3.2 follows from Eq. (3.19) to

$$S_i^T = S_i + \sum_{\substack{j=1 \\ j \neq i}}^n S_{ij} + \sum_{\substack{j=1 \\ j \neq i}}^n \sum_{\substack{k>j \\ k \neq i}}^n S_{ijk} + \dots + S_{12\dots n}, \quad (3.21)$$

that is, S_i^T is the sum of all sensitivity indices associated with x_i . Also, first order Sobol indices defined by Definition 3.1 and Definition 3.4 are equal: in general, $\mathbb{V}_x[x + a] = \mathbb{V}_x[x]$. It follows that $\mathbb{V}_{x_i}[f_i] = \mathbb{V}_{x_i}[\mathbb{E}_{\mathbf{x}_{\sim i}}[y|x_i]]$, where $f_i = \mathbb{E}_{\mathbf{x}_{\sim i}}[y|x_i] - f_0$ (see Eq. (3.14)).

3.3.3 Computation

In a brute-force attempt one could calculate the sensitivity indices with Monte Carlo integration. However, this would invoke double loops to resolve the multidimensional integrals, for example, for the first order indices: an inner loop for the expectation and an outer loop for the variance in Eq. (3.7). Therefore this approach becomes prohibitively expensive very quickly.

In practice, better strategies are needed to reduce the overall computational cost. There are computational schemes that exploit the special structure of the integrals and allow to compute a full set of first order and total indices – for each parameter – at the cost of

$$N_{\text{tot}} = N(n + 2) \quad (3.22)$$

model evaluations, where N is the number of Monte Carlo sample points and n the number of model input parameters [133, 135].

For a detailed presentation of the computational scheme used in this thesis see the Appendix of Paper C.

Research to improve the available computational schemes is very active [106, 107, 136] and many alternative formulations have already been introduced [25]. There are specialized formulations that greatly enhance the precision in certain scenarios [90]: for example, the Mauntz formula [139, 140] can be used for the computation of small indices while the Janon-Monod formula [141] can be employed in case of large first order indices. Martinez formula does not rely on precomputed samples but instead sequentially updates the approximation of the indices as soon as new sample points become available [142–144]. Of great importance are also methods for approximating the estimation error of the formulas. This can be done by random repetitions [145], based on asymptotic normality [141] or – the method used herein – by bootstrap methods [146].

3.3.4 Use cases

Sobol indices can be useful in a variety of different analysis contexts (see Section 3.2.1). Here, the most common ones are very briefly revisited and it is shown why a set of first order and total indices suffices to answer these key questions

Linearity of the model The additivity $A = \sum_{i=1}^n S_i$ is a measure of linearity of the model, where $0 \leq A \leq 1$. On the one hand, if A is close to 1 the model output can largely be described by the sum of individual, isolated influence of the input parameters. On the other hand, if A is close to 0 then the model is dominated by non-linear interaction terms. Likewise, $S_i^T - S_i$ gives, for a specific parameter x_i , the amount of output variance due to all the interactions associated with x_i (cf., Eq. (3.21)).

Parameter prioritization setting Assume, one attempts to reduce output uncertainty as much as possible by measuring one parameter exactly, that is, it is assumed all model parameters have a true but unknown value such that in theory they could get identified by experiments. In this case, Sobol's method tells us to choose the parameter with the highest first order index S_i .

Parameter fixing setting Often it is desirable to reduce the number of parameters to simplify model execution. This can, for example, be achieved by choosing reasonable values for un-influential parameters. Sobol indices allow to identify uninfluential parameters based on the total sensitivity index. Parameters with $S_i^T \approx 0$ are viable candidates for parameter fixing without having to worry too much about the precise value. The rational behind is that these parameters have, per definition of the total index, negligible overall influence on the model output over their complete range of variability.

4 Results I: gastric electromechanics

This chapter presents the results for the first active biomechanical system studied in this thesis: gastric electromechanics. The results are split into two sections. In the first section, the summary of Paper B presents a newly developed computational framework for gastric electromechanics. Details of the framework can be found in the reprint of the paper in the Appendix. Thereafter, an original global sensitivity analysis of this model is presented.

4.1 Paper B: Computational model of gastric motility with active-strain electromechanics

Sebastian Brandstaeter, Alessio Gizzi, Sebastian L. Fuchs, Amadeus M. Gebauer, Roland C. Aydin, Christian J. Cyron

published in

ZAMM - Journal of Applied Mathematics and Mechanics / Zeitschrift Für Angewandte Mathematik Und Mechanik, vol. 98, no. 12, pp. 2177–2197, 2018.

DOI: [10.1002/zamm.201800166](https://doi.org/10.1002/zamm.201800166).

Summary

Gastric motility is the coordinated contraction and relaxation of smooth muscle tissue in the stomach wall. There are several different motility patterns that each perform specific physiological tasks. For example, the ring-shaped, rhythmic contraction waves that travel along the stomach wall during gastric peristalsis ensure the mixing, grinding and propulsion of digesta. Gastric motility is realized by a close interaction between the gastric electrophysiological system, the muscular tissue, and hormonal and neural signalling. As a result of the intricate interaction between at least two cell types, interstitial cells of Cajal (ICCs) and smooth muscle cells (SMCs), the gastric electrophysiological system is very involved. ICCs are arranged in a continuous network spread across – most of – the stomach. They create and actively propagate synchronized, periodic bioelectrical signals called *slow waves*. Slow waves coordinate smooth muscle contractions of the stomach wall. They spread passively to the surrounding SMCs where the increased excitation then potentially triggers excitation-contraction coupling. Although, slow waves are permanently present in the stomach tissue, contractions only occur if suitable neural and hormonal signals coincide with the electrical stimulus.

In health, the propagation pattern of slow waves is very distinct. From a pacemaker region located on the greater curvature of the proximal stomach the waves spread in both circumferential and longitudinal, distal directions. Quickly, the activation pattern forms a ring spanning the

complete circumference. Three to four slow waves travel simultaneously towards the pylorus at a distance of approximately 60 mm. Slow waves do not spread proximally from the pacemaker region such that the fundus is electrically quiescent. This characteristic propagation pattern of the slow waves emerges from two essential phenomena. First, isolated ICCs generate slow waves at distinct intrinsic frequencies. The intrinsic frequencies of the cells decrease from the pacemaker region to the pylorus, which is known as the *intrinsic frequency gradient*. Second, in an intact network, the ICCs work at a single, synchronized frequency, which is equal to the highest frequency. This synchronization process is called *entrainment*.

In disease, the synchronized patterns can be disturbed. For example, some gastric motility disorders, like gastroparesis, have been associated with abnormal slow wave spreading: ectopic initiations or conduction blocks result in what is collectively referred to as *gastric dysrhythmia*.

In the past, experimental and computational studies of the individual subsystems have helped unravel their distinct features and key phenomena. Computational modelling of the multiphysics of gastric motility has received, however, much less attention and there remain many open questions with regard to the integrated system. To this end, the paper presents a phenomenological multiphysics framework. It combines a computationally robust model of gastric electrophysiology with an electromechanical finite elasticity model. Tissue electrophysiology is described by two, coupled monodomain formulations, one for each of the two cell types. Both cellular electrophysiology models are based on the same modified version of the two-variable Mitchell-Schaeffer model. The different properties of the cells – like the self-excitatory state of ICCs versus the excitatory one of SMCs – are reflected by choosing the model parameters accordingly. Tissue electromechanics is described by an active-strain finite elasticity approach.

The main findings of the article can be summarized as follows. First, the novel electrophysiological model is shown to remain stable also during long-term analyses in contrast to previous approaches. Second, in a series of numerical experiments, the paper shows that key phenomena, like entrainment across the organ and ring-shaped peristaltic contraction waves, can be reproduced successfully. Third, by varying the spatial distribution of the intrinsic ICC frequencies, the paper revealed that strong non-linearities govern the propagation pattern of slow waves and the mechanic activity in the stomach. Finally, the generality of the model is also displayed by replicating gastric dysrhythmias and demonstrating their impact on mechanical peristaltic contraction waves.

Nevertheless, several limitations of the model remain. In the proposed model, slow wave generation and propagation is solved in the reference configuration under incompressibility constraints thereby ignoring any potential mechano electric feedback (MEF). MEF can, however, be expected to be of great importance due to the known presence of stretch-activated currents or due to non-linear and stress-assisted diffusion. A homogeneous, isotropic neo-Hookean material model to describe the passive mechanical tissue behaviour was used. For this purpose, a more realistic constitutive model should be employed since the tissue properties are most likely anisotropic, viscoelastic and spatially heterogeneous. Another limitation is that the numerical examples were performed on simple schematic geometries such as, for example, rectangular tissue patches or cylinders. Thereby, the anatomical complexity of patient-specific stomach geometries has been neglected.

In summary, the article demonstrated that detailed insights to the coupled multiphysics underlying gastric motility on the organ level are possible with a computationally efficient, phe-

nomenological model framework. In the future, this framework could serve as a robust work-horse to further elucidate the fundamentals of gastric electromechanics in health and disease.

Author Contributions

S.B. and A.G. designed the mathematical model. **S.B.** and S.L.F. designed the computational framework. **S.B.**, S.L.F. and A.M.G. carried out the implementation. **S.B.**, A.G., and S.L.F. conceived and planned the numerical experiments. **S.B.** carried out all simulations. **S.B.**, A.G., S.L.F., A.M.G. and C.J.C. wrote the manuscript. **S.B.** prepared Figures 1-8. **S.B.** and S.L.F. prepared Figure 9. **All authors** discussed the content and commented on the manuscript. A.G. and C.J.C. conceived the original idea and were in charge of overall direction and planning.

4.2 Global sensitivity analysis of an active-strain electromechanics model for gastric peristalsis

This section presents a global sensitivity analysis as derived in Section 3.3 for the novel computational model of gastric electromechanics presented in Section 4.1 (see also Paper B). It focuses on an idealized, cylindrical model of a stomach during normal peristalsis similar to the one described in Section B.3.4. The main goal of this study is to investigate the influence of both electrophysiological and mechanical model parameters on the peristaltic contraction waves. In the following, the details of the setup of the analysis are described first. Next, the results of the analysis are presented.

4.2.1 Idealized model of gastric peristalsis

In the following, an idealized, three-dimensional model of a stomach showing normal gastric peristalsis is described in detail. The superscript $\phi \in \{i, m\}$ is used to distinguish between the two cells types: ICCs ($\phi = i$) and SMCs ($\phi = m$).

Geometry: The geometry of the stomach is approximated by a straight, circular, hollow, and open cylinder. The fundus does not experience the peristaltic contraction waves and is therefore neglected. The cylinder axis is aligned with the x -axis of the reference coordinate system. The length of the cylinder is $L_x = 250$ mm, its radius is $r = 50.930$ mm, and its thickness is $t = 3.5$ mm.

Boundary conditions: No-flux boundary conditions are applied at both ends of the cylinder for the electrophysiological part of the model. For the structural mechanical part, zero Dirichlet boundary conditions are prescribed in axial direction at both ends of the cylinder. Additionally, the displacements at both ends of the cylinder are restricted to the radial direction such that rigid body motions are prevented. A pressure load of $p = 3 \text{ N mm}^{-2}$ is applied to the inner surface of the stomach.

Spatial distribution of excitability: A unidirectional spatial distribution of the excitability parameter $a^i(x)$ is assumed according to Eq. (B.20) and Eq. (B.21) (see also Table B.2). Therefore, a^i only depends on the axial position x and contains four parameters: a_{\min}^i , a_{\max}^i , b_x and c_x . To ensure that $a^i(0) = a_{\max}^i$ and $a^i(L_x) = a_{\min}^i$ holds, $c_x = 1$ is set which reduces the number of free parameters to three. This choice of the spatial distribution of the excitability parameter

explicitly neglects the circumferential propagation of slow waves from the pacemaker region located at the greater curvature to the lesser curvature. This circumferential propagation is required to quickly form ring-shaped slow waves which result in equally ring-shaped contraction waves (see Section B.3.4). Here, the fully developed state of the contraction waves is of interest which motivates the neglect of the initial circumferential propagation.

Initial conditions: The initial conditions of the electrophysiology model are defined by the constant parameter values given in Table B.1. The reference configuration at zero pressure is defined by the geometry above. During the first ten time steps, the pressure is ramped up to the final value p which prestresses the stomach.

Computational setup: In contrast to the setup described in Section B.3.4, the above boundary conditions and the spatial distribution of the excitability parameter result in a rotational symmetry of the model around the cylinder axis. Therefore, the application of suitable symmetry Dirichlet boundary conditions allows to reduce the computational domain and to simulate only a wedge of the cylinder with an opening angle α_w in circumferential direction. This exploitation of the rotational symmetry significantly reduces the computational cost of the model. The model is numerically solved as described in Section B.3.1 (see also Section 1.2). In reference to the convergence analysis of Section B.3.2, a time step size of $dt = 0.1$ s is chosen and the mesh sizes of both electrophysiology and structural mechanics are $h = H = 0.5$ mm. The opening angle of the wedge α_w is chosen such that the elements have perfect quadratic shape: $\alpha_w \approx 0.563^\circ$. The model is solved for a total simulation time of $T = 500$ s. In Paper B, it was determined that the entrainment process takes 350 s. Only after this time interval, all ICCs can be assumed to be entrained and generate slow waves at a single, synchronized frequency. For this reason, the first 380 s of simulation time are discarded to ensure that the system has reached the entrained state. The remaining 120 s of simulation time constitute then the solution of the system.

4.2.2 Probability distributions of parameters

A priori assumptions on parameters

Overall, the model contains more than 25 parameters, but not all of them have to be included in the analysis. Some can be assumed to be known from measurements. Others are, a priori, assumed to play a minor role and are, therefore, not included in the study.

The geometry of the stomach can be obtained, for example, from medical imaging. Therefore, the values of L_x , r , and t are assumed to be known. They are chosen to represent a normal sized human stomach in the fed state. The pressure p inside the stomach can be measured by gastric manometry (see Paper A) and is, thus, assumed to be known.

Slow waves are actively propagated via the ICCs and passively spread to the SMCs [147, 148]. The electrical coupling between SMCs is assumed to be less tight compared to ICCs. In Paper B, this is reflected by setting the isotropic diffusion coefficient of SMCs to $\sigma^m = 0.1\sigma^i$, where σ^i is the isotropic diffusion coefficient of ICCs. This relation is kept here so that only σ^i remains a free parameter. In accordance with the passive, excitatory nature of SMCs, their excitability parameter is fixed to $a^m = 0$ (see Table B.1). The absolute value of the excitability parameter of the ICCs, a^i , ranges from a_{\min}^i to a_{\max}^i based on the spatial distribution of the excitability parameter (see previous subsection). The range defined by the values of a_{\min}^i and a_{\max}^i of Table B.1 is shown to cover the physiological range of frequencies between approximately 1–3 cpm (see

Table 4.1: Values of parameters that are fixed according to the a priori assumption described in Section 4.2.2.

Parameter		Value	Unit
<i>Geometry:</i>			
axial length of cylinder	L_x	250.0	mm
radius of cylinder	r	50.930	mm
thickness of wall	t	3.5	mm
<i>Boundary condition:</i>			
intraluminal pressure	p	3	N mm ⁻²
<i>ICC:</i>			
minimum excitability parameter	a_{\min}^i	$2.230\,75 \cdot 10^{-2}$	-
maximum excitability parameter	a_{\max}^i	$3.316\,00 \cdot 10^{-2}$	-
<i>SMC:</i>			
diffusion coefficient	σ^m	$0.1\sigma^i$	mm ² s ⁻¹
<i>Electromechanics:</i>			
opening voltage of VDCC	v_t	0.1	-
longitudinal intensity of active contraction	α_l	α	-
circumferential intensity of active contraction	α_c	α	-

Figure B.1 and [149]). For this reason, a_{\min}^i and a_{\max}^i themselves are considered fixed at the values given in Table B.1.

The voltage-dependent steady-states of the recovery variables h_{∞}^{ϕ} (see Eq. (B.3b)) contains a numerical smoothing parameter $\eta_{\text{gate}}^{\phi}$, where $\phi \in \{i, m\}$.

As described in [150], Eq. (B.3b) is equal to

$$h_{\infty}^{\phi}(v^{\phi}) = 1 - H(v^{\phi} - v_{\text{gate}}^{\phi}) \quad (4.1)$$

for the limit value $\eta_{\text{gate}}^{\phi} \rightarrow 0$. $H(\cdot)$ denotes the Heaviside step function.

Preliminary studies revealed that using Equation (4.1) in favour of Eq. (B.3b) does lead to almost identical result without introducing numerical instabilities. Therefore, Equation (4.1) is used for the present study which allows to omit $\eta_{\text{gate}}^{\phi}$.

In theory, the model allows to choose different material parameters α_l and α_c to control the intensities of the active muscle contractions of the longitudinal and the circumferential smooth muscle fibres, respectively. In Paper B, they are chosen to be equal which resulted in convincing contraction patterns. For this reason, the same assumption is applied here and a single parameter α is introduced which controls the intensity of both muscle fibres: $\alpha = \alpha_l = \alpha_c$.

Finally, a short outlook is required to complete the record of all a priori fixed parameters. As explained in necessary condition (NC2), v_t needs to be fixed at a suitable value to ensure physiologically meaningful solutions.

The values of the a priori fixed parameters are shown in Table 4.1. In the following subsections, probability distributions for the remaining parameters will be derived, as well as a suitable value for v_t .

Baseline probability distributions

After reducing the overall number of free parameters a total of 19 free parameters remain. A large influence of these parameters on the model outputs cannot be ruled out a priori. At the same time, data on these parameters is scarce, even for the few for which experimental studies exist. For example, the elastic properties of the stomach wall have been investigated experimentally in the past [151, 152]. However, these studies used different constitutive laws which impedes their use here. Thus, precise values of many parameters are unknown and these parameters are assumed to be distributed according to some probability distribution.

The limited availability of data implies that specific information on the probability distributions of these parameters is lacking. Therefore, uniform probability distributions are assumed for the parameters as described in the following. Paper B proposed point estimates for the parameters (see Tables B.1, B.2, and B.3). A detailed analysis of the model with these parameter values revealed that many important macroscopic quantities were within the respective experimentally observed ranges (see Section B.3.4). This included an entrained frequency of ICCs of approximately 3 cpm and 3–4 concurrent peristaltic contraction waves propagating distally at a velocity of approximately 3 mm s^{-1} [149]. For this reason, these parameter values are chosen as the mean values ξ_j of the individual uniform distributions $U_j(\theta_j, \chi_j)$, where the index j indicates one of the 19 free parameters. Large intervals are chosen to reflect the limited data: the bounds θ_j, χ_j are set to $\pm 50\%$ of the mean such that the lower bound is $\theta_j = 0.5\xi_j$ and the upper bound is $\chi_j = 1.5\xi_j$. In the literature, global sensitivity analyses of models of cardiac electrophysiology [153, 154] and electromechanics [155] have followed similar approaches to derive uniform probability distributions of model parameters. However, these studies used much smaller intervals of support by varying only up to $\pm 30\%$ around the mean.

Note that the above choice of distributions for $\tau_{\text{in}}^\phi, \tau_{\text{out}}^\phi, \tau_{\text{open}}^\phi$, and τ_{close}^ϕ respects the necessary conditions that these parameters have to fulfil: for all realisations, $\tau_{\text{in}}^\phi \ll \tau_{\text{out}}^\phi \ll \tau_{\text{open}}^\phi, \tau_{\text{close}}^\phi$ holds (see Section B.2.1.1 or [156]).

Finally, the baseline probability distributions of all parameters are summarized in Table 4.2.

Identification of admissible parameter bounds

This study is interested in physiological peristaltic contraction waves as experienced in healthy individuals. Therefore, all realisations from the distributions of parameters should result in physiologically meaningful solutions. To this end, the following two necessary conditions for rhythmic, peristaltic contraction waves can be stated:

(NC1) Non-zero intrinsic frequency of ICCs:

ICCs are active, self-excitatory pacemaker cells of the gastric electrophysiological system which continuously generate slow waves at a given intrinsic frequency [147, 148, 157]. If the intrinsic frequency was equal to zero, the cells would be in a passive, excitatory state. Clearly, this state would violate their primary physiological function as pacemaker cell. Therefore, parameter combinations that lead to ICCs with an intrinsic frequency equal to zero can be discarded as unphysiological.

(NC2) Maximum transmembrane potential of SMCs above activation threshold:

Excitation-contraction coupling is realised by Eq. (B.19), which describes the non-linear

Table 4.2: Baseline probability distributions of uncertain parameters. The parameters are distributed uniformly within the interval defined by $\pm 50\%$ of the given base value, except for the primary excitability parameter a^i . For values of a^i see Table 4.1.

Parameter		Base Value ξ_j	Base Distribution	Unit
<u>ICC:</u>				
primary excitability parameter	a^i	a_{\max}^i	$U_{a^i}(a_{\min}^i, a_{\max}^i)$	-
secondary excitability parameter	λ^i	$1.250\,00 \cdot 10^{-2}$		-
time constant of inward current	τ_{in}^i	$2.292\,74 \cdot 10^{-2}$		s
time constant of outward current	τ_{out}^i	$4.707\,19 \cdot 10^{-1}$		s
time constant of gate opening	τ_{open}^i	9.232 00		s
time constant of gate closing	τ_{close}^i	4.770 82		s
gating voltage	v_{gate}^i	$1.038\,25 \cdot 10^{-1}$		-
diffusion coefficient	σ^i	1.200 00		$\text{mm}^2 \text{s}^{-1}$
<u>SMC:</u>				
secondary excitability parameter	λ^m	$1.250\,00 \cdot 10^{-2}$		-
time constant of inward current	τ_{in}^m	$1.146\,37 \cdot 10^{-1}$		s
time constant of outward current	τ_{out}^m	$4.707\,19 \cdot 10^{-1}$		s
time constant of gate opening	τ_{open}^m	9.232 00	$U_j(0.5\xi_j, 1.5\xi_j)$	s
time constant of gate closing	τ_{close}^m	4.770 82		s
gating voltage	v_{gate}^m	$1.038\,25 \cdot 10^{-1}$		-
<u>Tissue electrophysiology:</u>				
resistance of gap junctions	D_{gap}	$5.000\,00 \cdot 10^{-1}$		s^{-1}
spread of excitability parameter a^i	b_x	3.162 20		-
<u>Electromechanics:</u>				
calcium dynamics	β_1	$1.000\,00 \cdot 10^1$		-
opening dynamics of VDCC	β_2	$1.000\,00 \cdot 10^1$		-
neo-Hooke material parameter	μ	$6.000\,00 \cdot 10^1$		N mm^{-2}
intensity of active contraction	α	$2.000\,00 \cdot 10^{-1}$		-

dependence of the active-strain activation γ on the transmembrane potential of the SMCs v^m : $\gamma(v^m)$. The function depends only on v^m but contains a threshold parameter v_t representing the opening voltage of voltage-dependent calcium channels (VDCCs). Contractions are possible only if $v^m > v_t$. Parameter combinations for which $v^m < v_t$ holds for all times, lead to the trivial, unphysiological solution of no contraction. Hence, for all parameter combinations $v_{\text{peak}}^m > v_t$ has to hold, where v_{peak}^m is the peak transmembrane potential of the SMC during a slow wave. Since v_{peak}^m depends on many parameters, also a v_t that always satisfies the above condition depends on other parameters. This violates, however, the assumption of independence (see Section 3.3.1). Therefore, v_t may not remain a free parameter and needs to be fixed to a suitable value. Then combinations of parameters that violate the above condition for v_{peak}^m can be discarded as unphysiological.

Conditions (NC1) and (NC2) depend only on parameters of the model of cellular electrophysiology because MEF is neglected (see Section 6.1.1). To verify whether the distributions defined

in the previous subsection result in physiologically feasible solutions, it suffices, therefore, to investigate a submodel for cellular electrophysiology. For this purpose, the following system of ordinary differential equations (ODEs) describing a single ICC coupled to a single SMC is introduced:

$$\begin{aligned}
\frac{\partial v^i}{\partial t} &= \frac{h^i}{\tau_{in}^i} (v^i + a^i) (v^i + a^i - \lambda^i) (1 - v^i) - \frac{v^i}{\tau_{out}^i} - D_{gap} (v^i - v^m) , \\
\frac{\partial h^i}{\partial t} &= \frac{h_{\infty}^i(v^i) - h^i}{\tau^i(v^i)} , \\
\frac{\partial v^m}{\partial t} &= \frac{h^m}{\tau_{in}^m} (v^m) (v^m - \lambda^m) (1 - v^m) - \frac{v^m}{\tau_{out}^m} + D_{gap} (v^i - v^m) , \\
\frac{\partial h^m}{\partial t} &= \frac{h_{\infty}^m(v^m) - h^m}{\tau^m(v^m)} ,
\end{aligned} \tag{4.2}$$

where the steady-states h_{∞}^{ϕ} are defined by Eq. (4.1) and voltage-dependent time constants $\tau^{\phi}(v^{\phi})$ are given by Eq. (B.3a) with $\phi \in \{i, m\}$. For a detailed description of the equations see Section B.2.1.

The model defined by Eq. (4.2) contains 14 uncertain parameters which are assumed to be independent. It is probed with a large, global, space-filling sample from the joint distribution of the parameters defined in Table 4.2. The sample of size $N = 8192$ is generated with Sobol sequences (see Section 3.3.3). For each sample point, Eq. (4.2) is solved and the mean frequency of the ICC f^i and the mean peak transmembrane potential of the SMC v_{peak}^m are computed. For this purpose, the model was implemented using the programming language *Python* and solved with a standard ODE solver of the *SciPy* library [158]. All variables are set to zero as initial conditions. The simulation time is at least 180 s of which 60 s are discarded to allow the system to reach its limit cycle. To properly resolve low frequency systems, the simulation time is dynamically increased up to a maximum of 7740 s if no slow waves are detected.

Verification of (NC1): A total of 1893 sample points show $f^i = 0$ and, therefore, violate (NC1). First, a detailed analysis revealed that unphysiological results are primarily evoked by an interaction between the parameters τ_{in}^i and τ_{out}^i . Namely, large values of τ_{in}^i in combination with small values of τ_{out}^i lead to $f^i = 0$. Consequentially, the bounds of these parameters have to be adapted to ensure physiologically feasible system behaviour. This can be achieved by choosing $\tau_{in}^i \in [0.0115, 0.022]$, $\tau_{out}^i \in [0.5, 0.706]$. Figure 4.1a illustrates the new bounds of the parameters by classifying the samples into ‘physiological’ ($f^i \neq 0$) and ‘unphysiological’ ($f^i = 0$). Only physiological sample points lie within the area enclosed by the newly identified physiological bounds of τ_{in}^i and τ_{out}^i . A second test of the model to verify the new bounds of τ_{in}^i and τ_{out}^i revealed that λ^i has to be restricted additionally. It showed that limiting $\lambda^i \in [0.0063, 0.016]$ successfully restricts the sample points to the ones in agreement with (NC1).

Verification of (NC2): Only those sample points of the second probing within the reduced intervals of τ_{in}^i , τ_{out}^i , and λ^i are considered for the verification of (NC2). The evaluation of the cumulative distribution function of v_{peak}^m reveals that 97 % of sample points are above 0.1. This finding justifies to choose the threshold parameter to $v_t = 0.1$. To ensure proper contractions, a safety factor of 1.5 is used for verification of (NC2). Therefore, the sample points can be identified as ‘physiological’ if $v_{peak}^m \geq 1.5v_t$ and as ‘unphysiological’ if $v_{peak}^m < 1.5v_t$. Again it is found that the interaction between two parameters results in the unphysiological model

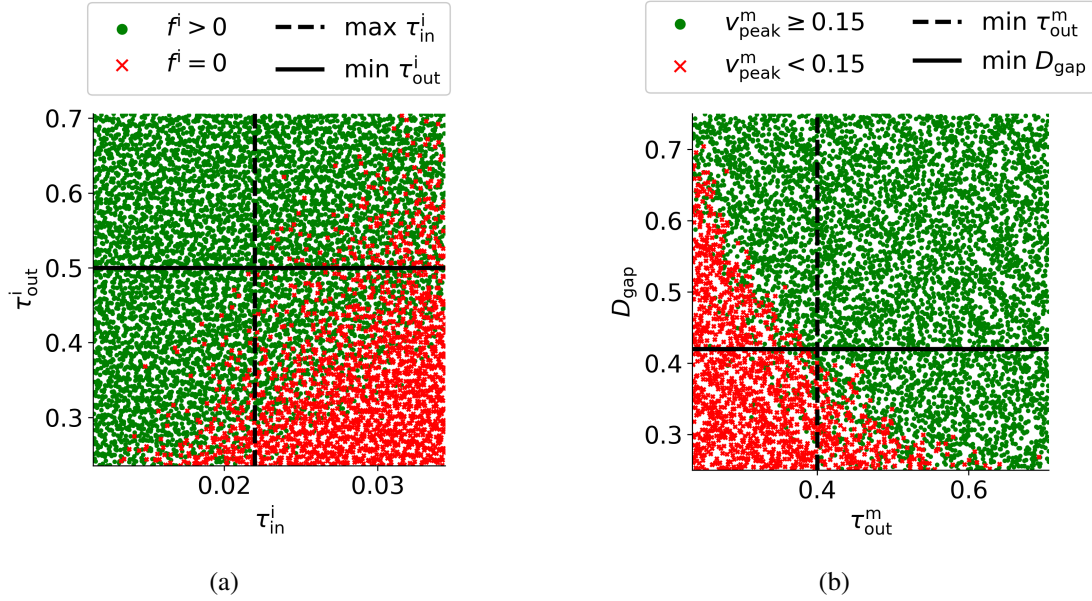


Figure 4.1: Scatterplots of space-filling samples from the 14 dimensional parameter space of model Eq. (4.2) showing the interaction between two selected parameters in relation to conditions (NC1) and (NC2) in (a) and (b), respectively. Sample points are classified into physiological (green) and unphysiological (red) points according to the respective condition. The black lines highlight the chosen rectangular subdomain that contain only sample points with physiological solutions.

behaviour: small values of τ_{out}^m combined with small values of D_{gap} result in $v_{peak}^m < 1.5v_t$. Hence, the bounds of these parameters have to be adjusted. The following physiological bounds can be identified: $\tau_{out}^m \in [0.4, 0.701]$ and $D_{gap} \in [0.42, 0.75]\text{s}^{-1}$. As illustrated in Figure 4.1b only physiological sample points lie within the area enclosed by these new, physiological bounds. In a third and final test of the model, the new parameter bounds were confirmed to only result in physiologically feasible solutions.

In addition to the study of physiologically admissible parameter bounds, a preliminary analysis of the full model of gastric electromechanics (see Section 4.2.1) revealed that the numerical stability of the model is critically determined by small values of the neo-Hooke parameter μ . Simulations with values of $\mu < 60 \text{ N mm}^{-2}$ failed. This can be explained by the applied membrane formulation of the structural discretization which neglects the bending stiffness in the surface tangent plane. Consequentially, values of μ that are too small lead to configurations that cannot be captured by the chosen formulation and potentially lead to buckling. For this reason, the lower bound of μ is increased such that $\mu \in [60, 90]\text{N mm}^{-2}$.

Finally, numerically and physiologically admissible probability distributions for all parameters can be given. They are summarized in Table 4.3.

Table 4.3: Probability distributions of uncertain parameters with numerically and physiologically admissible bounds as derived in Section 4.2.2. The parameters are distributed uniformly within the given bounds.

Parameter		Admissible Distribution		Unit
		$U_j(\theta_j, \chi_j)$		
		θ_j	χ_j	
<u>ICC:</u>				
primary excitability parameter	a^i	$2.230\,75 \cdot 10^{-2}$	$3.316\,00 \cdot 10^{-2}$	-
secondary excitability parameter	λ^i	$6.250\,00 \cdot 10^{-3}$	$1.600\,00 \cdot 10^{-2}$	-
time constant of inward current	τ_{in}^i	$1.146\,37 \cdot 10^{-2}$	$2.200\,00 \cdot 10^{-2}$	s
time constant of outward current	τ_{out}^i	$5.000\,00 \cdot 10^{-1}$	$7.060\,79 \cdot 10^{-1}$	s
time constant of gate opening	τ_{open}^i	4.616 00	$1.384\,80 \cdot 10^1$	s
time constant of gate closing	τ_{close}^i	2.385 41	7.156 23	s
gating voltage	v_{gate}^i	$5.191\,25 \cdot 10^{-2}$	$1.557\,38 \cdot 10^{-1}$	-
diffusion coefficient	σ^i	$6.000\,00 \cdot 10^{-1}$	1.800 00	mm ² s ⁻¹
<u>SMC:</u>				
secondary excitability parameter	λ^m	$6.250\,00 \cdot 10^{-3}$	$1.875\,00 \cdot 10^{-2}$	-
time constant of inward current	τ_{in}^m	$5.731\,85 \cdot 10^{-2}$	$1.719\,56 \cdot 10^{-1}$	s
time constant of outward current	τ_{out}^m	$4.000\,00 \cdot 10^{-1}$	$7.060\,79 \cdot 10^{-1}$	s
time constant of gate opening	τ_{open}^m	4.616 00	$1.384\,80 \cdot 10^1$	s
time constant of gate closing	τ_{close}^m	2.385 41	7.156 23	s
gating voltage	v_{gate}^m	$5.191\,25 \cdot 10^{-2}$	$1.557\,38 \cdot 10^{-1}$	-
<u>Tissue electrophysiology:</u>				
resistance of gap junctions	D_{gap}	$4.200\,00 \cdot 10^{-1}$	$7.500\,00 \cdot 10^{-1}$	s ⁻¹
spread of excitability parameter a^i	b_x	1.581 10	4.743 30	-
<u>Electromechanics:</u>				
calcium dynamics	β_1	5.000 00	$1.500\,00 \cdot 10^1$	-
opening dynamics of VDCC	β_2	5.000 00	$1.500\,00 \cdot 10^1$	-
neo-Hooke material parameter	μ	$6.000\,00 \cdot 10^1$	$9.000\,00 \cdot 10^1$	N mm ⁻²
intensity of active contraction	α	$1.000\,00 \cdot 10^{-1}$	$3.000\,00 \cdot 10^{-1}$	-

Fixing uninfluent parameters

In this section, the overall number of free parameters is reduced by exploiting the special structure of the idealized stomach model (see Section 4.2.1). The only coupling between electrophysiology and mechanics in the model happens via the excitation-contraction coupling of Eq. (B.19) (see also (NC2)). The coupling is unilateral because MEF is neglected. The parameters of the submodel of gastric electrophysiology can only influence the mechanical part of the model via γ , while the mechanical parameters cannot influence the electrophysiology part of the model. Hence, electrophysiological parameters that have little influence on γ will have even less influence on the mechanical behaviour of the coupled model. This scenario is a prime candidate for parameter fixation (see Section 3.2.1). By identifying and fixing the uninfluent electrophysiology parameters with respect to γ , resources for the analysis of the full model can be saved.

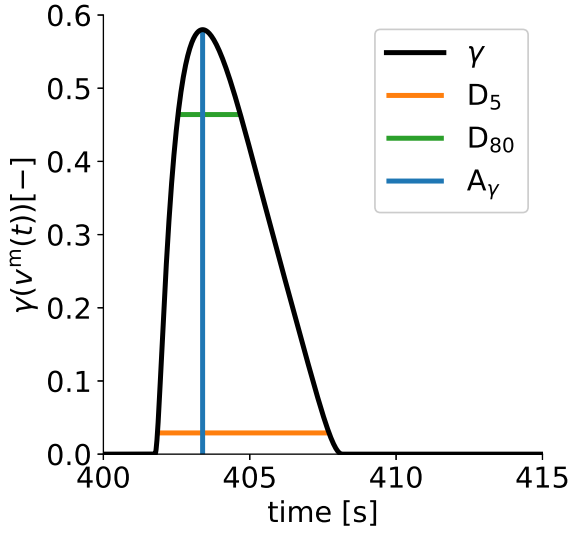
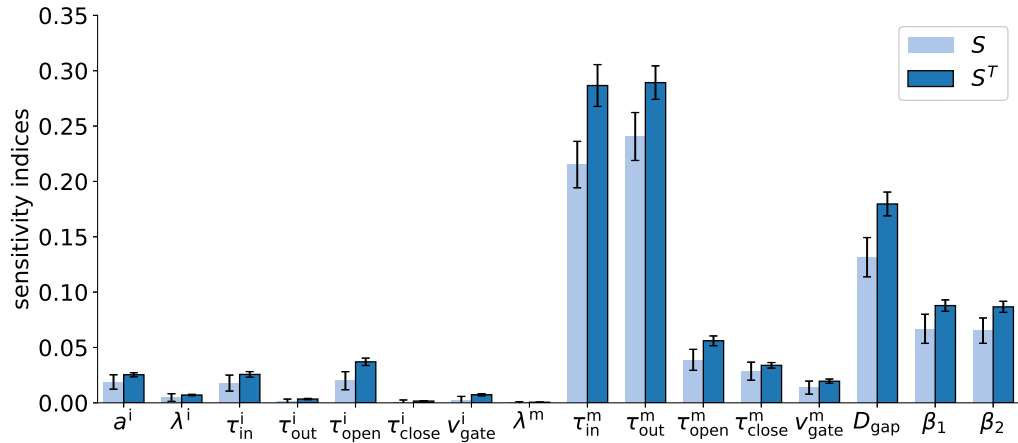


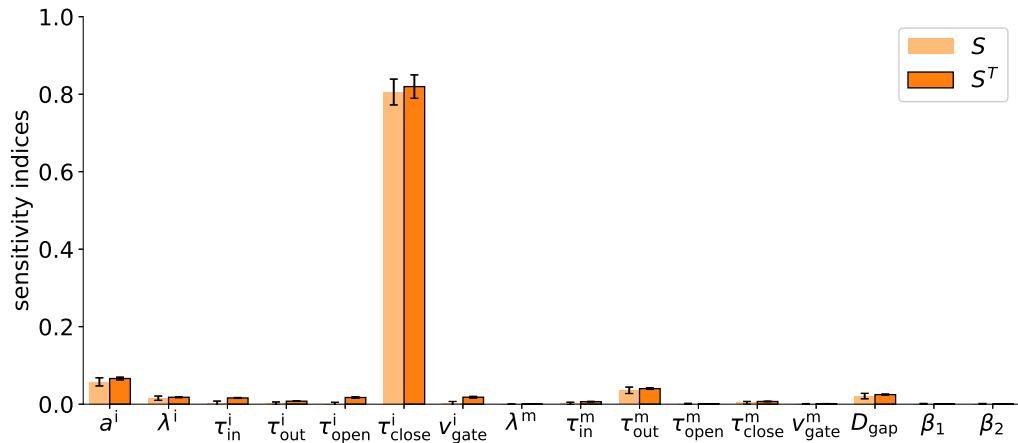
Figure 4.2: Three scalar quantities capturing the main properties of the active-strain activation $\gamma(t)$ during a slow wave. A_γ is the amplitude of the activation. The duration of activation D_5 is measured at 5 % of the maximum activation and the plateau duration D_{80} is measured at 80 %.

In the following a preliminary global sensitivity analysis of the submodel of gastric electrophysiology defined by Eq. (4.2) in combination with Eq. (B.19) is conducted. The computational setup remains as described in the previous section. In total, there are 16 free parameters (14 from Eq. (4.2) and 2 from Eq. (B.19)). The parameters are assumed to be distributed according to the physiologically admissible probability distributions derived in the previous section (see Table 4.3). Probing the model with a realization from the joint probability distribution of the parameters results in a time-dependent, periodic, functional output $\gamma(t)$ (see Figure 4.2). Similar to the analysis of cardiac action potentials in [153–155], three scalar quantities of interest are derived that describe the relevant properties of the signal. The first quantity is the *amplitude* A_γ . The second quantity is the *duration* of the activation D_5 measured as the width of the signal at 5 % of the maximal activation. The third one is the *plateau duration* of the activation D_{80} measured as the width of the signal at 80 % of the maximal activation. Figure 4.2 illustrates the quantities of interest for a single slow wave computed with the model at the base values given in Table 4.2.

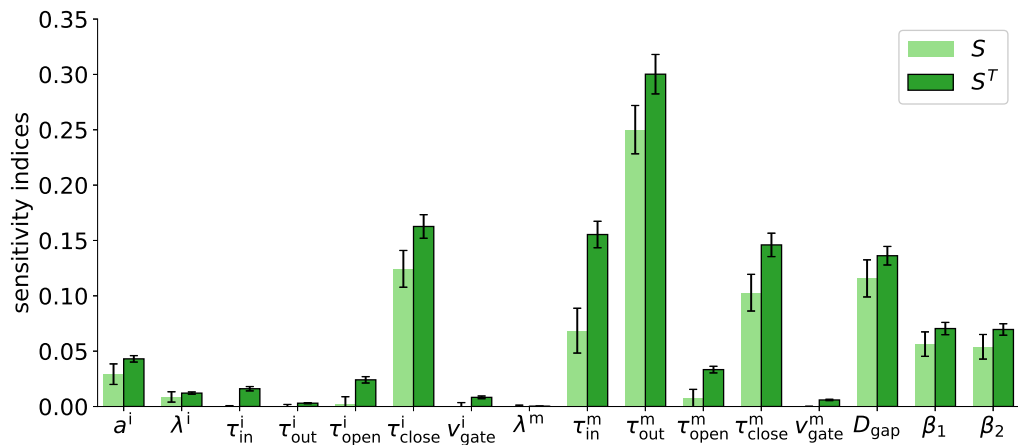
For each of the three quantities of interest, first order and total Sobol indices are computed based on a Monte Carlo sample of size $N = 4096$. An analysis of the individual probability density functions approximated by the 8192 independent sample points revealed that the overall variability of the quantities of interest was low. Their coefficients of variation (CVs) were between 0.28 and 0.38. Figure 4.3 depicts both first order and total indices of the 16 parameters together with their respective 95 % confidence intervals for each quantity of interest. A_γ is highly influenced by the time constants τ_{in}^m and τ_{out}^m , which have large total indices compared to the other parameters (Figure 4.3a). τ_{close}^i has by far the highest Sobol indices with respect to D_5 (see Figure 4.3b). Indeed, more than 80 % of the variability in D_5 can be explained alone by the uncertainty in τ_{close}^i . As illustrated in Figure 4.3c, the variability in D_{80} is caused to a large extent by τ_{out}^m . The second and third most influential parameters for D_{80} are also τ_{close}^i and τ_{in}^m . Most of the other parameters have negligible total indices for all three quantities of interest and can safely be fixed to their mean value according to the parameter fixing paradigm (see Section 3.3.4). Some have non-zero total indices, their values are, however, markedly smaller than



(a) amplitude A_γ



(b) duration D_5



(c) plateau duration D_{80}

Figure 4.3: First order and total Sobol indices and their 95 % confidence intervals for the quantities of interest A_γ , D_5 , D_{80} of model Eq. (4.2).

the ones of the above mentioned influential parameter. All in all, an outstanding significance of τ_{close}^i , τ_{in}^m , and τ_{out}^m for the active-strain activation γ can be ascertained. This justifies that all parameters except for these three are fixed at their base values given in Table 4.2 for the global sensitivity analysis of the full model of gastric electromechanics presented in the next section.

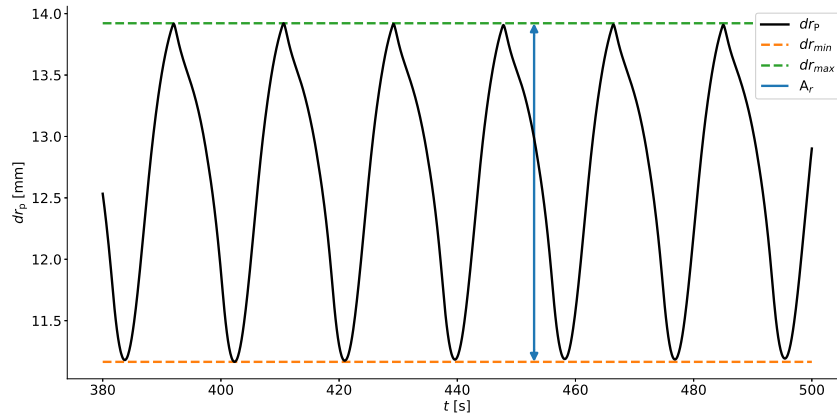
4.2.3 Quantities of interest

As described in Section 3.3, Sobol's method is defined only for scalar model outputs. Notwithstanding, the numerical solution of the model results in several spatiotemporal, vectorial fields, including the ones for electric transmembrane potential and mechanical displacement. Deriving descriptive scalar model outputs, called the quantities of interest, from these fields allows to resolve this mismatch. The main goal of this study is to investigate the influence of both electrophysiological and mechanical parameters on physiological, rhythmic peristaltic contraction waves travelling along the cylindrical stomach. For this purpose, scalar quantities of interest are defined in the following which capture shape and strength of the contractions as well as their propagation properties. All quantities are evaluated at the point P located at $x = L_x/2, y = r, z = 0$. P is chosen in the middle of the domain to reduce the influence of boundary conditions. Additionally, the displacements in y -direction are equal to the radial displacements dr_P there. As described in the previous section, the final 120 s of simulation time are used for the calculation of the scalar quantities of interest.

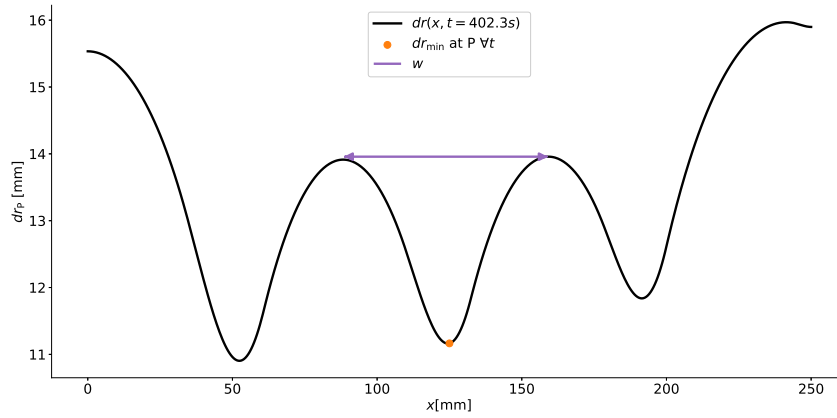
The contraction waves are characterized by four scalar quantities: the *uncontracted state* dr_{max} , their *amplitude* A_r and *width* w , and the *propagation speed* c_P . The maximal radial displacement at P, dr_{max} , is equivalent to the minimal contraction and, equally, the minimal displacement, dr_{min} , corresponds to the maximal contraction (see Figure 4.4a). The *uncontracted state* dr_{max} is defined by the minimal contraction at P over the final 120 s period. The *amplitude* A_r of a contraction is measured as the difference between minimum and maximum contraction and describes the strength of a contraction. The *width* of the contraction w is defined as the spatial distance between the two enclosing peaks of radial displacements – that is, the two closest, minimally contracted points – at the point in time of maximal contraction at P. In addition to their shape, the mean *propagation speed* c_P of the contraction waves is computed. It is measured by tracking the rising flanks of the contraction waves around P. Measuring the time Δt that a point on the rising flank needs to travel from $x_1 = 122.5$ mm to $x_2 = 127.5$ mm allows to compute the propagation speed c with

$$c = \frac{\Delta x}{\Delta t}, \quad (4.3)$$

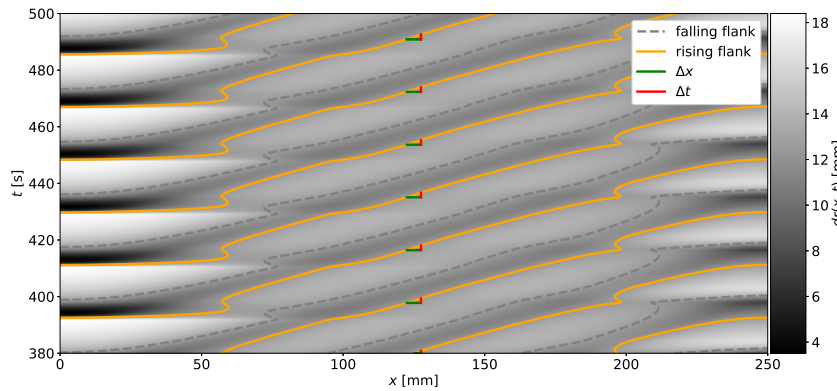
where $\Delta x = x_2 - x_1$. For this purpose, isolines at $A/2$ of the spatiotemporal radial displacement field are computed with the *measure* module of the open-source software *scikit-image* [159]. Falling flanks are dropped and for each of the detected rising flanks the conduction velocity is computed by Equation (4.3) (see Figure 4.4c). Finally, averaging these values results in the mean propagation speed of the contraction waves c_P .



(a) radial displacements over time at P



(b) radial displacements over axial position at $t = 402.3$ s



(c) spatiotemporal radial displacement field

Figure 4.4: Scalar quantities of interest derived from the spatiotemporal radial displacement field $dr(x, t)$ of an idealized model of gastric peristalsis. The quantities capture important features of the peristaltic contraction waves: (a) illustrates the amplitude A_r as well as the uncontracted state dr_{\max} at point P. (b) shows the width of the contraction at the point of maximum contraction in P. From the full spatiotemporal field depicted in (c) the propagation speed of the waves $c_P = \Delta x / \Delta t$ can be extracted.

4.2.4 Results

After fixing the uninfluential parameters of the electrophysiology model as described in Section 4.2.2, seven uncertain parameters remain in the idealized model of gastric electromechanics. These are the time constant of gate closing in ICCs τ_{close}^i , the time constant of the inward current of SMCs τ_{in}^m , the time constant of the outward current of SMCs τ_{in}^m , the isotropic diffusion coefficient of ICCs σ^i , the spread of the spatial distribution of the excitability $a^i(x)$, b_x , the intensity of the active-strain contractions α , and the neo-Hookean material parameter μ . The following global sensitivity analysis assumes physiologically admissible probability distributions for these parameters which were derived in Section 4.2.2 (see Table 4.3). Based on a Monte Carlo sample of size $N = 1024$, first order and total Sobol indices for each uncertain parameter and for each of the four quantities of interest (amplitude A_r , uncontracted state dr_{max} , width w , and propagation speed c_p) defined in Section 4.2.3 are computed. The computational approach presented in Section 3.3.3 is used. This implies that overall the model is evaluated 9216 times. The sample points can be separated into 2048 independent and 7168 cross sampled ones.

Probability distributions of quantities of interest

Figure 4.5 shows the probability density functions of the quantities of interest A_r , dr_{max} , w , and c_p . The densities are approximated by kernel density estimation (KDE) with Gaussian kernels based on the 2048 independent sample points.

The amplitude A_r of the peristaltic contraction waves generally remains small. The maximum amplitude observed is only 8.351 mm and more than 50 % of sample points result in amplitudes less than 2.5 mm. The mean amplitude is 2.647 mm. With a CV of 0.553, the variation in the amplitude is, however, comparably large. The variability of the uncontracted state dr_{max} is smaller. Its CV is 0.349 with a mean of 8.878 mm. The width of the contraction waves w experiences even less variability with a CV of only 0.171. Localized contractions of width 40 mm occur as well as far spread ones which, with a width of more than 100 mm, cover 40 % of the stomach's surface in a single contraction wave. Most contractions are, however, moderately spread and close to the mean width of 68.987 mm. The mean propagation speed is 3.461 mm s^{-1} . In a few sample points, the contraction waves propagate at a reduced speed of less than 2 mm s^{-1} . Many experience, however, higher propagation speeds up to the maximum value of 5.053 mm s^{-1} . Nevertheless, the variability of the propagation speed is small as the CV of c_p is only 0.175.

Sobol indices of parameters

Figure 4.6 shows the Sobol indices of the seven uncertain parameters for each of the four quantities of interest. The values of the indices are shown in Table 4.4. As illustrated in Figure 4.6a, the variance in the amplitude A_r is almost equally caused by five parameters. Still, the most influential parameter in terms of both indices is α but σ^i has only slightly smaller indices. The neo-Hooke material parameter μ and the spread of the excitability parameter distribution b_x do not influence the variability of A_r , since they both have negligible total indices of less than 0.005. Interactions play a minor role in the variability of A_r as indicated by a sum of first order indices of 0.888.

The variance of the uncontracted state dr_{max} is dominated by the uncertainty in μ . Almost 50 % of the variance is caused by this parameter alone. It is also not involved in parameter

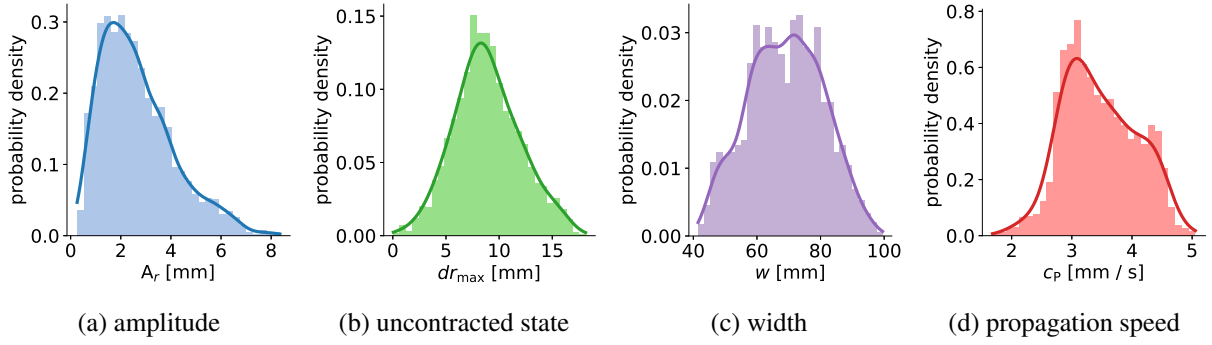


Figure 4.5: KDE for the probability density functions of the quantities of interest A_r , dr_{\max} , w , and c_P of the idealized model of gastric peristalsis described in Section 4.2.1.

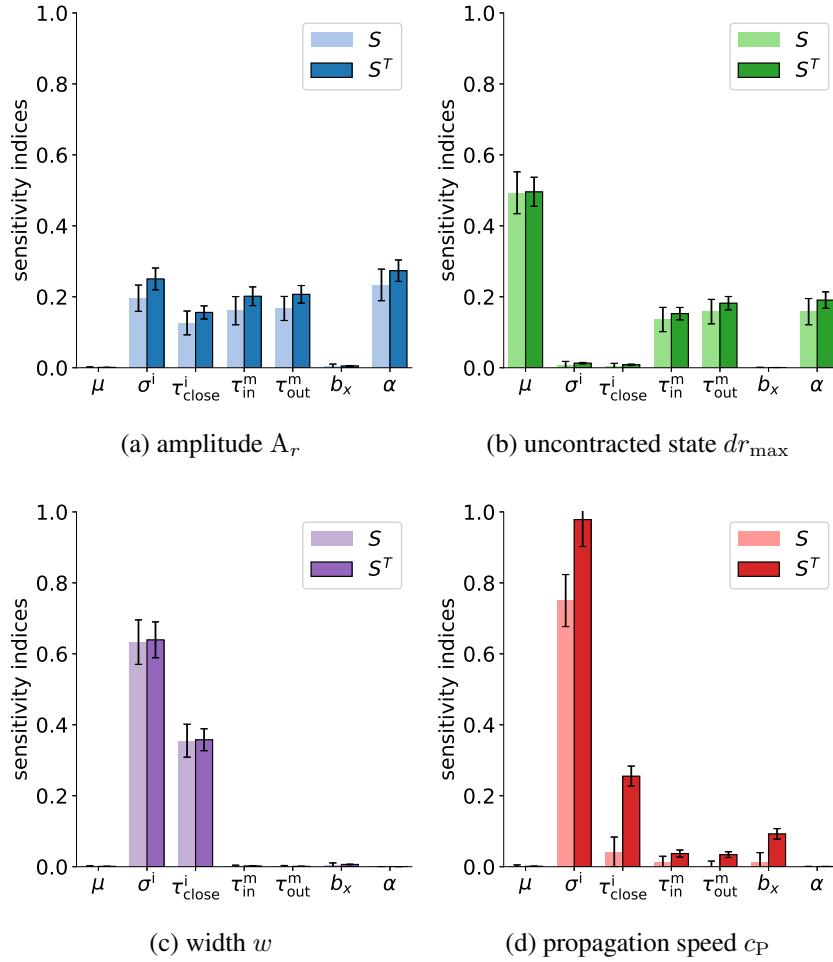


Figure 4.6: First order and total Sobol indices and their 95 % confidence intervals for the quantities of interest A_r , dr_{\max} , w , and c_P of an idealized model of gastric peristalsis (see Section 4.2.1).

Table 4.4: First order and total Sobol indices for each parameter and each quantity of interest. The sum of first order indices $\sum S_j$ depicted in the last row is a measure for the linearity of the respective model output. The amount of interactions a parameter is involved in is defined by $S_j^T - S_j$. For each quantity of interest the maximum total index are highlighted in bold letters.

Parameter	A_r		dr_{\max}		w		c_P	
	S_j	S_j^T	S_j	S_j^T	S_j	S_j^T	S_j	S_j^T
μ	0.000	0.001	0.493	0.496	0.000	0.001	0.002	0.001
σ^i	0.196	0.250	0.008	0.013	0.633	0.639	0.750	0.978
τ_{close}^i	0.126	0.156	0.004	0.009	0.355	0.358	0.042	0.255
τ_{in}^m	0.161	0.202	0.136	0.152	0.000	0.002	0.012	0.037
τ_{out}^m	0.167	0.207	0.158	0.182	0.001	0.001	0.001	0.034
b_x	0.004	0.005	0.000	0.001	0.004	0.006	0.012	0.093
α	0.233	0.274	0.158	0.191	0.000	0.000	0.000	0.001
sum:	0.888		0.957		0.993		0.817	

interactions as indicated by its almost identical first and total indices. Three other parameters, namely τ_{in}^m , τ_{out}^m and α , contribute also to the output variance of dr_{\max} . They all have similar total order indices of between 0.152 and 0.191 and constitute the complete amount of interactions. Overall, interactions between the parameters are, however, minimal ($\sum_j S_j = 0.957$). With total indices below 0.013, the influence of the other three parameters (σ^i , τ , and b_x) on dr_{\max} is negligible.

Only two parameters have non-zero total indices for the width w . These are the diffusion coefficient σ^i and the time constant τ_{close}^i . As indicated by their sum of first order indices practically no interaction between these two parameters occurs. Of the two influential parameters, σ^i is by far the most important one. It is responsible for more than 63 % of the variability in w ($S_{\sigma^i} = 0.633$). The remaining variance is almost entirely caused by τ_{close}^i ($S_{\tau_{\text{close}}^i} = 0.355$).

The variance in the propagation speed c_P is highly influenced by the uncertainty in the diffusion coefficient σ^i . It has a first order index of 0.750 and a total index of 0.978. While the first order indices of the other parameters are negligible, some of them have non-negligible total indices. Most notably τ_{close}^i has a total index of 0.255 but a first order index of only 0.042. The third most influential parameter is b_x with a total index of only 0.093. The mostly small first order indices indicate that there is a significant amount of interactions between the parameters. Indeed, with a value of 0.817, the sum of first order indices of c_P is markedly smaller than the ones of the other quantities of interest.

5 Results II: arterial growth and remodelling

This chapter presents the results for a model of the second active biomechanical system studied in this thesis: growth and remodelling of arterial tissue. A detailed global sensitivity analysis of a homogenized constrained mixture model of arterial growth and remodelling was performed which is presented in the form of a summary of Paper C. A comprehensive presentation of the analysis can be found in the reprint of the paper in Appendix.

5.1 Paper C: Global sensitivity analysis of a homogenized constrained mixture model of arterial growth and remodeling

Sebastian Brandstaeter, Sebastian L. Fuchs, Jonas Biehler, Roland C. Aydin,
Wolfgang A. Wall, Christian J. Cyron

published in

Journal of Elasticity, vol. 145, pp. 191–221, 2021. DOI: [10.1007/s10659-021-09833-9](https://doi.org/10.1007/s10659-021-09833-9).

Summary

During the past two decades, growth and remodelling of arterial tissue have been investigated in great detail. They have received substantial research interest not only due to their fundamental role for normal tissue maintenance but also due to their key role in diseases such as aneurysms.

Many different mathematical and computational models of arterial growth and remodelling have been developed. Among the most popular approaches are constrained mixture formulations. On the one hand, constrained mixture models have helped to significantly improve the understanding of the complex phenomena underlying aneurysm growth. On the other hand, their application in clinical practice, for example, to help make decisions on therapeutic options, remains uncharted territory. A multitude of studies have shown that constrained mixture models are capable of predicting aneurysm growth in principle. Many of these studies have relied on rough estimates of parameter values, for instance, in the form of population-average values. However, clinical applications call for reliable, individualized predictions which, in turn, require accurate, patient-specific model parameter values. Currently, it is impossible to measure all model parameters let alone patient-specifically. For this reason, it is paramount to identify the most impactful parameters with respect to the predictive capabilities of the models.

Global sensitivity analysis presents a great tool for answering these questions in a rational and well-founded way. Previous sensitivity and parameter studies of constrained mixture models have relied on local methods only. Local methods are, however, known to be inadequate for the investigation of non-linear models because they are incapable of detecting potential interactions between the model parameters. Additionally, global methods are better suited for the large variability of biological systems. This study presents such a global sensitivity analysis for a homogenized constrained mixture model of arterial growth and remodelling. By means of Sobol's variance-based sensitivity analysis approach, it is investigated how the uncertainty in the model output can be attributed to individual input parameters and their interactions.

The uncertainty in the evolution of the maximum diameter of an idealized, cylindrical abdominal aorta over the course of a 15 year period is studied in two representative examples. First, the blood vessel is subject to an elevated mean blood pressure, as seen during hypertension. Second, spontaneous loss of elastin potentially triggers the formation of an aneurysm. Between nine and ten uncertain parameters are varied simultaneously. The result of the global sensitivity analysis critically relies on how the uncertainty in these parameters is modelled. Here, it is assumed that each of the free parameters is distributed according to a uniform probability distribution that is independent from the other parameters. To appropriately cover the range of variability, the bounds of these distributions are based on experimental data where available. Where no experimental data is available, the study relied on previous theoretical studies to derive reasonable ranges.

From the two case studies, several key findings can be extracted. The studies revealed that interactions between the parameters can indeed play an important role in determining the variability of the radial expansion of blood vessels. This suggests that previous local analyses were able to reveal but a part of the parameters' influence and that future studies should indeed resort to global methods. Overall, three influential parameters are identified which essentially determine the inelastic deformation of the blood vessel due to growth and remodelling. These parameters are: the parameter that regulates the collagen production depending on the wall stress of the vessel, the average life time of collagen fibres, and one elastic parameter characterizing the strain stiffening of collagen fibres. The findings may guide future experimental and computational studies on the way to the clinical application of homogenized constrained mixture models. In computational studies, it may suffice to use population-average values for many of the model parameters. For experimental research, the results suggest to focus on the measurement of the three most influential parameters for the biggest increase in prediction reliability of AAA enlargement.

There are also some limitations of the study that should be mentioned. The studied model contains several assumptions and simplifications. Next to including potentially important phenomena like wall shear stress or intraluminal thrombus formation, the consideration of patient-specific geometries appears to be essential to improve individualized models of arterial growth and remodelling. Also the modelling of parameter uncertainties could be improved. Most likely, parameters of biological systems are neither uniformly distributed within their observed range nor are they all independent.

In conclusion, global sensitivity analysis based on Sobol indices was shown to be not only a viable but also a necessary tool for studying the influence of parameter uncertainties on the reliability of predictions of homogenized constrained mixture models for arterial growth and remodelling. It can give previously inaccessible model insights and quantitative statements which

allow comprehensive and reliable instructions for coming research. In this way, the study hopefully helps homogenized constrained mixture models to reach the level of sophistication necessary for their intended clinical application.

Author Contributions

S.B., J.B., and C.J.C conceived the original idea. **S.B.**, S.L.F. and J.B. designed the computational framework and carried out the implementation. **S.B.**, S.L.F. and C.J.C. conceived and planned the numerical experiments. **S.B.** carried out all simulations. **S.B.** and C.J.C. wrote the manuscript. S.L.F. prepared Figures 1 and 2. **S.B.** prepared Figures 3-8. **All authors** discussed the content and commented on the manuscript. C.J.C. was in charge of overall direction and planning.

6 Discussion

This chapter discusses the results obtained from studying two models of two different active biomechanical systems in the previous chapters (see Chapter 4 and Chapter 5). It begins by discussing the results for each model individually. Thereafter, a general perspective on global sensitivity analysis for models of active biomechanical systems is derived from these individual results.

6.1 Gastric electromechanics

This thesis presented two main results for the computational modelling of gastric electromechanics, which will be discussed in the following. The results found for the novel framework for the computational modelling of gastric peristalsis are discussed first. Then, the results of the global sensitivity analysis of this model is discussed.

6.1.1 Computational model of gastric motility

Computational models of gastric electromechanics remain scarce. Previous modelling studies focused mostly on the electrophysiological system of the gastrointestinal tract (see Section 2.4 for a detailed review with many additional references). The cellular models can be divided into biophysically based and phenomenological descriptions. Biophysical models attempt to replicate the mechanism and dynamics of the various ion channels involved in the bioelectrical activity. A host of biophysical models has been proposed in the past [160–165]. However, many of them appear to be outdated since novel experimental insights have contradicted their assumptions as described in the recent review by Mah et al. [166]. Despite the considerable research effort many of the biophysical details underlying the bioelectric activity of the gastrointestinal tract remain unknown. Therefore, simplified phenomenological descriptions that capture known signal properties macroscopically have also been developed. They go back to FitzHugh and Nagumo [167, 168] and have been proposed for the intestine [169, 170] and the stomach [171]. For tissue electrophysiology, three formulations of increasing generality have been proposed. These are the monodomain [169, 170, 172], the bidomain [171, 173–176] and the extended bidomain (or tridomain) [177–179] equations. The numerical simulation of the bidomain and tridomain formulations is costly and challenging. At the same time, the monodomain model has been shown to suffice for capturing key features of the system with manageable computational cost. For this reason, it remains a popular choice. So far, only a few studies have included electromechanical coupling in the intestine [172, 180–183] and even less in the stomach [184, 185]. Thus, what remains wanted is a computationally tractable, coupled multiphysics model that can be used to study the intricate interplay between electrophysiology and mechanics underlying the macroscopically, observed features of gastric motility in health and disease.

Paper B presented such a computational multiphysics framework for the phenomenological description of gastric peristalsis. The framework combines a robust gastric electrophysiology model with a finite elasticity model for the mechanics. Two coupled monodomain formulations describe the propagation of slow waves on the tissue scale: one for each of the two main cell types, ICCs and SMC. Both cellular models are based on the same modified version of the two-variable Mitchell-Schaeffer model. By choosing the model parameters accordingly, different properties of the cells – like self-excitatory ICCs versus excitatory SMCs – can be reproduced. An active-strain, finite elasticity approach is used to describe electromechanics.

Using only four state variables, the phenomenological model enabled an efficient, yet general description of gastric electrophysiology. Unlike previous formulations, the novel model remained stable for arbitrary simulation times. A series of numerical experiments proved that key phenomena of the integrated gastric electromechanical system in the physiological state, like entrainment and ring-shaped peristaltic contraction waves, can be reproduced successfully with the phenomenological modelling framework. Experimentally observed quantities like an entrained frequency of approximately 3 cpm (cycles per minute), 3–4 concurrent waves, and a propagation velocity of approximately 3 mm s⁻¹ are within the respective physiological ranges [149]. Additionally, the empirically observed coupling between dysrhythmias and gastroparesis was consolidated with the model. Inducing dysrhythmias via a conduction block allowed to study their influence on the mechanical contractions.

Naturally, the presented model also has limitations. First, electrophysiology is solved in the reference configuration and the model therefore ignores MEF. MEF can, for example, occur due to mechanosensitive ion channels [186–189] or due to non-linear [190, 191] and stress-assisted [3, 192, 193] diffusion. In their recent contribution, Klemm et al. [194] proposed an electro-chemomechanical model for gastric electromechanics including two MEF mechanisms: both the intrinsic frequency of ICCs and the peak potential of SMCs depend on the current deformation of the tissue. Second, a homogeneous, isotropic neo-Hookean material model to describe the passive mechanical tissue behaviour was used. There is, however, compelling experimental evidence that the properties of gastric tissue show both regional dependence and anisotropy [151, 152, 194, 195]. Finally, all examples were performed on simplified geometries such as tissue patches or cylinders. Thereby, the anatomical complexity of patient-specific stomach geometries has been neglected.

6.1.2 Global sensitivity analysis for the model of gastric motility

A global sensitivity analysis based on Sobol’s method was performed for an idealized, cylindrical model of a stomach during healthy peristalsis. A total of 20 free parameters were considered. Using a series of preliminary global parameter studies, physiologically feasible bounds for the uniform probability distributions of these parameters were derived. The unilateral coupling between the models of electrophysiology and structural mechanics allowed to perform an intermediate global sensitivity analysis of the model of gastric electrophysiology alone. In accordance with the parameter fixation paradigm, 13 uninfluential parameters could be fixed to their base values in this intermediate study. The seven remaining parameters were: the neo-Hooke material parameters μ , the intensity of active contraction α , the diffusion coefficient σ^i , the spread of spatial distribution of excitability b_x , the time constant of gate closing in ICCs τ_{close}^i , the time constant of the inward current of SMCs τ_{in}^m , and the time constant of the outward current of

SMCs τ_{out}^m . The influence of the input uncertainty in these seven parameters on the variance of four scalar model outputs was then analysed by computing pairs of first order and total Sobol indices for each parameter and each output. These four quantities of interest represent important properties of the peristaltic contraction waves: the amplitude, the uncontracted state, the width, and the propagation speed of the waves.

While the neo-Hooke material parameter μ heavily influenced the uncontracted state, it had zero influence on amplitude, width and propagation speed of the peristaltic contraction waves. The non-existing influence on the amplitude might be explained by the fact that it is computed based on the difference between the uncontracted and the maximally contracted state. As such, the amplitude appears to be a relative quantity with respect to the elastic properties of the stomach. More generally, this finding indicates that amplitude, width, and propagation speed are suitable quantities to characterize the active part of the contractions.

In addition to μ , the uncontracted state was also influenced by some of the other parameters. This can be explained by the fact that more than one contraction wave is present on the stomach's surface at any moment in time. These peripheral contraction waves influence the uncontracted state in the middle of the stomach.

Most parameters have a non-negligible influence on at least one quantity of interest. In part, this was expected, since some of them have been identified as important for the model of electrophysiology in the intermediate sensitivity study. Interactions between parameters played a minor role for all analysed quantities, except for the propagation speed.

The spread of the spatial distribution of the excitability parameter b_x was the only parameter that had negligible influence on all four quantities of interest. According to the parameter fixation paradigm, it can therefore be fixed to its base value in similar future studies. Yet, this result is surprising, since many previous studies stressed the importance of the intrinsic frequency gradient for gastric electrophysiology [187, 196, 197]. A possible explanation is that the frequency gradient might be more important in cases of disturbance of the system [197]. Herein, the system was, however, only studied under normal, undisturbed conditions.

The analysis of the probability density function (PDF) of the amplitude revealed that the amplitude was generally small. A comparison with values for peristaltic contraction waves extracted from magnetic resonance imaging (MRI) data confirms that these values are indeed too small. Typically, peristaltic contraction waves show amplitudes in the order of centimetres instead of millimetres [198, 199]. The presented global sensitivity analysis identified the intensity parameter α as the most influential parameter for the amplitude. Larger values of α would, therefore, most likely result in the necessary increase of the amplitude. Hence, future studies should aim to increase the possible range of α in order to reach more realistic values for the amplitude. A preliminary test showed that the model in its current form fails to do so due to numerical problems similar to the ones experienced for small μ values (see Section 4.2.2). While a fully resolved, three-dimensional structural mechanical formulation could certainly mitigate this problem, it would also substantially increase the computational costs. A promising compromise might be the use of shell formulations as recently suggested in [200]. In this way, the global sensitivity analysis of the model indicates a promising research direction for computational modelling of gastric electromechanics.

The diffusion coefficient σ^i is identified as the most important parameter of the model. The amplitude, the width, and the propagation speed are all heavily influenced by the diffusion coefficient σ^i . Measuring it experimentally would likely yield the greatest impact in terms of the

predictive capabilities of the model. Recently, some studies proposed approaches to efficiently determine the diffusion coefficient for cardiac electromechanics [201–205]. In the future, it appears, therefore, promising to attempt a transfer of these approaches to the field of gastric electromechanics.

Additionally, all four quantities of interest can be readily extracted *in-vivo* from standard MRI data [199, 206–209]. As discussed, many of them are dominated by at most two parameters with little interactions; this suggests that the identification of these parameters based on patient-specific, *in-vivo* data could be possible. Such a patient-specific identification of parameter values would greatly benefit the predictive capabilities of the model.

Altogether, the global sensitivity analysis of an idealized model of gastric peristalsis presented in this thesis revealed important model properties. Both advantageous qualities of the model and areas for possible improvements were identified. Promising approaches to implement these improvements were outlined.

Nevertheless, the presented study is subject to several limitations. Most notably, the model was studied under physiologically feasible conditions. To consolidate the importance of the study for the medical community the model should also be studied in pathophysiological condition in the future. Additionally, simplified assumptions on the probability distributions of the model parameters had to be assumed due to a lack of experimental data, which can be explained in part by the novelty of the model. Nevertheless, the study should be repeated in the future, when more experimental data becomes available. Finally, limitations and future directions for the chosen global sensitivity analysis approach as discussed in detail in Section 7.1 equally apply here.

6.2 Arterial growth and remodelling

Chapter 5 presented a global sensitivity analysis for a homogenized constrained mixture model for arterial growth and remodelling, which has previously been introduced by Cyron et al. [46]. The results of this analysis are discussed in the following section.

So far, mostly local parameter sensitivity studies of growth and remodelling models have been presented. Often new models are proposed together with a crude, local sensitivity analysis where the influence of individual parameters is demonstrated by evaluating the model with different parameter values. This approach can, for example, be seen in the following articles: [32, 35, 37, 38, 46, 48–50, 210–212]. There have also been more explicit parameter sensitivity studies that successfully investigated properties and hypothesis of existing models. Wilson et al. [42] illustrated the qualitative influence of the initial state on the evolving properties of AAAs by studying four different cases. In [213], a parameter study was presented where the importance of the properties of collagen turnover, like mass density production, collagen half-life and deposition stretch, for the evolution of AAAs is investigated by varying the parameters individually. The influence of the parameterized elastin damage on the anisotropy of aneurysmal tissue was analysed in [214]. While perhaps more exhaustive than some of the modelling studies, these parameter studies followed, however, the same local one-at-a-time approach of observing the qualitative change in output by varying isolated parameters. By studying the combined influence of two parameters on multiple model outputs, Valentín and Humphrey [215] presented a grid-based global approach and thereby a notable exception from the other studies. The study by Lee et al. [216] seems to

be the only one that used a true global sensitivity analysis method to investigate growth and remodelling so far. They investigate the total Sobol index of five parameters of a kinematic growth model for skin expansion which they calculated based on a multi-fidelity Gaussian process surrogate model. Unfortunately, they do not indicate the first order indices rendering it impossible to evaluate the amount of interactions between the parameters. While the authors supply confidence intervals for the indices, these do not include the additional uncertainties resulting from the surrogate approximation.

Thanks to all these previous studies, a deep understanding for the individual, local roles of the model parameters has been gained. What remains less examined is their global influence on model output variability if the complete parameter space is explored including interactions. To shed light on this question, Sobol's method of global, variance-based sensitivity analysis was applied to a homogenized constrained mixture model of arterial growth and remodelling.

In two case studies, the maximum diameter of an idealized, cylindrical abdominal aorta was tracked for 15 years. In the first case, a hypertensive aorta, subject to a sustained, increased mean blood pressure, was examined. In the second case, spontaneous loss of elastin occurs. Elastin damage has been hypothesized to potentially trigger AAA formation. Nine and ten uncertain parameters were varied respectively based on their uniform probability distributions. The additional parameter in the aneurysm case described the spatial spread of the elastin damage, which was not present in the hypertension case. All other parameters were identical between the cases. In the two examples, first order and total indices were computed for each of the parameters in one year intervals.

It was found that the sensitivity indices can change significantly over time. In both cases only three parameters influence the long-term radial expansion while some additional parameters influence the initial expansion but quickly loose influence afterwards. Interestingly, the three important parameters differed slightly between the cases. In the hypertension case, the orientation of collagen fibres in the vessel wall, the strain stiffening of collagen and the stress dependent collagen deposition were most influential. In the aneurysm case, the collagen fibre orientation was less important. Instead the collagen turnover time – which is closely linked to the half-life time – was found to be highly influential in combination with the other two important parameters of the hypertension case.

The mechanobiological stability theory introduced in [30, 31] presents a theoretical foundation for the discussion of the findings. The hypertension case was identified as a mechanobiologically stable system whereas the aneurysm is a potentially unstable one. The turnover time is identified as important in the initial, transient phase of the stable hypertensive aortas but also in the long-term for the potentially unstable aneurysm case. As predicted by the theory, it seemed crucial for growth and remodelling dynamics but less important for the mechanobiological equilibrium configuration. Contrarily, the collagen deposition was found influential in both initial and late phases of both cases. Again, this is coherent with the theory and consolidates the fact that collagen mass deposition is of major significance both for the rate of inelastic deformations during growth and remodelling as well as for the equilibrium state of stable systems. Only two elastic parameters have a major impact on the model output. To this end, the orientation of collagen fibres was found to be important for the elastic deformation of the system but less so for the inelastic ones from growth and remodelling. This is indicated by the fact that, in both case studies, an initially high influence decreases over time as the amount of inelastic deformation increases. In the stable hypertension case, the parameter maintains, however, some influence

because the overall inelastic deformation remains small compared to the elastic one. In both cases, the strain stiffening of collagen shows overall high importance, both initially and long-term. This reveals that the collagen strain stiffening strongly influences the elastic deformations as well as the inelastic ones.

Another notable difference between the two case studies was identified in terms of parameter interactions. While strong interactions between the three influential parameters were found in the aneurysm case, interactions played only a minor role in the hypertension case. This goes to show that it most likely does not suffice to measure one parameter alone. Instead, the full triplet of highly influential parameters needs to be measured with high precision to attain accurate model predictions. Furthermore, it shows that previous local studies might not have revealed the full picture. The strong interactions evidence the necessity for global sensitivity analysis methods to reveal true parameter influences on the model output of constrained mixture models.

Overall, it was concluded that it may suffice to use population-average values for many of the model parameters in similar, future computational studies. At the same time, it was suggested to focus future experimental research on the measurement of the three most influential parameters for the largest impact on prediction accuracy of AAA expansion.

The study suggests a host of future research directions including the lift of remaining limitations. Sobol's variance-based sensitivity analysis method has been used to investigate but one scalar output quantity, the maximum diameter. However, parameters that appear unimportant for one model output could be very influential on another and vice versa. Possible remedies include the combination of multiple scalar outputs into one as suggested in [217] but there are also more advanced methods [218, 219]. Additionally, the specific model investigated in the study simplified some known physical phenomena. These assumptions should be reconsidered in the future depending on the application context of the model. For example, the influence of blood flow and wall shear stress were neglected in accordance with many other studies of large, elastic arteries [42, 45, 48, 220]. In contrast, for smaller arteries these quantities have frequently been hypothesized to being essential [40, 221–223].

6.3 The big picture

From the discussion of the examples studied in this thesis, a bigger picture of variance-based global sensitivity analysis for models of active biomechanical systems arises. By quantifying the fraction of output variability that can be attributed to the uncertainty in individual and combinations of inputs, Sobol indices indicate how the current predictive capabilities of a model can be improved most efficiently both in terms of accuracy and computational cost. The identification of the most influential parameters allows for attempts to reduce uncertainties in these parameters which, in turn, will greatly increase the prediction accuracy of the model. In contrast, the uncertainty in uninfluential parameters can be neglected thereby reducing the computational cost of model predictions significantly without compromising the accuracy too much.

Pinpointing the potential for improvement of the model certainly is the main achievement of a global sensitivity analysis and worthwhile on its own. However, there are several additional insights that emerge naturally in the process and can therefore be leveraged without almost any additional cost. First and foremost, any good global sensitivity analysis is precluded by an uncertainty quantification, which serves to assess the current uncertainty in the model output due to the

input uncertainties. In other words, uncertainty quantification determines the current reliability of model predictions depending on the inevitably uncertain inputs. In the case of Sobol's method, the quantification of the overall output variability is an integral part of the method. Nevertheless, it should always be evaluated and analysed explicitly because it can have strong influence on the interpretation of the results. Second, the global nature of the analysis indicates that also interactions between parameters can be investigated. In its presented form, Sobol indices allow for the quantification of the overall interactions of each parameter. While this information is useful to detect the presence of interactions, it does neither reveal which other parameters are involved nor the nature of the input-output relation. This means that if one finds a parameter that is involved in interactions, one does not get to know whether it is an interaction with one specific parameter or multiple parameters and which ones are involved precisely. In theory, such information could be easily attained within the analysis framework (see Definition 3.4). In practice, it is, however, prohibitively expensive to calculate the higher order indices in most cases. Even if all indices – including higher order ones – were known, the nature of the input-output relations would still remain unknown. What is meant by 'nature of the input-output relation' is most easily explained with an example. Say one finds a large second order index for parameters A and B . Then one knows that interactions between A and B are responsible for a significant amount of output variability. What remains unexplored is how they interact. It could, for example, be that high values of A together with low values of B result in low output values. However, it could certainly also be that it is the combination of small values in A and B that result in large output values or any other relation between the parameters for that matter. Indeed, this argument applies equivalently to first order indices, that is, the input-output relations of single parameters. While the sensitivity indices alone can not reveal the details of the input-output relations, the information obtained during their computation can be used to investigate them. There is no straightforward way of doing so. Notwithstanding, this thesis showed that visual methods, like parallel coordinates plots, are readily available tools that can help significantly in studying the nature of input-output relations in general, and parameter interactions in particular, without any additional cost. In this way, quantitative and qualitative methods complement each other to form a powerful analysis framework that can be used to attain deep model knowledge.

7 Conclusion and outlook

This thesis proposed a novel computational framework for gastric electromechanics capable of describing, for the first time, gastric peristalsis in health and disease. Next, it presented variance-based global sensitivity analyses based on Sobol indices for both this new model of gastric electromechanics and a well-established homogenized constrained mixture model of arterial growth and remodelling. For each model, a set of first order and total sensitivity indices was computed and analysed for representative scalar model outputs in multiple application scenarios.

The novel model of gastric electromechanics successfully represented key phenomena of the integrated gastric electromechanical system in the physiological state, like entrainment of ICCs and ring-shaped peristaltic contraction waves. Many of the experimentally observable quantities were shown to lie within the respective physiological ranges. Additionally, the influence of gastric dysrhythmias on the peristaltic contractions was analysed for the first time. Thus, the model could be used to study the pathological processes underlying the empirically observed coupling between dysrhythmias and gastroparesis in the future.

The global sensitivity analyses for two models of active biomechanical systems performed in this thesis proved that Sobol indices are a powerful tool capable of overcoming the limitations of current standard methods. The comparison between first order and total indices allowed for the quantification of the overall amount of parameter interactions. The analyses revealed that indeed significant amounts of parameter interactions can occur in models of active biomechanical systems. For example, more than 42 % of the long-term output variance in the maximum diameter of an AAA resulted from parameter interactions. This finding demonstrates the necessity for global methods to study models of active biomechanical systems and that previous studies might have underestimated the influence of some parameters.

Variance-based global sensitivity analysis was shown to be of great use also with regard to the analysis of parameter uncertainties. On the one hand, this thesis revealed that the influence of the uncertainty in many parameters on the uncertainty in the output of models of active biomechanical systems can be neglected. For example, the number of uncertain parameters could be reduced from 20 to six in the study of properties of gastric peristaltic contraction waves. This result shows that Sobol indices can be used to systematically reduce the complexity of future model predictions significantly without introducing large errors. On the other hand, this thesis found that the uncertainty in the output of the models was frequently dominated by the uncertainty in very few parameters. For instance, in the hypertensive aorta example, the uncertainty in the collagen mass deposition alone was responsible for 68.8 % of the output variability. For future research, the most influential parameters yield the best return of investment: acquiring additional knowledge on these parameters, that is, reducing their uncertainty, will likely reduce output uncertainty the most.

Additionally, the thesis showed that visual methods complement the mathematically rigorous analysis by Sobol's method perfectly. For example, parallel coordinates plots can be used to analyse the nature of the identified interactions. In the case of the model of gastric elec-

tromechanics, this helped to identify physiologically feasible regions of the input space. Which allowed to concentrate the analysis of the model to this region of interest.

Overall, the main result can be summarized as follows: global sensitivity analysis should become an essential part of the development process of models of active biomechanical systems. By demonstrating its applicability to a broad class of models, this thesis can hopefully inspire others to adopt and advance the approach in the future. With regards to models of active biomechanical systems, global sensitivity analysis optimistically brings them closer to the clinical application they are destined for.

7.1 Future Perspectives for global sensitivity analysis of models of active biomechanical systems

The results obtained with Sobol's variance-based, global sensitivity analysis approach as presented herein are very encouraging. Global analysis methods were identified as a necessary extension of the more common, local approaches. However, there are also some limitations and open questions that should be addressed in the future.

First of all, the results of a global sensitivity analysis critically rely on how the input uncertainties are modelled. In this thesis, independent, uniform distributions for all parameters were assumed due to a lack of available data. However, it appears very likely that biological parameters are neither uniformly distributed nor necessarily independent from each other. In part this issue can be mitigated over time if additional data becomes available through specifically designed experimental studies. For example, Seyedsalehi et al. have shown in [224] how existing knowledge can be incorporated into complex prior distributions including correlations between the parameters and with age. Another promising approach was presented in [225] where Biehler et al. demonstrated how to infer probabilistic models of key AAA parameters, like wall thickness and stiffness, from more easily accessible explanatory variables with advanced Bayesian regression techniques. What remains pending is to analyse the sensitivity of models of active biomechanical systems to such advanced probabilistic models of input uncertainty. In part this might be because the treatment of dependent inputs still poses a big challenge to global sensitivity analysis. While the definition of the indices (see Definition 3.1 and Definition 3.2) remains valid also in the dependent parameter case their interpretability based on Definition 3.3 gets lost. For example, total indices smaller than the corresponding first order ones can occur in case of negative correlations [226]. This loss of correspondence between indices and model structure renders the method inappropriate for dependent inputs. Research in the field is very active and a variety of studies have suggested approaches to generalize Sobol's method. Notable attempts include the generalizations of the ANOVA decomposition [227, 228], copula-based approaches [226, 229], and methods using Rosenblatt and Nataf transformations to derive independent representations of dependent random variables [230, 231]. Other approaches treat special cases like inputs on non-rectangular domains, which arise, for example, in case of algebraic constraints, [134]. Algebraic constraints could, for example, arise in homogenized constrained mixture model with more than 2 constituents, because their mass fractions have to fulfil the partition of unity property. Additionally, the so-called Shapley Effects have recently been proposed as promising, generalized sensitivity measures based on game-theory [94, 130–132]. So far, these

advanced sensitivity analysis methods have been studied mostly with academic examples and their application to more complex models remains largely unexplored.

Second, the models studied herein generally result in spatiotemporal solution fields. Sobol's method is, however, defined only for scalar-valued model outputs. This thesis showed how to derive such scalar output quantities from the functional output, for example, by identifying special points of interest in the domain, like the apex of an AAA, and by considering discrete points in time. In future studies, none of the above approaches might adequately reduce the dimension of the model output and therefore more sophisticated methods are required. Research progress in generalizing Sobol indices to functional output has been made [232, 233] but application examples remain scarce. A more common approach is to decompose the output, for example, by functional principal component analysis [218, 219] or by wavelet transformation [234]. The actual sensitivity analysis is then performed with regards to the most important coefficients. To a certain degree, such decompositions allow to compute sensitivity indices for functional outputs. However, the interpretation of the resulting indices can be difficult, because the relation of the coefficients to the solution is sometimes not straightforward.

Finally, the extreme computational cost of Sobol's method should be mentioned. The method requires many model evaluations – typically at least in the thousands – which can very quickly become prohibitively expensive. This can either be due to a high cost of the individual model evaluations or due to a high number of uncertain inputs. In this thesis, the computational cost is kept at bay mostly by exploiting the special structure of the models like, for example, geometric symmetries. Additionally, the evaluation is facilitated by an efficient use of the available computing infrastructure. Nevertheless, the direct application of global sensitivity analysis as presented herein to more expensive problems, for example, to models with patient-specific geometries, will likely remain very challenging. There are two ways of decreasing the overall cost, that is, the number of required model evaluations. On the one hand, cheaper but less accurate screening methods like Morris' elementary effects method [109, 110] (see also Section 3.2.2) can be used to decrease the number of uncertain inputs prior to a detailed analysis. Parameters that are identified as uninfluential by the Morris Screening can be fixed to a certain value – typically to the mean value – in the preceding, quantitative analysis with Sobol's method. This approach is in part justified by the link that was established between Morris' Screening and the total index in [110] (see also Section 3.3.4). On the other hand, a common approach to handle expensive models is to first fit a surrogate model (often also referred to as meta-model or emulator) to a smaller input-output sample. The sensitivity analysis is then carried out on the surrogate whose individual evaluation cost is considered negligible in comparison to the full model. Surrogate modelling is a vast and active research field [66, 235]. The most common surrogates for sensitivity analysis are based on Gaussian processes [236, 237] or Polynomial Chaos expansion [233, 238]. More recently multi-fidelity approaches have gained popularity in uncertainty quantification [19, 28, 235] and first studies began to apply them to sensitivity analysis [27]. Another new advancement is based on physics-informed machine learning [239–242]. However, more research is needed to elucidate the use of these novel methods in the context of sensitivity analysis. Generally, it should be mentioned that surrogate models introduce an additional source of epistemic uncertainty stemming from limited data. Therefore, their use mandates at least a very careful validation of the surrogate model. Ideally the additional uncertainty should, however, be propagated through to the estimates of the sensitivity indices as, for example, proposed by [243]. Future research in this regard will allow the consistent application of global sensitivity

analysis to models that seem unattainable today. In this way, the synergy between mathematical modelling and global sensitivity analysis will continue to grow and foster many more exciting scientific discoveries in the field of biomechanics.

Bibliography

- [1] A. Gizzi, C. Cherubini, S. Filippi and A. Pandolfi, ‘Theoretical and Numerical Modeling of Nonlinear Electromechanics with applications to Biological Active Media’, *Communications in Computational Physics*, vol. 17, no. 1, pp. 93–126, 2015. DOI: [10.4208/cicp.091213.260614a](https://doi.org/10.4208/cicp.091213.260614a).
- [2] S. Land *et al.*, ‘Verification of cardiac mechanics software: Benchmark problems and solutions for testing active and passivematerial behaviour’, *Proceedings of the Royal Society A: Mathematical, Physical and Engineering Sciences*, vol. 471, no. 2184, 2015. DOI: [10.1098/rspa.2015.0641](https://doi.org/10.1098/rspa.2015.0641).
- [3] A. Loppini, A. Gizzi, R. Ruiz-Baier, C. Cherubini, F. H. Fenton and S. Filippi, ‘Competing mechanisms of stress-assisted diffusivity and stretch-activated currents in cardiac electromechanics’, *Frontiers in Physiology*, vol. 9, no. December, pp. 1–16, 2018. DOI: [10.3389/fphys.2018.01714](https://doi.org/10.3389/fphys.2018.01714).
- [4] M. R. Pfaller, J. M. Hörmann, M. Weigl, A. Nagler, R. Chabiniok, C. Bertoglio and W. A. Wall, ‘The importance of the pericardium for cardiac biomechanics: from physiology to computational modeling’, *Biomechanics and Modeling in Mechanobiology*, vol. 18, no. 2, pp. 503–529, 2019. DOI: [10.1007/s10237-018-1098-4](https://doi.org/10.1007/s10237-018-1098-4).
- [5] C. J. Cyron and J. D. Humphrey, ‘Growth and remodeling of load-bearing biological soft tissues’, *Meccanica*, vol. 52, no. 3, pp. 645–664, 2017. DOI: [10.1007/s11012-016-0472-5](https://doi.org/10.1007/s11012-016-0472-5).
- [6] J. F. Eichinger, L. J. Haeusel, D. Paukner, R. C. Aydin, J. D. Humphrey and C. J. Cyron, ‘Mechanical homeostasis in tissue equivalents: a review’, *Biomechanics and Modeling in Mechanobiology*, 2021. DOI: [10.1007/s10237-021-01433-9](https://doi.org/10.1007/s10237-021-01433-9).
- [7] J. D. Humphrey, ‘Constrained Mixture Models of Soft Tissue Growth and Remodeling – Twenty Years After’, *Journal of Elasticity*, vol. 145, pp. 49–75, 2021. DOI: [10.1007/s10659-020-09809-1](https://doi.org/10.1007/s10659-020-09809-1).
- [8] O. Röhrle, U. Ş. Yavuz, T. Klotz, F. Negro and T. Heidlauf, ‘Multiscale modeling of the neuromuscular system: Coupling neurophysiology and skeletal muscle mechanics’, *Wiley Interdisciplinary Reviews: Systems Biology and Medicine*, vol. 11, no. 6, pp. 681–701, 2019. DOI: [10.1002/wsbm.1457](https://doi.org/10.1002/wsbm.1457).
- [9] R. Kuravi, K. Leichsenring, M. Böl and A. Ehret, ‘3D finite element models from serial section histology of skeletal muscle tissue – The role of micro-architecture on mechanical behaviour’, *Journal of the Mechanical Behavior of Biomedical Materials*, vol. 113, p. 104 109, 2021. DOI: [10.1016/j.jmbbm.2020.104109](https://doi.org/10.1016/j.jmbbm.2020.104109).

- [10] World Health Organisation, *The top 10 causes of death*, 2020. [Online]. Available: <https://www.who.int/news-room/fact-sheets/detail/the-top-10-causes-of-death> (visited on 10/04/2021).
- [11] National Heart and Lung and Blood Institute and National Institute of Diabetes and Digestive and Kidney Diseases; National Institutes of Health; U.S. Department of Health and Human Services, *Clinical guidelines on the identification, evaluation, and treatment of overweight and obesity in adults: the evidence report*, 98-4083. NIH Publication, 1998.
- [12] National Heart and Lung and Blood Institute; National Institutes of Health; U.S. Department of Health and Human Services, *Managing Overweight and Obesity in Adults Systematic Evidence Review From the Obesity Expert Panel*, 2013. 2013.
- [13] World Health Organisation, *Noncommunicable diseases: Risk factors*. [Online]. Available: <https://www.who.int/data/gho/data/themes/topics/topic-details/GHO/ncd-risk-factors> (visited on 14/04/2021).
- [14] S. Brandstaeter, S. L. Fuchs, R. C. Aydin and C. J. Cyron, ‘Mechanics of the stomach: A review of an emerging field of biomechanics’, *GAMM-Mitteilungen*, vol. 42, no. 3, e201900001, 2019. DOI: [10.1002/gamm.201900001](https://doi.org/10.1002/gamm.201900001).
- [15] T. G. Trucano, L. P. Swiler, T. Igusa, W. L. Oberkampf and M. Pilch, ‘Calibration, validation, and sensitivity analysis: What’s what’, *Reliability Engineering and System Safety*, vol. 91, no. 10-11, pp. 1331–1357, 2006. DOI: [10.1016/j.res.2005.11.031](https://doi.org/10.1016/j.res.2005.11.031).
- [16] C. A. Taylor, M. T. Draney, J. P. Ku, D. Parker, B. N. Steele, K. Wang and C. K. Zarins, ‘Predictive Medicine: Computational Techniques in Therapeutic Decision-Making’, *Computer Aided Surgery*, vol. 4, no. 5, pp. 231–247, 1999. DOI: [10.3109/10929089909148176](https://doi.org/10.3109/10929089909148176).
- [17] V. G. Eck, W. P. Donders, J. Sturdy, J. Feinberg, T. Delhaas, L. R. Hellevik and W. Huberts, ‘A guide to uncertainty quantification and sensitivity analysis for cardiovascular applications’, *International Journal for Numerical Methods in Biomedical Engineering*, vol. 32, no. 8, e02755, 2016. DOI: [10.1002/cnm.2755](https://doi.org/10.1002/cnm.2755).
- [18] S. Roccabianca, C. A. Figueroa, G. Tellides and J. D. Humphrey, ‘Quantification of regional differences in aortic stiffness in the aging human’, *Journal of the Mechanical Behavior of Biomedical Materials*, vol. 29, pp. 618–634, 2014. DOI: [10.1016/j.jmbbm.2013.01.026](https://doi.org/10.1016/j.jmbbm.2013.01.026).
- [19] J. Biehler, M. W. Gee and W. A. Wall, ‘Towards efficient uncertainty quantification in complex and large-scale biomechanical problems based on a Bayesian multi-fidelity scheme’, *Biomechanics and Modeling in Mechanobiology*, vol. 14, no. 3, pp. 489–513, 2015. DOI: [10.1007/s10237-014-0618-0](https://doi.org/10.1007/s10237-014-0618-0).
- [20] J. S. Tran, D. E. Schiavazzi, A. M. Kahn and A. L. Marsden, ‘Uncertainty quantification of simulated biomechanical stimuli in coronary artery bypass grafts’, *Computer Methods in Applied Mechanics and Engineering*, vol. 345, pp. 402–428, 2019. DOI: [10.1016/j.cma.2018.10.024](https://doi.org/10.1016/j.cma.2018.10.024).

-
- [21] J. Biehler, ‘Efficient Uncertainty Quantification for Large-Scale Biomechanical Models Using a Bayesian Multi-Fidelity Approach’, Dissertation, Technical University of Munich, 2016. [Online]. Available: <http://nbn-resolving.de/urn/resolver.pl?urn:nbn:de:bvb:91-diss-20161215-1294756-1-1>.
- [22] A. Quaglino, S. Pezzuto, P. S. Koutsourelakis, A. Auricchio and R. Krause, ‘Fast uncertainty quantification of activation sequences in patient-specific cardiac electrophysiology meeting clinical time constraints’, *International Journal for Numerical Methods in Biomedical Engineering*, vol. 34, no. 7, e2985, 2018. DOI: [10.1002/cnm.2985](https://doi.org/10.1002/cnm.2985).
- [23] A. Saltelli, K. Aleksankina, W. Becker, P. Fennell, F. Ferretti, N. Holst, S. Li and Q. Wu, ‘Why so many published sensitivity analyses are false: A systematic review of sensitivity analysis practices’, *Environmental Modelling and Software*, vol. 114, pp. 29–39, 2019. DOI: [10.1016/j.envsoft.2019.01.012](https://doi.org/10.1016/j.envsoft.2019.01.012).
- [24] T. Sullivan, *Introduction to Uncertainty Quantification*, S. Antman, L. Greengard and P. Holmes, Eds., ser. Texts in Applied Mathematics. Cham: Springer International Publishing, 2015, vol. 63. DOI: [10.1007/978-3-319-23395-6](https://doi.org/10.1007/978-3-319-23395-6).
- [25] R. Ghanem, H. Owhadi and D. Higdon, *Handbook of uncertainty quantification*, R. Ghanem, D. Higdon and H. Owhadi, Eds. Cham: Springer International Publishing, 2017, pp. 1–2053. DOI: [10.1007/978-3-319-12385-1](https://doi.org/10.1007/978-3-319-12385-1).
- [26] S. Razavi *et al.*, ‘The Future of Sensitivity Analysis: An essential discipline for systems modeling and policy support’, *Environmental Modelling and Software*, vol. 137, no. December 2020, p. 104 954, 2021. DOI: [10.1016/j.envsoft.2020.104954](https://doi.org/10.1016/j.envsoft.2020.104954).
- [27] E. Qian, B. Peherstorfer, D. O’Malley, V. V. Vesselinov and K. Willcox, ‘Multifidelity monte carlo estimation of variance and sensitivity indices’, *SIAM-ASA Journal on Uncertainty Quantification*, vol. 6, no. 2, pp. 683–706, 2018. DOI: [10.1137/17M1151006](https://doi.org/10.1137/17M1151006).
- [28] J. Nitzler, J. Biehler, N. Fehn, P. S. Koutsourelakis and W. A. Wall, ‘A generalized probabilistic learning approach for multi-fidelity uncertainty propagation in complex physical simulations’, *arXiv*, arXiv:2001.02892, 2020.
- [29] J. Humphrey, *Cardiovascular Solid Mechanics*. Springer New York, 2002. DOI: [10.1007/978-0-387-21576-1](https://doi.org/10.1007/978-0-387-21576-1).
- [30] C. J. Cyron and J. D. Humphrey, ‘Vascular homeostasis and the concept of mechanobiological stability’, *International Journal of Engineering Science*, vol. 85, pp. 203–223, 2014. DOI: [10.1016/j.jengsci.2014.08.003](https://doi.org/10.1016/j.jengsci.2014.08.003).
- [31] C. J. Cyron, J. S. Wilson and J. D. Humphrey, ‘Mechanobiological stability: a new paradigm to understand the enlargement of aneurysms?’, *Journal of The Royal Society Interface*, vol. 11, no. 100, p. 20 140 680, 2014. DOI: [10.1098/rsif.2014.0680](https://doi.org/10.1098/rsif.2014.0680).
- [32] F. A. Braeu, A. Seitz, R. C. Aydin and C. J. Cyron, ‘Homogenized constrained mixture models for anisotropic volumetric growth and remodeling’, *Biomechanics and Modeling in Mechanobiology*, vol. 16, no. 3, pp. 889–906, 2017. DOI: [10.1007/s10237-016-0859-1](https://doi.org/10.1007/s10237-016-0859-1).

- [33] F. A. Braeu, R. C. Aydin and C. J. Cyron, ‘Anisotropic stiffness and tensional homeostasis induce a natural anisotropy of volumetric growth and remodeling in soft biological tissues’, *Biomechanics and Modeling in Mechanobiology*, vol. 18, no. 2, pp. 327–345, 2019. DOI: [10.1007/s10237-018-1084-x](https://doi.org/10.1007/s10237-018-1084-x).
- [34] J. D. Humphrey and K. R. Rajagopal, ‘A Constrained Mixture Model For Growth And Remodeling Of Soft Tissue’, *Mathematical Models and Methods in Applied Sciences*, vol. 12, no. 3, pp. 407–430, 2002. DOI: [10.1142/S0218202502001714](https://doi.org/10.1142/S0218202502001714).
- [35] P. N. Watton, N. A. Hill and M. Heil, ‘A mathematical model for the growth of the abdominal aortic aneurysm’, *Biomechanics and Modeling in Mechanobiology*, vol. 3, no. 2, pp. 98–113, 2004. DOI: [10.1007/s10237-004-0052-9](https://doi.org/10.1007/s10237-004-0052-9).
- [36] P. N. Watton and N. A. Hill, ‘Evolving mechanical properties of a model of abdominal aortic aneurysm’, *Biomechanics and Modeling in Mechanobiology*, vol. 8, no. 1, pp. 25–42, 2009. DOI: [10.1007/s10237-007-0115-9](https://doi.org/10.1007/s10237-007-0115-9).
- [37] C. A. Figueroa, S. Baek, C. A. Taylor and J. D. Humphrey, ‘A computational framework for fluid–solid–growth modeling in cardiovascular simulations’, *Computer Methods in Applied Mechanics and Engineering*, vol. 198, no. 45–46, pp. 3583–3602, 2009. DOI: [10.1016/j.cma.2008.09.013](https://doi.org/10.1016/j.cma.2008.09.013).
- [38] I. Karšaj, J. Sorić and J. D. Humphrey, ‘A 3-D framework for arterial growth and remodeling in response to altered hemodynamics’, *International Journal of Engineering Science*, vol. 48, no. 11, pp. 1357–1372, 2010. DOI: [10.1016/j.ijengsci.2010.06.033](https://doi.org/10.1016/j.ijengsci.2010.06.033).
- [39] A. Sheidaei, S. C. Hunley, S. Zeinali-Davarani, L. G. Raguin and S. Baek, ‘Simulation of abdominal aortic aneurysm growth with updating hemodynamic loads using a realistic geometry’, *Medical Engineering and Physics*, vol. 33, no. 1, pp. 80–88, 2011. DOI: [10.1016/j.medengphy.2010.09.012](https://doi.org/10.1016/j.medengphy.2010.09.012).
- [40] I. Karšaj and J. D. Humphrey, ‘A multilayered wall model of arterial growth and remodeling’, *Mechanics of Materials*, vol. 44, pp. 110–119, 2012. DOI: [10.1016/j.mechmat.2011.05.006](https://doi.org/10.1016/j.mechmat.2011.05.006).
- [41] S. Zeinali-Davarani and S. Baek, ‘Medical image-based simulation of abdominal aortic aneurysm growth’, *Mechanics Research Communications*, vol. 42, pp. 107–117, 2012. DOI: [10.1016/j.mechrescom.2012.01.008](https://doi.org/10.1016/j.mechrescom.2012.01.008).
- [42] J. S. Wilson, S. Baek and J. D. Humphrey, ‘Importance of initial aortic properties on the evolving regional anisotropy, stiffness and wall thickness of human abdominal aortic aneurysms’, *Journal of the Royal Society Interface*, vol. 9, no. 74, pp. 2047–2058, 2012. DOI: [10.1098/rsif.2012.0097](https://doi.org/10.1098/rsif.2012.0097).
- [43] J. S. Wilson, L. Virag, P. Di Achille, I. Karšaj and J. D. Humphrey, ‘Biochemomechanics of intraluminal thrombus in abdominal aortic aneurysms’, *Journal of Biomechanical Engineering*, vol. 135, no. 2, pp. 1–14, 2013. DOI: [10.1115/1.4023437](https://doi.org/10.1115/1.4023437).
- [44] L. Virag, J. S. Wilson, J. D. Humphrey and I. Karšaj, ‘A Computational Model of Biochemomechanical Effects of Intraluminal Thrombus on the Enlargement of Abdominal Aortic Aneurysms’, *Annals of Biomedical Engineering*, vol. 43, no. 12, pp. 2852–2867, 2015. DOI: [10.1007/s10439-015-1354-z](https://doi.org/10.1007/s10439-015-1354-z).

-
- [45] M. Farsad, S. Zeinali-Davarani, J. Choi and S. Baek, ‘Computational growth and remodeling of abdominal aortic aneurysms constrained by the spine’, *Journal of Biomechanical Engineering*, vol. 137, no. 9, pp. 1–12, 2015. DOI: [10.1115/1.4031019](https://doi.org/10.1115/1.4031019).
- [46] C. J. Cyron, R. C. Aydin and J. D. Humphrey, ‘A homogenized constrained mixture (and mechanical analog) model for growth and remodeling of soft tissue’, *Biomechanics and Modeling in Mechanobiology*, vol. 15, no. 6, pp. 1389–1403, 2016. DOI: [10.1007/s10237-016-0770-9](https://doi.org/10.1007/s10237-016-0770-9).
- [47] L. Virag, J. S. Wilson, J. D. Humphrey and I. Karšaj, ‘Potential biomechanical roles of risk factors in the evolution of thrombus-laden abdominal aortic aneurysms’, *International Journal for Numerical Methods in Biomedical Engineering*, vol. 33, no. 12, pp. 1–18, 2017. DOI: [10.1002/cnm.2893](https://doi.org/10.1002/cnm.2893).
- [48] A. Grytsan, T. S. Eriksson, P. N. Watton and T. Gasser, ‘Growth description for Vessel Wall adaptation: A Thick-Walled mixture model of abdominal aortic aneurysm evolution’, *Materials*, vol. 10, no. 9, pp. 1–19, 2017. DOI: [10.3390/ma10090994](https://doi.org/10.3390/ma10090994).
- [49] N. Horvat, L. Virag, G. A. Holzapfel, J. Sorić and I. Karšaj, ‘A finite element implementation of a growth and remodeling model for soft biological tissues: Verification and application to abdominal aortic aneurysms’, *Computer Methods in Applied Mechanics and Engineering*, vol. 352, pp. 586–605, 2019. DOI: [10.1016/j.cma.2019.04.041](https://doi.org/10.1016/j.cma.2019.04.041).
- [50] S. J. Mousavi, S. Farzaneh and S. Avril, ‘Patient-specific predictions of aneurysm growth and remodeling in the ascending thoracic aorta using the homogenized constrained mixture model’, *Biomechanics and Modeling in Mechanobiology*, vol. 18, no. 6, pp. 1895–1913, 2019. DOI: [10.1007/s10237-019-01184-8](https://doi.org/10.1007/s10237-019-01184-8).
- [51] S. Brandstaeter, A. Gizzi, S. L. Fuchs, A. M. Gebauer, R. C. Aydin and C. J. Cyron, ‘Computational model of gastric motility with active-strain electromechanics’, *ZAMM - Journal of Applied Mathematics and Mechanics / Zeitschrift für Angewandte Mathematik und Mechanik*, vol. 98, no. 12, pp. 2177–2197, 2018. DOI: [10.1002/zamm.201800166](https://doi.org/10.1002/zamm.201800166).
- [52] S. Brandstaeter, S. L. Fuchs, J. Biehler, R. C. Aydin, W. A. Wall and C. J. Cyron, ‘Global Sensitivity Analysis of a Homogenized Constrained Mixture Model of Arterial Growth and Remodeling’, *Journal of Elasticity*, vol. 145, pp. 191–221, 2021. DOI: [10.1007/s10659-021-09833-9](https://doi.org/10.1007/s10659-021-09833-9).
- [53] *BACI: A Comprehensive Multi-Physics Simulation Framework*, 2021. [Online]. Available: <https://baci.pages.gitlab.lrz.de/website>.
- [54] A.-T. Vuong, ‘A Computational Approach to Coupled Poroelastic Media Problems’, Dissertation, Technical University of Munich, 2016. [Online]. Available: <http://nbn-resolving.de/urn/resolver.pl?urn:nbn:de:bvb:91-diss-20161214-1341399-1-5>.
- [55] P. W. Farah, ‘Mortar Methods for Computational Contact Mechanics Including Wear and General Volume Coupled Problems’, Dissertation, Technical University of Munich, 2018. [Online]. Available: <http://nbn-resolving.de/urn/resolver.pl?urn:nbn:de:bvb:91-diss-20170411-1363363-1-5>.

- [56] F. A. Bräu, ‘Three-dimensional Homogenized Constrained Mixture Model of Anisotropic Vascular Growth and Remodeling’, Dissertation, Technical University of Munich, 2019, p. 89. [Online]. Available: <http://nbn-resolving.de/urn/resolver.pl?urn:nbn:de:bvb:91-diss-20191010-1483186-1-5>.
- [57] J. Biehler, J. Nitzler, S. Brandstaeter, W. A. Wall and V. Gravemeier, *QUEENS – A Software Platform for Uncertainty Quantification, Physics-Informed Machine Learning, Bayesian Optimization, Inverse Problems and Simulation Analytics: User Guide*. AdCo Engineering GW GmbH, 2021.
- [58] J. Herman and W. Usher, ‘SALib: An open-source Python library for Sensitivity Analysis’, *The Journal of Open Source Software*, vol. 2, no. 9, p. 97, 2017. DOI: [10.21105/joss.00097](https://doi.org/10.21105/joss.00097).
- [59] H. Stachowiak, *Allgemeine Modelltheorie*. Wien: Springer-Verlag Wien, 1973.
- [60] K. Rogers, *Scientific modeling*. [Online]. Available: <https://www.britannica.com/science/scientific-modeling>.
- [61] A. Saltelli, M. Ratto, T. Andres, F. Campolongo, J. Cariboni, D. Gatelli, M. Saisana and S. Tarantola, *Global Sensitivity Analysis. The Primer*. Chichester, UK: John Wiley & Sons, Ltd, 2008, pp. 1–292. DOI: [10.1002/9780470725184](https://doi.org/10.1002/9780470725184).
- [62] F. Pianosi, K. Beven, J. Freer, J. W. Hall, J. Rougier, D. B. Stephenson and T. Wagener, ‘Sensitivity analysis of environmental models: A systematic review with practical workflow’, *Environmental Modelling & Software*, vol. 79, pp. 214–232, 2016. DOI: [10.1016/j.envsoft.2016.02.008](https://doi.org/10.1016/j.envsoft.2016.02.008).
- [63] R. C. Smith, *Uncertainty Quantification: Theory, Implementation, and Applications*, D. Estep, Ed. Philadelphia, Pa.: SIAM, 2014.
- [64] G. Qian and A. Mahdi, ‘Sensitivity analysis methods in the biomedical sciences’, *Mathematical Biosciences*, vol. 323, no. August 2019, p. 108 306, 2020. DOI: [10.1016/j.mbs.2020.108306](https://doi.org/10.1016/j.mbs.2020.108306).
- [65] E. Borgonovo and E. Plischke, ‘Sensitivity analysis: A review of recent advances’, *European Journal of Operational Research*, vol. 248, no. 3, pp. 869–887, 2016. DOI: [10.1016/j.ejor.2015.06.032](https://doi.org/10.1016/j.ejor.2015.06.032).
- [66] B. Sudret, S. Marelli and J. Wiart, ‘Surrogate models for uncertainty quantification: An overview’, in *2017 11th European Conference on Antennas and Propagation (EUCAP)*, IEEE, 2017, pp. 793–797. DOI: [10.23919/EuCAP.2017.7928679](https://doi.org/10.23919/EuCAP.2017.7928679).
- [67] G. Box, ‘Robustness in the Strategy of Scientific Model Building’, in *Robustness in Statistics*, Elsevier, 1979, pp. 201–236. DOI: [10.1016/B978-0-12-438150-6.50018-2](https://doi.org/10.1016/B978-0-12-438150-6.50018-2).
- [68] G. E. Box and N. R. Draper, *Empirical Model-Building and Response Surfaces*, ser. Wiley Series in Probability and Statistics. Wiley, 1987.
- [69] M. C. Kennedy and A. O’Hagan, ‘Bayesian calibration of computer models’, *Journal of the Royal Statistical Society: Series B (Statistical Methodology)*, vol. 63, no. 3, pp. 425–464, 2001. DOI: [10.1111/1467-9868.00294](https://doi.org/10.1111/1467-9868.00294).

- [70] A. O'Hagan and J. E. Oakley, 'Probability is perfect, but we can't elicit it perfectly', *Reliability Engineering and System Safety*, vol. 85, no. 1-3, pp. 239–248, 2004. DOI: [10.1016/j.res.2004.03.014](https://doi.org/10.1016/j.res.2004.03.014).
- [71] G. E. Box, 'Science and statistics', *Journal of the American Statistical Association*, vol. 71, no. 356, pp. 791–799, 1976. DOI: [10.1080/01621459.1976.10480949](https://doi.org/10.1080/01621459.1976.10480949).
- [72] A. Saltelli, 'A short comment on statistical versus mathematical modelling', *Nature Communications*, vol. 10, no. 1, p. 3870, 2019. DOI: [10.1038/s41467-019-11865-8](https://doi.org/10.1038/s41467-019-11865-8).
- [73] G. A. Holzapfel, *Nonlinear Solid Mechanics: A Continuum Approach for Engineering*. Wiley, 2000.
- [74] C. Truesdell, W. Noll, C. Truesdell and W. Noll, *The Non-Linear Field Theories of Mechanics*. 2004, pp. 1–579. DOI: [10.1007/978-3-662-10388-3_1](https://doi.org/10.1007/978-3-662-10388-3_1).
- [75] A. Popp, 'Mortar Methods for Computational Contact Mechanics and General Interface Problems', Dissertation, Technical University of Munich, 2012. [Online]. Available: <http://nbn-resolving.de/urn/resolver.pl?urn:nbn:de:bvb:91-diss-20120917-1109994-0-1>.
- [76] J. Keener and J. Sneyd, *Mathematical Physiology I: Cellular Physiology*, S. Antman, J. Marsden and L. Sirovich, Eds., ser. Interdisciplinary Applied Mathematics. New York, NY: Springer New York, 2009, vol. 8/1. DOI: [10.1007/978-0-387-75847-3](https://doi.org/10.1007/978-0-387-75847-3).
- [77] J. Keener and J. Sneyd, *Mathematical Physiology II: Systems Physiology*, S. Antman, J. Marsden and L. Sirovich, Eds., ser. Interdisciplinary Applied Mathematics. Springer New York, 2009, vol. 8/2. DOI: [10.1007/978-0-387-79388-7](https://doi.org/10.1007/978-0-387-79388-7).
- [78] P. C. Franzone, L. F. Pavarino and S. Scacchi, *Mathematical Cardiac Electrophysiology*, 1st ed., ser. MS&A 1. Springer International Publishing, 2014, vol. 13. DOI: [10.1007/978-3-319-04801-7](https://doi.org/10.1007/978-3-319-04801-7).
- [79] P. Wriggers, *Nonlinear Finite Element Methods*. Berlin, Heidelberg: Springer Berlin Heidelberg, 2008. DOI: [10.1007/978-3-540-71001-1](https://doi.org/10.1007/978-3-540-71001-1).
- [80] K.-J. Bathe, *Finite Element Procedures*. Prentice Hall, Pearson Education, Inc, 2014.
- [81] R. Brown, R. Prajapati, D. McGrouther, I. Yannas and M. Eastwood, 'Tensional homeostasis in dermal fibroblasts: Mechanical responses to mechanical loading in three-dimensional substrates', *Journal of Cellular Physiology*, vol. 175, no. 3, pp. 323–332, 1998. DOI: [10.1002/\(SICI\)1097-4652\(199806\)175:3<323::AID-JCP10>3.0.CO;2-6](https://doi.org/10.1002/(SICI)1097-4652(199806)175:3<323::AID-JCP10>3.0.CO;2-6).
- [82] J. D. Humphrey, E. R. Dufresne and M. A. Schwartz, 'Mechanotransduction and extracellular matrix homeostasis', *Nature Reviews Molecular Cell Biology*, vol. 15, no. 12, pp. 802–812, 2014. DOI: [10.1038/nrm3896](https://doi.org/10.1038/nrm3896).
- [83] J. F. Eichinger, D. Paukner, J. M. Szafron, R. C. Aydin, J. D. Humphrey and C. J. Cyron, 'Computer-controlled biaxial bioreactor for investigating cell-mediated homeostasis in tissue equivalents', *Journal of Biomechanical Engineering*, vol. 142, no. 7, pp. 1–8, 2020. DOI: [10.1115/1.4046201](https://doi.org/10.1115/1.4046201).

- [84] J. D. Humphrey and M. Latorre, ‘Biomechanics and Mechanobiology of Extracellular Matrix Remodeling’, in *Multi-scale Extracellular Matrix Mechanics and Mechanobiology. Studies in Mechanobiology, Tissue Engineering and Biomaterials*, Z. Y., Ed., Cham: Springer, 2020, pp. 1–20. DOI: [10.1007/978-3-030-20182-1_1](https://doi.org/10.1007/978-3-030-20182-1_1).
- [85] T. Matsumoto and K. Hayashi, ‘Response of Arterial Wall to Hypertension and Residual Stress’, in *Biomechanics: Functional Adaptation and Remodeling*, K. Hayashi, A. Kamiya and K. Ono, Eds. Tokyo: Springer Japan, 1996, pp. 93–119.
- [86] M. Latorre and J. D. Humphrey, ‘Modeling mechano-driven and immuno-mediated aortic maladaptation in hypertension’, *Biomechanics and Modeling in Mechanobiology*, vol. 17, no. 5, pp. 1497–1511, 2018. DOI: [10.1007/s10237-018-1041-8](https://doi.org/10.1007/s10237-018-1041-8).
- [87] E. L. Chaikof, R. L. Dalman, M. K. Eskandari, B. M. Jackson, W. A. Lee, M. A. Mansour, T. M. Mastracci, M. Mell, M. H. Murad, L. L. Nguyen, G. S. Oderich, M. S. Patel, M. L. Schermerhorn and B. W. Starnes, ‘The Society for Vascular Surgery practice guidelines on the care of patients with an abdominal aortic aneurysm’, *Journal of Vascular Surgery*, vol. 67, no. 1, 2–77.e2, 2018. DOI: [10.1016/j.jvs.2017.10.044](https://doi.org/10.1016/j.jvs.2017.10.044).
- [88] D. G. Cacuci, *Sensitivity and Uncertainty Analysis, Volume I*. Chapman and Hall/CRC, 2003. DOI: [10.1201/9780203498798](https://doi.org/10.1201/9780203498798).
- [89] D. G. Cacuci, M. Ionescu-Bujor and I. M. Navon, *Sensitivity and Uncertainty Analysis, Volume II*. CRC Press, 2005. DOI: [10.1201/9780203483572](https://doi.org/10.1201/9780203483572).
- [90] B. Iooss and P. Lemaître, ‘A Review on Global Sensitivity Analysis Methods’, in *Uncertainty Management in Simulation-Optimization of Complex Systems: Algorithms and Applications*, G. Dellino and C. Meloni, Eds. Boston, MA: Springer US, 2015, pp. 101–122. DOI: [10.1007/978-1-4899-7547-8_5](https://doi.org/10.1007/978-1-4899-7547-8_5).
- [91] T. J. Santner, B. J. Williams and W. I. Notz, *The Design and Analysis of Computer Experiments*, ser. Springer Series in Statistics. New York, NY: Springer New York, 2018, pp. 1–436. DOI: [10.1007/978-1-4939-8847-1](https://doi.org/10.1007/978-1-4939-8847-1).
- [92] M. T. Wentworth, R. C. Smith and H. T. Banks, ‘Parameter selection and verification techniques based on global sensitivity analysis illustrated for an HIV model’, *SIAM-ASA Journal on Uncertainty Quantification*, vol. 4, no. 1, pp. 266–297, 2016. DOI: [10.1137/15M1008245](https://doi.org/10.1137/15M1008245).
- [93] D. Douglas-Smith, T. Iwanaga, B. F. Croke and A. J. Jakeman, ‘Certain trends in uncertainty and sensitivity analysis: An overview of software tools and techniques’, *Environmental Modelling and Software*, vol. 124, no. September 2019, p. 104588, 2020. DOI: [10.1016/j.envsoft.2019.104588](https://doi.org/10.1016/j.envsoft.2019.104588).
- [94] B. Iooss and C. Prieur, ‘Shapley effects for sensitivity analysis with correlated inputs: comparisons with Sobol’ indices, numerical estimation and applications’, *International Journal for Uncertainty Quantification*, vol. 9, no. 5, pp. 493–514, 2019. DOI: [10.1615/Int.J.UncertaintyQuantification.2019028372](https://doi.org/10.1615/Int.J.UncertaintyQuantification.2019028372).

-
- [95] B. Iooss and A. Saltelli, ‘Introduction to Sensitivity Analysis’, in *Handbook of Uncertainty Quantification*, R. Ghanem, H. Owhadi and D. Higdon, Eds., Cham: Springer International Publishing, 2017, ch. 31, pp. 1103–1122. DOI: [10.1007/978-3-319-12385-1_31](https://doi.org/10.1007/978-3-319-12385-1_31).
- [96] M. Nodet and A. Vidard, ‘Variational Methods’, in *Handbook of Uncertainty Quantification*, R. Ghanem, H. Owhadi and D. Higdon, Eds., Cham: Springer International Publishing, 2017, ch. 32, pp. 1123–1142. DOI: [10.1007/978-3-319-12385-1_32](https://doi.org/10.1007/978-3-319-12385-1_32).
- [97] D. Hwang, D. W. Byun and M. Talat Odman, ‘An automatic differentiation technique for sensitivity analysis of numerical advection schemes in air quality models’, *Atmospheric Environment*, vol. 31, no. 6, pp. 879–888, 1997. DOI: [10.1016/S1352-2310\(96\)00240-3](https://doi.org/10.1016/S1352-2310(96)00240-3).
- [98] C. P. Robert and G. Casella, *Monte Carlo Statistical Methods*. Springer New York, 2004. DOI: [10.1007/978-1-4757-4145-2](https://doi.org/10.1007/978-1-4757-4145-2).
- [99] M. D. McKay, R. J. Beckman and W. J. Conover, ‘A Comparison of Three Methods for Selecting Values of Input Variables in the Analysis of Output from a Computer Code’, *Technometrics*, vol. 21, no. 2, p. 239, 1979. DOI: [10.2307/1268522](https://doi.org/10.2307/1268522).
- [100] J. Helton and F. Davis, ‘Latin hypercube sampling and the propagation of uncertainty in analyses of complex systems’, *Reliability Engineering & System Safety*, vol. 81, no. 1, pp. 23–69, 2003. DOI: [10.1016/S0951-8320\(03\)00058-9](https://doi.org/10.1016/S0951-8320(03)00058-9).
- [101] R. Sheikholeslami and S. Razavi, ‘Progressive Latin Hypercube Sampling: An efficient approach for robust sampling-based analysis of environmental models’, *Environmental Modelling & Software*, vol. 93, pp. 109–126, 2017. DOI: [10.1016/j.envsoft.2017.03.010](https://doi.org/10.1016/j.envsoft.2017.03.010).
- [102] I. Sobol’, ‘On the distribution of points in a cube and the approximate evaluation of integrals’, *USSR Computational Mathematics and Mathematical Physics*, vol. 7, no. 4, pp. 86–112, 1967. DOI: [10.1016/0041-5553\(67\)90144-9](https://doi.org/10.1016/0041-5553(67)90144-9).
- [103] S. Joe and F. Y. Kuo, ‘Remark on Algorithm 659: Implementing Sobol’s quasirandom sequence generator’, *ACM Transactions on Mathematical Software*, vol. 29, no. 1, pp. 49–57, 2003. DOI: [10.1145/641876.641879](https://doi.org/10.1145/641876.641879).
- [104] S. Joe and F. Y. Kuo, ‘Constructing Sobol Sequences with Better Two-Dimensional Projections’, *SIAM Journal on Scientific Computing*, vol. 30, no. 5, pp. 2635–2654, 2008. DOI: [10.1137/070709359](https://doi.org/10.1137/070709359).
- [105] I. M. Sobol’, D. Asotsky, A. Kreinin and S. Kucherenko, ‘Construction and Comparison of High-Dimensional Sobol’ Generators’, *Wilmott*, vol. 2011, no. 56, pp. 64–79, 2011. DOI: [10.1002/wilm.10056](https://doi.org/10.1002/wilm.10056).
- [106] S. Kucherenko, D. Albrecht and A. Saltelli, ‘Exploring multi-dimensional spaces: a Comparison of Latin Hypercube and Quasi Monte Carlo Sampling Techniques’, *arXiv e-prints*, arXiv:1505.02350, 2015. [Online]. Available: <http://arxiv.org/abs/1505.02350>.
- [107] S. Lo Piano, F. Ferretti, A. Puy, D. Albrecht and A. Saltelli, ‘Variance-based sensitivity analysis: The quest for better estimators and designs between explorativity and economy’, *Reliability Engineering and System Safety*, vol. 206, p. 107 300, 2021. DOI: [10.1016/j.res.2020.107300](https://doi.org/10.1016/j.res.2020.107300).

- [108] D. C. Woods and S. M. Lewis, ‘Design of Experiments for Screening’, in *Handbook of Uncertainty Quantification*, R. Ghanem, H. Owhadi and D. Higdon, Eds., Cham: Springer International Publishing, 2017, ch. 33, pp. 1143–1185. DOI: [10.1007/978-3-319-12385-1_33](https://doi.org/10.1007/978-3-319-12385-1_33).
- [109] M. D. Morris, ‘Factorial Sampling Plans for Preliminary Computational Experiments’, *Technometrics*, vol. 33, no. 2, pp. 161–174, 1991. DOI: [10.1080/00401706.1991.10484804](https://doi.org/10.1080/00401706.1991.10484804).
- [110] F. Campolongo, A. Saltelli and J. Cariboni, ‘From screening to quantitative sensitivity analysis. A unified approach’, *Computer Physics Communications*, vol. 182, no. 4, pp. 978–988, 2011. DOI: [10.1016/j.cpc.2010.12.039](https://doi.org/10.1016/j.cpc.2010.12.039).
- [111] I. M. Sobol, ‘On sensitivity estimation for nonlinear mathematical models’, *Matematicheskoe Modelirovanie*, vol. 2, no. 1, pp. 112–118, 1990.
- [112] I. M. Sobol, ‘Sensitivity Estimates for Nonlinear Mathematical Models’, *Math. Modeling Comput. Exp.*, vol. 1, no. 4, pp. 407–414, 1993.
- [113] T. Homma and A. Saltelli, ‘Importance measures in global sensitivity analysis of nonlinear models’, *Reliability Engineering and System Safety*, vol. 52, no. 1, pp. 1–17, 1996. DOI: [10.1016/0951-8320\(96\)00002-6](https://doi.org/10.1016/0951-8320(96)00002-6).
- [114] P. C. Young, G. M. Hornberger and R. C. Spear, ‘Modeling badly defined systems: some further thoughts’, in *Proceedings SIMSIG Conference, Canberra*, 1978, pp. 24–32.
- [115] R. Spear, ‘Eutrophication in peel inlet—II. Identification of critical uncertainties via generalized sensitivity analysis’, *Water Research*, vol. 14, no. 1, pp. 43–49, 1980. DOI: [10.1016/0043-1354\(80\)90040-8](https://doi.org/10.1016/0043-1354(80)90040-8).
- [116] R. C. Spear, T. M. Grieb and N. Shang, ‘Parameter uncertainty and interaction in complex environmental models’, *Water Resources Research*, vol. 30, no. 11, pp. 3159–3169, 1994. DOI: [10.1029/94WR01732](https://doi.org/10.1029/94WR01732).
- [117] D. M. Hamby, ‘A review of techniques for parameter sensitivity analysis of environmental models’, *Environmental Monitoring and Assessment*, vol. 32, no. 2, pp. 135–154, 1994. DOI: [10.1007/BF00547132](https://doi.org/10.1007/BF00547132).
- [118] F. Sarrazin, F. Pianosi and T. Wagener, ‘Global Sensitivity Analysis of environmental models: Convergence and validation’, *Environmental Modelling and Software*, vol. 79, pp. 135–152, 2016. DOI: [10.1016/j.envsoft.2016.02.005](https://doi.org/10.1016/j.envsoft.2016.02.005).
- [119] E. Borgonovo, ‘A new uncertainty importance measure’, *Reliability Engineering & System Safety*, vol. 92, no. 6, pp. 771–784, 2007. DOI: [10.1016/j.res.2006.04.015](https://doi.org/10.1016/j.res.2006.04.015).
- [120] C. K. Park and K.-I. Ahn, ‘A new approach for measuring uncertainty importance and distributional sensitivity in probabilistic safety assessment’, *Reliability Engineering & System Safety*, vol. 46, no. 3, pp. 253–261, 1994. DOI: [10.1016/0951-8320\(94\)90119-8](https://doi.org/10.1016/0951-8320(94)90119-8).
- [121] B. Krykacz-Hausmann, ‘Epistemic sensitivity analysis based on the concept of entropy’, in *SAMO 2001: Third International Symposium on Sensitivity Analysis of Model Output*, Madrid: Editorial CIEMAT, 2001, pp. 53–57.

-
- [122] H. Liu, W. Chen and A. Sudjianto, ‘Relative Entropy Based Method for Probabilistic Sensitivity Analysis in Engineering Design’, *Journal of Mechanical Design*, vol. 128, no. 2, p. 326, 2006. DOI: [10.1115/1.2159025](https://doi.org/10.1115/1.2159025).
- [123] F. Pianosi and T. Wagener, ‘A simple and efficient method for global sensitivity analysis based on cumulative distribution functions’, *Environmental Modelling & Software*, vol. 67, pp. 1–11, 2015. DOI: [10.1016/j.envsoft.2015.01.004](https://doi.org/10.1016/j.envsoft.2015.01.004).
- [124] F. Pianosi and T. Wagener, ‘Distribution-based sensitivity analysis from a generic input-output sample’, *Environmental Modelling & Software*, vol. 108, pp. 197–207, 2018. DOI: [10.1016/j.envsoft.2018.07.019](https://doi.org/10.1016/j.envsoft.2018.07.019).
- [125] S. Kucherenko, M. Rodriguez-Fernandez, C. Pantelides and N. Shah, ‘Monte Carlo evaluation of derivative-based global sensitivity measures’, *Reliability Engineering & System Safety*, vol. 94, no. 7, pp. 1135–1148, 2009. DOI: [10.1016/j.res.2008.05.006](https://doi.org/10.1016/j.res.2008.05.006).
- [126] I. Sobol’ and S. Kucherenko, ‘Derivative based global sensitivity measures and their link with global sensitivity indices’, *Mathematics and Computers in Simulation*, vol. 79, no. 10, pp. 3009–3017, 2009. DOI: [10.1016/j.matcom.2009.01.023](https://doi.org/10.1016/j.matcom.2009.01.023).
- [127] S. Razavi and H. V. Gupta, ‘A new framework for comprehensive, robust, and efficient global sensitivity analysis: 1. Theory’, *Water Resources Research*, vol. 52, no. 1, pp. 423–439, 2016. DOI: [10.1002/2015WR017558](https://doi.org/10.1002/2015WR017558).
- [128] S. Razavi and H. V. Gupta, ‘A new framework for comprehensive, robust, and efficient global sensitivity analysis: 2. Application’, *Water Resources Research*, vol. 52, no. 1, pp. 440–455, 2016. DOI: [10.1002/2015WR017559](https://doi.org/10.1002/2015WR017559).
- [129] R. Sheikholeslami and S. Razavi, ‘A Fresh Look at Variography: Measuring Dependence and Possible Sensitivities Across Geophysical Systems From Any Given Data’, *Geophysical Research Letters*, vol. 47, no. 20, 2020. DOI: [10.1029/2020GL089829](https://doi.org/10.1029/2020GL089829).
- [130] A. B. Owen, ‘Sobol’ Indices and Shapley Value’, *SIAM/ASA Journal on Uncertainty Quantification*, vol. 2, no. 1, pp. 245–251, 2014. DOI: [10.1137/130936233](https://doi.org/10.1137/130936233).
- [131] E. Song, B. L. Nelson and J. Staum, ‘Shapley Effects for Global Sensitivity Analysis: Theory and Computation’, *SIAM/ASA Journal on Uncertainty Quantification*, vol. 4, no. 1, pp. 1060–1083, 2016. DOI: [10.1137/15M1048070](https://doi.org/10.1137/15M1048070).
- [132] A. B. Owen and C. Prieur, ‘On Shapley Value for Measuring Importance of Dependent Inputs’, *SIAM/ASA Journal on Uncertainty Quantification*, vol. 5, no. 1, pp. 986–1002, 2017. DOI: [10.1137/16M1097717](https://doi.org/10.1137/16M1097717).
- [133] A. Saltelli, P. Annoni, I. Azzini, F. Campolongo, M. Ratto and S. Tarantola, ‘Variance based sensitivity analysis of model output. Design and estimator for the total sensitivity index’, *Computer Physics Communications*, vol. 181, no. 2, pp. 259–270, 2010. DOI: [10.1016/j.cpc.2009.09.018](https://doi.org/10.1016/j.cpc.2009.09.018).
- [134] S. Kucherenko, O. V. Klymenko and N. Shah, ‘Sobol’ indices for problems defined in non-rectangular domains’, *Reliability Engineering and System Safety*, vol. 167, pp. 218–231, 2017. DOI: [10.1016/j.res.2017.06.001](https://doi.org/10.1016/j.res.2017.06.001).

- [135] A. Saltelli, ‘Making best use of model evaluations to compute sensitivity indices’, *Computer Physics Communications*, vol. 145, no. 2, pp. 280–297, 2002. DOI: [10.1016/S0010-4655\(02\)00280-1](https://doi.org/10.1016/S0010-4655(02)00280-1).
- [136] S. Kucherenko and S. Song, ‘Different numerical estimators for main effect global sensitivity indices’, *Reliability Engineering and System Safety*, vol. 165, no. February, pp. 222–238, 2017. DOI: [10.1016/j.res.2017.04.003](https://doi.org/10.1016/j.res.2017.04.003).
- [137] A. Saltelli and S. Tarantola, ‘On the Relative Importance of Input Factors in Mathematical Models’, *Journal of the American Statistical Association*, vol. 97, no. 459, pp. 702–709, 2002. DOI: [10.1198/016214502388618447](https://doi.org/10.1198/016214502388618447).
- [138] I. M. Sobol, ‘Global sensitivity indices for nonlinear mathematical models and their Monte Carlo estimates’, *Mathematics and Computers in Simulation*, vol. 55, no. 1-3, pp. 271–280, 2001. DOI: [10.1016/S0378-4754\(00\)00270-6](https://doi.org/10.1016/S0378-4754(00)00270-6).
- [139] I. Sobol’, S. Tarantola, D. Gatelli, S. Kucherenko and W. Mauntz, ‘Estimating the approximation error when fixing unessential factors in global sensitivity analysis’, *Reliability Engineering & System Safety*, vol. 92, no. 7, pp. 957–960, 2007. DOI: [10.1016/j.res.2006.07.001](https://doi.org/10.1016/j.res.2006.07.001).
- [140] A. Saltelli and P. Annoni, ‘How to avoid a perfunctory sensitivity analysis’, *Environmental Modelling and Software*, vol. 25, no. 12, pp. 1508–1517, 2010. DOI: [10.1016/j.envsoft.2010.04.012](https://doi.org/10.1016/j.envsoft.2010.04.012).
- [141] A. Janon, T. Klein, A. Lagnoux, M. Nodet and C. Prieur, ‘Asymptotic normality and efficiency of two Sobol index estimators’, *ESAIM: Probability and Statistics*, vol. 18, pp. 342–364, 2014. DOI: [10.1051/ps/2013040](https://doi.org/10.1051/ps/2013040).
- [142] J.-M. Martinez, ‘Analyse de sensibilité globale par décomposition de la variance’, in *Presentation in “Journée des GdR Ondes & Mascot Num”*, Paris: Institut Henri Poincaré, 2011. [Online]. Available: https://forge.scilab.org/index.php/p/nisp/issues/attachment/68/GdR_Ondes_Janvier_2011_-_Analyse_de_sensibilite_globale_-_Martinez.pdf (visited on 17/06/2021).
- [143] M. Baudin, K. Boumhaout, T. Delage, B. Iooss and J.-M. Martinez, ‘Numerical stability of Sobol’ indices estimation formula’, in *Proceedings of the 8th International Conference on Sensitivity Analysis of Model Output (SAMO 2016)*, Le Tampon, 2016, pp. 50–51. [Online]. Available: https://samo2016.sciencesconf.org/data/pages/Proceedings_Samo.2016.pdf (visited on 17/06/2021).
- [144] T. Terraz, A. Ribes, Y. Fournier, B. Iooss and B. Raffin, ‘Melissa: Large scale in transit sensitivity analysis avoiding intermediate files’, in *Proceedings of the International Conference for High Performance Computing, Networking, Storage and Analysis, SC 2017*, New York, NY, USA: ACM, 2017, pp. 1–14. DOI: [10.1145/3126908.3126922](https://doi.org/10.1145/3126908.3126922).
- [145] B. Iooss, F. Van Dorpe and N. Devictor, ‘Response surfaces and sensitivity analyses for an environmental model of dose calculations’, *Reliability Engineering & System Safety*, vol. 91, no. 10-11, pp. 1241–1251, 2006. DOI: [10.1016/j.res.2005.11.021](https://doi.org/10.1016/j.res.2005.11.021).

- [146] G. E. Archer, A. Saltelli and I. M. Sobol, ‘Sensitivity measures, anova-like techniques and the use of bootstrap’, *Journal of Statistical Computation and Simulation*, vol. 58, no. 2, pp. 99–120, 1997. DOI: [10.1080/00949659708811825](https://doi.org/10.1080/00949659708811825).
- [147] K. M. Sanders, S. M. Ward and S. D. Koh, ‘Interstitial Cells: Regulators of Smooth Muscle Function’, *Physiological Reviews*, vol. 94, no. 3, pp. 859–907, 2014. DOI: [10.1152/physrev.00037.2013](https://doi.org/10.1152/physrev.00037.2013).
- [148] K. M. Sanders, Y. Kito, S. J. Hwang and S. M. Ward, ‘Regulation of Gastrointestinal Smooth Muscle Function by Interstitial Cells’, *Physiology*, vol. 31, no. 5, pp. 316–326, 2016. DOI: [10.1152/physiol.00006.2016](https://doi.org/10.1152/physiol.00006.2016).
- [149] G. O’Grady, P. Du, L. K. Cheng, J. U. Egbuji, W. J. E. P. Lammers, J. A. Windsor and A. J. Pullan, ‘Origin and propagation of human gastric slow-wave activity defined by high-resolution mapping’, *American Journal of Physiology-Gastrointestinal and Liver Physiology*, vol. 299, no. 3, G585–G592, 2010. DOI: [10.1152/ajpgi.00125.2010](https://doi.org/10.1152/ajpgi.00125.2010).
- [150] K. Djabella, M. Landau and M. Sorine, ‘A two-variable model of cardiac action potential with controlled pacemaker activity and ionic current interpretation’, in *2007 46th IEEE Conference on Decision and Control*, Institute of Electrical & Electronics Engineers (IEEE), 2007, pp. 5186–5191. DOI: [10.1109/cdc.2007.4434970](https://doi.org/10.1109/cdc.2007.4434970).
- [151] R. Aydin, S. Brandstaeter, F. Braeu, M. Steigenberger, R. Marcus, K. Nikolaou, M. Notohamiprodjo and C. Cyron, ‘Experimental characterization of the biaxial mechanical properties of porcine gastric tissue’, *Journal of the Mechanical Behavior of Biomedical Materials*, vol. 74, pp. 499–506, 2017. DOI: [10.1016/j.jmbbm.2017.07.028](https://doi.org/10.1016/j.jmbbm.2017.07.028).
- [152] M. Bauer, E. Morales-Orcajo, L. Klemm, R. Seydewitz, V. Fiebach, T. Siebert and M. Böl, ‘Biomechanical and microstructural characterisation of the porcine stomach wall: Location- and layer-dependent investigations’, *Acta Biomaterialia*, vol. 102, pp. 83–99, 2020. DOI: [10.1016/j.actbio.2019.11.038](https://doi.org/10.1016/j.actbio.2019.11.038).
- [153] P. Pathmanathan, J. M. Cordeiro and R. A. Gray, ‘Comprehensive Uncertainty Quantification and Sensitivity Analysis for Cardiac Action Potential Models’, *Frontiers in Physiology*, vol. 10, 2019. DOI: [10.3389/fphys.2019.00721](https://doi.org/10.3389/fphys.2019.00721).
- [154] G. Del Corso, R. Verzicco and F. Viola, ‘Sensitivity analysis of an electrophysiology model for the left ventricle’, *Journal of the Royal Society Interface*, vol. 17, no. 171, 2020. DOI: [10.1098/rsif.2020.0532rsif20200532](https://doi.org/10.1098/rsif.2020.0532rsif20200532).
- [155] D. E. Hurtado, S. Castro and P. Madrid, ‘Uncertainty quantification of 2 models of cardiac electromechanics’, *International Journal for Numerical Methods in Biomedical Engineering*, vol. 33, no. 12, pp. 1–21, 2017. DOI: [10.1002/cnm.2894](https://doi.org/10.1002/cnm.2894).
- [156] C. C. Mitchell and D. G. Schaeffer, ‘A two-current model for the dynamics of cardiac membrane’, *Bulletin of Mathematical Biology*, vol. 65, no. 5, pp. 767–793, 2003. DOI: [10.1016/S0092-8240\(03\)00041-7](https://doi.org/10.1016/S0092-8240(03)00041-7).
- [157] K. M. Sanders, S. D. Koh, S. Ro and S. M. Ward, ‘Regulation of gastrointestinal motility - insights from smooth muscle biology’, *Nat Rev Gastroenterol Hepatol*, vol. 9, no. 11, pp. 633–645, 2012. DOI: [10.1038/nrgastro.2012.168](https://doi.org/10.1038/nrgastro.2012.168).

- [158] P. Virtanen *et al.*, ‘SciPy 1.0: fundamental algorithms for scientific computing in Python’, *Nature Methods*, vol. 17, no. 3, pp. 261–272, 2020. DOI: [10.1038/s41592-019-0686-2](https://doi.org/10.1038/s41592-019-0686-2).
- [159] S. van der Walt, J. L. Schönberger, J. Nunez-Iglesias, F. Boulogne, J. D. Warner, N. Yager, E. Gouillart and T. Yu, ‘scikit-image: image processing in Python’, *PeerJ*, vol. 2, e453, 2014. DOI: [10.7717/peerj.453](https://doi.org/10.7717/peerj.453).
- [160] J. B. Youm, N. Kim, J. Han, E. Kim, H. Joo, C. H. Leem, G. Goto, A. Noma and Y. E. Earm, ‘A mathematical model of pacemaker activity recorded from mouse small intestine’, *Philosophical Transactions of the Royal Society of London A: Mathematical, Physical and Engineering Sciences*, vol. 364, no. 1842, pp. 1135–1154, 2006. DOI: [10.1098/rsta.2006.1759](https://doi.org/10.1098/rsta.2006.1759).
- [161] A. Corrias and M. L. Buist, ‘A Quantitative Model of Gastric Smooth Muscle Cellular Activation’, *Annals of Biomedical Engineering*, vol. 35, no. 9, pp. 1595–1607, 2007. DOI: [10.1007/s10439-007-9324-8](https://doi.org/10.1007/s10439-007-9324-8).
- [162] A. Corrias and M. L. Buist, ‘Quantitative cellular description of gastric slow wave activity’, *American Journal of Physiology - Gastrointestinal and Liver Physiology*, vol. 294, no. 4, G989–G995, 2008. DOI: [10.1152/ajpgi.00528.2007](https://doi.org/10.1152/ajpgi.00528.2007).
- [163] R. A. Faville, A. J. Pullan, K. M. Sanders, S. D. Koh, C. M. Lloyd and N. P. Smith, ‘Biophysically Based Mathematical Modeling of Interstitial Cells of Cajal Slow Wave Activity Generated from a Discrete Unitary Potential Basis’, *Biophysical Journal*, vol. 96, no. 12, pp. 4834–4852, 2009. DOI: [10.1016/j.bpj.2009.03.058](https://doi.org/10.1016/j.bpj.2009.03.058).
- [164] R. Lees-Green, S. J. Gibbons, G. Farrugia, J. Sneyd and L. K. Cheng, ‘Computational modeling of anoctamin 1 calcium-activated chloride channels as pacemaker channels in interstitial cells of Cajal’, *American Journal of Physiology - Gastrointestinal and Liver Physiology*, vol. 306, no. 8, G711–G727, 2014. DOI: [10.1152/ajpgi.00449.2013](https://doi.org/10.1152/ajpgi.00449.2013).
- [165] J. B. Youm, C. H. Leem, S. R. Lee, I.-S. Song, H. K. Kim, H. J. Heo, B. J. Kim, N. Kim and J. Han, ‘Modeling of stochastic behavior of pacemaker potential in interstitial cells of Cajal’, *Progress in Biophysics and Molecular Biology*, vol. 116, no. 1, pp. 56–69, 2014. DOI: [10.1016/j.pbiomolbio.2014.09.002](https://doi.org/10.1016/j.pbiomolbio.2014.09.002).
- [166] S. A. Mah, R. Avci, L. K. Cheng and P. Du, ‘Current applications of mathematical models of the interstitial cells of Cajal in the gastrointestinal tract’, *Wiley Interdisciplinary Reviews: Systems Biology and Medicine*, no. September, pp. 1–15, 2020. DOI: [10.1002/wsbm.1507](https://doi.org/10.1002/wsbm.1507).
- [167] R. FitzHugh, ‘Impulses and Physiological States in Theoretical Models of Nerve Membrane’, *Biophysical Journal*, vol. 1, no. 6, pp. 445–466, 1961.
- [168] J. Nagumo, S. Arimoto and S. Yoshizawa, ‘An Active Pulse Transmission Line Simulating Nerve Axon’, *Proceedings of the IRE*, vol. 50, no. 10, pp. 2061–2070, 1962. DOI: [10.1109/JRPROC.1962.288235](https://doi.org/10.1109/JRPROC.1962.288235).
- [169] R. R. Aliev, W. Richards and J. P. Wikswo, ‘A Simple Nonlinear Model of Electrical Activity in the Intestine’, *Journal of Theoretical Biology*, vol. 204, no. 1, pp. 21–28, 2000. DOI: [10.1006/jtbi.2000.1069](https://doi.org/10.1006/jtbi.2000.1069).

- [170] A. Gizzi, C. Cherubini, S. Migliori, R. Alloni, R. Portuesi and S. Filippi, 'On the electrical intestine turbulence induced by temperature changes', *Physical Biology*, vol. 7, no. 1, p. 16 011, 2010. DOI: [10.1088/1478-3975/7/1/016011](https://doi.org/10.1088/1478-3975/7/1/016011).
- [171] A. J. Pullan, L. K. Cheng, R. Yassi and M. L. Buist, 'Modelling gastrointestinal bioelectric activity', *Progress in Biophysics and Molecular Biology*, vol. 85, no. 2-3, pp. 523–550, 2004. DOI: [10.1016/j.pbiomolbio.2004.02.003](https://doi.org/10.1016/j.pbiomolbio.2004.02.003).
- [172] A. Gizzi, A. Pandolfi and M. Vasta, 'Viscoelectromechanics modeling of intestine wall hyperelasticity', *International Journal for Computational Methods in Engineering Science and Mechanics*, vol. 17, no. 3, pp. 143–155, 2016. DOI: [10.1080/15502287.2015.1082678](https://doi.org/10.1080/15502287.2015.1082678).
- [173] M. L. Buist, L. K. Cheng, R. Yassi, L. A. Bradshaw, W. O. Richards and A. J. Pullan, 'An anatomical model of the gastric system for producing bioelectric and biomagnetic fields', *Physiological Measurement*, vol. 25, no. 4, p. 849, 2004.
- [174] L. K. Cheng, R. Komuro, T. M. Austin, L. Buist M. and A. J. Pullan, 'Anatomically realistic multiscale models of normal and abnormal gastrointestinal electrical activity', *World Journal of Gastroenterology*, vol. 13, no. 9, pp. 1378–1383, 2007. DOI: [10.3748/wjg.v13.i9.1378](https://doi.org/10.3748/wjg.v13.i9.1378).
- [175] M. L. Buist, L. K. Cheng, K. M. Sanders and A. J. Pullan, 'Multiscale modelling of human gastric electric activity: can the electrogastragram detect functional electrical uncoupling?', *Experimental Physiology*, vol. 91, no. 2, pp. 383–390, 2006. DOI: [10.1113/expphysiol.2005.031021](https://doi.org/10.1113/expphysiol.2005.031021).
- [176] A. Corrias, P. Pathmanathan, D. J. Gavaghan and M. L. Buist, 'Modelling tissue electrophysiology with multiple cell types: applications of the extended bidomain framework', *Integrative Biology*, vol. 4, no. 2, pp. 192–201, 2012. DOI: [10.1039/C2IB00100D](https://doi.org/10.1039/C2IB00100D).
- [177] F. B. Sachse, A. P. Moreno, G. Seemann and J. A. Abildskov, 'A model of electrical conduction in cardiac tissue including fibroblasts', *Annals of Biomedical Engineering*, vol. 37, no. 5, pp. 874–889, 2009. DOI: [10.1007/s10439-009-9667-4](https://doi.org/10.1007/s10439-009-9667-4).
- [178] M. L. Buist and Y. C. Poh, 'An Extended Bidomain Framework Incorporating Multiple Cell Types', *Biophysical Journal*, vol. 99, no. 1, pp. 13–18, 2010. DOI: [10.1016/j.bpj.2010.03.054](https://doi.org/10.1016/j.bpj.2010.03.054).
- [179] S. Sathar, M. L. Trew, G. O'Grady and L. K. Cheng, 'A Multiscale Tridomain Model for Simulating Bioelectric Gastric Pacing', *Biomedical Engineering, IEEE Transactions on*, vol. 62, no. 11, pp. 2685–2692, 2015. DOI: [10.1109/TBME.2015.2444384](https://doi.org/10.1109/TBME.2015.2444384).
- [180] R. N. Miftakhov and G. R. Abdusheva, 'Numerical simulation of excitation-contraction coupling in a locus of the small bowel', *Biological Cybernetics*, vol. 74, no. 5, pp. 455–467, 1996. DOI: [10.1007/BF00206712](https://doi.org/10.1007/BF00206712).
- [181] V. Gajendiran and M. L. Buist, 'A quantitative description of active force generation in gastrointestinal smooth muscle', *International Journal for Numerical Methods in Biomedical Engineering*, vol. 27, no. 3, pp. 450–460, 2011. DOI: [10.1002/cnm.1419](https://doi.org/10.1002/cnm.1419).

- [182] P. Du, Y. C. Poh, J. L. Lim, V. Gajendiran, G. O’Grady, M. L. Buist, A. J. Pullan and L. K. Cheng, ‘A Preliminary Model of Gastrointestinal Electromechanical Coupling’, *Biomedical Engineering, IEEE Transactions on*, vol. 58, no. 12, pp. 3491–3495, 2011. DOI: [10.1109/TBME.2011.2166155](https://doi.org/10.1109/TBME.2011.2166155).
- [183] P. Du, J. L. Lim and L. K. Cheng, ‘A Model of Electromechanical Coupling in the Small Intestine’, in *Multiscale Computer Modeling in Biomechanics and Biomedical Engineering*, ser. Studies in Mechanobiology, Tissue Engineering and Biomaterials, A. Gefen, Ed., vol. 14, Springer Berlin Heidelberg, 2013, pp. 179–207. DOI: [10.1007/8415_2012_153](https://doi.org/10.1007/8415_2012_153).
- [184] R. Miftahof and N. Akhmadeev, ‘Dynamics of the human stomach’, in *Modelling in Medicine and Biology VIII*, ser. WIT Transactions on Biomedicine and Health, Vol 13, vol. 13, 2009. DOI: [10.2495/BIO090181](https://doi.org/10.2495/BIO090181).
- [185] R. N. Miftahof, ‘Stress-Strain Analysis In The Stomach’, in *V European Conference on Computational Fluid Dynamics (ECCOMAS CFD 2010)*, J. C. F. Pereira, A. Sequeira and J. M. C. Pereira, Eds., vol. 5, 2010.
- [186] K.-J. Won, K. M. Sanders and S. M. Ward, ‘Interstitial cells of Cajal mediate mechano-sensitive responses in the stomach’, *Proceedings of the National Academy of Sciences*, vol. 102, no. 41, pp. 14 913–14 918, 2005. DOI: [10.1073/pnas.0503628102](https://doi.org/10.1073/pnas.0503628102).
- [187] J. D. Huizinga and W. J. E. P. Lammers, ‘Gut peristalsis is governed by a multitude of cooperating mechanisms’, *American Journal of Physiology - Gastrointestinal and Liver Physiology*, vol. 296, no. 1, G1–G8, 2009. DOI: [10.1152/ajpgi.90380.2008](https://doi.org/10.1152/ajpgi.90380.2008).
- [188] A. Beyder, R. Lees-Green and G. Farrugia, ‘Role of Ion Channel Mechanosensitivity in the Gut: Mechano-Electrical Feedback Exemplified By Stretch-Dependence of Nav1.5’, in *New Advances in Gastrointestinal Motility Research*, ser. Lecture Notes in Computational Vision and Biomechanics, L. K. Cheng, A. J. Pullan and G. Farrugia, Eds., vol. 10, Springer Netherlands, 2013, pp. 7–27. DOI: [10.1007/978-94-007-6561-0_2](https://doi.org/10.1007/978-94-007-6561-0_2).
- [189] J. D. Huizinga, ‘The Physiology and Pathophysiology of Interstitial Cells of Cajal: Pace-making, Innervation, and Stretch Sensation’, in *Physiology of the Gastrointestinal Tract*, Sixth Edit, Elsevier Inc., 2018, pp. 305–335. DOI: [10.1016/B978-0-12-809954-4.00013-X](https://doi.org/10.1016/B978-0-12-809954-4.00013-X).
- [190] D. E. Hurtado, S. Castro and A. Gizzi, ‘Computational modeling of non-linear diffusion in cardiac electrophysiology: A novel porous-medium approach’, *Computer Methods in Applied Mechanics and Engineering*, vol. 300, no. Supplement C, pp. 70–83, 2016. DOI: [10.1016/j.cma.2015.11.014](https://doi.org/10.1016/j.cma.2015.11.014).
- [191] A. Gizzi, A. Loppini, R. Ruiz-Baier, A. Ippolito, A. Camassa, A. La Camera, E. Emmi, L. Di Perna, V. Garofalo, C. Cherubini and S. Filippi, ‘Nonlinear diffusion and thermo-electric coupling in a two-variable model of cardiac action potential’, *Chaos: An Interdisciplinary Journal of Nonlinear Science*, vol. 27, no. 9, p. 93 919, 2017. DOI: [10.1063/1.4999610](https://doi.org/10.1063/1.4999610).
- [192] C. Cherubini, S. Filippi, A. Gizzi and R. Ruiz-Baier, ‘A note on stress-driven anisotropic diffusion and its role in active deformable media’, *Journal of Theoretical Biology*, vol. 430, no. Supplement C, pp. 221–228, 2017. DOI: [10.1016/j.jtbi.2017.07.013](https://doi.org/10.1016/j.jtbi.2017.07.013).

- [193] A. Propp, A. Gizzi, F. Levrero-Florencio and R. Ruiz-Baier, ‘An orthotropic electro-viscoelastic model for the heart with stress-assisted diffusion’, *Biomechanics and Modeling in Mechanobiology*, vol. 19, no. 2, pp. 633–659, 2020. DOI: [10.1007/s10237-019-01237-y](https://doi.org/10.1007/s10237-019-01237-y).
- [194] L. Klemm, R. Seydewitz, M. Borsdorf, T. Siebert and M. Böl, ‘On a coupled electro-chemomechanical model of gastric smooth muscle contraction’, *Acta Biomaterialia*, vol. 109, pp. 163–181, 2020. DOI: [10.1016/j.actbio.2020.04.007](https://doi.org/10.1016/j.actbio.2020.04.007).
- [195] C. Fontanella, C. Salmaso, I. Toniolo, N. de Cesare, A. Rubini, G. De Benedictis and C. E.L., ‘Computational models for the mechanical investigation of stomach tissues and structure’, *Annals of Biomedical Engineering*, vol. in press, pp. 1–13, 2019. DOI: [10.1007/s10439-019-02229-w](https://doi.org/10.1007/s10439-019-02229-w).
- [196] S. K. Sarna, E. E. Daniel and Y. J. Kingma, ‘Simulation of the electric-control activity of the stomach by an array of relaxation oscillators’, *The American Journal of Digestive Diseases*, vol. 17, no. 4, pp. 299–310, 1972. DOI: [10.1007/BF02231729](https://doi.org/10.1007/BF02231729).
- [197] P. Du, N. Paskaranandavadivel, G. O’Grady, S.-J. Tang and L. K. Cheng, ‘A theoretical study of the initiation, maintenance and termination of gastric slow wave re-entry’, *Mathematical Medicine and Biology*, vol. 32, no. 4, pp. 405–423, 2015. DOI: [10.1093/imammb/dqu023](https://doi.org/10.1093/imammb/dqu023).
- [198] M. J. Ferrua and R. P. Singh, ‘Modeling the Fluid Dynamics in a Human Stomach to Gain Insight of Food Digestion’, *Journal of Food Science*, vol. 75, no. 7, R151–R162, 2010.
- [199] M. J. Ferrua and R. P. Singh, ‘Computational modelling of gastric digestion: current challenges and future directions’, *Current Opinion in Food Science*, vol. 4, pp. 116–123, 2015. DOI: [10.1016/j.cofs.2015.06.005](https://doi.org/10.1016/j.cofs.2015.06.005).
- [200] A. Nitti, J. Kiendl, A. Gizzi, A. Reali and M. D. de Tullio, ‘A curvilinear isogeometric framework for the electromechanical activation of thin muscular tissues’, *Computer Methods in Applied Mechanics and Engineering*, vol. 382, p. 113 877, 2021. DOI: [10.1016/j.cma.2021.113877](https://doi.org/10.1016/j.cma.2021.113877).
- [201] L. S. Graham and D. Kilpatrick, ‘Estimation of the Bidomain Conductivity Parameters of Cardiac Tissue From Extracellular Potential Distributions Initiated by Point Stimulation’, *Annals of Biomedical Engineering*, vol. 38, no. 12, pp. 3630–3648, 2010. DOI: [10.1007/s10439-010-0119-y](https://doi.org/10.1007/s10439-010-0119-y).
- [202] H. Yang and A. Veneziani, ‘Estimation of cardiac conductivities in ventricular tissue by a variational approach’, *Inverse Problems*, vol. 31, no. 11, p. 115 001, 2015. DOI: [10.1088/0266-5611/31/11/115001](https://doi.org/10.1088/0266-5611/31/11/115001).
- [203] A. Barone, F. Fenton and A. Veneziani, ‘Numerical sensitivity analysis of a variational data assimilation procedure for cardiac conductivities’, *Chaos: An Interdisciplinary Journal of Nonlinear Science*, vol. 27, no. 9, p. 093 930, 2017. DOI: [10.1063/1.5001454](https://doi.org/10.1063/1.5001454).

- [204] A. Barone, A. Gizzi, F. Fenton, S. Filippi and A. Veneziani, ‘Experimental validation of a variational data assimilation procedure for estimating space-dependent cardiac conductivities’, *Computer Methods in Applied Mechanics and Engineering*, vol. 358, p. 112 615, 2020. DOI: [10.1016/j.cma.2019.112615](https://doi.org/10.1016/j.cma.2019.112615).
- [205] A. Barone, M. G. Carlino, A. Gizzi, S. Perotto and A. Veneziani, ‘Efficient estimation of cardiac conductivities: A proper generalized decomposition approach’, *Journal of Computational Physics*, vol. 423, p. 109 810, 2020. DOI: [10.1016/j.jcp.2020.109810](https://doi.org/10.1016/j.jcp.2020.109810).
- [206] A. Pal, K. Indireskumar, W. Schwizer, B. Abrahamsson, M. Fried and J. G. Brasseur, ‘Gastric flow and mixing studied using computer simulation’, *Proceedings of the Royal Society of London B: Biological Sciences*, vol. 271, no. 1557, pp. 2587–2594, 2004. DOI: [10.1098/rspb.2004.2886](https://doi.org/10.1098/rspb.2004.2886).
- [207] L. Marciani, ‘Assessment of gastrointestinal motor functions by MRI: A comprehensive review’, *Neurogastroenterology and Motility*, vol. 23, no. 5, pp. 399–407, 2011. DOI: [10.1111/j.1365-2982.2011.01670.x](https://doi.org/10.1111/j.1365-2982.2011.01670.x).
- [208] A. Menys, C. Hoad, R. Spiller, S. M. Scott, D. Atkinson, L. Marciani and S. A. Taylor, ‘Spatio-temporal motility MRI analysis of the stomach and colon’, *Neurogastroenterology and Motility*, vol. 31, no. 5, 2019. DOI: [10.1111/nmo.13557](https://doi.org/10.1111/nmo.13557).
- [209] S. Hosseini, R. Avci, N. Paskaranandavadivel, N. Palmada, V. Suresh and L. K. Cheng, ‘A Novel Method for Time-Dependent Numerical Modeling of Gastric Motility Directly from Magnetic Resonance Imaging’, in *2020 42nd Annual International Conference of the IEEE Engineering in Medicine & Biology Society (EMBC)*, vol. 2020-July, IEEE, 2020, pp. 2384–2387. DOI: [10.1109/EMBC44109.2020.9175607](https://doi.org/10.1109/EMBC44109.2020.9175607).
- [210] S. Baek, K. R. Rajagopal and J. D. Humphrey, ‘A Theoretical Model of Enlarging Intracranial Fusiform Aneurysms’, *Journal of Biomechanical Engineering*, vol. 128, no. 1, pp. 142–149, 2006. DOI: [10.1115/1.2132374](https://doi.org/10.1115/1.2132374).
- [211] M. Kroon and G. A. Holzapfel, ‘A model for saccular cerebral aneurysm growth by collagen fibre remodelling’, *Journal of Theoretical Biology*, vol. 247, no. 4, pp. 775–787, 2007. DOI: [10.1016/j.jtbi.2007.03.009](https://doi.org/10.1016/j.jtbi.2007.03.009).
- [212] J. D. Laubrie, J. S. Mousavi and S. Avril, ‘A new finite-element shell model for arterial growth and remodeling after stent implantation’, *International Journal for Numerical Methods in Biomedical Engineering*, vol. 36, no. 1, pp. 1–19, 2020. DOI: [10.1002/cnm.3282](https://doi.org/10.1002/cnm.3282).
- [213] J. S. Wilson, S. Baek and J. D. Humphrey, ‘Parametric study of effects of collagen turnover on the natural history of abdominal aortic aneurysms’, *Proceedings of the Royal Society A: Mathematical, Physical and Engineering Sciences*, vol. 469, no. 2150, 2013. DOI: [10.1098/rspa.2012.0556](https://doi.org/10.1098/rspa.2012.0556).
- [214] J. S. Wilson and J. D. Humphrey, ‘Evolving anisotropy and degree of elastolytic insult in abdominal aortic aneurysms: Potential clinical relevance?’, *Journal of Biomechanics*, vol. 47, no. 12, pp. 2995–3002, 2014. DOI: [10.1016/j.jbiomech.2014.07.003](https://doi.org/10.1016/j.jbiomech.2014.07.003).

- [215] A. Valentín and J. D. Humphrey, ‘Parameter sensitivity study of a constrained mixture model of arterial growth and remodeling’, *Journal of Biomechanical Engineering*, vol. 131, no. 10, pp. 1–11, 2009. DOI: [10.1115/1.3192144](https://doi.org/10.1115/1.3192144).
- [216] T. Lee, I. Bilonis and A. B. Tepole, ‘Propagation of uncertainty in the mechanical and biological response of growing tissues using multi-fidelity Gaussian process regression’, *Computer Methods in Applied Mechanics and Engineering*, vol. 359, p. 112 724, 2020. DOI: [10.1016/j.cma.2019.112724](https://doi.org/10.1016/j.cma.2019.112724).
- [217] F. Gamboa, A. Janon, T. Klein and A. Lagnoux, ‘Sensitivity indices for multivariate outputs’, *Comptes Rendus Mathématique*, vol. 351, no. 7-8, pp. 307–310, 2013. DOI: [10.1016/j.crma.2013.04.016](https://doi.org/10.1016/j.crma.2013.04.016).
- [218] K. Campbell, M. D. McKay and B. J. Williams, ‘Sensitivity analysis when model outputs are functions’, *Reliability Engineering and System Safety*, vol. 91, no. 10-11, pp. 1468–1472, 2006. DOI: [10.1016/j.res.2005.11.049](https://doi.org/10.1016/j.res.2005.11.049).
- [219] T. Sumner, E. Shephard and I. D. Bogle, ‘A methodology for global-sensitivity analysis of time-dependent outputs in systems biology modelling’, *Journal of the Royal Society Interface*, vol. 9, no. 74, pp. 2156–2166, 2012. DOI: [10.1098/rsif.2011.0891](https://doi.org/10.1098/rsif.2011.0891).
- [220] S. Zeinali-Davarani, A. Sheidaei and S. Baek, ‘A finite element model of stress-mediated vascular adaptation: application to abdominal aortic aneurysms’, *Computer Methods in Biomechanics and Biomedical Engineering*, vol. 14, no. 9, pp. 803–817, 2011. DOI: [10.1080/10255842.2010.495344](https://doi.org/10.1080/10255842.2010.495344).
- [221] J. R. Cebal, M. A. Castro, J. E. Burgess, R. S. Pergolizzi, M. J. Sheridan and C. M. Putman, ‘Characterization of cerebral aneurysms for assessing risk of rupture by using patient-specific computational hemodynamics models’, *American Journal of Neuroradiology*, vol. 26, no. 10, pp. 2550–2559, 2005. DOI: [10.1016/s0098-1672\(08\)70473-9](https://doi.org/10.1016/s0098-1672(08)70473-9).
- [222] P. Watton and Y. Ventikos, ‘Modelling evolution of saccular cerebral aneurysms’, *Journal of Strain Analysis for Engineering Design*, vol. 44, no. 5, pp. 375–389, 2009. DOI: [10.1243/03093247JSA492](https://doi.org/10.1243/03093247JSA492).
- [223] D. M. Sforza, K. Kono, S. Tateshima, F. Viñuela, C. Putman and J. R. Cebal, ‘Hemodynamics in growing and stable cerebral aneurysms’, *Journal of NeuroInterventional Surgery*, vol. 8, no. 4, pp. 407–412, 2016. DOI: [10.1136/neurintsurg-2014-011339](https://doi.org/10.1136/neurintsurg-2014-011339).
- [224] S. Seyedsalehi, L. Zhang, J. Choi and S. Baek, ‘Prior distributions of material parameters for Bayesian calibration of growth and remodeling computational model of abdominal aortic wall’, *Journal of Biomechanical Engineering*, vol. 137, no. 10, pp. 1–13, 2015. DOI: [10.1115/1.4031116](https://doi.org/10.1115/1.4031116).
- [225] J. Biehler, S. Kehl, M. W. Gee, F. Schmies, J. Pelisek, A. Maier, C. Reeps, H. H. Eckstein and W. A. Wall, ‘Probabilistic noninvasive prediction of wall properties of abdominal aortic aneurysms using Bayesian regression’, *Biomechanics and Modeling in Mechanobiology*, vol. 16, no. 1, pp. 45–61, 2017. DOI: [10.1007/s10237-016-0801-6](https://doi.org/10.1007/s10237-016-0801-6).
- [226] S. Kucherenko, S. Tarantola and P. Annoni, ‘Estimation of global sensitivity indices for models with dependent variables’, *Computer Physics Communications*, vol. 183, no. 4, pp. 937–946, 2012. DOI: [10.1016/j.cpc.2011.12.020](https://doi.org/10.1016/j.cpc.2011.12.020).

- [227] G. Chastaing, F. Gamboa and C. Prieur, ‘Generalized Hoeffding-Sobol decomposition for dependent variables - application to sensitivity analysis’, *Electronic Journal of Statistics*, vol. 6, pp. 2420–2448, 2012. DOI: [10.1214/12-EJS749](https://doi.org/10.1214/12-EJS749).
- [228] G. Chastaing, F. Gamboa and C. Prieur, ‘Generalized Sobol sensitivity indices for dependent variables: numerical methods’, *Journal of Statistical Computation and Simulation*, vol. 85, no. 7, pp. 1306–1333, 2015. DOI: [10.1080/00949655.2014.960415](https://doi.org/10.1080/00949655.2014.960415).
- [229] N. C. Do and S. Razavi, ‘Correlation Effects? A Major but Often Neglected Component in Sensitivity and Uncertainty Analysis’, *Water Resources Research*, vol. 56, no. 3, 2020. DOI: [10.1029/2019WR025436](https://doi.org/10.1029/2019WR025436).
- [230] T. A. Mara, S. Tarantola and P. Annoni, ‘Non-parametric methods for global sensitivity analysis of model output with dependent inputs’, *Environmental Modelling & Software*, vol. 72, pp. 173–183, 2015. DOI: [10.1016/j.envsoft.2015.07.010](https://doi.org/10.1016/j.envsoft.2015.07.010).
- [231] S. Tarantola and T. A. Mara, ‘Variance-Based sensitivity indices of computer models with dependent inputs: the fourier amplitude sensitivity test’, *International Journal for Uncertainty Quantification*, vol. 7, no. 6, pp. 511–523, 2017. DOI: [10.1615/Int.J.UncertaintyQuantification.2017020291](https://doi.org/10.1615/Int.J.UncertaintyQuantification.2017020291).
- [232] F. Gamboa, A. Janon, T. Klein and A. Lagnoux, ‘Sensitivity analysis for multidimensional and functional outputs’, *Electronic Journal of Statistics*, vol. 8, no. 1, 2014. DOI: [10.1214/14-EJS895](https://doi.org/10.1214/14-EJS895).
- [233] A. Alexanderian, P. A. Gremaud and R. C. Smith, ‘Variance-based sensitivity analysis for time-dependent processes’, *Reliability Engineering & System Safety*, vol. 196, p. 106 722, 2020. DOI: [10.1016/j.ress.2019.106722](https://doi.org/10.1016/j.ress.2019.106722).
- [234] A. Marrel, B. Iooss, M. Jullien, B. Laurent and E. Volkova, ‘Global sensitivity analysis for models with spatially dependent outputs’, *Environmetrics*, vol. 22, no. 3, pp. 383–397, 2011. DOI: [10.1002/env.1071](https://doi.org/10.1002/env.1071).
- [235] J. Biehler, M. Mäck, J. Nitzler, M. Hanss, P.-S. Koutsourelakis and W. A. Wall, ‘Multi-fidelity approaches for uncertainty quantification’, *GAMM-Mitteilungen*, vol. 42, no. 2, e201900008, 2019. DOI: [10.1002/gamm.201900008](https://doi.org/10.1002/gamm.201900008).
- [236] J. E. Oakley and A. O’Hagan, ‘Probabilistic sensitivity analysis of complex models: A Bayesian approach’, *Journal of the Royal Statistical Society. Series B: Statistical Methodology*, vol. 66, no. 3, pp. 751–769, 2004. DOI: [10.1111/j.1467-9868.2004.05304.x](https://doi.org/10.1111/j.1467-9868.2004.05304.x).
- [237] A. Marrel, B. Iooss, B. Laurent and O. Roustant, ‘Calculations of Sobol indices for the Gaussian process metamodel’, *Reliability Engineering and System Safety*, vol. 94, no. 3, pp. 742–751, 2009. DOI: [10.1016/j.ress.2008.07.008](https://doi.org/10.1016/j.ress.2008.07.008).
- [238] B. Sudret, ‘Global sensitivity analysis using polynomial chaos expansions’, *Reliability Engineering & System Safety*, vol. 93, no. 7, pp. 964–979, 2008. DOI: [10.1016/j.ress.2007.04.002](https://doi.org/10.1016/j.ress.2007.04.002).
- [239] M. Raissi, P. Perdikaris and G. Karniadakis, ‘Physics-informed neural networks: A deep learning framework for solving forward and inverse problems involving nonlinear partial differential equations’, *Journal of Computational Physics*, vol. 378, pp. 686–707, 2019. DOI: [10.1016/j.jcp.2018.10.045](https://doi.org/10.1016/j.jcp.2018.10.045).

-
- [240] E. Haghighat, M. Raissi, A. Moure, H. Gomez and R. Juanes, ‘A physics-informed deep learning framework for inversion and surrogate modeling in solid mechanics’, *Computer Methods in Applied Mechanics and Engineering*, vol. 379, p. 113 741, 2021. DOI: [10.1016/j.cma.2021.113741](https://doi.org/10.1016/j.cma.2021.113741).
- [241] M. Arnst, C. Soize and K. Bulthuis, ‘Computation of Sobol Indices in Global Sensitivity Analysis From Small Data Sets by Probabilistic Learning on Manifolds’, *International Journal for Uncertainty Quantification*, vol. 11, no. 2, pp. 1–23, 2021. DOI: [10.1615/Int.J.UncertaintyQuantification.2020032674](https://doi.org/10.1615/Int.J.UncertaintyQuantification.2020032674).
- [242] M. Rixner and P.-S. Koutsourelakis, ‘A probabilistic generative model for semi-supervised training of coarse-grained surrogates and enforcing physical constraints through virtual observables’, *Journal of Computational Physics*, vol. 434, p. 110 218, 2021. DOI: [10.1016/j.jcp.2021.110218](https://doi.org/10.1016/j.jcp.2021.110218).
- [243] A. Janon, M. Nodet and C. Prieur, ‘Uncertainties Assessment in Global Sensitivity Indices Estimation From Metamodels’, *International Journal for Uncertainty Quantification*, vol. 4, no. 1, pp. 21–36, 2014. DOI: [10.1615/Int.J.UncertaintyQuantification.201204291](https://doi.org/10.1615/Int.J.UncertaintyQuantification.201204291).
- [244] Encyclopædia Britannica, *Human digestive system*. [Online]. Available: <https://www.britannica.com/science/human-digestive-system#/media/1/1081754/1087> (visited on 17/06/2021).
- [245] Encyclopædia Britannica, *Structures of the human stomach*. [Online]. Available: <https://www.britannica.com/science/human-digestive-system#/media/1/1081754/68634> (visited on 17/06/2021).
- [246] H. P. Parkman and M. P. Jones, ‘Tests of Gastric Neuromuscular Function’, *Gastroenterology*, vol. 136, no. 5, pp. 1526–1543, 2009. DOI: [10.1053/j.gastro.2009.02.039](https://doi.org/10.1053/j.gastro.2009.02.039).
- [247] B. E. Lacy, K. L. Koch and M. D. Crowell, ‘Manometry’, in *Schuster atlas of gastrointestinal motility in health and disease*, M. M. Schuster, M. D. Crowell and K. L. Koch, Eds., Second, Hamilton, Ontario: BC Decker Inc., 2002, ch. 10, pp. 135–150.
- [248] M. J. Ferrua, Z. Xue and R. P. Singh, ‘On the kinematics and efficiency of advective mixing during gastric digestion - A numerical analysis’, *Journal of Biomechanics*, vol. 47, no. 15, pp. 3664–3673, 2014. DOI: [10.1016/j.jbiomech.2014.09.033](https://doi.org/10.1016/j.jbiomech.2014.09.033).

Appended publications

A

Mechanics of the stomach: A review of an emerging field of biomechanics

Sebastian Brandstaeter*, Sebastian L. Fuchs*, Roland C. Aydin, Christian J. Cyron

* these authors contributed equally to this work.

published in

GAMM - Mitteilungen, vol. 42, no. 3, e201900001, 2019. DOI: [10.1002/gamm.201900001](https://doi.org/10.1002/gamm.201900001).

Reprinted from [14], licensed under a Creative Commons Attribution 4.0 International License (<https://creativecommons.org/licenses/by/4.0/>).

FIGURE 1 (on p. 97 of this thesis) reprinted from [244], copyright (2010), with permission from Encyclopædia Britannica, Inc.

FIGURE 2 (on p. 98 of this thesis) reprinted from [245], copyright (2010), with permission from Encyclopædia Britannica, Inc.

FIGURE 3 (on p. 99 of this thesis) reprinted from [246], copyright (2009), who adapted from [247], both with permission from Elsevier.

FIGURE 4 (on p. 102 of this thesis) reprinted from [248], copyright (2014), with permission from Elsevier.

ORIGINAL PAPER



Mechanics of the stomach: A review of an emerging field of biomechanics

Sebastian Brandstaeter¹ | Sebastian L. Fuchs^{1,2} | Roland C. Aydin³ | Christian J. Cyron^{2,3}

¹Institute for Computational Mechanics, Technical University of Munich, Garching, Germany

²Institute of Continuum and Materials Mechanics, Hamburg University of Technology, Hamburg, Germany

³Institute of Materials Research, Materials Mechanics, Helmholtz-Zentrum Geesthacht, Geesthacht, Germany

Correspondence

Christian J. Cyron, Institute of Continuum and Materials Mechanics, Hamburg University of Technology, Eissendorfer Str. 42, 21073, Hamburg, Germany.
Email: christian.cyron@tuhh.de

Funding Information

This research was supported by the German Research Foundation (Deutsche Forschungsgemeinschaft), CY 75/3-1.

Mathematical and computational modeling of the stomach is an emerging field of biomechanics where several complex phenomena, such as gastric electrophysiology, fluid mechanics of the digesta, and solid mechanics of the gastric wall, need to be addressed. Developing a comprehensive multiphysics model of the stomach that allows studying the interactions between these phenomena remains one of the greatest challenges in biomechanics. A coupled multiphysics model of the human stomach would enable detailed in-silico studies of the digestion of food in the stomach in health and disease. Moreover, it has the potential to open up unprecedented opportunities in numerous fields such as computer-aided medicine and food design. This review article summarizes our current understanding of the mechanics of the human stomach and delineates the challenges in mathematical and computational modeling which remain to be addressed in this emerging area.

KEYWORDS

digesta, gastric electrophysiology, gastric mechanics, gastric wall, multiphysics model

1 | INTRODUCTION

Healthcare problems related to the stomach are among the most important causes of morbidity in industrialized countries. For example, healthcare costs of obesity have nearly doubled from \$79 billion in 1998 to \$147 billion in 2008 in the United States,^[1,2] where in 2010, the prevalence of obesity was an estimated 36% (17% in the EU³). More than 250 000 bariatric surgeries are performed per year in the United States and EU together^[4,5] with a cost of €5000–€15 000 per procedure.^[6,7] The economic footprint of gastro-esophageal reflux disease (GERD) amounts to an estimated \$20 billion/year in the United States.⁸ Moreover, 10%–45% of the general population suffer from dyspepsia (indigestion),^[9] which seriously compromises individual well-being and economic productivity. These highly prevalent health problems are closely linked to gastric mechanics (ie, mechanics of the stomach). For example, obesity can be permanently resolved by irreversible changes of gastric geometry and mechanics as performed in bariatric surgery.^[10] GERD results from a misbalance between intragastric pressure and closing pressure of the sphincter between stomach and esophagus. Dyspepsia is often related to control disturbances of gastric smooth muscle.

Sebastian Brandstaeter and Sebastian L. Fuchs contributed equally to this work.

ABBREVIATIONS: ACW, antral contraction wave; DPM, discrete particle method; GERD, gastro-esophageal reflux disease; ICC, interstitial cell of Cajal; ICC-IM, intramuscular ICC; ICC-MY, myenteric ICC; MRI, magnetic resonance imaging; PDGFR α^+ , platelet-derived growth factor receptor α positive; SMC, smooth muscle cell; SPH, smoothed particle hydrodynamics.

This is an open access article under the terms of the Creative Commons Attribution License, which permits use, distribution and reproduction in any medium, provided the original work is properly cited.

© 2019 The Authors. *GAMM - Mitteilungen* published by Wiley-VCH Verlag GmbH & Co. KGaA on behalf of Gesellschaft für Angewandte Mathematik und Mechanik

Perhaps even more importantly, the stomach and its mechanics play a key role not only in the digestion of food, one of the most essential processes in living organisms, but also for drug administration. Around 70% of all drugs are administered orally, and their processing and effectiveness thus depend crucially on gastric mechanics.^[11–13]

This tremendous importance of gastric mechanics is not at all reflected by current research efforts as is best revealed by a comparison with cardiovascular mechanics. Healthcare costs of cardiovascular diseases (\$149 billion in the United States in 2008^[14]) are comparable to the ones related to the stomach. However, in the program of the 8th World Congress of Biomechanics in 2018 with more than 4500 presentations common cardiovascular keywords* are found 414 times, whereas prominent keywords related to the stomach[†] do not appear at all. Hundreds of experimental articles about cardiovascular tissue mechanics over the last decades are contrasted by just a small number of articles on experimental gastric tissue mechanics. The situation is similar in modeling. Three-dimensional computational fluid mechanics was first applied to arteries around 1990,^[15,16] to the stomach only in 2007.^[17] Computational models incorporating fluid-structure interactions were developed for the vasculature already in the mid-1990s.^[18] Recently pioneering steps in this direction have been taken for the intestine^[19–21] but no such model has been proposed for the stomach so far. In short, modeling of the stomach lags around 20 years behind modeling of the cardiovascular system.

Several reasons have delayed the progress of gastric compared to cardiovascular biomechanics, in particular the sophisticated and for a long time poorly understood electrophysiology of the stomach,^[22] the complex mechanics of *digesta* (ie, food undergoing digestion) compared to blood, and the limited understanding of neural and hormonal mechanisms controlling gastric mechanics. Over the last decade, substantial progress has been made in all these fields,^[22–39] and rapid advances in computational power allow addressing even complex multiphysics problems nowadays.

Benefitting from these recent advances, the time has come now to tackle one of the still open big questions of biomechanics, which is the development of a comprehensive mathematical and computational multiphysics model of the stomach, which allows for detailed in-silico studies of the mechanics and mathematical principles governing the digestion of food in the stomach. Such a model has the potential to open up new horizons and unprecedented opportunities in numerous fields such as computer-aided medicine and food design. This review article is intended to provide a comprehensive summary of our current understanding of the mechanics of the human stomach. It may serve as a convenient starting point in particular for applied mathematicians and engineers who have interest to start research in this emerging area of biomechanics.

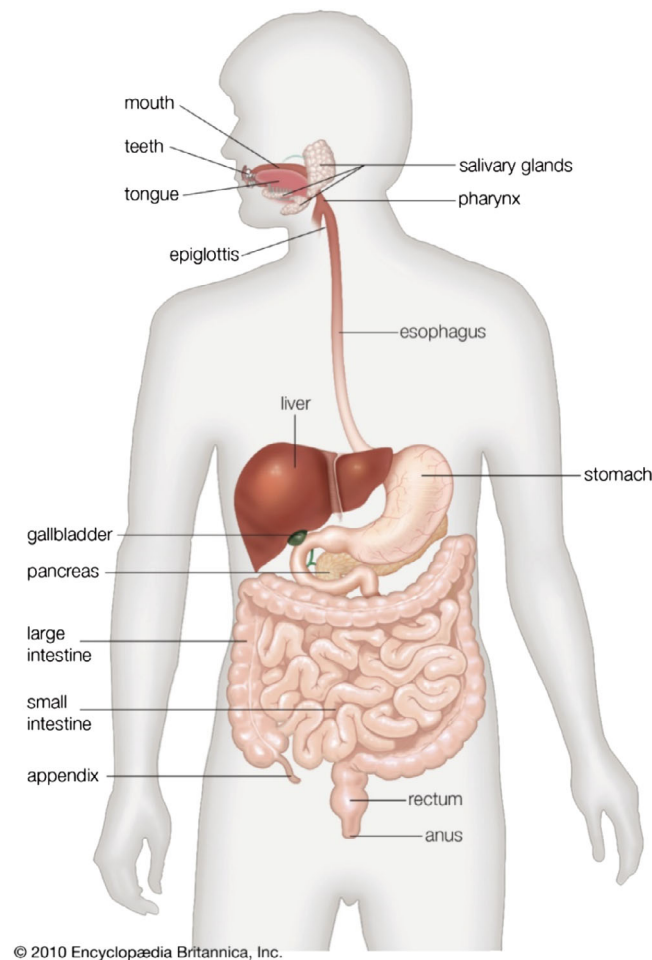
2 | ANATOMY AND PHYSIOLOGY OF THE HUMAN STOMACH

The human gastrointestinal tract is composed of several roughly tube-like organs in series (cf. Figure 1). Food enters via the mouth and is swallowed through the esophagus into the stomach, passing through a muscular cuff (the lower esophageal sphincter) that opens during swallowing. In the stomach, the *digesta* are stored, mixed, diluted with gastric juice, and mechanically as well as chemically disintegrated. Subsequently, they are released at a tightly controlled rate through the pylorus, a rhythmically opening muscular cuff, into the duodenum,^[40] the first part of the small intestine. After the small intestine, where most nutrients are extracted, *digesta* pass through the large intestine where more nutrients, ions and in particular water are extracted, leaving nearly solid feces, that are excreted through the anus. Positions in the gastrointestinal tract are denoted by the terms proximal (closer to the mouth) vs distal (closer to the anus).

The stomach is as a J-shaped muscular bag curved in the frontal plane (cf. Figure 1). Its volume is determined by the amount of stored *digesta* and normally ranges between 25 mL in the fasted and 1500 mL in the fed state.^[11] After a typical meal of ~1000 mL, the stomach measures around 30 cm along its greater curvature and exhibits a maximal width of around 10 cm.^[41] Anatomically, the stomach can be divided into three regions (from proximal to distal): fundus, corpus or body, and antrum (cf. Figure 2). While the gross histology is consistent throughout the organ (cf. Figure 2), the regions of the stomach can also be distinguished based on their detailed histological properties.^[42] The fundus is a muscular bag that relaxes upon ingestion of food to increase its storage capacity (gastric accommodation). Peristaltic muscular contraction waves, that is, ring-like contraction that constrict the stomach circumferentially, running from the corpus through the antrum to the pylorus, are mixing and grinding the food in the distal part of the stomach (cf. Figure 3). Temporal coordination of these so-called antral contraction waves (ACWs) with the aperture of the pylorus controls release of the *digesta* into the duodenum.

2.1 | Gastric lumen: Fluid mechanics and chemical reactions

Mastication breaks solid food down into small fragments that are mixed with saliva in the mouth^[43] and, after swallowing, with gastric juice in the stomach. *Digesta* in the lumen (ie, inside space) of the stomach can be modeled as in general non-Newtonian fluids, carrying a solid phase of particles (cf. Figure 3) and fibers.^[44–46] In general, one distinguishes between three types of gastric mixing processes, that is, solid-solid, solid-liquid, and liquid-liquid mixing, depending on the consistency of the *digesta*.^[47]



© 2010 Encyclopædia Britannica, Inc.

FIGURE 1 Major regions of gastrointestinal tract from mouth to anus[‡]

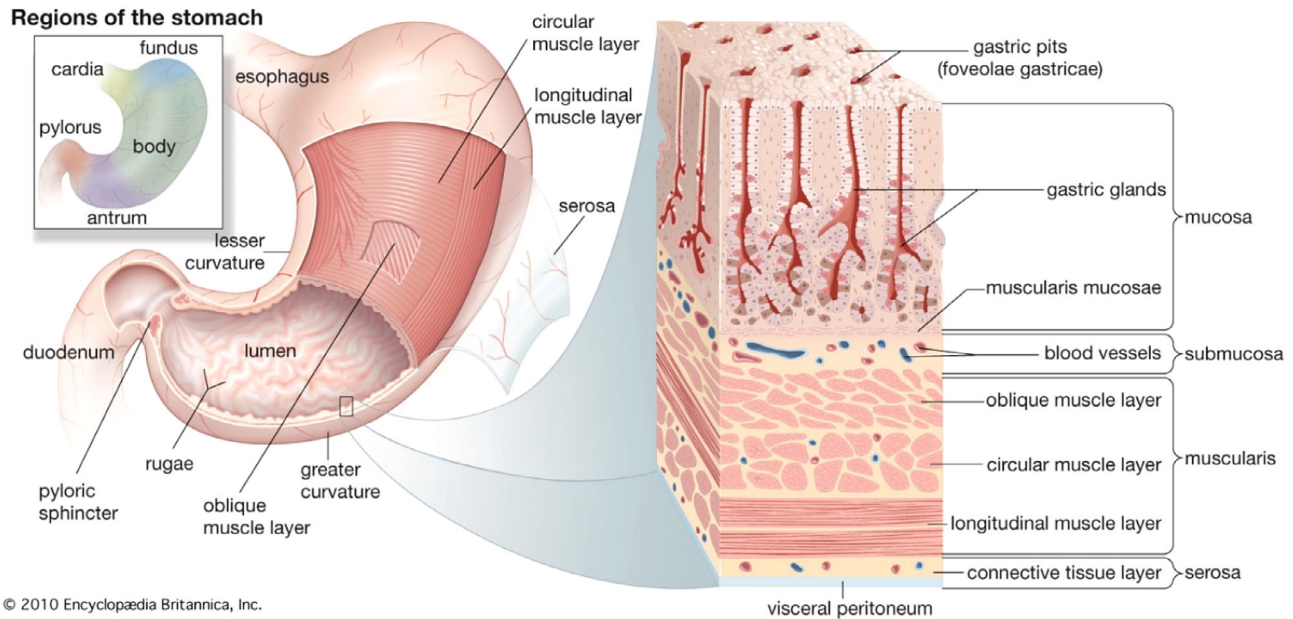
In the stomach, solid particles are disintegrated by fragmentation (cleavage into smaller pieces of roughly similar size) and erosion (abrasion of the surface by fluid shear stress).^[43,46,48] For tough small particles—like carrot or nut particles of a few millimeters in diameter—erosion dominates.^[49] Chemical reactions tenderize the food matrix, promoting thereby both mechanical fragmentation and erosion. Disintegration reduces the size of food particles over time following an exponential, sigmoidal, or delayed sigmoidal function, depending on the rate of simultaneous swelling of the particles due to absorption of gastric juice.^[46]

2.2 | Gastric wall: Solid mechanics

The gastric wall is around 3–4 mm thick and is comprised of four major layers, the mucosa, submucosa, muscularis, and serosa.^[50,51] Wall elasticity and stress can be divided into a passive part, determined by the strain of elastic fibers mainly in the submucosa and muscularis, and an active part governed by the (adaptable) tone of smooth muscle fibers mainly in the muscularis. The muscularis consists of up to three sublayers (the oblique, longitudinal, and circumferential sublayer) with muscle fibers oriented in respective directions (cf. Figure 2).

One of the primary functions of the stomach is storage of ingested food until it is further processed in the intestine. Gastric volume between the fasted and postprandial state can change by a factor of 60 by unfolding and stretching (by up to ~160%^[52]) of the gastric wall. The mechanics of gastrointestinal tissue is much less explored than the one of cardiovascular tissue. There have been a few papers on the constitutive behavior of the esophagus,^[53–57] small intestine,^[58–64] and large intestine,^[58,61,65–71] and around 20 on the mechanical properties of the gastric wall.^[61,72–89] These revealed that the constitutive properties and thickness of the different layers of the gastric wall differ significantly between different regions of the stomach, corresponding to their respective physiological functions. Most papers on gastric tissue mechanics report results of uniaxial tests only,^[61,72–76,79,80,87] which are insufficient to characterize the biaxial deformation (in both circumferential and longitudinal direction) observed in vivo, noting the in general significant anisotropy of gastric tissue.^[73,88]

Recently, a study identified for the first time the quasi-static passive biaxial mechanical properties of porcine gastric tissue.^[88] The authors conducted biaxial tests including seven different stretch ratios of tissue patches extracted from the three main regions of the stomach, that is, fundus, corpus, and antrum. Experimental data was fitted to a Fung-type strain energy function



© 2010 Encyclopædia Britannica, Inc.

FIGURE 2 Structure of human stomach (left) and gastric wall (right)⁸

(cf. Section 3.2). The study confirmed a pronounced anisotropy of gastric tissue. In addition, it showed that the three regions of the gastric wall exhibit specific mechanical properties consistent with their respective physiological functions. However, the study did not conduct layer specific biaxial experiments and was limited to porcine tissue.

Another recent study investigated extensively the active mechanical properties of porcine fundic smooth muscle tissue.^[89] The study quantified the force-length and force-velocity relations of fundic smooth muscle strips. Additionally, the dependency of force generation on preceding length changes, so called history effects, was examined. Notably, the study suggested the importance of history-dependent effects for the physiological function of the fundus, that is, mainly gastric accommodation (cf. sSection 2.3.1). While ref. [89] presented extensive data on the active properties of porcine gastric smooth muscle, the experiments were limited to fundic tissue, omitting corporal and antral tissue. Corporal and antral regions might, however, show different active mechanical properties adapted to their specific physiological functions, that is, mixing and grinding of ingested food as well as emptying toward the duodenum (cf. Section 2.3).

Unfortunately, experiments with animal tissue^[61,73,74] are not directly applicable to humans due to significant interspecies differences.^[74] Only two authors reported biaxial mechanical tests of human gastric tissue.^[77,78,81] Focussing on equibiaxial, highly dynamic load only,^[81] does not provide sufficient data to establish, for example, a nonlinear strain energy function for gastric tissue. Like ref. [81], also refs. [77, 78] studied only passive elasticity, neglecting the role of smooth muscle tension, and did not examine differences between the layers of the gastric wall.

Despite significant recent progress, there is still a pressing need for more experimental data about the mechanics of the human gastric wall, distinguishing between different regions, wall layers as well as active and passive elasticity and anticipating the complex physiological deformations of the stomach. Nevertheless, there exists already at least a basic collection of published experimental data about the mechanical properties of the gastric wall that can serve as a reasonable basis for mathematical and computational modeling.

2.3 | Gastric wall: Electrophysiology and electromechanics

In general, changes of the gastric geometry by contraction or relaxation of the smooth muscle in the muscularis of the gastric wall are referred to as gastric motility. One can distinguish three kinds of gastric motility: gastric accommodation, gastric mixing and emptying via ACWs, and migrating motor complexes.

2.3.1 | Gastric accommodation

The reflex leading to gastric muscle tone reduction predominantly in the proximal stomach after ingestion of food is called gastric accommodation (cf. Figure 3). It enables the stomach to expand its volume without significant increase of intragastric pressure. Thereby, gastric accommodation supports the physiological function of (temporary) food storage.^[36,37,90] Gastric accommodation comprises two main responses: receptive and adaptive relaxation.^[91,92] Eating stimulates the oropharynx and esophagus which triggers the relaxation of smooth muscle in the proximal stomach shortly after (within seconds). This response

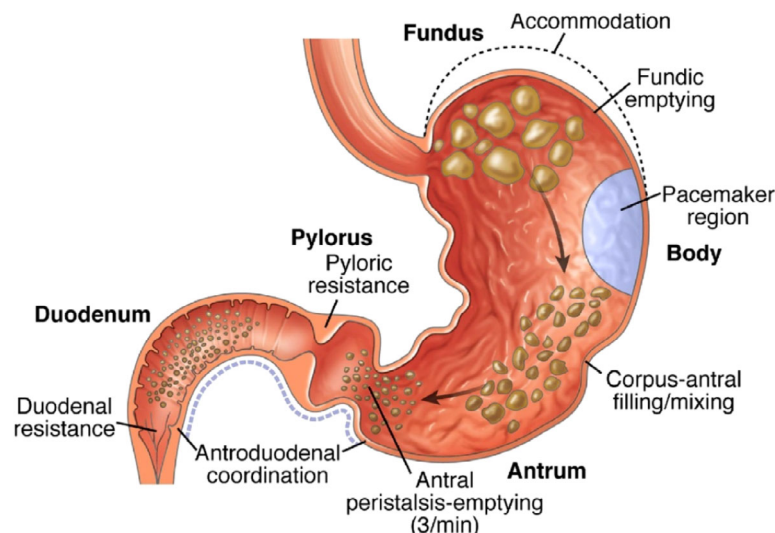


FIGURE 3 Schematic representation of gastric motility patterns including accommodation and antral contraction waves resulting in mixing and grinding of luminal content[¶]

is called receptive relaxation. Adaptive relaxation is a slower mechanism adjusting fundic muscle tone in response to gastric and duodenal distension and increased gastric intraluminal pressure. Possibly nutrient sensing in the duodenum also plays a role. Consequently, the specific properties of the ingested food influence adaptive relaxation.^[93] Impaired gastric accommodation is often associated with gastric disorders like GERD and dyspepsia.^[9] Normal muscle tension is restored during gastric emptying.^[94]

2.3.2 | Antral contraction waves

The motility pattern responsible for gastric emptying and gastric mixing (cf. Figure 3) is at its core the same: antral peristalsis or ACWs. ACWs appear as ring-shaped muscular contractions of the gastric wall which move along the stomach. They make the antrum act as a peristaltic food pump.^[40,94] The complex interplay between pyloric opening and closing and arriving ACWs on one hand mixes and grinds digesta and on the other hand regulates gastric emptying, that is, the release of gastric content into the duodenum.

ACWs are controlled by periodic electrical signals, called slow waves, propagating through the gastric wall. The underlying electrophysiology is similar to the heart^[95] but yet significantly more sophisticated due to a complex interplay between at least two cell types: smooth muscle cells (SMCs) and interstitial cells of Cajal (ICC).^[6,22,96] SMCs are responsible for generating the mechanical force leading to contractions of the gastric wall. ICC are largely responsible for generating the electric signals that stimulate contractions of SMCs. In the following, we will discuss some details of this big picture. In corpus, antrum, and pylorus, a dense network of ICC can be found at the myenteric plexus which is a branching network of cells in the space between the longitudinal and circumferential sublayer of the muscularis. ICC located there are called myenteric ICC (ICC-MY). ICC-MY are not present in the fundus.^[97] In all regions of the stomach, ICC can be found inside the longitudinal and the circumferential muscle layers, so called intramuscular ICC (ICC-IM). In addition to ICC, also platelet-derived growth factor receptor α positive (PDGFR α^+) cells are located at the myenteric plexus and inside the muscle layers. They play a role in controlling gastric electrophysiology by transducing input signals from the enteric nervous system. Both PDGFR α^+ cells and ICC-IM are found in close proximity to the endings of enteric motor neurons.^[96,98–101] SMCs, ICC and PDGFR α^+ cells are coupled electrically via gap junctions, effectively forming a multicellular syncytium. This syncytium plays the role of the pacemaker system for gastric motility. Additionally, it acts as the mediator for regulatory inputs from the enteric nervous and endocrine systems^[96,102] and mechanical stimuli. Slow waves are generated by ICC-MY which harbor biochemical pacemaker units.^[33,96,103–108] Anoctamin 1 (Ano1) calcium-activated chloride channels have been identified as key pacemaker channels in ICC-MY and are essential for slow wave generation.^[109–112] Another important mechanism for pacemaker activity is calcium-induced calcium release from intracellular stores into microdomains close to the plasma membrane.^[96,104,105,108,113] Within the ICC network, slow waves are propagated actively via a voltage-dependent mechanism involving T-type calcium channels and calcium-induced calcium release from the endoplasmic reticulum.^[108,113–115] However, slow waves conduct only passively to the surrounding SMCs.^[96,116] SMCs are not capable of actively generating slow waves. Instead, SMCs get depolarized by arriving slow waves such that calcium entry through (voltage-gated) T-type calcium channels is initiated.^[104,105] The resulting increase of intracellular calcium constitutes the initial step of a complex biochemical excitation-contraction mechanism^[117–119] which is essential to translate

the rhythmic electrical pacemaker activity of ICC-MY into the iconic ring-shaped ACWs. Slow waves decay quickly in tissue lacking a network of ICC-MY.^[6,102] The fundus lacks ICC-MY and is thus electrically largely quiescent. While slow waves are nonintermittently generated by ICC-MY, smooth muscle contractions occur only if appropriate neural,^[4] endocrine^[120] and mechanical^[121] inputs coincide with the electrical excitation. The transduction of inputs from the enteric nervous system is realized by the PDGFR α ⁺ and ICC-IM.^[122–124] Additionally, ICC-IM are electrically coupled to ICC-MY indicating their relevance in transmitting slow waves from ICC-MY deeper into the muscle layers. ICC also play an important role in mechanotransduction via stretch-activated currents.^[121,125,126] Despite substantial research efforts, many details concerning the complex biophysical mechanisms that control the generation and propagation of slow waves within the multicellular electrophysiological system of the stomach remain unknown.

Individual ICC generates slow waves at a cell-specific intrinsic frequency. An important feature of the ICC-MY network is the proximal to distal intrinsic frequency gradient describing the fact that the intrinsic frequency decreases from approximately 3 cpm (cycles per minute) at the proximal corpus to 0.8–1.8 cpm at the distal antrum. In an intact network, ICC synchronize their activity to the highest intrinsic frequency within the network, a process called entrainment. The precise way how the myriad ICC are entrained in a single wave remains controversial^[26,32,127,128] and forms a promising future application area for mathematical modeling. Sensitivity of ICC-internal processes to surrounding electric potential may play a role.^[32,129] Therefore, the region with the highest intrinsic frequency is referred to as the pacemaker site. In the human stomach, it is located at the proximal corpus on the side of the greater curvature (cf. Figure 3).^[30,43] Frequency gradient and entrainment are essential features for the formation of the physiological slow wave propagation pattern on the organ level.^[130] Recent progress in high-resolution electrical mapping techniques has facilitated the identification of slow wave propagation patterns in health and disease.^[29,30,131–137] In the healthy human stomach, slow waves are initiated at the pacemaker site (cf. Figure 3) at a frequency of 3cpm and from there propagate distally toward the pylorus. Increased circumferential propagation velocity ensures the rapid formation of a closed ring. Slow waves do not spread proximally from the pacemaker site such that the fundus is void of slow wave activity. Between three and four slow waves travel toward the pylorus at a spacing of approximately 60 mm at the same time. Slow waves are unable to pass the pylorus. Therefore, the pylorus acts as separator for the electrical activity of the stomach and the small intestine.^[138]

A frequent health problem is gastric dysrhythmia, that is, improperly coordinated slow waves that result in uncoordinated ACWs.^[26,139] Over the past years, various types of gastric dysrhythmias have been identified and successfully linked to different functional disorders of the stomach including gastroparesis and GERD.^[140,141] To disclose its still poorly understood physiological origin, two avenues of research appear promising: first, the development of biophysically more accurate mathematical models of gastric electrophysiology, second, a careful computational examination of the coupling between electric slow wave propagation and gastric solid and fluid mechanics, noting the pronounced mechanosensitivity of the ICC.^[142] The second approach could significantly benefit from a comprehensive computational multiphysics model of the stomach (cf. Section 3).

2.3.3 | Migrating motor complexes

Gastric accommodation and ACWs are the dominant forms of gastric motility in the postprandial stomach (ie, directly after a meal). By contrast, in the fasted stomach between meals so-called migrating motor complexes are observed. They sweep indigestible solids from the stomach through the intestine by means of very strong electromechanical contraction waves. They are typically repeating every 120 minutes.^[45] So far, most of the publications concerning gastric mechanics focus on the postprandial rather than the interdigestive stomach, although models of migrating motor complexes may be of great use for computer-aided drug design.

2.3.4 | Examination of gastric motility

The current gold standard to assess gastric accommodation is the so-called gastric barostat,^[90] an inflatable balloon that is placed in the (proximal) stomach and connected by a tube through the esophagus to an external air supply which ensures a given constant pressure. If gastric smooth muscle relaxes by gastric accommodation, the volume of the balloon will increase as additional air can be accommodated at the given pressure. This increase of volume is a, though only coarse, measure of gastric accommodation. The gastric barostat is fairly invasive^[143] and time consuming and thus often not well-tolerated by patients. Moreover, it alters ACWs and secretion of gastric juice, making a simultaneous evaluation of normal gastric motility and digestion impossible. Some variations of the gastric barostat (imposing, for example, not a constant pressure but volume or wall tension^[144]) share the same drawbacks. It has therefore been suggested to replace it by a less invasive procedure such as the measurement of the intragastric pressure^[90] (for which a small manometric catheter suffices) or the imaging of postprandial gastric volume (using, eg, magnetic resonance imaging [MRI]).^[145] However, neither alone can characterize gastric accommodation. On one hand, intragastric pressure cannot fully characterize gastric accommodation because for a given ingested volume it also depends on the (unknown) individual anatomy. On the other hand, the gastric volume measured by imaging is primarily determined by the ingested volume (plus some gastric juice) rather than by muscular relaxation.^[37,143,146,147] The latter can only roughly be

estimated from changes of gastric volume over time by emptying.^[147] Therefore, the gastric barostat is still the clinical gold standard to assess gastric accommodation.

ACWs are assessed in clinical practice by antroduodenal manometry. It requires time-consuming placement of a manometric catheter in the stomach and duodenum and can presumably detect by far not all contractions accurately (and also perturbs normal gastric function). Again, imaging has been discussed as a noninvasive alternative.^[148–154] However, a standardized interpretation of imaging data is still lacking (despite some suggestions like the gastric motility index^[155]), which prevents clinical application so far.^[147,156]

3 | MATHEMATICAL AND COMPUTATIONAL MODELING

3.1 | Gastric lumen: Fluid mechanics of the digesta

Examination of gastric fluid mechanics in vivo and ex vivo is difficult and often nearly impossible due to technical hurdles and ethical concerns, especially in humans. In vitro models have greatly helped to advance our understanding of gastric fluid mechanics^[157–160] but can hardly mimic the real gastric geometry and motility.^[41] Therefore, first computational fluid dynamics models of the stomach were developed around 15 years ago. After first attempts in two dimensions,^[40,161,162] in 2007, the first three-dimensional (finite element) model^[17,41,49,163–165] was proposed (and slightly modified in ref. [166]). Recently, a promising smooth particle hydrodynamics (SPH) computational model developed originally for the intestine^[19,20,167] was applied also to a stomach-like geometry examining gastric motility and emptying.^[168,169] These computational models revealed important patterns in gastric flow. For low viscosity^[40,161] dominant retrograde jets in the antrum, circulatory flow between the ACWs, and a so-called “stomach road,” along which gastric emptying occurs predominantly, were reported. In contrast, for higher viscosity more ordered patterns prevail.^[164,170] The importance of buoyancy^[170] and antral recirculation^[166] for gastric mixing were disclosed by different techniques.^[161,164,165] Food disintegration has been studied so far only using highly simplified models (assuming, for example, a fixed amount of erosion each time a particle is passing through an ACW^[171]).

Despite their great merits, all current computational models of the human stomach suffer from several important limitations:

- The gastric wall is modeled as rigid and its deformation during ACWs, if modeled at all, is kinematically prescribed. It is experimentally well confirmed that altered properties of the digesta^[17,151,171–178] or also altered gastric geometry^[179] can significantly change gastric flow, motility, and emptying. Current models with a prescribed wall motion can by design not account for these dependencies and do thus not allow predictive simulations of the impact of substantial parameter changes in the stomach. Such predictive simulations would require coupled multiphysics models accounting for interactions between flow of the digesta and viscoelasticity and electrophysiology of the wall.
- Current models have never been applied with person-specific in vivo geometries and associated data about gastric motility (ie, muscular contractions).
- Mechanical and chemical food disintegration is currently not modeled explicitly. The effect of gastric juice is generally neglected despite its significant impact on food disintegration and thus also on the time-dependent viscosity of the digesta and gastric flow.

In general, the fluid flow in the gastric lumen is assumed to show laminar and incompressible behavior^[41,49,164] being expressed by a balance of mass and a balance of momentum in Eulerian form

$$\nabla \cdot \mathbf{u} = 0 \quad (1)$$

$$\rho \left(\frac{\partial \mathbf{u}}{\partial t} + \mathbf{u} \cdot \nabla \mathbf{u} \right) = -\nabla p + \nabla \cdot \boldsymbol{\tau} + \rho \mathbf{g} \quad (2)$$

with fluid density ρ , velocity field \mathbf{u} , pressure p , gravity \mathbf{g} , and viscous stress tensor $\boldsymbol{\tau}$. The viscous stress tensor $\boldsymbol{\tau}$ is typically expressed in terms of the strain rate tensor $\mathbf{E} = \frac{1}{2}(\nabla \mathbf{u} + (\nabla \mathbf{u})^T)$. As a first approximation, dilute digesta can be modeled as a Newtonian fluid, which is characterized by a linear relationship of the strain rate tensor \mathbf{E} and the viscous stress tensor $\boldsymbol{\tau}$ via a dynamic viscosity μ :

$$\boldsymbol{\tau} = 2\mu \mathbf{E}. \quad (3)$$

The fluid viscosity of gastric juice in the stomach typically varies from 0.01 to 2 Pa · s.^[45] Experiments in vitro showed that the viscosity of digesta decreases within 40 minutes from a maximum of 17 Pa · s to 2.2 Pa · s^[180] caused by intragastric dilution^[45] with gastric juice. While the assumption of a Newtonian fluid may be appropriate as a reasonable approximation for dilute digesta, there are obviously many cases where it appears not applicable. Then a non-Newtonian fluid with a nonlinear relation between strain rate and shear stress has to be assumed, typically with shear thinning behavior.^[45,49,164]

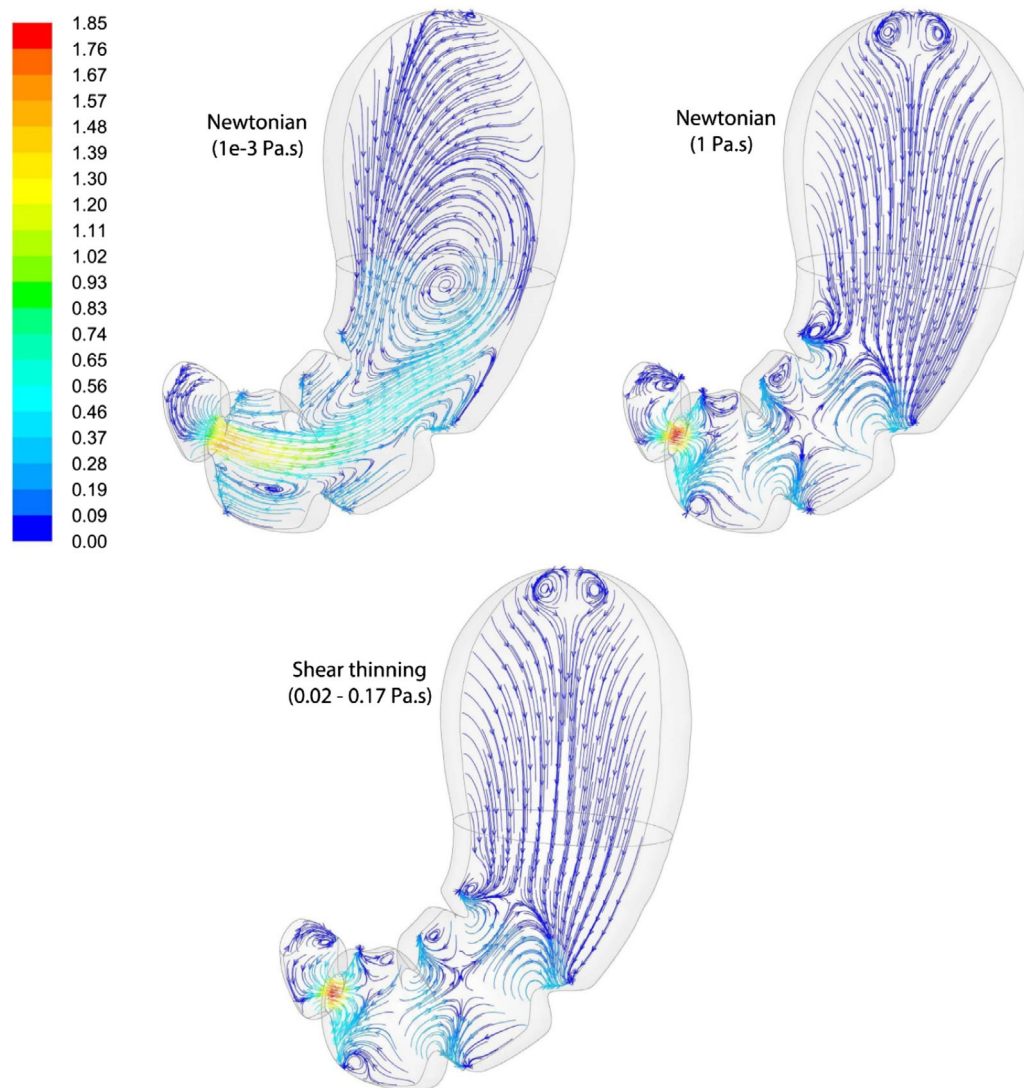


FIGURE 4 Simulation results of a three-dimensional gastric model: streamlines for different rheological properties of the fluid during ACWs, colored by velocity magnitude (cm/s)^{||}

Another intricacy to be considered in modeling gastric fluid mechanics is the multiphasic nature which digesta often exhibit. In general, they are a mixture of solid and liquid phases (Figure 4).

Two common approaches to model dispersed multiphase flows as observed in the gastric lumen are the discrete particle method (DPM) and the Eulerian multifluid model.^[181,182] The Eulerian multifluid model (also called Euler-Euler model or two-fluid model [TFM]) describes different phases as homogenized, interpenetrating fluids. It allows arbitrarily high volume fractions of the solid phase, but requires the derivation of suitable constitutive relations from kinetic theory. Assumptions or approximations typically applied in this derivation often compromise the quantitative reliability of the approach. This difficulty is avoided by the DPM where particle-particle interactions can directly be modeled by soft sphere or hard sphere contact algorithms. However, for high volume fractions of the solid phase, the DPM suffers from numerical problems.

A promising approach to model multiphase flows specifically in the gastric lumen is the method of smoothed particle hydrodynamics (SPH), which has already been successfully applied in computational modeling of the small intestine.^[167] SPH, first introduced in refs. [183, 184], is a mesh-free computational method, which is by its Lagrangian nature^[185,186] particularly suitable for modeling multiphase flows and flows with large deformations of the fluid domain, which both occurs in the stomach.

So far, multiphase flow in the stomach has been addressed only phenomenologically by an Euler-Euler model.^[165] More realistic models (eg. using particle-based methods as DPM or SPH) still remain wanted.

3.2 | Gastric wall: Solid mechanics

Continuum mechanical modeling of gastric tissue considerably lacks behind the modeling of other soft tissues. Gregersen and Kassab^[187] were among the first to suggest a generic exponential stress-strain relation in gastrointestinal tissue. Still

continuum mechanical modeling attempts of the passive properties of gastric tissue largely remain restricted to Fung-type exponential strain energy functions ψ of the form

$$\psi = \frac{1}{2}c(e^{b_1 E_{11}^2 + b_2 E_{22}^2 + 2b_3 E_{11} E_{22}} - 1) \quad (4)$$

with the ij -components E_{ij} of the Green-Lagrange strain tensor \mathbf{E} and where $c > 0$ defines a spatial energy density and b_i , $i = 1 \dots 3$ are nondimensional material parameters.^[88] One of the major drawbacks of simple, phenomenological Fung-type exponential strain energy functions is that they do not distinguish between the structural components of the tissue. Structurally based constitutive models have however been shown to be superior for other tissue types, for example, for vascular tissue.^[188]

In 2009, Gao and colleagues^[189] proposed a component-specific duodenal wall model distinguishing between the passive contributions of elastin and collagen fibers and the active tension created by smooth muscle fibers. The passive model consisted of a single linear-elastic elastin fiber and multiple parallel linear-elastic collagen fibers with distributed unstressed lengths. The collagen fibers were assumed to carry zero stress below a certain length. The smooth muscle model was based on a logarithmic strain energy function combined with a phenomenological muscle tone function. While a component specific modeling approach seems promising, the assumption of linear fiber elasticity adopted in ref. [189] may be questioned.^[73,75,88]

A promising approach modeling gastric tissue might be to adapt the structurally based anisotropic hyperelastic strain energy function originally developed by Holzapfel et al. for the arterial wall.^[188] For this model has already been found to be suitable for various collagenous soft tissues. The general idea of this modeling approach is to describe each tissue layer by an additively decomposed strain energy function of the type

$$\psi = \psi_{vol} + \underbrace{\psi_{iso} + \psi_{aniso}}_{\text{isochoric}} \quad (5)$$

where the indices *vol*, *iso* and *aniso* indicate the volumetric, the isotropic deviatoric and the anisotropic deviatoric part, respectively. The volumetric part in (5) can as a first approximation for soft tissues often be chosen such that it models nearly incompressible material behavior. For the individual summands in (5), various formulations have been proposed in the context of constitutive modeling of soft biological tissues in the gastrointestinal tract and related organs. For example, Sommer and colleagues^[57] studied esophageal tissue. They modeled the isotropic elasticity contribution, which presumably mainly results from the elastin matrix in the tissue, by a Neo-Hookean function

$$\psi_{iso,NH} = \frac{c}{2}(\bar{I}_1 - 3) \quad (6)$$

where $c > 0$ is a stress-like material parameter and $\bar{I}_1 = \text{tr}(\bar{\mathbf{C}})$ is the first invariant of the modified Cauchy-Green tensor $\bar{\mathbf{C}} = \mathbf{J}^{-\frac{2}{3}} \mathbf{C}$ with Cauchy-Green tensor \mathbf{C} and determinant of the deformation gradient \mathbf{J} .^[190] Gizzi and colleagues^[191] used a Mooney-Rivlin like function to describe the isotropic elasticity contribution of intestinal tissue. The isotropic contribution in (5) then becomes

$$\psi_{iso,MR} = \frac{1}{2}(c_1(\bar{I}_1 - 3) + c_2(\bar{I}_2 - 3)) \quad (7)$$

where c_1 , c_2 are stiffness related material parameters, $\bar{I}_1 = \text{tr}(\bar{\mathbf{C}})$ is the first and $\bar{I}_2 = \frac{1}{2}(\text{tr}(\bar{\mathbf{C}})^2 - \text{tr}(\bar{\mathbf{C}}^2))$ the second invariant of the modified Cauchy-Green tensor $\bar{\mathbf{C}}$ as defined above.

Both refs. [57, 191] use Fung-type exponential strain energy functions to describe the anisotropic elasticity contribution from collagen fibers. This contribution can be modeled by

$$\psi_{aniso} = \sum_{i=1}^N \frac{k_{1,i}}{2k_{2,i}} [\exp\{k_{2,i}(\lambda_i^2 - 1)^2\} - 1] \quad (8)$$

where the index i indicates the i th fiber family out of a total of N fiber families; $k_{1,i} > 0$ are stress-like material parameters, $k_{2,i} > 0$ are dimensionless material parameters and λ_i is the elastic stretch of the material in direction of the i th fiber family.

While the above-mentioned formulations have been used successfully to describe the passive constitutive behavior of various fibrous soft biological tissues,^[192–195] their applicability to gastric tissue still needs to be carefully evaluated. For this purpose, suitable experimental data from multiaxial layer-specific tensile tests are required. In particular, detailed mathematical models of smooth muscle tension in the gastric wall still remain to be developed. To this end, work on similar tissues such as vascular smooth muscle^[196] or smooth muscle of the urinary bladder^[197,198] may serve as a guideline.

3.3 | Gastric wall: Electrophysiology and electromechanics

In contrast to the heart where propagation of electrical signals and excitation contraction both are realized (mainly) by cardiomyocytes, in the stomach, these functionalities are fundamentally split among at least two cell types: generation and propagation

of slow waves is realized by ICC. SMCs get electrically excited by slow waves and transform these signals into mechanical responses (cf. Section 2.3.2). Mathematical descriptions of gastric electrophysiology should take into account its multicellular nature including the complex coupling between the structural components. A computational model of gastric electrophysiology must address phenomena across multiple length and time scales. On the cellular scale, the triggering and modulation of slow waves which are essentially oscillations of the transmembrane electric potential must be described. This is possible either phenomenologically, using a simple oscillating system of ordinary differential equations,^[139,199] or by detailed biophysical cell models.^[33,34,127,128,200,201] In biophysical cell models, the spatiotemporal scale associated with the description of the kinetics of ion channels and other intracellular mechanisms is even smaller than the one of the processes on the cellular level. All contributions of one type of ion channel are typically compiled to a single, averaged contribution instead of modeling all ion channels of a type individually.^[202] There have been detailed reviews of existing biophysical cell models of gastric electrophysiology.^[203,204] Only the parameters of biophysical models have a direct biophysical interpretation and are thus appropriate for the detailed exploration of the cellular and subcellular foundations of gastric electrophysiology. Yet, even phenomenological models of gastric electrophysiology are sufficient to reproduce and study the phenomenon of slow waves in realistic geometries when combined with models of electric wave propagation through the gastric wall. Such models in general rely on partial differential equations describing the transport of electric potential through the gastric wall. These partial differential equations can be solved, for example, by finite element discretizations.^[22,35] Three increasingly general models have been proposed to model the propagation of electric signals through the gastric wall: the monodomain,^[139,191,199,205] bidomain,^[206–210] and extended bidomain (also called tridomain)^[211–213] model, where the first one is sufficient to model slow waves qualitatively and the last one allows the detailed examination of even advanced phenomena such as external electric stimulation of the stomach. The three models mainly differ in the number of incorporated cell types and the description of the coupling between the cells. From the extended bidomain formulation the bi- and monodomain models may be regained under special simplifying assumptions. The extended bidomain model explicitly models the intracellular space of two different cell types, smooth muscle cells and ICC, as well as a shared intercellular space. These three spaces are coupled via electric currents. Based on the principle of conservation of total current, the extended bidomain model leads to the equations

$$\nabla \cdot (\sigma_i^{(1)} \nabla \phi_i^{(1)}) = A_m^{(1)} \left(C_m^{(1)} \left(\frac{\partial \phi_i^{(1)}}{\partial t} - \frac{\partial \phi_e}{\partial t} \right) + I_{ion}^{(1)} - I_{stim}^{(1)} \right) + A_{gap} I_{gap} \quad (9)$$

$$\nabla \cdot (\sigma_i^{(2)} \nabla \phi_i^{(2)}) = A_m^{(2)} \left(C_m^{(2)} \left(\frac{\partial \phi_i^{(2)}}{\partial t} - \frac{\partial \phi_e}{\partial t} \right) + I_{ion}^{(2)} - I_{stim}^{(2)} \right) - A_{gap} I_{gap} \quad (10)$$

$$\nabla \cdot (\sigma_e \nabla \phi_e) + \nabla \cdot (\sigma_i^{(1)} \nabla \phi_i^{(1)}) + \nabla \cdot (\sigma_i^{(2)} \nabla \phi_i^{(2)}) + I_{stim}^{ext} = 0 \quad (11)$$

where the superscripts (1) and (2) are used to distinguish between the two cell types (ICC and smooth muscle cells) and the subscripts i and e denote quantities related to the intracellular and extracellular space, respectively. The three principle unknowns are the intracellular electrical potentials $\phi_i^{(1)}$, $\phi_i^{(2)}$ and the extracellular potential ϕ_e . $\sigma_i^{(1)}$, $\sigma_i^{(2)}$, and σ_e are the associated conductivity tensors. $A_m^{(1)}$, $A_m^{(2)}$, and A_{gap} are surface to volume ratios describing either the amount of cell membrane surface per reference volume (index: m) or the amount of cell membrane surface per reference volume covered by gap junctions between the cells. $C_m^{(1)}$ and $C_m^{(2)}$ are the capacitances of the cellular membranes. $I_{ion}^{(1)}$ and $I_{ion}^{(2)}$ are the total sum of all ionic membrane currents for each cell type. The individual ionic conductances are described by functions of the three principle unknowns and additional internal variables. $I_{stim}^{(1)}$ and $I_{stim}^{(2)}$ are stimulus currents into the respective cells and I_{stim}^{ext} is the total external stimulus current into the extracellular space. I_{gap} describes the current through the gap junctions connecting ICC and SMC, often modeled as an ohmic conductance depending on the difference between the intracellular potentials.

There are multiple ways of reducing the extended bidomain model to a simple bidomain model. The most natural way is the simplifying assumption that only one cell type plays a significant role for propagation of electric signals in the tissue. Mathematically, this means $A_m^{(2)} = A_{gap} = 0$. Then, the second equation of the bidomain model can be dropped and together with it the superscripts distinguishing between cell types because only one cell type remains important. The bidomain equations then follow naturally from (9)–(11) as:

$$\nabla \cdot (\sigma_i \nabla \phi_i) = A_m \left(C_m \left(\frac{\partial \phi_i}{\partial t} - \frac{\partial \phi_e}{\partial t} \right) + I_{ion} - I_{stim} \right) \quad (12)$$

$$\nabla \cdot (\sigma_e \nabla \phi_e) + \nabla \cdot (\sigma_i \nabla \phi_i) + I_{stim}^{ext} = 0. \quad (13)$$

To account for the involvement of the two cell types while using the bidomain tissue formulation (12)–(13), one needs to resort to a geometrically explicit description of the separate tissue layers.^[206,208,210]

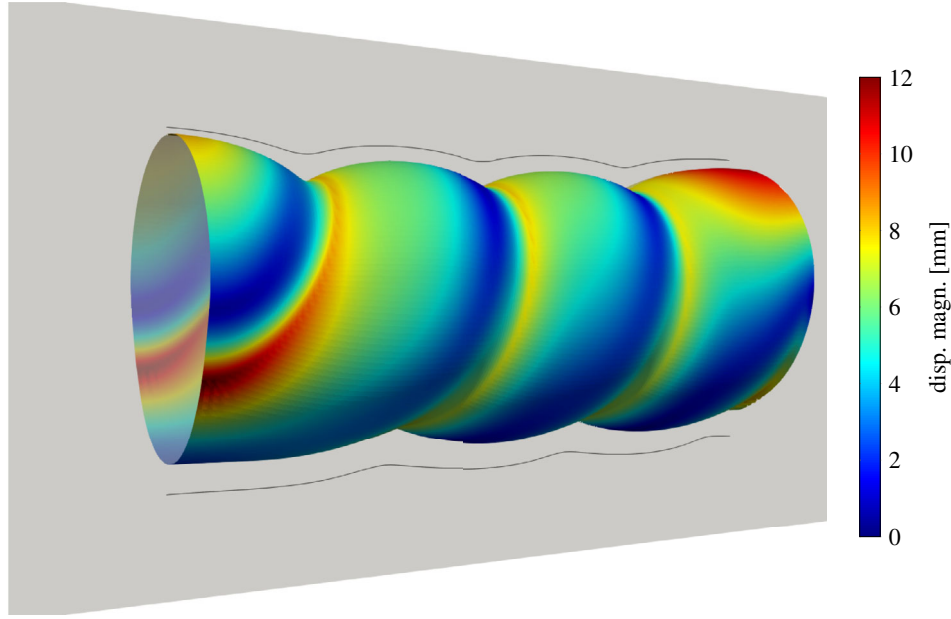


FIGURE 5 Simulation results of an active-strain electromechanics model applied to study ACWs on an idealized cylindrical geometry. The model can represent coordinated propagation of the ACWs based on the underlying entrained slow waves**

The numerical solution of the bidomain and extended bidomain models are both computationally challenging and expensive.^[213–215] Therefore, the so called monodomain model remains a popular alternative. Again, there are multiple ways of deriving a monodomain formulation from the (extended) bidomain model.^[216] One possibility is to assume equal anisotropy of the extra- and intracellular conductivity tensors, that is, a simple proportionality relation between both. Another possibility is to assume a highly conductive extracellular space, that is, $\sigma_e \gg \sigma_i^{(1)}, \sigma_i^{(2)}$. Following the latter approach, it is straight forward to arrive at the following coupled monodomain models (one for each cell type) for gastric electrophysiology:

$$\nabla \cdot (\sigma_i^{(1)} \nabla \phi_i^{(1)}) = A_m^{(1)} \left(C_m^{(1)} \frac{\partial \phi_i^{(1)}}{\partial t} + I_{ion}^{(1)} - I_{stim}^{(1)} \right) + A_{gap} I_{gap} \quad (14)$$

$$\nabla \cdot (\sigma_i^{(2)} \nabla \phi_i^{(2)}) = A_m^{(2)} \left(C_m^{(2)} \frac{\partial \phi_i^{(2)}}{\partial t} + I_{ion}^{(2)} - I_{stim}^{(2)} \right) - A_{gap} I_{gap}. \quad (15)$$

In a recent contribution, ref. [139] has shown that many of the key phenomena of physiological and pathophysiological gastric slow wave propagation such as entrainment, anisotropic conduction patterns, and dysrhythmias can be appropriately modeled by a simple monodomain model (Figure 5).

Gastric electrophysiology and wall mechanics are closely related, for example, via mechanosensitive ion channels in the membrane of the ICC.^[142,217] Disregard of this interplay severely limits nearly all current models of gastric electrophysiology.^[135] In an initial attempt to examine the interplay between mechanics and electrophysiology in the stomach, Brandstaeter and colleagues^[139] have used an active-strain electromechanics formulation to couple electrical slow waves unidirectionally to a continuum mechanical membrane model. With their phenomenological approach, the authors were able to represent the coordinated propagation of ACWs on an idealized stomach geometry as well as the effect of gastric dysrhythmias on the mechanical contractions of the muscle tissue.

The two only coupled electromechanical models of the stomach proposed so far^[52,139] still do not yet incorporate fluid mechanics and thus the important effect of fluid-structure interactions on wall deformation. Combining gastric electrophysiology, fluid mechanics and solid mechanics within a coupled multiphysics model of the whole stomach remains one of the greatest challenges in the field and can be hoped to pave the way to significant insights into gastric mechanics and motility in health and disease.

4 | FUTURE APPLICATIONS AREAS

Detailed mathematical and computational models of the human stomach have the potential to provide insights that may lead to important progress in several application areas ranging from medicine to food industries. In this section, we will briefly illustrate a selection of these potential applications.

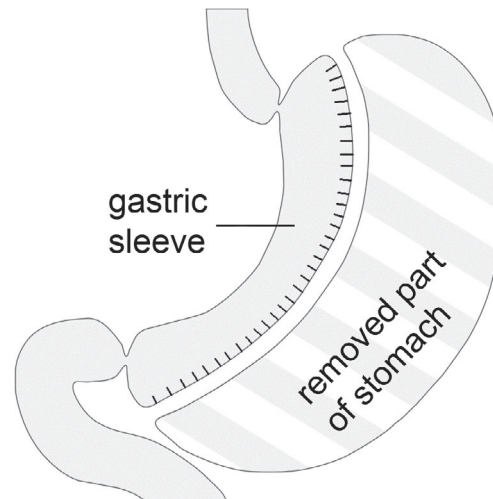


FIGURE 6 sleeve gastrectomy reduces gastric volume by around 75% by stapling, leaving a narrow gastric sleeve

4.1 | Obesity and bariatric surgery

Conservative therapies against obesity, such as a change of life style or medication, seldom reduce body weight by more than 10%, leaving bariatric surgery often as the only option in cases of morbid obesity.^[218] Bariatric surgery directly changes gastric geometry and mechanics, but has recently been discovered to induce also subtle biochemical long-term changes such as genetic switches and altered gastrointestinal microbiota.^[10] The inability of pharmacological measures to produce such long-term changes suggests a remarkable interplay between mechanics and biochemistry in the gastrointestinal tract which remains poorly understood but might be the key to effective therapies of obesity. Currently, more than 250 000 bariatric surgeries per year are performed in the United States and EU together.^[4,5] They typically reduce the effective gastric volume (eg, by downsizing, confining, or bypassing) and pay off within 2–4 years thanks to vastly reduced health care costs.^[7] Over recent years, sleeve gastrectomy (cf. Figure 6) has become the by far dominant bariatric surgical procedure in the United States with a market share of around 60% in 2014^[219] (compared to only 17% in 2011 [4]). A similar global trend is expected, noting that sleeve gastrectomy is increasingly considered the definitive bariatric operation.^[179] Currently, sleeve gastrectomy is performed in practice in a largely heuristic way. Computer-aided planning of these surgical interventions has a significant potential to reduce adverse side effects and is thus an important future application area of mathematical and computational multiphysics models of the human stomach.

4.2 | Dyspepsia

Dyspepsia (indigestion) is one of the most frequent health problems with a prevalence estimated between 10% and 45%.^[9] Often an organic reason such as a peptic ulcer or GERD can be diagnosed. However, between 5% and 10% of the general population suffer from so-called functional dyspepsia, where no organic reason can be identified. Several conditions associated with functional dyspepsia are closely related to gastric mechanics such as increased sensitivity to gastric distension, insufficient gastric accommodation, and delayed gastric emptying (possibly owing to antral hypomotility). Clinically, it is important to distinguish reliably at least between the latter two cases, because muscle relaxing drugs may improve gastric accommodation but impair ACWs and thus gastric emptying, while prokinetic agents would have the opposite effect.

As a highly prevalent and yet fairly unspecific problem, functional dyspepsia is likely to have often not only one single cause but rather to result from an unfavorable combination of several factors. Detailed computational multiphysics models of the stomach could help to unravel the interplay between these factors and identify new therapeutic strategies.

4.3 | Food, satiation, and satiety

Satiation and satiety are thought to be mainly governed by mechanoreceptors in the stomach and nutrient sensing in the intestine^[220–222] and both have been shown to contribute to total satiation nearly additively.^[220] For a given nutrient content, satiation and satiety can therefore be maximized by maximal stimulation of the gastric mechanoreceptors. It remains controversial whether these sense strain or stress^[144,223–231] and currently both should be taken into consideration. In either case, however, designing food so as to maximize gastric retention time appears a promising way to maximize satiation. This idea has already been pursued in a few experimental studies^[232–236] as an approach to tackle obesity. This approach fits with a generally rapidly increasing interest in food design^[233,237] and can be elegantly combined with other approaches from process engineering.^[238,239]

A computational multiphysics model of the stomach could help to speed up the progress in this field significantly by replacing time-consuming and costly experiments by fast and cheap in-silico studies.

5 | CONCLUSIONS

Gastric mechanics is a highly promising field of biomechanics. However, modeling of the human stomach at the moment lags around 20 years behind modeling of the cardiovascular system. So far, there exists no computational multiphysics model of the human stomach combining gastric electrophysiology, fluid mechanics of the digesta, and solid mechanics of the gastric wall. The development of such a model has long been impaired by a limited understanding in these fields and a limited availability of robust computational methods enabling convenient simulations of such complex multiphysics problems. Additionally, research effort in the individual fields has been unevenly distributed in the past, that is, a stronger focus has been put on gastric electrophysiology compared to gastric solid mechanics. In recent years, substantial progress has been made in all mentioned fields, now providing a deeper knowledge and more computational resources to develop and apply a computational multiphysics model of the human stomach.

A general computational multiphysics model of the human stomach bears great potential to serve as a valuable tool for examining the link between gastric mechanics and health problems such as functional dyspepsia, GERD, or morbid obesity, and for developing new therapies. Additionally, a computational multiphysics model of the human stomach could be applied to examine gastric motility, for example, migrating motor complexes, which could support future computer-aided drug design.

These promising application areas are expected to stimulate over the next years fast growing research efforts dedicated to mathematical and computational modeling of the stomach.

ACKNOWLEDGEMENTS

The authors gratefully acknowledge funding from the German Research Foundation (Deutsche Forschungsgemeinschaft) within the Project CY 75/3-1 (“Computational Multiphysics Modeling of the Postprandial Human Stomach”).

ENDNOTES

* *Cardio, cardiac, vascular, heart, coronary, aneurysm, artery, arteries, arterial, athero/arteriosclerotic.*

† *Stomach, gastric, gastro, oesophagus, esophageal, esophagus.*

‡ By courtesy of Encyclopaedia Britannica, Inc., copyright 2010; used with permission.

§ By courtesy of Encyclopaedia Britannica, Inc., copyright 2010; used with permission.

¶ Reprinted from ref. [91]. Copyright (2009), who adapted from Lacy, B. E., Koch, K. L., Crowell, M. D., Chapter 10: Manometry. In: Schuster atlas of gastrointestinal motility in health and disease, Schuster, M. M., Crowell, M. D., Koch, K. L., eds. Second edition 2002, BC Decker Inc., 135-150, both with permission from Elsevier.

|| Reprinted from ref. [164]. Copyright (2014), with permission from Elsevier.

** Reprinted from ref. [139]. Licensed under CC BY 4.0 (<https://creativecommons.org/licenses/by/4.0/legalcode>).

REFERENCES

- [1] E. A. Finkelstein, J. G. Trogon, J. W. Cohen, W. Dietz, *Health Aff.* 2009, **28**(5), w822.
- [2] M. Camilleri, D. Dubois, B. Coulie, M. Jones, P. J. Kahrilas, A. M. Rentz, A. Sonnenberg, V. Stanghellini, W. F. Stewart, J. Tack, N. J. Talley, W. Whitehead, D. A. Revicki, *Clin. Gastroenterol. Hepatol.* 2005, **3**(6), 543.
- [3] OECD, *Overweight and Obesity among Adults*, OECD Publishing, Paris 2012.
- [4] J. D. Wood, *Physiol. Gastrointest. Tract* 2018, 361.
- [5] O. Borisenko, Z. Colpan, B. Dillemans, P. Funch-Jensen, J. Hedenbro, A. R. Ahmed, *Obes. Surg.* 2015, **25**(8), 1408.
- [6] G. W. Hennig, N. J. Spencer, *Physiol. Gastrointest. Tract* 2018, 469.
- [7] P. Y. Cremieux, H. Buchwald, S. A. Shikora, A. Ghosh, H. E. Yang, M. Buessing, *Am. J. Manag. Care* 2008, **14**(9), 589.
- [8] A. J. Gawron, D. D. French, J. E. Pandolfino, C. W. Howden, *PharmacoEconomics* 2014, **32**(8), 745.
- [9] P. Oustamanolakis, J. Tack, *J. Clin. Gastroenterol.* 2012, **46**(3), 175.
- [10] K. K. Ryan, V. Tremaroli, C. Clemmensen, P. Kovatcheva-Datchary, A. Myronovych, R. Karns, H. E. Wilson-Pérez, D. A. Sandoval, R. Kohli, F. Bäckhed, R. J. Seeley, *Nature* 2014, **509**(7499), 183.
- [11] E. A. Klausner, E. Lavy, M. Friedman, A. Hoffman, *J. Control. Release* 2003, **90**(2), 143.
- [12] S. S. Palla, R. Kotha, A. Paladugu, E. R. K. Reddy, S. L. Adavi, K. R. Reddy, *Int. J. Pharmaceut. Sci. Nanotechnol.* 2013, **6**(3), 2097.
- [13] S. Cascone, F. De Santis, G. Lamberti, *J. Drug Deliv. Sci. Technol.* 2017, **41**, 454.
- [14] J. G. Trogon, E. A. Finkelstein, I. A. Nwaise, F. K. Tangka, D. Orenstein, *Health Promot. Pract.* 2007, **8**(3), 234.
- [15] C. C. Rindt, A. A. van Steenhoven, J. D. Janssen, R. S. Reneman, A. Segal, *J. Biomech.* 1990, **23**(5), 461.
- [16] K. Perktold, M. Resch, R. O. Peter, *J. Biomech.* 1991, **24**(6), 409.

- [17] S. K. Singh, *PhD Thesis*, University of California (Davis, CA, USA) 2007.
- [18] K. Perktold, G. Rappitsch, *J. Biomech.* 1995, **28**(7), 845.
- [19] M. D. Sinnott, P. W. Cleary, P. G. Dinning, J. W. Arkwright, M. Costa, *Comput Part Mech* 2015, 1.
- [20] M. D. Sinnott, P. W. Cleary, J. W. Arkwright, P. G. Dinning, *Comput. Biol. Med.* 2012, **42**(4), 492.
- [21] B. Hari, S. Bakalis, P. Fryer, in *Proceedings of the 2012 COMSOL Conf. in Milan*, COMSOL, Incorporation, Burlington, MA 2012.
- [22] P. Du, G. O'Grady, J. B. Davidson, L. K. Cheng, A. J. Pullan, *Crit. Rev. Biomed. Eng.* 2010, **38**(3), 225.
- [23] P. Du, J. Gao, G. O'Grady, L. K. Cheng, *Conf. Proc. IEEE Eng. Med. Biol. Soc.* 2013, **2013**, 6547.
- [24] P. Du, S. Li, G. O'Grady, L. K. Cheng, A. J. Pullan, J. D. Chen, *Am. J. Physiol. Gastrointest. Liver Physiol.* 2009, **297**(4), G672.
- [25] P. Du, G. O'Grady, L. K. Cheng, A. J. Pullan, *Biophys. J.* 2010, **99**(9), 2784.
- [26] P. Du, G. O'Grady, J. Gao, S. Sathar, L. K. Cheng, *Wiley Interdiscip. Rev. Syst. Biol. Med.* 2013, **5**(4), 481.
- [27] P. Du, G. O'Grady, J. A. Windsor, L. K. Cheng, A. J. Pullan, *I.E.E.E. Trans. Biomed. Eng.* 2009, **56**(12), 2755.
- [28] P. Du, Y. C. Poh, J. L. Lim, V. Gajendiran, G. O'Grady, M. L. Buist, A. J. Pullan, L. K. Cheng, *I.E.E.E. Trans. Biomed. Eng.* 2011, **58**(12), 3491.
- [29] G. O'Grady, T. L. Abell, *Gastroenterol. Clin. N. Am.* 2015, **44**(1), 169.
- [30] G. O'Grady, P. Du, L. K. Cheng, J. U. Egbuji, W. J. Lammers, J. A. Windsor, A. J. Pullan, *Am. J. Physiol. Gastrointest. Liver Physiol.* 2010, **299**(3), G585.
- [31] G. O'Grady, P. Du, J. U. Egbuji, W. J. Lammers, A. Wahab, A. J. Pullan, L. K. Cheng, J. A. Windsor, *Surg. Endosc.* 2009, **23**(12), 2842.
- [32] M. L. Buist, A. Corrias, Y. C. Poh, *Ann. Biomed. Eng.* 2010, **38**(9), 3022.
- [33] A. Corrias, M. L. Buist, *Am. J. Physiol. Gastrointest. Liver Physiol.* 2008, **294**(4), G989.
- [34] A. Corrias, M. L. Buist, *Ann. Biomed. Eng.* 2007, **35**(9), 1595.
- [35] A. Corrias, P. Du, M. L. Buist, in *New Advances in Gastrointestinal Motility Research*, Springer, Dordrecht 2013, p. 167–195.
- [36] H. Ehrlein, M. Schemann, *Gastrointestinal Motility*, Technische Universität München, Munich 2005.
- [37] S. Kindt, J. Tack, *Gut* 2006, **55**(12), 1685.
- [38] S. J. Kentish, A. J. Page, *Physiol. Behav.* 2014, **136**, 170.
- [39] A. C. Meyer-Gerspach, B. Wolnerhanssen, B. Beglinger, F. Nessenius, M. Napitupulu, F. H. Schulte, R. E. Steinert, C. Beglinger, *Physiol. Behav.* 2014, **129**, 265.
- [40] A. Pal, K. Indreshkumar, W. Schwizer, B. Abrahamsson, M. Fried, J. G. Brasseur, *Proc. R. Soc. Lond. B Biol. Sci.* 2004, **271**(1557), 2587.
- [41] M. Ferrua, R. Singh, *J. Food Sci.* 2010, **75**(7), R151.
- [42] D. A. Owen, *Am. J. Surg. Pathol.* 1986, **10**, 48.
- [43] M. Koziolok, G. Garbacz, M. Neumann, W. Weitschies, *Mol. Pharm.* 2013, **10**(5), 1610.
- [44] R. G. Lentle, P. W. Janssen, *J. Comp. Physiol. B* 2008, **178**(6), 673.
- [45] F. Kong, R. Singh, *J. Food Sci.* 2008, **73**(5), R67.
- [46] F. Kong, R. P. Singh, *Food Biophys* 2009, **4**(3), 180.
- [47] G. M. Bornhorst, *Annu. Rev. Food Sci. Technol.* 2017, **8**, 523.
- [48] M. Boland, M. Golding, H. Singh, *Food Structures, Digestion and Health*, Elsevier Science, Academic Press, London, UK 2014.
- [49] M. J. Ferrua, F. Kong, R. P. Singh, *Trends Food Sci. Technol.* 2011, **22**(9), 480.
- [50] G. L. Rapaccini, A. Aliotta, M. Pompili, A. Grattagliano, M. Anti, B. Merlino, G. Gambassi, *Gastrointest. Radiol.* 1988, **13**(3), 197.
- [51] A. L. Kierszenbaum, L. Tres, *Histology and Cell Biology: An Introduction to Pathology*, Elsevier Health Sciences, Saunders, Philadelphia, PA 2015.
- [52] N. R. Akhmadeev, R. Miftahof, in *Modelling in Medicine and Biology* (Ed. C. A. Brebbia), WIT Press, Southampton, UK 2011, pp. 3–20.
- [53] W. Yang, T. C. Fung, K. S. Chian, C. K. Chong, *J. Biomech. Eng.* 2006, **128**(6), 899.
- [54] R. K. Goyal, P. Biancani, A. Phillips, H. M. Spiro, *J. Clin. Invest.* 1971, **50**(7), 1456.
- [55] A. N. Natali, E. L. Carniel, H. Gregersen, *Med. Eng. Phys.* 2009, **31**(9), 1056.
- [56] B. K. Tay, J. Kim, M. A. Srinivasan, *I.E.E.E. Trans. Biomed. Eng.* 2006, **53**(11), 2129.
- [57] G. Sommer, A. Schriefel, G. Zeindlinger, A. Katzensteiner, H. Ainödhofer, A. Saxena, G. A. Holzapfel, *Acta Biomater.* 2013, **9**(12), 9379.
- [58] E. L. Carniel, C. G. Fontanella, L. Polese, S. Merigliano, A. N. Natali, *Technol. Health Care* 2013, **21**(3), 271.
- [59] H. Hoeg, A. B. Slatkin, J. W. Burdick, W. S. Grundfest, in *Robotics and Automation, 2000. Proc. ICRA '00. IEEE Int. Conf. IEEE*, Piscataway, NJ 2000.
- [60] C. Bellini, P. Glass, M. Sitti, E. S. Di Martino, *J. Mech. Behav. Biomed. Mater.* 2011, **4**(8), 1727.
- [61] J. Rosen, J. D. Brown, S. De, M. Sinanan, B. Hannaford, *J. Biomech. Eng.* 2008, **130**(2), 021020.
- [62] J. B. Frokjaer, S. D. Andersen, A. M. Drewes, H. Gregersen, *Dig. Dis. Sci.* 2006, **51**(9), 1662.
- [63] D. Liao, J. Zhao, H. Gregersen, *J. Biomech.* 2010, **43**(11), 2079.
- [64] E. L. Carniel, A. Rubini, A. Frigo, A. N. Natali, *Comput. Med. Prog. Bio.* 2014, **113**(1), 338.
- [65] A. E. Bharucha, R. D. Hubmayr, I. J. Ferber, A. R. Zinsmeister, *Am. J. Physiol. Gastrointest. Liver Physiol.* 2001, **281**(2), G459.
- [66] D. A. Watters, A. N. Smith, M. A. Eastwood, K. C. Anderson, R. A. Elton, J. W. Mugerwa, *Gut* 1985, **26**(4), 384.
- [67] D. A. Watters, A. N. Smith, M. A. Eastwood, K. C. Anderson, R. A. Elton, *Q. J. Exp. Physiol.* 1985, **70**(1), 151.
- [68] P. Ciarletta, P. Dario, F. Tendick, S. Micera, *Int. J. Robot. Res.* 2009, **28**(10), 1279.
- [69] J. M. Price, P. Patitucci, Y. C. Fung, *Am. J. Phys.* 1977, **233**(1), C47.
- [70] J. M. Price, P. J. Patitucci, Y. C. Fung, *Am. J. Phys.* 1979, **236**(5), C211.
- [71] E. L. Carniel, V. Gramigna, C. G. Fontanella, C. Stefanini, A. N. Natali, *J. Biomed. Mater. Res. A* 2014, **102**(5), 1243.
- [72] V. I. Egorov, I. V. Schastlivtsev, E. V. Prut, A. O. Baranov, R. A. Turusov, *J. Biomech.* 2002, **35**(10), 1417.
- [73] J. Zhao, D. Liao, P. Chen, P. Kunwald, H. Gregersen, *J. Biomech.* 2008, **41**(16), 3441.
- [74] J. Zhao, D. Liao, H. Gregersen, *Neurogastroenterol. Motil.* 2005, **17**(3), 388.
- [75] Z. G. Jia, W. Li, Z. R. Zhou, *J. Biomech.* 2015, **48**(4), 651.
- [76] R. N. Miftakhov, in *Hydroelasticity of Shells*, Academy of Sciences of the USSR (in Russian), Moscow, 1983, pp. 163–171.
- [77] R. N. Miftakhov, in *Hydroelasticity of Shells*, Academy of Sciences of the USSR (in Russian), Moscow, 1983, pp. 172–181.
- [78] R. N. Miftakhov, in *Investigations in the Theory of Plates and Shells*, Kazan University Press (in Russian), Kazan, Russia, 1985, pp. 35–46.
- [79] F. Nonogaki, *J. Kyoto Prefect. Univ. Med.* 1960, **67**, 1140.
- [80] Y. Fukuyama, *J. Kyoto Prefect. Univ. Med.* 1961, **69**, 261.
- [81] M. K. Howes, *PhD Thesis*, Virginia Polytechnic Institute and State University (USA), Blacksburg, Virginia (U. S.) 2013.
- [82] H. Saraf, K. T. Ramesh, A. M. Lennon, A. C. Merkle, J. C. Roberts, *J. Biomech.* 2007, **40**(9), 1960.
- [83] Y.-J. Lim, D. Deo, T. P. Singh, D. B. Jones, S. De, *Surg. Endosc.* 2009, **23**(6), 1298.
- [84] R. N. Miftakhov, in *Shell Interactions with Fluids*, Academy of Sciences of the USSR (in Russian), Moscow, 1981, pp. 197–204.
- [85] R. N. Miftakhov, in *Shell Interactions with Fluids*, Academy of Sciences of the USSR (in Russian), Moscow, 1981, pp. 205–214.
- [86] W. Avenhaus, B. Kemper, G. von Bally, W. Domschke, *Gastrointest. Endosc.* 2001, **54**(4), 496.
- [87] H. Gregersen, O. H. Gilja, T. Hausken, A. Heimdal, C. Gao, K. Matre, S. Odegaard, A. Berstad, *Am. J. Physiol. Gastrointest. Liver Physiol.* 2002, **283**(2), G368.

- [88] R. C. Aydin, S. Brandstaeter, F. A. Braeu, M. Steigenberger, R. P. Marcus, K. Nikolaou, M. J. Mech. Behav. Biomed. Mater. 2017, **74**, 499.
- [89] A. Tomalka, M. Borsdorf, M. Böl, T. Siebert, *Front. Physiol.* 2017, **8**, 1.
- [90] P. Janssen, S. Verschueren, H. Giao Ly, R. Vos, L. Van Oudenhove, J. Tack, *Neurogastroenterol. Motil.* 2011, **23**(4), 316.
- [91] H. P. Parkman, M. P. Jones, *Gastroenterology* 2009, **136**, 1526.
- [92] T. Arakawa, H. Uno, T. Fukuda, K. Higuchi, K. Kobayashi, T. Kuroki, *J. Smooth Muscle Res.* 1997, **33**, 81.
- [93] W. Schwizer, A. Steingotter, M. Fox, T. Zur, M. Thumshirn, P. Bosiger, M. Fried, *Gut* 2002, **51**, i59.
- [94] K. Indireskumar, J. G. Brasseur, H. Faas, G. S. Hebbard, P. Kunz, J. Dent, C. Feinle, M. Li, P. Boesiger, M. Fried, W. Schwizer, *Am. J. Physiol. Gastrointest. Liver Physiol.* 2000, **278**(4), G604.
- [95] G. Tse, E. T. H. Lai, J. M. Yeo, V. Tse, S. H. Wong, *Front. Physiol.* 2016, **7**.
- [96] K. M. Sanders, Y. Kito, S. J. Hwang, S. M. Ward, *Physiology* 2016, **31**, 316.
- [97] A. J. Burns, T. M. Herbert, S. M. Ward, K. M. Sanders, *Cell Tissue Res.* 1997, **290**, 11.
- [98] K. M. Sanders, S. M. Ward, S. D. Koh, *Physiol. Rev.* 2014, **94**, 859.
- [99] P. J. Blair, Y. Bayguinov, K. M. Sanders, S. M. Ward, *Cell Tissue Res.* 2012, **350**, 199.
- [100] S. A. Baker, G. W. Hennig, A. K. Salter, M. Kurahashi, S. M. Ward, K. M. Sanders, *J. Physiol.* 2013, **591**, 6193.
- [101] T. Komuro, K. Seki, K. Horiguchi, *Arch. Histol. Cytol.* 1999, **62**, 295.
- [102] B. T. Drumm, S. A. Baker, *Adv. Physiol. Educ.* 2017, **41**, 100.
- [103] C. P. Fall, J. E. Keizer, *J. Theor. Biol.* 2001, **210**(2), 151.
- [104] H. Zheng, B. T. Drumm, S. Earley, T. S. Sung, S. D. Koh, K. M. Sanders, *Sci. Signal.* 2018, **11**.
- [105] B. T. Drumm, T. S. Sung, H. Zheng, S. A. Baker, S. D. Koh, K. M. Sanders, *Cell Calcium* 2018, **72**, 1.
- [106] K. M. Sanders, S. D. Koh, S. Ro, S. M. Ward, *Nat. Rev. Gastroenterol. Hepatol.* 2012, **9**, 633.
- [107] S. M. Ward, T. Ördög, S. D. Koh, S. A. Baker, J. Y. Jun, G. Amberg, K. Monaghan, K. M. Sanders, *J. Physiol.* 2000, **525**, 355.
- [108] M. H. Zhu, T. S. Sung, K. O'Driscoll, S. D. Koh, K. M. Sanders, *Am. J. Physiol. Cell Physiol.* 2015, **308**, C608.
- [109] P. J. Gomez-Pinilla, S. J. Gibbons, M. R. Bardsley, A. Lorincz, M. J. Pozo, P. J. Pasricha, M. V. de Rijn, R. B. West, M. G. Sarr, M. L. Kendrick, R. R. Cima, E. J. Dozois, D. W. Larson, T. Ordog, G. Farrugia, *Am. J. Physiol. Gastrointest. Liver Physiol.* 2009, **296**, G1370.
- [110] S. J. Hwang, N. Basma, K. M. Sanders, S. M. Ward, *Br. J. Pharmacol.* 2016, **173**, 1339.
- [111] S. J. Hwang, P. J. A. Blair, F. C. Britton, K. E. O'Driscoll, G. Hennig, Y. R. Bayguinov, J. R. Rock, B. D. Harfe, K. M. Sanders, S. M. Ward, *J. Physiol.* 2009, **587**, 4887.
- [112] M. H. Zhu, T. W. Kim, S. Ro, W. Yan, S. M. Ward, S. D. Koh, K. M. Sanders, *J. Physiol.* 2009, **587**, 4905.
- [113] B. T. Drumm, G. W. Hennig, M. J. Battersby, E. K. Cunningham, T. S. Sung, S. M. Ward, K. M. Sanders, S. A. Baker, *J. Gen. Physiol.* 2017, **149**, 703.
- [114] H. Zheng, K. S. Park, S. D. Koh, K. M. Sanders, *AJP: Cell Physiology* 2014, **306**, C705.
- [115] S. A. Baker, B. T. Drumm, D. Saur, G. W. Hennig, S. M. Ward, K. M. Sanders, *J. Physiol.* 2016, **594**, 3317.
- [116] H. M. Cousins, F. R. Edwards, H. Hickey, C. E. Hill, G. D. S. Hirst, *J. Physiol.* 2003, **550**, 829.
- [117] K. N. Bitar, *Am. J. Med.* 2003, **115**, 15.
- [118] K. N. Bitar, R. R. Gilmont, S. Raghavan, S. Somara, in *Physiology of the Gastrointestinal Tract*, Academic Press, 2012, pp. 489–509.
- [119] B. A. Perrino, *J. Neurogastroenterol. Motil.* Academic Press, London, UK 2016, Korean Society of Neurogastroenterology and Motility, 213.
- [120] F. M. Gribble, F. Reimann, G. P. Roberts, *Physiol. Gastrointest. Tract* 2018, 31.
- [121] J. D. Huizinga, *Physiol. Gastrointest. Tract* 2018, 305.
- [122] M. Grover, C. E. Bernard, P. J. Pasricha, H. P. Parkman, T. L. Abell, L. A. Nguyen, W. Snape, K. R. Shen, M. Sarr, J. Swain, M. Kendrick, S. Gibbons, T. Ordog, G. Farrugia, *Neurogastroenterol. Motil.* 2012, **24**, 844.
- [123] K. M. Sanders, S. M. Ward, *Br. J. Pharmacol.* 2018, 1.
- [124] T. S. Sung, S. J. Hwang, S. D. Koh, Y. Bayguinov, L. E. Peri, P. J. Blair, T. I. Webb, D. M. Pardo, J. R. Rock, K. M. Sanders, S. M. Ward, *J. Physiol.* 2018, **596**, 1549.
- [125] P. R. Strege, Y. Ou, L. Sha, A. Rich, S. J. Gibbons, J. H. Szurszewski, M. G. Sarr, G. Farrugia, *Am. J. Physiol. Gastrointest. Liver Physiol.* 2003, **285**, G1111.
- [126] S. J. Park, C. M. McKay, Y. Zhu, J. D. Huizinga, *Am. J. Physiol. Gastrointest. Liver Physiol.* 2005, **289**, G791.
- [127] R. Faville, A. Pullan, K. Sanders, S. Koh, C. Lloyd, N. Smith, *Biophys. J.* 2009, **96**(12), 4834.
- [128] R. A. Faville, A. J. Pullan, K. M. Sanders, N. P. Smith, *Biophys. J.* 2008, **95**(1), 88.
- [129] K. M. Sanders, S. D. Koh, S. M. Ward, *Annu. Rev. Physiol.* 2006, **68**, 307.
- [130] D. F. Va. Helden, D. R. Laver, J. Holdsworth, M. S. Intiaz, *Clin. Exp. Pharmacol. Physiol.* 2010, **37**, 516.
- [131] W. J. E. P. Lammers, B. Stephen, K. Arafat, G. W. Manefield, *Neurogastroenterol. Motil.* 1996, **8**, 207.
- [132] G. O'Grady, T. R. Angeli, P. Du, C. Lahr, W. J. E. P. Lammers, J. A. Windsor, T. L. Abell, G. Farrugia, A. J. Pullan, L. K. Cheng, *Gastroenterology* 2012, **143**, 589.e3.
- [133] T. R. Angeli, N. Paskaranandavadi, L. K. Cheng, P. Du, *Food Struct. Dig. Health* 2014, 273.
- [134] P. Du, A. Hameed, T. R. Angeli, C. Lahr, T. L. Abell, L. K. Cheng, G. O'Grady, *Neurogastroenterol. Motil.* 2015, **27**, 1409.
- [135] R. Berry, L. K. Cheng, P. Du, N. Paskaranandavadi, T. R. Angeli, T. Mayne, G. Beban, G. O'Grady, G. O'Grady, *Obes. Surg.* 2017, **27**, 1.
- [136] N. Paskaranandavadi, L. K. Cheng, P. Du, J. M. Rogers, G. O'Grady, *Am. J. Physiol.-Gastrointest. Liver Physiol.* 2017, **313**, G265.
- [137] A. Farajidavar, *Brain Res.* 2018, **1693**, 169.
- [138] W. J. E. P. Lammers, B. Stephen, E. Adeghate, S. Ponery, O. Pozzan, *Neurogastroenterol. Motil.* 1998, **10**, 339.
- [139] S. Brandstaeter, A. Gizzi, S. L. Fuchs, A. M. Gebauer, R. C. Aydin, C. J. Cyron, *ZAMM-J. Appl. Math. Mech.* 2018, **98**, 2177.
- [140] G. O'Grady, T. H. H. Wang, P. Du, T. Angeli, W. J. Lammers, L. K. Cheng, *Clin. Exp. Pharmacol. Physiol.* 2014, **41**, 854.
- [141] P. Du, S. Calder, T. R. Angeli, S. Sathar, N. Paskaranandavadi, G. O'Grady, L. K. Cheng, *Front. Physiol.* 2018, **8**, 1136.
- [142] Z. Y. Wang, Y. F. Han, X. Huang, P. Zhao, H. L. Lu, Y. C. Kim, W. X. Xu, *J. Biomech.* 2010, **43**(11), 2214.
- [143] I. M. de Zwart, J. J. Haans, P. Verbeek, P. H. Eilers, A. de Roos, A. A. Masclee, *Am. J. Physiol. Gastrointest. Liver Physiol.* 2007, **292**(1), G208.
- [144] E. Distrutti, F. Azpiroz, A. Soldevilla, J. R. Malagelada, *Gastroenterology* 1999, **116**(5), 1035.
- [145] I. M. de Zwart, B. Mearadji, H. J. Lamb, P. H. Eilers, A. A. Masclee, A. de Roos, P. Kunz, *Radiology* 2002, **224**(2), 592.
- [146] B. D. van den Elzen, R. J. Bennink, R. E. Wieringa, G. N. Tytgat, G. E. Boeckxstaens, *Gut* 2003, **52**(11), 1548.
- [147] W. Schwizer, A. Steingotter, M. Fox, *Scand. J. Gastroenterol.* 2006, **41**(11), 1245.
- [148] W. Schwizer, R. Fraser, J. Borovicka, G. Crelier, P. Boesiger, M. Fried, *Dig. Dis. Sci.* 1994, **39**(12), 1015.
- [149] W. Schwizer, H. Maecke, M. Fried, *Gastroenterology* 1992, **103**(2), 369.
- [150] M. K. Stehling, D. F. Evans, G. Lamont, R. J. Ordidge, A. M. Howseman, B. Chapman, R. Coxon, P. Mansfield, J. D. Hardcastle, R. E. Coupland, *Radiology* 1989, **171**(1), 41.
- [151] K. Schulze, *Neurogastroenterol. Motil.* 2006, **18**(3), 172.

- [152] K. S. Schulze, *Acta Physiol.* 2015, **213**(2), 394.
- [153] L. Marciani, P. Young, J. Wright, R. Moore, N. Coleman, P. A. Gowland, R. C. Spiller, *Neurogastroenterol. Motil.* 2001, **13**(5), 511.
- [154] A. Steingötter, *PhD Thesis*, Swiss Federal Institute of Technology Zurich, Zurich, CH, Swiss 2005.
- [155] W. Ajaj, S. C. Goehde, N. Papanikolaou, G. Holtmann, S. G. Ruehm, J. F. Debatin, T. C. Lauenstein, *Gut* 2004, **53**(9), 1256.
- [156] W. Schwizer, M. Fox, A. Steingötter, *Gut* 2003, **52**(suppl 4), iv34.
- [157] H. Koza, I. Kobayashi, M. A. Neves, M. Nakajima, K. Uemura, S. Sato, S. Ichikawa, *Food Funct.* 2014, **5**(8), 1839.
- [158] Q. Guo, A. Ye, M. Lad, M. Ferrua, D. Dalgleish, H. Singh, *Food Funct.* 2015, **6**(3), 756.
- [159] F. Kong, R. P. Singh, *J. Food Sci.* 2010, **75**(9), E627.
- [160] K. Verhoeckx, P. Cotter, I. López-Expósito, C. Kleiveland, T. Lea, A. Mackie, T. Requena, D. Swiatecka, H. Wichers, *The Impact of Food Bio-Actives on Gut Health: In Vitro and Ex Vivo Models*, Springer, Cham 2015.
- [161] A. Pal, J. G. Brasseur, B. Abrahamsson, *J. Biomech.* 2007, **40**(6), 1202.
- [162] H. Koza, I. Kobayashi, M. Nakajima, K. Uemura, S. Sato, S. Ichikawa, *Food Biophys.* 2010, **5**(4), 330.
- [163] M. J. Ferrua, R. P. Singh, *Procedia Food Sci.* 2011, **1**, 1465.
- [164] M. J. Ferrua, Z. Xue, R. P. Singh, *J. Biomech.* 2014, **47**(15), 3664.
- [165] Z. Xue, M. J. Ferrua, P. Singh, *Alimentos Hoy* 2012, **21**(27), 3.
- [166] Y. Imai, I. Kobayashi, S. Ishida, T. Ishikawa, M. Buist, T. Yamaguchi, *Am. J. Physiol. Gastrointest. Liver Physiol.* 2013, **304**(5), G536.
- [167] M. D. Sinnott, P. W. Cleary, S. M. Harrison, *Appl. Math. Model.* 2017, **44**, 143.
- [168] P. Cleary, M. Sinnott, B. Hari, S. Bakalis, S. Harrison, *Chapter 10 - Modelling food digestion*. in *Modeling Food Processing Operations* (Eds: S. Bakalis, K. Knoerzer, P. Fryer), Elsevier Science & Technology, Cambridge 2015.
- [169] S. M. Harrison, P. W. Cleary, M. D. Sinnott, *Food Funct.* 2018, **9**, 3202.
- [170] M. J. Ferrua, R. P. Singh, *Curr. Opin. Food Sci.* 2015, **4**, 116.
- [171] M. Schemann, H. J. Ehrlein, *Digestion* 1982, **25**(3), 194.
- [172] N. Washington, *Antacids and Anti Reflux Agents*, Taylor & Francis, Boca Raton 1991.
- [173] D. Kumar, S. Gustavsson, *An Illustrated Guide to Gastrointestinal Motility*, John Wiley & Sons Ltd, Chichester 1988.
- [174] H. J. Ehrlein, O. Keinke, M. Schemann, *Studies on the process of gastric emptying*. in *Gastrointestinal Motility* (Ed: C. Roman), Springer, Netherlands, Dordrecht 1983, p. 111.
- [175] O. Keinke, H. J. Ehrlein, *Q. J. Exp. Physiol.* 1983, **68**(4), 675.
- [176] P. M. King, A. Pryde, R. C. Heading, *Dig. Dis. Sci.* 1988, **33**(12), 1537.
- [177] J. Russell, P. Bass, *Am. J. Physiol. Gastrointest. Liver Physiol.* 1985, **249**(6), G662.
- [178] R. G. Lentle, P. W. Janssen, K. Goh, P. Chambers, C. Hulls, *Dig. Dis. Sci.* 2010, **55**(12), 3349.
- [179] M. Laffin, J. Chau, R. S. Gill, D. W. Birch, S. Karmali, *J. Obes.* 2013, **2013**.
- [180] L. Marciani, P. A. Gowland, R. C. Spiller, P. Manoj, R. J. Moore, P. Young, S. Al-Sahab, D. Bush, J. Wright, A. J. Fillery-Travis, *J. Nutr.* 2000, **130**, 122.
- [181] Wörner, M., *A Compact Introduction to the Numerical Modeling of Multiphase Flows*. Karlsruhe Institut of Technology, Karlsruhe 2003.
- [182] N. G. Deen, M. Van Sint Annaland, M. A. Van der Hoef, J. A. M. Kuipers, *Chem. Eng. Sci.* 2007, **62**(1–2), 28.
- [183] R. A. Gingold, J. J. Monaghan, *Mon. Not. R. Astron. Soc.* 1977, **181**, 375.
- [184] L. B. Lucy, L. B. Lucy, *Astron. J.* 1977, **82**, 1013.
- [185] J. J. Monaghan, *Rep. Prog. Phys.* 2005, **68**, 1703.
- [186] M. B. Liu, G. R. Liu, *Arch. Comput. Method Eng.* 2010, **17**, 25.
- [187] H. Gregersen, G. Kassab, *Neurogastroenterol. Motil.* 1996, **8**, 277.
- [188] G. A. Holzapfel, T. C. Gasser, R. W. Ogden, *J. Elast. Phys. Sci. Solids* 2000, **61**, 1.
- [189] F. Gao, D. Liao, A. M. Drewes, H. Gregersen, *Neurogastroenterol. Motil.* 2009, **21**, 914.
- [190] G. A. Holzapfel, *Nonlinear Solid Mechanics: A Continuum Approach for Engineering*. John Wiley & Sons Ltd, Chichester 2000.
- [191] A. Gizzi, A. Pandolfi, M. Vasta, *Int. J. Comput. Method Eng. Sci. Mech.* 2016, **17**(3), 143.
- [192] M. Vasta, A. Gizzi, A. Pandolfi, *Int. J. Non-Linear Mech.* 2018, **106**, 258.
- [193] A. Gizzi, A. Pandolfi, M. Vasta, *J. Eng. Math.* 2018, **109**, 211.
- [194] A. Pandolfi, A. Gizzi, M. Vasta, *Meccanica* 2017, **1**.
- [195] A. Pandolfi, A. Gizzi, M. Vasta, *J. Biomech.* 2016, **49**, 2436.
- [196] S. I. Murtada, J. D. Humphrey, G. A. Holzapfel, *Biophys. J.* 2017, **113**, 714.
- [197] R. Seydewitz, R. Menzel, T. Siebert, M. Böhl, *J. Mech. Behav. Biomed. Mater.* 2017, **75**, 128.
- [198] E. Morales-Orcajo, T. Siebert, M. Böhl, *Acta Biomater.* 2018, **75**, 263.
- [199] R. R. Aliev, W. Richards, J. P. Wikswo, *J. Theor. Biol.* 2000, **204**(1), 21.
- [200] J. B. Youm, N. Kim, J. Han, E. Kim, H. Joo, C. H. Leem, G. Goto, A. Noma, Y. E. Earm, *Philos Trans A Math Phys Eng Sci* 2006, **364**(1842), 1135.
- [201] R. Lees-Green, S. J. Gibbons, G. Farrugia, J. Sneyd, L. K. Cheng, *Am. J. Physiol. Gastrointest. Liver Physiol.* 2014, **306**, G711.
- [202] J. Keener, J. Sneyd, *Mathematical Physiology I: Cellular Physiology*, Vol. **8/1** Springer, New York, NY 2009.
- [203] R. Lees-Green, P. Du, G. O'Grady, A. Beyder, G. Farrugia, A. J. Pullan, *Front. Physiol.* 2011, **2**.
- [204] B. B. Barth, X. Shen, *Brain Res.* 2018, **1693**, 174.
- [205] A. Gizzi, C. Cherubini, S. Migliori, R. Alloni, R. Portuesi, S. Filippi, *Phys. Biol.* 2010, **7**, 16011.
- [206] M. L. Buist, L. K. Cheng, R. Yassi, L. A. Bradshaw, W. O. Richards, A. J. Pullan, *Physiol. Meas.* 2004, **25**, 849.
- [207] A. J. Pullan, L. K. Cheng, R. Yassi, M. L. Buist, *Prog. Biophys. Mol. Biol.* 2004, **85**, 523.
- [208] L. K. Cheng, R. Komuro, T. M. Austin, M. L. Buist, A. J. Pullan, *World J. Gastroenterol.* 2007, **13**, 1378.
- [209] A. Corrias, P. Pathmanathan, D. J. Gavaghan, M. L. Buist, *Integr. Biol.* 2012, **4**, 192.
- [210] M. L. Buist, L. K. Cheng, K. M. Sanders, A. J. Pullan, *Exp. Physiol.* 2006, **91**, 383.
- [211] F. B. Sachse, A. P. Moreno, G. Seemann, J. A. Abildskov, *Ann. Biomed. Eng.* 2009, **37**, 874.
- [212] M. L. Buist, Y. C. Poh, *Biophys. J.* 2010, **99**(1), 13.
- [213] S. Sathar, M. L. Trew, G. O'Grady, L. K. Cheng, *Biomed. Eng. IEEE Trans.* 2015, **62**, 2685.
- [214] E. J. Vigmond, F. Aguel, N. A. Trayanova, *Biom. Eng. IEEE Trans.* 2002, **49**, 1260.
- [215] J. A. Southern, G. Plank, E. J. Vigmond, J. P. Whiteley, *Biomed. Eng.*, IEEE Transactions on 2009, **56**, 2404.
- [216] P. C. Franzone, L. F. Pavarino, S. Scacchi, *Mathematical Cardiac Electrophysiology* Springer, Cham 2014, p. 13.
- [217] A. Beyder, R. Lees-Green, G. Farrugia, *Role of Ion Channel Mechanosensitivity in the Gut: Mechano-Electrical Feedback Exemplified By Stretch-Dependence of Nav1.5*. in *New Advances in Gastrointestinal Motility Research* (Eds: L. K. Cheng, A. J. Pullan, G. Farrugia), Springer, Netherlands, Dordrecht 2013, p. 7.
- [218] H. R. Berthoud, A. C. Shin, H. Zheng, *Physiol. Behav.* 2011, **105**(1), 106.

- [219] J. Esteban Varela, N. T. Nguyen, *Surg. Obes. Relat. Dis.* 2015.
- [220] T. L. Powley, R. J. Phillips, *Physiol. Behav.* 2004, **82**(1), 69.
- [221] R. E. Steinert, A. C. Meyer-Gerspach, C. Beglinger, *Am. J. Physiol. Endocrinol. Metab.* 2012, **302**(6), E666.
- [222] P. Janssen, P. Vande Berghe, S. Verschueren, A. Lehmann, I. Depoortere, J. Tack, *Aliment. Pharmacol. Ther.* 2011, **33**(8), 880.
- [223] J. Tack, B. Coulie, A. Wilmer, A. Andrioli, J. Janssens, *Gut* 2000, **46**(4), 468.
- [224] H. Piessevaux, J. Tack, A. Wilmer, B. Coulie, A. Geubel, J. Janssens, *Gut* 2001, **49**(2), 203.
- [225] P. Janssen, H. Pottel, R. Vos, J. Tack, *Aliment. Pharmacol. Ther.* 2011, **33**(5), 607.
- [226] R. Notivol, B. Coffin, F. Azpiroz, F. Mearin, J. Serra, J. R. Malagelada, *Gastroenterology* 1995, **108**(2), 330.
- [227] A. Iggo, *J. Physiol.* 1955, **128**(3), 593.
- [228] L. Ashley Blackshaw, D. Grundy, T. Scratcherd, *J. Auton. Nerv. Syst.* 1987, **18**(1), 19.
- [229] S. Carmagnola, P. Cantu, R. Penagini, *Am. J. Gastroenterol.* 2005, **100**(8), 1704.
- [230] J. D. Barlow, H. Gregersen, D. G. Thompson, *Am. J. Physiol. Gastrointest. Liver Physiol.* 2002, **282**(4), G683.
- [231] T. Takeda, T. Nabae, G. Kassab, J. Liu, R. K. Mittal, *Neurogastroenterol. Motil.* 2004, **16**(6), 721.
- [232] L. Marciani, N. Hall, S. E. Pritchard, E. F. Cox, J. J. Totman, M. Lad, C. L. Hoad, T. J. Foster, P. A. Gowland, R. C. Spiller, *J. Nutr.* 2012, **142**(7), 1253.
- [233] A. R. Mackie, H. Rafiee, P. Malcolm, L. Salt, G. van Aken, *Am. J. Physiol. Gastrointest. Liver Physiol.* 2013, **304**(11), G1038.
- [234] L. Marciani, S. E. Pritchard, C. Hellier-Woods, C. Costigan, C. L. Hoad, P. A. Gowland, R. C. Spiller, *Eur. J. Clin. Nutr.* 2013, **67**(7), 754.
- [235] L. Marciani, M. Wickham, G. Singh, D. Bush, B. Pick, E. Cox, A. Fillery-Travis, R. Faulks, C. Marsden, P. A. Gowland, R. C. Spiller, *Am. J. Physiol. Gastrointest. Liver Physiol.* 2007, **292**(6), G1607.
- [236] L. Marciani, R. Faulks, M. S. Wickham, D. Bush, B. Pick, J. Wright, E. F. Cox, A. Fillery-Travis, P. A. Gowland, R. C. Spiller, *Br. J. Nutr.* 2009, **101**(6), 919.
- [237] H. Singh, A. Ye, M. J. Ferrua, *Curr. Opin. Food Sci.* 2015, **3**, 85.
- [238] I. Norton, P. Fryer, S. Moore, *AIChE J.* 2006, **52**(5), 1632.
- [239] I. Norton, S. Moore, P. Fryer, *Obes. Rev.* 2007, **8**, 83.

How to cite this article: Brandstaeter S, Fuchs SL, Aydin RC, Cyron CJ. Mechanics of the stomach: A review of an emerging field of biomechanics. *GAMM-Mitteilungen*. 2019;42:e201900001. <https://doi.org/10.1002/gamm.201900001>

B

Computational model of gastric motility with active-strain electromechanics

Sebastian Brandstaeter, Alessio Gizzi, Sebastian L. Fuchs, Amadeus M. Gebauer, Roland C. Aydin, Christian J. Cyron




published in

ZAMM - Journal of Applied Mathematics and Mechanics / Zeitschrift Für Angewandte Mathematik Und Mechanik, vol. 98, no. 12, pp. 2177–2197, 2018.

DOI: [10.1002/zamm.201800166](https://doi.org/10.1002/zamm.201800166).

Reprinted from [51], licensed under a Creative Commons Attribution 4.0 International License (<https://creativecommons.org/licenses/by/4.0/>).

Computational model of gastric motility with active-strain electromechanics

Sebastian Brandstaeter¹  | Alessio Gizzi²  | Sebastian L. Fuchs^{1,3} |
Amadeus M. Gebauer¹ | Roland C. Aydin¹ | Christian J. Cyron^{3,4} 

¹Institute for Computational Mechanics, Technical University of Munich, Boltzmannstrasse 15, 85748, Garching, Germany

²Department of Engineering, Campus Bio-Medico University of Rome, Via A. del Portillo 21, 00128, Rome, Italy

³Institute of Continuum and Materials Mechanics, Hamburg University of Technology, Eissendorfer Str. 42, 21073, Hamburg, Germany

⁴Institute of Materials Research, Materials Mechanics, Helmholtz-Zentrum Geesthacht, Max-Planck-Strasse 1, 21502, Geesthacht, Germany

Correspondence

Christian J. Cyron, Institute of Continuum and Materials Mechanics, Hamburg University of Technology, Eissendorfer Str. 42, 21073, Hamburg, Germany
Email: christian.cyron@tuhh.de

Funding information

Erasmus+; Deutsche Forschungsgemeinschaft, Grant/Award Number: CY 75/3-1; Italian National Group of Mathematical Physics (GNFM); Istituto Nazionale di Alta Matematica "Francesco Severi"; COST-CA16119, Grant/Award Number: STSM-38666

Present Address

Institute of Continuum and Materials Mechanics, Hamburg University of Technology, Eissendorfer Str. 42, 21073 Hamburg, Germany

We present an electro-mechanical constitutive framework for the modeling of gastric motility, including pacemaker electrophysiology and smooth muscle contractility. In this framework, we adopt a phenomenological description of the gastric tissue. Tissue electrophysiology is represented by a set of two minimal two-variable models and tissue electromechanics by an active-strain finite elasticity approach. We numerically investigate the implication of the spatial distribution of pacemaker cells on the entrainment and synchronization of the slow waves characterizing gastric motility in health and disease. On simple schematic model geometries, we demonstrate that the proposed computational framework is amenable to large scale in-silico analyses of the complex gastric motility including the underlying electro-mechanical coupling.

KEYWORDS

active-strain electro-mechanics, electrophysiology, finite elasticity, gastric motility

1 | INTRODUCTION

Gastric motility is a coordinated dynamics of the stomach wall that typically results in rhythmic contractions, which accomplishes several physiological functions such as mixing, grinding and propulsion of ingested food.^[1] Gastric motility is partly

Abbreviations: ICC, interstitial cell of Cajal; ICC-MY, myenteric interstitial cell of Cajal; SMC, smooth muscle cell; VDCC, voltage-dependent calcium channel; cpm, cycles per minute

This is an open access article under the terms of the Creative Commons Attribution License, which permits use, distribution and reproduction in any medium, provided the original work is properly cited.

© 2018 The Authors. ZAMM - Journal of Applied Mathematics and Mechanics published by Wiley-VCH Verlag GmbH & Co. KGaA

governed by the electric activity of the gastric electrophysiological system.^[2,3] The electric activity of the gastric tissue controls the contractile stress exerted by the smooth muscle cells (SMC) of the tissue via synchronized propagating bioelectrical waves, known as slow waves.^[4] Slow waves are permanently present in most of the regions of the gastrointestinal tract. However, smooth muscle contraction only occurs if certain neuronal and hormonal signals coincide with these electrical signals.^[5] Slow waves are generated by specialized pacemaker cells, termed interstitial cells of Cajal (ICC), i.e., located between the longitudinal and circular muscle layer. Gastric slow waves are characterized by four distinct phases: in the initial upstroke phase, the cell depolarizes rapidly from a resting potential to a peak potential. The initial upstroke is followed by a pronounced plateau phase, in which the potential stays close to the peak potential. In the repolarization phase, the membrane potential returns to its resting value and during the refractory phase, it remains there. It has been shown that Ano1 channels, a type of Ca^{2+} -activated Cl^- channel, play a fundamental role in slow wave generation of ICC.^[6] It is hypothesized that calcium-induced calcium release from internal stores into microdomains might be an important mechanism for pacemaker functionality.^[7] ICC are spatially distributed in a continuous network-like arrangement. Within this network, slow waves propagate across ICC via voltage-dependent mechanisms.^[3,8] Therefore, the pacemaker system of the stomach is spread across the whole organ, unlike in the heart where specific nodes dictate the pacemaker activity.^[9] Overall, several details of the complex biophysical mechanisms ruling the electrophysiology of slow waves remain unknown, despite considerable research efforts.^[2,3,6,7,10–13]

While isolated ICC generate slow waves at distinct intrinsic frequencies, they synchronize to the highest frequency in an undamaged network. This process is called *entrainment*. In the healthy human stomach, the driving *pacemaker region* is located on the greater curvature of the proximal stomach. There, the ICC with the highest intrinsic frequency of approximately 3 cpm (cycles per minute) can be found. From the pacemaker region, the intrinsic frequency degrades towards the pylorus, a fact known as (intrinsic) *frequency gradient*. In the distal antrum the intrinsic frequency is between 0.8 cpm to 1.8 cpm. The frequency gradient, combined with the process of entrainment, is essential for the coordinated onset and propagation of slow waves in distal direction resulting in the characteristic shape of ring wavefronts. Under healthy conditions, between three and four slow waves simultaneously travel at a distance of approximately 60 mm towards the pylorus. The fundus has been shown to be electrically quiescent so that slow waves do not spread proximally from the pacemaker region into the fundus.^[9,14,15]

In the presence of pathologies, abnormal slow waves are observed and associated with different gastric motility disorders. In particular, the physiological entrainment regulated by ICC may degenerate leading to ectopic initiations, conduction blocks etc.,^[16] usually named *dysrhythmias*. Most of these phenomena appear astonishingly similar to what is known from cardiac tissue, e.g., in the form of cardiac arrhythmias,^[17] further emphasizing the shared biophysical features between different active biological media.^[18]

The specific electro-mechanical activity of the stomach is realized through the coordinated interplay between ICC and SMC. The slow waves generated and actively propagated by ICC spread passively to the surrounding SMC via dedicated proteic connections, the so-called gap junctions.^[19] These localized structures furnish a direct electrical coupling between different cells forming a so-called syncytium. SMC are depolarized by the conduction of slow waves. The depolarization activates L-type voltage-dependent Ca^{2+} channels (VDCC);^[3] the initial event to start complex multiscale mechanisms, e.g., calcium-induced calcium release,^[20,21] which result in the smooth muscle contractions deforming the gastric wall as a whole in a coordinated and synchronous manner.

In the last decades, simplified phenomenological, mathematical approaches, based on FitzHugh-Nagumo-like dynamical systems, have been proposed for modeling the ICC-SMC electrical coupling both in the intestine^[22,23] and the stomach.^[24] In these models, the coupled ICC-SMC system is represented with a minimal level of complexity by a pair of two state variables for each cell type, namely the normalized transmembrane voltage, v , and a local recovery variable, r . Unfortunately, this specific modeling approach suffers from an inherent instability which typically arises for simulation times longer than just a couple of seconds. The approach is thus practically not applicable for long-term in-silico analyses. Moreover, despite significant and ongoing research efforts (see Du *et al.*^[16] for a recent review), several mechanisms controlling gastric motility are still not yet fully understood, which makes it difficult to develop detailed mechanistic models. Therefore, there is a pressing need for a simple phenomenological continuum-scale model of gastric electrophysiology that is computationally robust, efficient and stable.

Modeling gastric motility requires, however, not only a model of gastric electrophysiology but also of the active muscular contractions and electro-mechanical coupling giving rise to the peristaltic waves observed during the digestion of food.^[16] Active biological tissues are intrinsically characterized by multiphysics and multiscale behavior involving several length and time scales.^[25,26] The study of such complex microstructured materials fosters a continuous forefront research in applied mathematics and mechanics, including innovative theoretical formulations^[27] and homogenization procedures,^[28,29] as well as experimental^[30–33] and numerical tools.^[34,35] So far advanced theoretical and computational studies of soft tissue contractility have addressed mainly the nonlinear behavior of skeletal^[36–38] and cardiac muscles^[39–42] including a wide and variegated literature.^[43] Much less attention, though, has been dedicated to modeling the multiphysics of gastrointestinal motility, which

distinguishes itself by a particularly high structural and functional complexity.^[3,44,45] Only a few contributions have so far addressed the mechanics of active contractions in the gastrointestinal tract.^[46,47] For the small intestine, Gizzi *et al.*^[48] recently proposed a generalized thermodynamical framework with a statistical description of the intestinal wall microstructure.^[49–51] Moreover, some attempts to characterize the altered mechanical contractility of human colon strips in the presence of unbalanced thermal states were proposed over the last years.^[23,52] What remains wanted so far is a computational model that combines a simple phenomenological, and computationally robust model of gastric electrophysiology with an electro-mechanical finite elasticity framework, enabling thereby comprehensive studies of the complex multiphysical nature of gastric motility on the organ level.

The present contribution aims at partially filling this gap. We propose a simple phenomenological approach coupling a modified-version of the two-variable Mitchell-Schaeffer electrophysiological model^[53,54] with an active-strain electro-mechanical description of the gastric tissue.^[40,55] Our aim is to establish a robust computational framework amenable to large scale in-silico analyses of the complex gastrointestinal motility including the underlying electro-mechanical coupling in a finite-strain framework. We directly relate the contractility dynamics in the stomach with the transmembrane voltage of SMC neglecting more complex biophysical phenomena due to neural, hormonal and mechano-electric effects. Our modeling approach can successfully reproduce several experimentally observed key phenomena as indicated by a number of computational tests. We demonstrate the broad applicability of the model by simulating both normal and dysrhythmic dynamics within a finite elasticity electro-mechanical framework varying both electrophysiological material properties and mechanical boundary conditions. This paper is mainly dedicated to general, phenomenological aspects of the mathematical modeling of the electro-mechanical coupling in the stomach. Therefore, all the computational examples were accomplished on simplified model domains such as rectangular tissue patches or cylindrical tubes, which resemble the gastric geometry but still skip the anatomical complexity of realistic geometries.

2 | MODEL FORMULATION

2.1 | Gastric electrophysiology

Across the gastric wall, there is a distribution of ICC and SMC which both respond to electric signals. In particular, the ICC generate the electric signals and therefore have the ability to trigger SMC. The electrical behavior of individual cells is intrinsically coupled to adjacent cells by the transport of electric potential through dedicated proteic structures. The coupling between the electrophysiological processes at the cell level and the transport of electric potential at the tissue scale gives rise then to ordered electric patterns (emerging behavior) known as gastric slow waves at the organ level. In the following two subsections, we will first introduce a simple phenomenological two-variable model of cell electrophysiology and, subsequently, the monodomain model for the transport of electric potential across the tissue. Thereby, we provide a system of coupled partial differential equations that can reproduce the phenomenon of electric propagation of slow waves within the gastric wall.

2.1.1 | Cell electrophysiology

To model cell electrophysiology, we adopt a phenomenological approach based on a modified version of the Mitchell-Schaeffer model,^[53] originally introduced to describe the cardiac action potential, and here characterized for gastric slow wave propagation. The dynamical features of this model, delineated in the following, justify its usage for the phenomenological description of gastric electrophysiology following a wide literature on the subject.^[56] The model, in fact, is capable of reproducing both pacemaker signals, needed to model ICC, and smooth muscle excitation signals, necessary to model SMC,^[54] improving and stabilizing the phenomenological approach of Aliev *et al.*^[22]. The mathematical formulation assumes that gastric electrophysiology on the level of single cells can be modeled phenomenologically both in ICC and SMC by two state variables each. These are the normalized transmembrane voltage $v^\phi \in [0, 1]$ and the gating (recovery) variable $h^\phi \in [0, 1]$, which mimics time constants and morphology of subcellular ionic currents within ICC and SMC, respectively. The index $\phi \in \{i, m\}$ distinguishes herein between ICC (index: i) and SMC (index: m). The evolution in time of these state variables is assumed to be governed by the system of coupled ordinary differential equations (ODEs):

$$\frac{\partial v^\phi}{\partial t} = I_{\text{in}}^\phi(v^\phi, h^\phi) + I_{\text{out}}^\phi(v^\phi) + I_{\text{stim}}^\phi(t), \quad (1a)$$

$$\frac{\partial h^\phi}{\partial t} = \frac{h_\infty^\phi(v^\phi) - h^\phi}{\tau^\phi(v^\phi)}. \quad (1b)$$

Equation 1a describes the conservation of ionic and capacitive currents across the cell membrane, a fundamental physical law of theoretical electrophysiology.^[57] Ions are transported into cells by the inward transmembrane ionic current $I_{\text{in}}^{\phi}(v^{\phi}, h^{\phi}) \geq 0$ or possibly also by some time-dependent external stimulus current I_{stim}^{ϕ} applied to the tissue (e.g., due to some biomedical device). At the same time, charged ions are withdrawn from the cells by the outward transmembrane ionic current $I_{\text{out}}^{\phi}(v^{\phi}) \leq 0$. The conservation of ionic fluxes requires that these three currents equal rate of change of the ionic charge across the membrane (capacitive effect). Herein, all currents are normalized with respect to the capacitance of the cell membrane. Therefore the left-hand side contribution is represented by the rate of change $\partial v^{\phi} / \partial t$ of the transmembrane potential. From biophysical experiments, we know that the in- and outward transmembrane ionic currents depend on the transmembrane voltage v^{ϕ} .^[3,6,12,13,58] To reproduce such complex behavior, we use herein simplified, FitzHugh-Nagumo-like cubic reaction functions

$$I_{\text{in}}^{\phi}(v^{\phi}, h^{\phi}) = \frac{h^{\phi}}{\tau_{\text{in}}^{\phi}} (v^{\phi} + a^{\phi}) (v^{\phi} + a^{\phi} - \lambda^{\phi}) (1 - v^{\phi}), \quad (2a)$$

$$I_{\text{out}}^{\phi}(v^{\phi}) = -\frac{v^{\phi}}{\tau_{\text{out}}^{\phi}}, \quad (2b)$$

where τ_{in}^{ϕ} and τ_{out}^{ϕ} are time constants, a^{ϕ} and λ^{ϕ} represent excitability parameters. The formulation is able to reproduce ICC self-oscillation (pacemaker activity), i.e., periodic electric signals with a defined intrinsic frequency, as well as the excitable (passive) SMC dynamics via the adjustment of these excitability parameters. In Equation 1b, the voltage-dependent time constant $\tau^{\phi}(v^{\phi})$ and the voltage-dependent steady state value $h_{\infty}^{\phi}(v^{\phi})$ are defined by

$$\tau^{\phi}(v^{\phi}) = \frac{\tau_{\text{open}}^{\phi} \tau_{\text{close}}^{\phi}}{\tau_{\text{open}}^{\phi} + h_{\infty}^{\phi}(v^{\phi}) (\tau_{\text{close}}^{\phi} - \tau_{\text{open}}^{\phi})}, \quad (3a)$$

$$h_{\infty}^{\phi}(v^{\phi}) = \frac{1}{2} \left(1 - \tanh \left(\frac{v^{\phi} - v_{\text{gate}}^{\phi}}{\eta_{\text{gate}}^{\phi}} \right) \right), \quad (3b)$$

where $\tau_{\text{open}}^{\phi}$ and $\tau_{\text{close}}^{\phi}$ are time constants phenomenologically related to subcellular ionic dynamics and the parameters v_{gate}^{ϕ} and $\eta_{\text{gate}}^{\phi}$ modify the sign of the steady-state value. We note that this model is well-known to be valid under the assumption $\tau_{\text{in}}^{\phi} \ll \tau_{\text{out}}^{\phi} \ll \tau_{\text{open}}^{\phi}, \tau_{\text{close}}^{\phi}$.^[53]

2.1.2 | Transport of electric potential on organ scale

Electric slow waves result from an interplay between electric oscillations triggered by the ICC at each point in the tissue and a transport of electric potential on the tissue scale through cell-cell communication. We model this transport process on the domain $\Omega_0 \subset \mathbb{R}^d$, $d = 1, 2, 3$, in the time interval $[0, T]$. Let $v^i, v^m : \Omega_0 \times [0, T] \rightarrow [0, 1]$ be the normalized transmembrane voltage of ICC and SMC, respectively. We assume that the transport of electric potential happens across both types of cells. For each cell type, it is modeled by a so-called monodomain continuum formulation (also known as cable equation)^[22,59,60] according to the following reaction-diffusion system:

$$\frac{\partial v^i}{\partial t} = \sigma^i \Delta v^i - D_{\text{gap}} (v^i - v^m) + I_{\text{tot}}^i(v^i, h^i; \mathbf{X}), \quad (4)$$

$$\frac{\partial v^m}{\partial t} = \sigma^m \Delta v^m + D_{\text{gap}} (v^i - v^m) + I_{\text{tot}}^m(v^m, h^m; \mathbf{X}), \quad (5)$$

where σ^i, σ^m denote the isotropic diffusion coefficients for electric potential for ICC and SMC, respectively; D_{gap} describes the homogenized resistance of gap junction proteins between the two cell types; and the normalized currents $I_{\text{tot}}^i, I_{\text{tot}}^m$ are defined by the right-hand side of ODEs (1), differentiated in the parameter choices in Table 1 and assumed space-dependent. Δ denotes the Laplace operator on Ω_0 , which is linked to the Nabla operator ∇ on Ω_0 via $\Delta = \nabla^2$. The problem formulation is closed by suitable initial conditions, $v^{\phi}(t = 0) = v_0^{\phi}$, $h^{\phi}(t = 0) = h_0^{\phi}$ for $\phi \in \{i, m\}$ (see Table 1), and with Neumann zero-flux boundary conditions (representing an insulated tissue) on the boundary $\partial\Omega_0$ of the domain Ω_0 with outward normal \mathbf{n} , i.e.,

$$\nabla v^{\phi} \cdot \mathbf{n} = 0 \quad \text{on} \quad \partial\Omega_0 \times [0, T] \quad \forall \phi \in \{i, m\}, \quad (6)$$

where (\cdot) denotes the scalar product.

TABLE 1 Electrophysiology parameters for ICC and SMC used in the application examples are described here

Parameter	Value		Unit
	ICC ($\phi = i$)	SMC ($\phi = m$)	
τ_{in}^{ϕ}	2.29274×10^{-2}	1.14637×10^{-1}	s
τ_{out}^{ϕ}	4.70719×10^{-1}	4.70719×10^{-1}	s
τ_{open}^{ϕ}	9.23200	9.23200	s
τ_{close}^{ϕ}	4.77082	4.77082	s
a_{min}^{ϕ}	3.31600×10^{-2}	0.00000	—
a_{max}^{ϕ}	2.23075×10^{-2}	0.00000	—
λ^{ϕ}	1.25000×10^{-2}	1.25000×10^{-2}	—
v_{gate}^{ϕ}	1.03825×10^{-1}	1.03825×10^{-1}	—
η_{gate}^{ϕ}	4.50362×10^{-2}	4.50362×10^{-2}	—
σ^{ϕ}	1.20000	1.20000×10^{-1}	$\text{mm}^2 \text{s}^{-1}$
D_{gap}	5.00000×10^{-1}	5.00000×10^{-1}	s^{-1}
v_0^{ϕ}	3.41438×10^{-2}	3.41438×10^{-2}	—
h_0^{ϕ}	6.78747×10^{-1}	6.78747×10^{-1}	—
v_r^{ϕ}	5.76016×10^{-3}	2.05112×10^{-3}	—
h_r^{ϕ}	4.96258×10^{-1}	5.24102×10^{-1}	—

2.2 | Continuum mechanical framework

In this section, we briefly summarize the equations of continuum mechanics governing the finite-strain deformation of the stomach. The kinematics of a homogeneous continuum body, the concept of active contraction, and the associated constitutive behavior are recalled. For the sake of conciseness, the fundamental balance principles of continuum mechanics, i.e., the balance of linear and angular momentum, essential to pose the initial boundary value problem are not stated herein.

2.2.1 | Kinematics

Let \mathbf{X} denote a material point in a body Ω_0 at time $t = 0$ in the three-dimensional Euclidean Space, which is also called reference or material configuration. Herein, we assume that the reference configuration is load- and stress-free. At times $t > 0$, the body may undergo a transformation, i.e., motion and deformation, to the current or spatial configuration $\Omega_t \subset \mathbb{R}^d$. Hereby, the material point \mathbf{X} is related to the spatial point \mathbf{x} in the spatial (deformed) configuration by the nonlinear deformation map $\varphi_t : \Omega_0 \rightarrow \Omega_t$, $\mathbf{X} \mapsto \mathbf{x}$. We introduce the deformation gradient $\mathbf{F} = \partial \mathbf{x} / \partial \mathbf{X}$ and its determinant $J = \det \mathbf{F} > 0$, which describes the local volume change from the material to the spatial configuration.

Describing the active contraction of the gastric tissue, we follow an active-strain approach.^[40] The reliability of such an approach with respect to others (e.g., active stress) has been theoretically and biophysically motivated in previous contributions. In particular, the active-strain approach can be derived from thermodynamical arguments^[61] respecting the notion of *distorsions* in continuum mechanics. At the same time, the multiscale nature of excitable contractile cells, such as SMC, justifies the adoption of such a concept to reproduce calcium and voltage-based intra-cellular mechanisms leading to the sliding of proteic filaments (actin and myosin) generating the motion. In fact, these dynamics occur within the cell at a much smaller temporal and spatial scale with respect to our macroscopic modeling framework. Accordingly, we assume that the active deformation of the tissue due to smooth muscle contraction can be represented by a change of the local traction-free configuration of the infinitesimal volume elements of the tissue. This change of the local traction-free configuration can be represented - similar to plastic deformation in plasticity theory - by a multiplicative decomposition of the deformation gradient \mathbf{F} into a part \mathbf{F}_a resulting from local active-strain deformation rather than external loading and a complementary elastic part \mathbf{F}_e such that

$$\mathbf{F} = \mathbf{F}_e \mathbf{F}_a. \quad (7)$$

If smooth muscle contraction, i.e., \mathbf{F}_a , is known, \mathbf{F}_e can be computed in a standard fashion from two conditions, first the balance of momentum and second the geometric compatibility of the deformed configuration Ω_t . The effect of the active deformation

\mathbf{F}_a is often illustrated via a so-called intermediate configuration Ω_a on which \mathbf{F}_a maps the reference configuration and which itself is mapped on the current configuration Ω_t by the elastic \mathbf{F}_e .

Due to the high amount of water in gastrointestinal tissue, we assume the material to be incompressible, i.e., $J = 1$. Also, we require that both the elastic and the active part of the deformation gradient tensor fulfill such a condition, i.e., $J_e = \det \mathbf{F}_e = 1$, and $J_a = \det \mathbf{F}_a = 1$. We finally introduce the right Cauchy-Green deformation tensor

$$\mathbf{C} = \mathbf{F}^T \mathbf{F}, \quad (8)$$

as well as the so-called elastic Cauchy-Green deformation tensor

$$\mathbf{C}_e = \mathbf{F}_e^T \mathbf{F}_e = \mathbf{F}_a^{-T} \mathbf{C} \mathbf{F}_a^{-1}. \quad (9)$$

2.2.2 | Passive material behavior

We assume a passive hyperelastic material behavior with strain energy density Ψ , which is a function of the elastic deformation gradient \mathbf{F}_e :

$$\Psi = \Psi(\mathbf{F}) = \Psi_e(\mathbf{F}_e). \quad (10)$$

Though more general assumptions could be made, for simplicity and in order to focus on key aspects of electromechanical coupling herein, we assume an isotropic, incompressible neo-Hookean material model

$$\Psi_e(I_1^e) = \mu(I_1^e - 3), \quad (11)$$

with scalar stiffness parameter μ and the first invariant of the elastic right Cauchy-Green tensor $I_1^e := \text{tr } \mathbf{C}_e$.

According to the active-strain approach, the first Piola-Kirchhoff stress tensor reads

$$\mathbf{P} = \frac{\partial \Psi}{\partial \mathbf{F}} = \frac{\partial \Psi_e(\mathbf{F}_e)}{\partial \mathbf{F}_e} \frac{\partial \mathbf{F}_e}{\partial \mathbf{F}} = \mathbf{P}_e \mathbf{F}_a^{-T}, \quad (12)$$

in which we do not consider additional mechano-electric feedback. In the previous relation, we have introduced the elastic first Piola-Kirchhoff stress tensor \mathbf{P}_e , which describes the stresses induced by the elastic deformation \mathbf{F}_e on the intermediate configuration Ω_a . A detailed derivation of Equation 12 is provided in the Appendix. The second Piola-Kirchhoff stress tensor \mathbf{S} and its counterpart on the intermediate configuration \mathbf{S}_e can be derived as

$$\mathbf{S} = \mathbf{F}^{-1} \mathbf{P} = \mathbf{F}_a^{-1} \mathbf{S}_e \mathbf{F}_a^{-T}. \quad (13)$$

For efficient computational schemes one typically needs the tangent of the passive material $\mathbb{C}_e = 2\partial \mathbf{S}_e / \partial \mathbf{C}_e$. We identify (8) and (13) as the pull-back of strains and stresses from the intermediate configuration into the reference configuration and apply the same pull-back operation on \mathbb{C}_e . In Einstein's index notation, the resulting fourth order material tangent reads:

$$\mathbb{C}_{IJKL} = (\mathbf{F}_a^{-1})_{Ii} (\mathbf{F}_a^{-1})_{Jj} (\mathbf{F}_a^{-1})_{Kk} (\mathbf{F}_a^{-1})_{Ll} (\mathbb{C}_e)_{ijkl}. \quad (14)$$

Note that (14) only holds if the active part of the deformation gradient \mathbf{F}_a is independent of the deformation \mathbf{F} .

2.2.3 | Active material behavior

Gastric tissue typically exhibits two layers of smooth muscle with distinct fiber orientations, circumferential and longitudinal, with respect to the main geometric axis of the stomach. Therefore, modeling the active contraction of the stomach requires the introduction of an anisotropic material behavior.

Let $\mathbf{N}_c, \mathbf{N}_l$ be orthogonal unit vectors in the fiber directions of the circumferential and longitudinal muscle layer, respectively, in the reference configuration. $\mathbf{N}_n = \mathbf{N}_c \times \mathbf{N}_l$ represents the unit vector in thickness direction of the gastric wall.

Allowing for active deformation in circumferential and longitudinal directions, we assume that the active part of the deformation gradient takes the following form^[40]

$$\mathbf{F}_a = \mathbf{I} - \gamma (\alpha_c \mathbf{N}_c \otimes \mathbf{N}_c + \alpha_l \mathbf{N}_l \otimes \mathbf{N}_l) + \gamma_n \mathbf{N}_n \otimes \mathbf{N}_n. \quad (15)$$

where \otimes denotes the usual tensor product, $\gamma = \gamma(v^m) \in [0, 1]$ is a smooth activation function depending on the excitation state, and α_c and α_l are material parameters controlling the intensity of the active contraction in circumferential and longitudinal direction, respectively. We introduce the additional parameter γ_n to enforce the incompressibility condition of the active deformation gradient by a stretch orthogonal to the smooth muscle layers in direction \mathbf{N}_n . Note that this means that we assume that incompressibility manifests solely in a thickness change of the gastric wall.

Making use of the orthogonality requirement of the fiber directions, we can define the Jacobian of the active deformation gradient as

$$\det \mathbf{F}_a = (1 - \gamma\alpha_c) (1 - \gamma\alpha_l) (1 + \gamma_n) \stackrel{!}{=} 1. \quad (16)$$

Solving (16) for γ_n results in

$$\gamma_n = \frac{1 - (1 - \gamma\alpha_c) (1 - \gamma\alpha_l)}{(1 - \gamma\alpha_c) (1 - \gamma\alpha_l)}. \quad (17)$$

In order to ensure that the fibers cannot contract to zero or negative lengths, we enforce each factor in the denominator of (17) to be positive. For an arbitrary $\gamma \in [0, 1]$, this condition is equivalent to

$$\alpha_c < 1 \wedge \alpha_l < 1. \quad (18)$$

Note that negative values of α_c and α_l describe lengthening of the muscle fibers.

2.2.4 | Excitation-contraction coupling

The generation of active force within gastrointestinal smooth muscle cells depends on the intracellular Ca^{2+} concentration.^[21] The Ca^{2+} concentration itself is regulated by complex spatio-temporal dynamics involving both VDCC and intra-cellular stochastic mechanisms.^[58] In order to keep the computational cost of the proposed model minimal, in this first contribution, we neglect such intra-cellular multiscale Ca^{2+} -dynamics and propose a direct relation between the transmembrane voltage of the SMC, v^m , and the active-strain activation parameter γ in the form

$$\gamma(v^m) = \left(1 - e^{-\beta_1(v^m - v_t)}\right) \left(1 - e^{-\beta_2(v^m - v_t)}\right) H(v^m - v_t). \quad (19)$$

Here, v_t is the normalized opening voltage of the VDCC, β_1 is a parameter resembling the homogenized Ca^{2+} dynamics, and β_2 describes the opening dynamics of the VDCC. $H(x)$ denotes the Heaviside step function.

3 | NUMERICAL EXAMPLES

3.1 | General

We implemented the coupling of the two-variable Mitchell-Schaeffer electrophysiology model with the active-strain electro-mechanical description of the gastric tissue as described in Sec. 2 in our in-house research simulation code BACI (written in C++) and we performed a series of computational tests ensuring numerical reliability of the proposed computational model. The scalar transport problem and the structural mechanics problem are solved numerically using the finite element method. The geometry is discretized by scalar transport elements and standard nonlinear membrane finite elements. Our implementation allows for non-matching meshes of both discretizations in order to reduce the overall computational costs.

A membrane is considered to be a thin-walled hyperelastic structure without bending stiffness in the surface tangent plane. Plane stress is assumed in the membrane. Nevertheless, a pressure load may act in the normal direction on the membrane surface and be balanced by the in-plane stresses and membrane curvature. In general, membranes exhibit a highly nonlinear behavior due to simultaneous presence of both geometrical and material nonlinearities.

3.2 | Preliminary study on a one-dimensional gastric electrophysiology model

To verify the correct implementation and the numerical properties of the proposed mathematical model, we set up a one-dimensional (1D) gastric electrophysiology model, not including any mechanics yet. The one-dimensional domain with

TABLE 2 Parameters for the spatial distribution functions $a^i(x)$ of type (20) and $a^i(x, y)$ of type (22). The functions f_θ with $\theta \in \{x, y\}$ are defined by (21)

Parameter	f_x	f_y		
		Isotropic	Anisotropic	Unidirectional
b_θ	3.1622	3.1622	0.1	3.1622
c_θ	0	0	0.9	1

$x \in [0, L_x]$ and $L_x = 250$ mm represents a line on the stomach's surface from the pacemaker region to the pylorus along the greater curvature. We apply no-flux boundary conditions at the two end points, $x = 0$ mm and $x = 250$ mm. In this 1D numerical analysis, we consider a time step size of $dt = 3.125$ ms and a mesh size of $h = 15.625$ μ m, corresponding to 16000 two-noded linear scalar transport elements. The electrophysiology parameters for ICC and SMC together with the initial conditions are collected in Table 1.

In the gastric tissue, only the ICC exhibit the ability to actively trigger electric waves. Therefore, for the SMC the excitability parameter $a^m = 0$. For the ICC the excitability parameter, as introduced in Equation 2a, is in general unequal to zero and varies in space. Its exact spatial distribution can be expected to vary patient-specifically. Here, we assume it to be given by the smooth scalar function

$$a^i(x) = a_{\min}^i + (a_{\max}^i - a_{\min}^i) f_x\left(\frac{x}{L_x}\right), \quad (20)$$

where a_{\min}^i, a_{\max}^i are the desired minimal and maximal excitability parameter values¹; f_x is a normalized function controlling the spatial variation of the excitability in x-direction. For simplicity, we herein assume the function to be of the Gaussian-like type

$$f_\theta(\xi_\theta) = 1 - \frac{c_\theta - 1}{\exp[-b_\theta] - 1} (1 - \exp[-b_\theta(\xi_\theta)^2]), \quad \xi_\theta \in [0, 1], \quad (21)$$

where the index θ indicates the correlation between the normalized variable $\xi_\theta = \theta/L_\theta$ to the physical variable θ , L_θ is the chosen reference length. In the present case, we have $\theta = x$. In (21), the shape parameter b_θ is linked to the variance of the underlying Gaussian and the parameter c_θ is defined such that $f_\theta(1) = c_\theta$. Note that $f_\theta(0) = 1$ holds for all $b_\theta \in \mathbb{R}^{\neq 0}, c_\theta \in \mathbb{R}$.

All electrophysiology parameters for ICC and SMC together with the initial conditions are collected in Table 1. The constitutive model parameters for distribution function (20) are provided in Table 1 and Table 2.

Entrainment Analysis

A key feature of gastrointestinal electrophysiology is the so-called *entrainment* process. This process is a form of emergent behavior. In the upper, proximal part of the stomach the excitability parameter and therefore the intrinsic frequency of electric oscillations on cell level is higher than in the lower, distal part, towards the pylorus. Therefore, if isolated from each other, the ICC in different regions of the stomach would exhibit electric oscillations with different frequencies. However, due to the coupling of the ICC by the transport of electric potential across the tissue on the continuum scale, the ICC in the lower part of the stomach are entrained. That is, the frequency of their electrostatic oscillations on cellular level is forced towards the higher intrinsic frequency of the ICC in the upper part of the stomach. The region containing the ICC with the highest intrinsic frequency, located in the upper part of the stomach, is therefore also referred to as *pacemaker region*.

With such a phenomenology in mind, Figure 1 shows the temporal evolution of the frequency of the oscillations of the electric potential at each point in the domain as observed in our computational model.

In the beginning, at each point the frequency is given by the intrinsic frequency of the ICC at this point, that is, determined by a^i . Therefore, one observes a significant gradient of the frequency across the domain at $t = 0$. Over time this gradient diminishes. At $t = 500$ s, the electric oscillations of the ICC exhibit nearly the same frequency in the whole domain, which is equal to the initial frequency of the ICC in the upper part of the domain (i.e., at $x = 0$). That indicates that the ICC at the opposite end of the domain have been entrained to these pacemaker ICC in the upper part. According to experimental evidence,^[14,15] the frequency entrainment values obtained with our phenomenological model fall within the physiological range with good accuracy. As

¹ Note that the excitability parameter a is found to govern the intrinsic frequency of slow wave generation on the cellular scale.

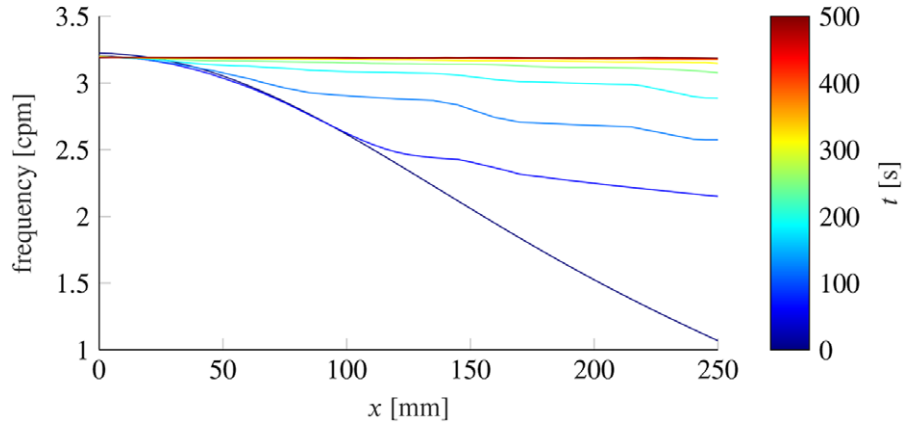


FIGURE 1 Temporal evolution of ICC frequency gradient. The color indicates the time of the respective frequency measurement (see colorbar)

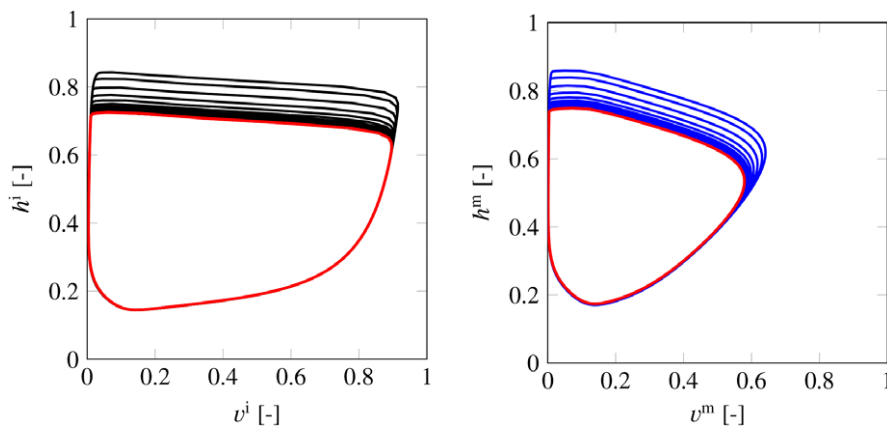


FIGURE 2 Development of phase portraits from the intrinsic to the entrained state of ICC (left) and SMC (right) located in the middle of the domain at $x = 125$ mm. The resulting stable limit cycle is depicted in red

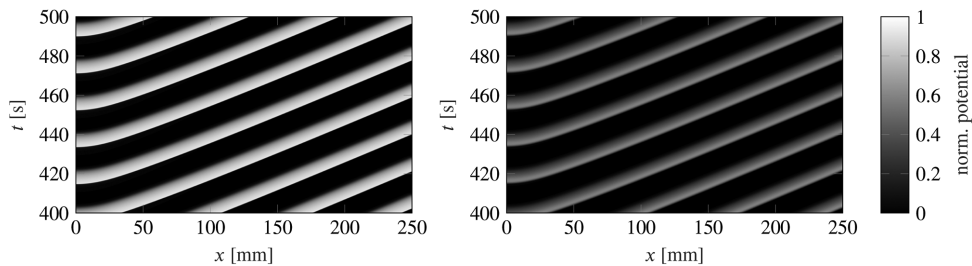


FIGURE 3 Spatiotemporal plot of normalized transmembrane potential of ICC v^i (left) and of SMC v^m (right) over space (horizontal axis) and time (vertical axis). The colorbar applies to both figures. (left) Slow waves of ICC (grey to white areas) are generated in the pacemaker region and travel distally, i.e. from left to right in space, with almost constant conduction velocity. Areas of rest are depicted in black. (right) The excitation of SMC follows the slow waves closely but with reduced amplitude (note the overall darker tone) and with a slightly delayed peak (see also Figure 4)

indicated by straight horizontal lines, for $t > 350$ s the entrainment is stable over the whole domain. This result ensures that our phenomenological modeling is capable of reproducing a physiological entrainment process.

To further confirm such behavior, we provide in Figure 2 the development of the phase portrait of the two electrophysiological state variables from the intrinsic to the entrained state for both ICC and SMC. We highlight in red the last 40 s showing that both cell types develop a stable limit cycle. In addition, Figure 3 shows the space-time propagation pattern of the ICC transmembrane potential v^i during the last 100 s, where a clear periodic entrained state is recognized. Slow waves (grey to white areas), marked by a steep activation front, are initiated at the pacemaker site and travel along the domain, i.e., from left to right, with a constant conduction velocity. We also observe stable refractory phases at the resting potential of $v^i = 0$ (see also Figure 4). The excitation of SMC follows the slow waves generated by the ICC closely. However, the amplitude is smaller and the peak occurs slightly

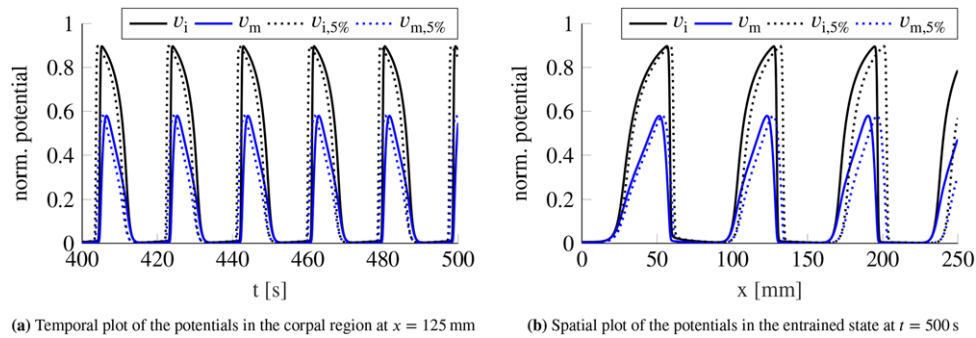


FIGURE 4 Normalized transmembrane potential v^i of ICC (depicted in black) and normalized transmembrane potential v^m of SMC (depicted in blue). Solid lines depict a reference solution computed with $dt = 3.125$ ms, $h = 15.625$ μ m, dashed lines depict the solution obtained with a much coarser discretization with time step and mesh size $dt = 0.1$ ms, $h = 0.5$ mm. The relative difference is small; for the conduction velocity (CV) it remains below 5% (see also Figure 5)

delayed (see also Figure 4). It is worth noticing that such robust periodic behavior is one of the major advantages with respect to previous phenomenological models.^[22]

Conduction Velocity Analysis

The conduction velocity (CV) of a slow wave can be estimated from the gradient of the sharp activation lines separating bright and black regions in the space-time plot in Figure 3. At a certain distance from the pacemaker region a constant CV of 3.6 mm s^{-1} establishes, whereas within the pacemaker region (up to approx. $x = 50$ mm) CV exhibits a negative gradient. Since equal boundary conditions are applied at both ends of the one-dimensional simulation domain, the computed CV variation is due to the spatial gradient of excitability nonlinearly linked to the entrainment process (see Figure 1). Averaging the conduction velocity over the whole simulation domain results in the value 3.8 mm s^{-1} which, again, falls within the expected physiological range.^[15]

For illustrative purposes, Figure 4a shows the temporal evolution of the transmembrane potentials of ICC and SMC in the center of the domain, which corresponds to a vertical cut through Figure 3 at $x = 125$ mm. Figure 4b shows the potentials over space in the entrained state (horizontal cut through Figure 3 at $t = 500$ s). The obtained slow waves are stable and entrain to a constant frequency for both ICC and SMC. In fact, the activation of the SMC follows the pacemaker potential of the ICC with a slight delay (modeling the complex intra-cellular calcium mechanisms) and the SMC experience a lower maximal depolarization. This result, as well as the general shape of the slow waves, is in agreement with experimental recordings.^[62]

Numerical Convergence Analysis

It is well known that the conduction velocity of reaction-diffusion systems in general depends on the numerical solution scheme.^[63] Therefore, we examined the influence of the numerical parameters, namely the time step size dt and the mesh size h , on the computed CV. We chose to evaluate the CV in the middle of the simulation domain in order to minimize the influence of the no-flux boundary conditions and after approximately $T = 500$ s of simulated time, ensuring a complete entrainment of the system. The CV is determined by tracking the propagation of the wave front (threshold $v^i = 0.5$) for 0.6 s.

In the convergence study, we varied the time step and mesh size in the ranges 3.125 ms $\leq dt \leq 0.2$ s, 15.625 μ m $\leq h \leq 1.0$ mm, each subsequently by a factor of two, performing a total of 49 simulations in the selected parameter space. As a reference solution, we choose the simulation result achieved with the smallest time step and mesh size (used for the analysis above). The convergence plot in Figure 5 shows the CV for each pair of numerical parameters dt and h . Distinctly, the CV converges with decreasing time step size and decreasing mesh size and justifies the choice of our reference solution.

The black contour line in Figure 5 indicates a 5% relative deviation of the CV from the one computed with the finest discretization in space and time (i.e., the reference solution used above). To balance computational cost and numerical accuracy, we select $dt = 0.1$ s, $h = 0.5$ mm (with a CV relative error less than 5%, refer to Figure 5) for the solution of the electrophysiological problem in all subsequent examples. The dashed traces in Figure 4 show the solution of the model using the selected space-time discretization compared to the finest solution, depicted in solid lines. The visual comparison of the two solutions reveals that the shape of the simulated slow waves does not change significantly (see also Figure 4a). While a slight variation of CV appears, the spatial offset remains, however, basically constant.

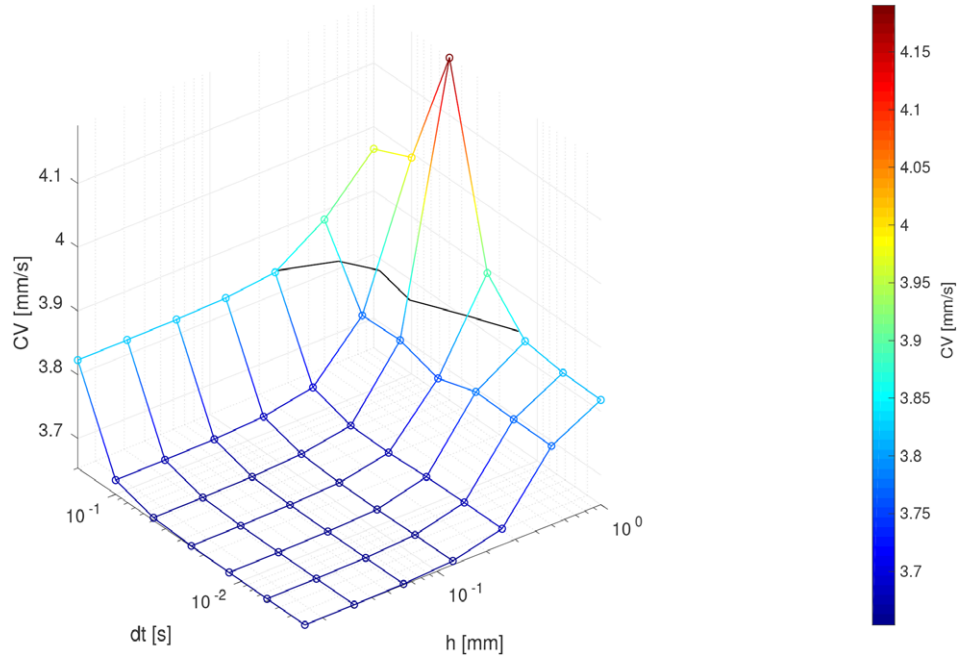


FIGURE 5 Convergence of the conduction velocity (CV) depending on time step size dt and mesh size h . The black line corresponds to 5% relative error with respect to the conduction velocity at the smallest time step and mesh size ($dt = 3.125$ ms, $h = 15.625$ μ m)

3.3 | Electro-mechanical coupling on a two-dimensional tissue patch

We continue the set of examples with a two-dimensional tissue patch incorporating an active-strain based electro-mechanical coupling. Our model domain is $\{(x, y) \in [0, L_x] \times [0, L_y]\}$ with $L_x = 250$ mm and $L_y = 160$ mm. This domain can be imagined to resemble, for example, the half lateral surface of an idealized cylindrical stomach that has been cut-open along the greater and lesser curvature and flattened in the xy -plane, neglecting the electrically quiescent fundus area. The x -axis is aligned with the longitudinal direction and the y -axis is aligned with the former circumferential direction of the half lateral surface of the stomach. We expect structural displacements to occur in such a flattened tissue patch solely in-plane of the patch, while thickness adjustments due to the incompressibility constraints occur normal to the patch. In the reference configuration, the thickness of the membrane is set to $t = 3.5$ mm.^[64]

Motivated by the previous convergence analysis, the numerical parameters are fixed to $dt = 0.1$ s, $h = 0.5$ mm for the electrophysiological model throughout the remaining examples. For the structural mechanical part, instead, we use a mesh size of $H = 2.0$ mm, with the purpose of reducing the computational costs. Such a choice is in line with similar studies in which a relation between electrophysiological and mechanical meshes has been investigated, setting the maximal mesh resolution for the mechanical problem between twice and eight times the size of the electrical one (see e.g. Cherubini *et al.*^[39] or Colli Franzone *et al.*^[65]). Our choice results in 160000 four-noded bilinear quadrilateral scalar transport finite elements for the electrophysiological domain and 10000 four-noded bilinear quadrilateral membrane finite elements for the structural mechanical problem.

As before, we prescribe no-flux boundary conditions on the whole boundary for the electrophysiological model. The structural boundary conditions of the planar patch, instead, are chosen to constrain displacements normal to the boundary whereas displacements tangential to the boundary are unconstrained. Namely at the vertical boundary lines ($x = 0, y \in [0, L_y]$) and ($x = L_x, y \in [0, L_y]$) displacements in x -direction are constrained to be zero. On the horizontal boundary lines ($x \in [0, L_x], y = 0$) and ($x \in [0, L_x], y = L_y$) displacements in y -direction are constrained to be zero. These boundary conditions are chosen such that they resemble the ones to which a half-stomach can be expected to be subject in vivo. There, the plane through minor and major curvature is in good approximation a symmetry plane of the stomach. The corresponding symmetry boundary condition is applied in our model on the boundaries in y -direction. At the same time, the stomach appears at both ends to be rather tethered in axial direction (by esophageal sphincter and pylorus) but - at least to some extent - unconstrained perpendicular to the axial direction. In our example, on the whole two-dimensional patch out-of-plane displacements of the membrane are constrained to be zero (mimicking the idea of a tissue patch flattened for experimental testing).

TABLE 3 Parameters for active and passive mechanical behavior used in the examples presented in section 3.3

Parameter	Value	Unit
μ	6.0×10^1	N mm^{-2}
α_1	2.0×10^{-1}	–
α_c	2.0×10^{-1}	–
β_1	1.0×10^1	–
β_2	1.0×10^1	–
v_t	2.5×10^{-1}	–

For the two-dimensional computational models examined below, we assume the spatial distribution function of the excitability parameter to be described by the smooth scalar function

$$a^i(x, y) = a_{\min}^i + (a_{\max}^i - a_{\min}^i) f_x \left(\frac{x}{L_x} \right) f_y \left(\frac{y}{L_y} \right), \quad (22)$$

where a_{\min}^i, a_{\max}^i are the desired minimal and maximal excitability parameter values; f_x and f_y are normalized functions controlling the spatial variation of the excitability in x - and y -direction, respectively. We assume each of these functions to be of the Gaussian-like type defined by (21) meaning we introduce two normalized variables $\xi_\theta, \theta \in \{x, y\}$ with distinct sets of parameters (see Table 2).

In the following, we discuss a series of numerical examples with isotropic, anisotropic, and unidirectional distributions of the excitability parameter a^i . Constitutive model parameters are provided in Table 2 and the corresponding contour plots of the resulting distributions are depicted in Figure 6a, 6b and 7a. All remaining model parameters together with the applied initial conditions are summarized in Table 1 and Table 3. As described in Sec. 3.2, the system needs approximately 350 s to reach the entrained state. To ensure an entrained state, we study in the following subsections electro-mechanical results at $t = 500$ s.

3.3.1 | Isotropic spatial distribution of the excitability parameter

First, we investigate the influence of the spatial distribution of the excitability parameter $a^i(x, y)$ on the two-dimensional propagation pattern of the resulting slow waves as well as on the mechanical response (see Figure 6 (left)).

We begin with an isotropic distribution of the excitability parameter $a^i(x, y)$ of ICC (see Table 2 for parameter values) illustrated by the contour plot in Figure 6a. We consider the pacemaker region to be located at the origin of the coordinate system ($x = 0, y = 0$) where we prescribe the maximum amplitude a_{\max}^i that isotropically reduces to a_{\min}^i , at a radius of 250 mm from the pacemaker site.

Figure 6c shows the spatial propagation pattern of the ICC transmembrane potential v^i . Slow waves are initiated periodically at the origin. From there they propagate through the tissue in an almost perfect circular pattern until reaching the boundary at the top ($y = 160$ mm). This indicates that the CV in this set up is isotropic. Due to the influence of the no-flux boundary condition,^[66] the slow waves straighten slightly once they have spread over the complete circumferential length but continue to travel in longitudinal direction whereby they heavily bend. Notably, there are always between three and four slow waves on the domain, which conforms with experimental gastric recordings.^[67]

Figure 6e shows patterns of mechanical activation following the electrical slow waves, implying that also in the two-dimensional case the electrical activation of the SMC is synchronized with the ICC pacemaker signal. While the general spatial pattern is, as expected, very similar to that of the ICC transmembrane potential, we recognize complex mechanical deformations far from the pacemaker site (see Figure 6g). These non-trivial patterns are due to the delay of the electrical activation of SMC (see Figure 4b), the threshold behavior of the active-strain electro-mechanical coupling (see Equation 19), the nonlinearity of the adopted material model, and the effect of boundary conditions. The magnitude of the in-plane displacements, in particular, is closely linked to the mechanical activation parameter $\gamma(v^m)$ as can be observed in Figure 6g. In general, the maximum structural contractions occur in the region of the maximum activation parameter $\gamma(v^m)$. In addition, localized and alternating contracted and relaxed regions follow positive and negative gradients of the electrical activation waves. Note that the effect of the structural boundary conditions is clearly visible as soon as a propagating contraction wave reaches the boundary of the simulation domain.

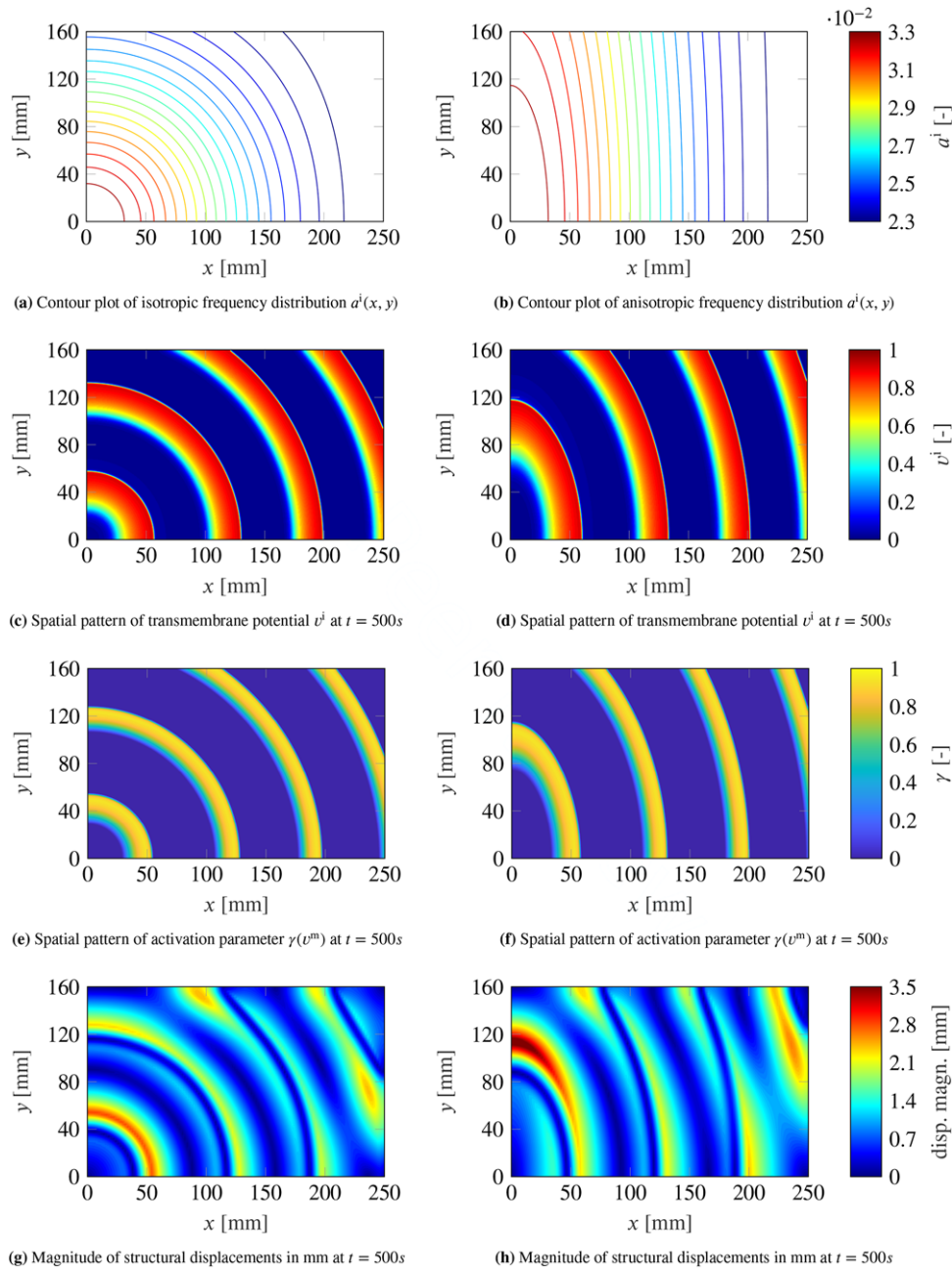


FIGURE 6 Collection of spatial plots illustrating the influence of different spatial distributions of the excitability parameter $a^i(x, y)$ on the gastric electro-mechanical model. The left column shows the case of an isotropic distribution, the right column the case of an anisotropic distribution. The colorbars apply to both columns

3.3.2 | Anisotropic spatial distribution of the excitability parameter

In this section, we investigate the influence of an anisotropic distribution of the excitability parameter $a^i(x, y)$ comparing and contrasting the results with the isotropic case (see Figure 6 (right)). The parameters for the distribution function f_x in x-direction remain unchanged while the distribution function f_y in y-direction is built so as to achieve a far slower descent of the excitability parameter (see Table 2). A contour plot of the anisotropic excitability parameter $a^i(x, y)$ is depicted in Figure 6b.

As expected from the preliminary 1D analysis, the decreased gradient of the excitability in y-direction results in an increased CV, yielding an elliptical shaped propagation pattern of the slow waves (see Figure 6d). Once again, under the influence of no-flux boundary conditions, the CV of incoming slow waves at the upper boundary is slightly increased in y-direction leading to a lower curvature of the shape of the wave front.

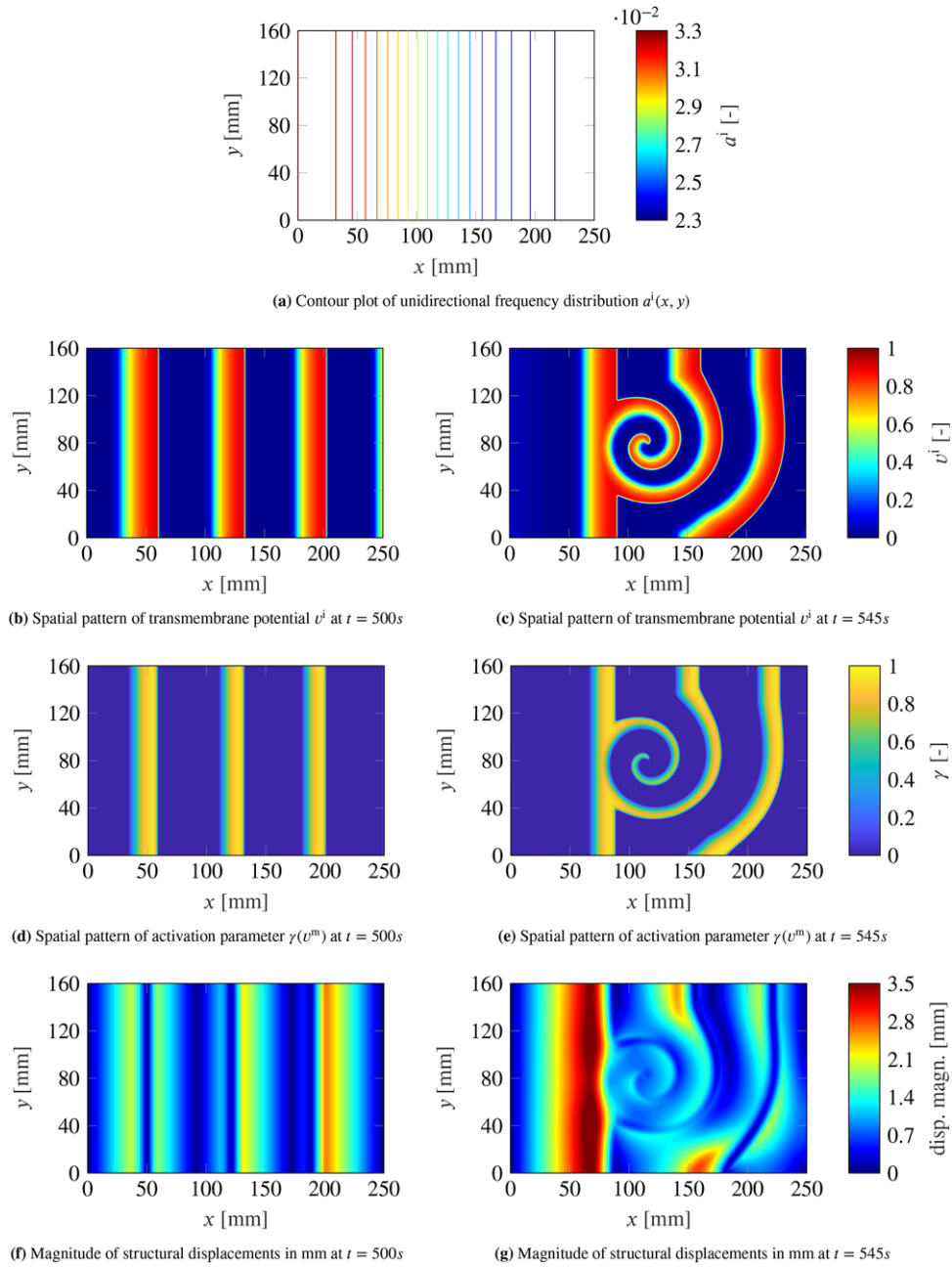


FIGURE 7 Collection of spatial plots illustrating the effects of gastric dysrhythmias induced by a conduction block on the electro-mechanical model. The left column shows the physiological case, the right column the pathological case, where a spiral developed. The colorbars apply to both columns

From the mechanical point of view, similar to the isotropic case, the spatial pattern of the mechanical activation (see Figure 6f) follows the transmembrane potential with a slight delay. However, the magnitude of the in-plane displacements illustrated in Figure 6h appears much less ordered in the presence of an anisotropic excitation. In particular, the highest magnitude of displacements is observed already on the first wave front propagating in y -direction and multiple shear-like bands appear within the tissue. These mechanical bands are of extreme importance for the correct motility and physiological function of the gastric wall.

These results confirm that the model is capable of representing different spatial electro-mechanical propagation patterns that have a large influence on the structural mechanical response.

3.3.3 | Unidirectional distribution of the excitability parameter with conduction block

In the literature, it has been shown, both in experiments^[68] and numerical studies,^[23,69] that conduction blocks can cause gastric dysrhythmias. In this section, we address such a complex phenomenon through our electro-mechanical framework, by

perturbating the electrophysical activity of the tissue during the entrained state. To begin with, we revisit the unidirectional distribution of the excitability parameter of Sec. 3.2 and apply it to the two-dimensional tissue patch. Figure 7a shows the resulting contour plot of the excitability parameter a . This leads to a perfectly synchronized activation along the y -axis at $x = 0$ mm. From there, completely straight slow waves propagate in x -direction, as shown in Figure 7b. The Figures 7d and 7f show the spatial pattern of the activation parameter $\gamma(v^m)$ and the resulting structural displacements. As expected, the mechanical activation parameter follows the straight slow waves and results in displacements occurring only in x -direction with modulated amplitude along the excitability gradient.

Starting from the fully entrained system, we induce a rectangular conduction block (width: $l_x = 50$ mm, height: $l_y = 80$ mm, origin: $x = 125$ mm, $y = 40$ mm) in the simulation domain at $t = 500$ s in the following way: we reset the state variables v^ϕ, h^ϕ to the fixed values v_r^ϕ, h_r^ϕ for all $\phi \in \{i, m\}$ on the domain of the conduction block for the duration of one single time step (refer to Table 1 for values). This perturbation leads to an emerging retrograde activation wave initiated at the top edge of the former conduction block by the remaining upper half of the slow wave (not shown). The resulting electrophysiological activity is a stable rotating spiral wave, significantly altering the slow wave propagation behavior, as depicted in Figure 7c. Figure 7c shows the established spiral wave at $t = 545$ s, and the nonlinear interaction (annihilation) with the slow waves generated by the pacemaker. An inhomogeneous conduction delay is clearly recognized from the bending of the slow wave in the lower parts while the upper part of the tissue remains less affected at this stage.

The resulting mechanical activation pattern is shown in Figure 7e and Figure 7g illustrates the magnitude of the resulting displacements. Clearly, the displacement magnitude is very elevated in the area where an approaching slow wave encounters the stable spiral. At the same time, the area covered by the spiral itself shows relatively small displacement magnitude in line with pathological scenarios, e.g. the so called *paralytic ileus*.^[23,70] It is important to note that in a clinical setting such extreme perturbations of the displacement field could not be reconstructed nor analyzed in a straightforward manner from a simple measurement of the electrical activity in the stomach. Rather, to achieve a detailed understanding of such a situation one needs a detailed understanding of the electro-mechanical coupling in the stomach, for which in the future reliable computational multiphysics models of the stomach as the one introduced in this paper will be required. Altogether the example in this section demonstrates that the proposed electro-mechanical computational model is able to reproduce also complex perturbation protocols and dysrhythmias in gastric tissue.

3.4 | Idealized three-dimensional electro-mechanical model for gastrointestinal motility

We conclude the set of examples with a three-dimensional idealized electro-mechanical stomach model. To focus on fundamental aspects of our computational model rather than geometric details, we greatly simplify the stomach's geometry and assume a straight circular hollow cylindrical shape. We neglect the electrically quiescent fundus area that does not show the typical peristaltic contraction waves.^[71] The cylinder has a length of $L_x = 250$ mm, a radius of $r = 50.930$ mm, and a membrane thickness of $t = 3.5$ mm. The cylinder axis is aligned with the x axis. Both ends of the cylinder are open. The greater curvature of the stomach corresponds in our idealized model to the line that lies within the xy -plane at $z = r$, whereas the lesser curvature is thought to be the line in the same plane at $z = -r$.

Motivated by the convergence analysis in Sec. 3.2, we chose a time step size of $dt = 0.1$ s and a mesh size of $h = 0.5$ mm for the electrophysiological part of the model. To reduce the computational costs, we use a mesh size parameter of $H = 2.0$ mm for the structural mechanical part. The above choice of numerical parameters results in a total number of 320000 four-noded bilinear quadrilateral scalar transport finite elements for the electrophysiological domain. The structural mechanical domain is discretized by 20000 four-noded bilinear quadrilateral nonlinear membrane finite elements. The thickness adjustments due to the incompressibility constraints occur normal to the membrane surface.

For the electrophysiological problem, we prescribe no-flux boundary conditions at both ends of the cylinder. For the mechanical problem, we apply zero Dirichlet boundary conditions in axial direction at both ends of the cylinder. To suppress rigid body motions, additionally the displacements of three points are constrained appropriately. Namely at $(x, y, z) = (L_x, 0, r)$ displacements in z -direction are constrained and at $(x, y, z) = (L_x, \pm r, 0)$ displacements in y -direction. Additionally, we prescribe a pressure load of $p = 3.0$ N mm⁻² on the inner surface of the cylinder.^[72,73]

The values of all model parameters together with suitable initial conditions are summarized in Table 3 and Table 1. Approximately 350 s of simulation time are needed to ensure the system's entrainment (see Sec. 3.2). Therefore, we evaluate the results well after this point.

To ensure the rapid formation of ring-shaped contractions as observed experimentally in the stomach,^[74] an increased circumferential CV is essential. We therefore resort to the anisotropic excitability parameter distribution (see Table 2). We map the

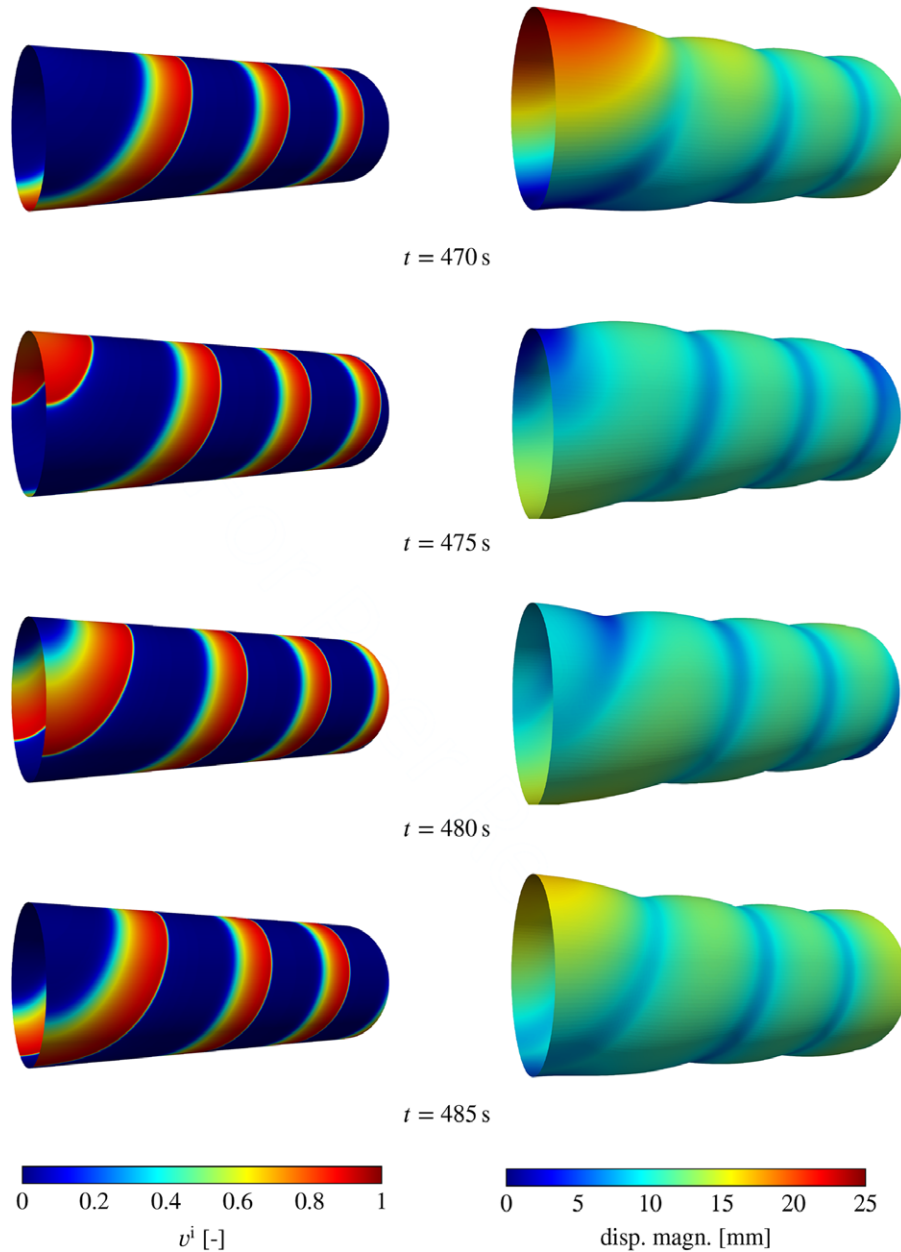


FIGURE 8 Idealized cylindrical electro-mechanical stomach model at different points of simulation time. The left column shows the normalized ICC transmembrane potential v^i . The magnitude of the displacements is depicted in the right column together with the resulting deformation. The colorbars apply to the respective column, where v^i is dimensionless and the displacement magnitude is depicted in mm

planar distribution function onto the cylinder surface such that the pacemaker site with the highest intrinsic frequency is located at $(x, y, z) = (0, 0, r)$. As described in Sec. 3.3.2, we expect this to result in the desired anisotropic conduction behavior.

The left column of Figure 8 shows the spatial distribution of the transmembrane voltage v^i at different points in time. At $t = 475$ s the pacemaker site (top, left) is in the refractory phase just before activation. Once initiated at the pacemaker site, the slow waves propagate both axially and symmetrically in radial direction ($t = 475$). As desired, the CV in radial direction is higher than in axial direction ($t = 480$). Therefore, the slow waves form a closed ring within approximately 20 s after initiation (see previous wave in ($t = 470$)). The closed slow wave ring travels in axial direction until it phases out at the right boundary, $x = L_x$. This slow wave propagation pattern is stable. The slow waves are generated with a frequency of approximately 3 cpm, resulting in a spatial distance between subsequent waves of 40 mm. Both values are within the experimentally established physiological range.^[74]

The right column of Figure 8 visualizes the resulting deformation. Compared to its load-free configuration, the cylinder is inflated by the applied inner pressure to a radius of $R = 70.485$ mm. In this deformed state the electric slow waves induce, via

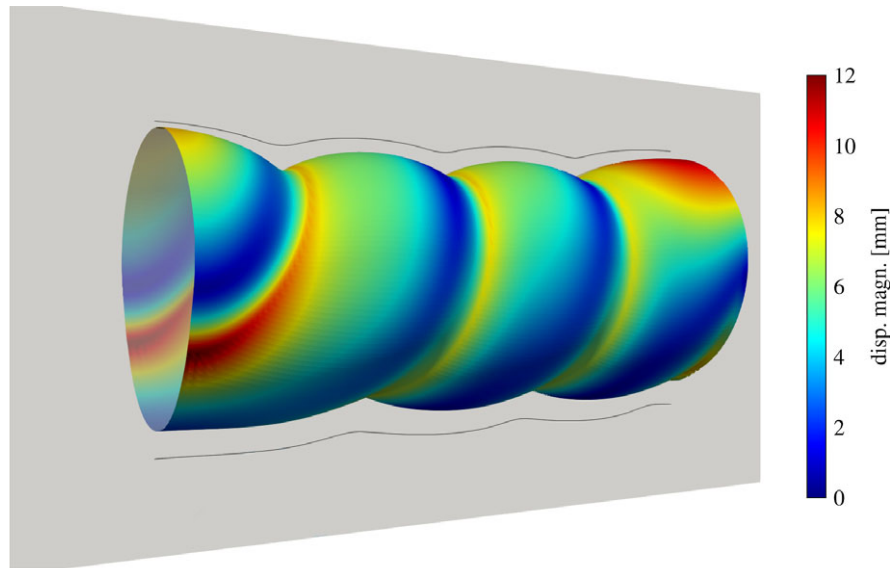


FIGURE 9 Solution with increased values of $\alpha_1 = \alpha_c = 0.5$. For comparison, the black line shows the outline of the solution with $\alpha_1 = \alpha_c = 0.25$ in the xz -plane (grey). The colorbar shows the displacement magnitude in mm. By adjusting α_1 and α_c , the model is capable of representing different intensities of the contractions. The contraction waves become more pronounced for higher α_1 and α_c values

the resulting muscular contraction, ring-shaped contraction waves which propagate axially in a synchronized and coordinated pattern. We investigated the influence of the contractility parameters α_1 and α_c on the mechanical deformation. As depicted in Figure 9, the model is capable of representing different intensities of the peristaltic gastric contractions by adjusting the values of α_1 and α_c . The higher these values are, the more pronounced the resulting contraction waves become. This example clearly demonstrates that our electro-mechanical model is in principle able to reproduce the essential features of peristaltic contraction waves as observed in the stomach.

4 | CONCLUSION

In this paper, we propose a computational model of the electro-mechanical coupling in the stomach based on an active-strain finite elasticity approach. Within this framework, gastric electrophysiology is represented by a simplified phenomenological model relying on two internal state variables considering two coupled modified Mitchell-Schaeffer models. Using a series of computational examples, we demonstrated that this multiphysics approach is sufficient to capture essential phenomena of gastric electro-mechanics such as slow wave generation and entrainment across the organ, gastric dysrhythmias as well as the propagation of stable ring-shaped peristaltic contraction waves along the stomach.

Our computational analyses reveal that the spatial propagation patterns of electric and mechanic activity in the gastrointestinal tissue strongly depend on the underlying distributions of the excitability parameter which controls the intrinsic frequencies at which ICC trigger electric signals within SMC (in the absence of any entrainment due to coupling with surrounding ICC).

As a novel contribution, the present study links gastric electrophysiology and dysrhythmias to the mechanical properties of the stomach highlighting the strong mechanical nonlinearities that characterize the gastric wall. Though several experimental evidences have shown the tight coupling between dysrhythmias and gastroparesis (e.g., irregular initiation, aberrant conduction, low amplitude etc. ^[75]), this link remains largely unexplored so far from a modeling and computational viewpoint and we aim at stimulating further investigations in the future.

Altogether, the computational model of gastric electro-mechanics presented in this paper can be understood as a computationally efficient and, at the same time, robust workhorse for future computational studies of the role of the electro-mechanical coupling in the stomach in health and disease.

Nevertheless, several limitations of the proposed model should be mentioned here. In our model the problem of electrophysiological wave generation and propagation is solved on the reference configuration under incompressibility constraints. This implicitly assumes a one-way coupling between electrophysiology and mechanics, neglecting any feedback from the mechanical deformation on the electrophysiology, known as mechano-electric feedback (MEF).^[76] Such feedback might, however, play

an important role in reality, e.g., via stretch-activated currents^[77,78] or nonlinear^[79,80] and stress-assisted diffusion.^[42] We aim to include the effects of MEF in a future contribution generalizing the present theoretical and computational framework and to validate it against in vivo electro-mechanical data.^[73,81,82]

Another rather obvious limitation of our model is the purely phenomenological approach to model the spatio-temporal dynamics of cell electrophysiology. In fact, incorporating a detailed multiscale, biophysical description of the intra-cellular processes governing gastric electrophysiology might be a valuable goal for future work. In particular, we aim at validating the present active-strain electro-mechanical framework against experimental evidences in terms of biophysical electrophysiological couplings.^[13,83,84]

From the computational point of view, a deeper investigation of the CV in the circumferential direction using a more realistic gastric geometry should be accomplished, considering also the presence of the fundus, which is electrically quiescent but responsible for other, specific mechanical effects, namely the storage function of the stomach. Also, more efficient numerical schemes^[85–87] and GPU-based codes^[88,89] are foreseen to speed-up the wide numerical analyses necessary to fully characterize a complex organ like the stomach.

Finally, also a more realistic mechanical model of the gastric tissue should be employed. It is well-known that the gastric tissue exhibits inhomogeneous and in general also anisotropic mechanical properties, which may also strongly depend on the age of an individual.^[90–94] Exploring the precise effect of the mechanical properties on the electro-mechanical coupling might be a key to better understand the origin of certain gastric pathologies. Also the effect of the amplitude of muscular contraction should be studied in more depth in the future. Overall, the model results should also be validated against electro-mechanical data sets in order to expand the model's predictive significance.

Addressing all these and in fact several other open points proposes a host of interesting avenues of future research in the still emerging field of gastric electro-mechanics.

ACKNOWLEDGMENTS

The authors gratefully acknowledge funding from the German Research Foundation (Deutsche Forschungsgemeinschaft) within the Project CY 75/3-1 (“Computational Multiphysics Modeling of the Postprandial Human Stomach”). The authors also wish to thank the support from the Italian National Group of Mathematical Physics (GNFM) and Istituto Nazionale di Alta Matematica (INdAM) “Francesco Severi”, the COST-CA16119 (STSM-38666) and the Erasmus+ Programme.

ORCID

Sebastian Brandstaeter  <http://orcid.org/0000-0001-9594-1302>

Alessio Gizzi  <http://orcid.org/0000-0001-5350-8156>

Christian J. Cyron  <http://orcid.org/0000-0001-8264-0885>

REFERENCES

- [1] E. N. Marieb, K. Hoehn, *Human Anatomy & Physiology 9th edn.*, Pearson Education **2013**.
- [2] J. D. Huizinga, W. J. E. P. Lammers, *American Journal of Physiology - Gastrointestinal and Liver Physiology* **2009**, 296, G1.
- [3] K. M. Sanders, Y. Kito, S. J. Hwang, S. M. Ward, *Physiology* **2016**, 31, 316.
- [4] J. H. Szurszewski, *The American Journal of Physiology* **1998**, 274, G447.
- [5] K. M. Sanders, S. D. Koh, S. M. Ward, *Annual Review of Physiology* **2006**, 68, 307.
- [6] S. J. Hwang, P. J. A. Blair, F. C. Britton, K. E. O'Driscoll, G. Hennig, Y. R. Bayguinov, J. R. Rock, B. D. Harfe, K. M. Sanders, S. M. Ward, *Journal of Physiology* **2009**, 587, 4887.
- [7] M. H. Zhu, T. S. Sung, K. O'Driscoll, S. D. Koh, K. M. Sanders, *American Journal of Physiology - Cell Physiology* **2015**, 308, C608.
- [8] K. J. Park, G. W. Hennig, H.-T. Lee, N. J. Spencer, S. M. Ward, T. K. Smith, K. M. Sanders, *American Journal of Physiology-Cell Physiology* **2006**, 290, C1411.
- [9] T. R. Angeli, G. O'Grady, W. J. E. P. Lammers, *The Electrical Regulation of GI Motility at the Whole-Organ Level* (Eds: L. K. Cheng, A. J. Pullan, G. Farrugia), Springer Netherlands, Dordrecht **2013**, pp. 95–112.
- [10] D. F. Van Helden, M. S. Imtiaz, K. Nurgaliyeva, P.-Y. von der Weid, P. J. Dosen, *The Journal of Physiology* **2000**, 524, 245.
- [11] D. F. Van Helden, D. R. Laver, J. Holdsworth, M. S. Imtiaz, *Clinical and Experimental Pharmacology and Physiology* **2010**, 37, 516.
- [12] Q. Xiao, K. Yu, P. Perez-Cornejo, Y. Cui, J. Arreola, H. C. Hartzell, *Proc. Natl. Acad. Sci.* **2011**, 108, 8891.

- [13] R. Lees-Green, S. J. Gibbons, G. Farrugia, J. Sneyd, L. K. Cheng, *American Journal of Physiology - Gastrointestinal and Liver Physiology* **2014**, 306, G711.
- [14] R. A. Hinder, K. A. Kelly, *The American Journal of Surgery* **1977**, 133, 29.
- [15] T. R. Angeli, N. Paskaranandavadi, L. K. Cheng, P. Du, *An Improved Understanding of Gut Function through High-Resolution Mapping and Multiscale Computational Modeling of the Gastrointestinal Tract*, Academic Press **2014**.
- [16] P. Du, S. Calder, T. R. Angeli, S. Sathar, N. Paskaranandavadi, G. O'Grady, L. K. Cheng, *Frontiers in Physiology* **2018**, 8, 1136.
- [17] A. Karma, *Annu. Rev. Condens. Matter Phys.* **2013**, 4, 313.
- [18] D. Bini, C. Cherubini, S. Filippi, A. Gizzi, P. E. Ricci, *Communications in Computational Physics* **2010**, 8, 610.
- [19] M. Hanani, G. Farrugia, T. Komuro, *Intercellular Coupling of Interstitial Cells of Cajal in the Digestive Tract*, vol 242, Academic Press, **2005**, pp. 249–282.
- [20] S. J. Kim, S. C. Ahn, J. K. Kim, Y. C. Kim, I. So, K. W. Kim, *American Journal of Physiology - Cell Physiology* **1997**, 273, C1947.
- [21] V. Gajendiran, M. L. Buist, *International Journal for Numerical Methods in Biomedical Engineering* **2011**, 27, 450.
- [22] R. R. Aliev, A. W. Richards, J. P. Wikswo, *Journal of Theoretical Biology* **2000**, 204, 21.
- [23] A. Gizzi, C. Cherubini, S. Migliori, R. Alloni, R. Portuesi, S. Filippi, *Physical Biology* **2010**, 7, 016011.
- [24] A. J. Pullan, L. K. Cheng, R. Yassi, M. L. Buist, *Progress in Biophysics and Molecular Biology* **2004**, 85, 523.
- [25] S.-I. Murtada, J. D. Humphrey, G. A. Holzapfel, *Biophys. J.* **2017**, 113, 714.
- [26] S.-I. Murtada, M. Kroon, G. A. Holzapfel, *Biomechanics and Modeling in Mechanobiology* **2010**, 9, 749.
- [27] A. Gizzi, C. Cherubini, S. Filippi, A. Pandolfi, *Communication in Computational Physics* **2015**, 17, 93.
- [28] C. J. Cyron, R. C. Aydin, J. D. Humphrey, *Biomechanics and Modeling in Mechanobiology* **2016**, 15, 1389.
- [29] C. J. Cyron, R. C. Aydin, *ZAMM* **2017**, 97, 1011.
- [30] A. Gizzi, E. M. Cherry, R. F. Gilmour Jr., S. Luther, S. Filippi, F. H. Fenton, *Frontiers in Physiology* **2013**, 4, 71.
- [31] M. Böhl, A. E. Ehret, K. Leichsenring, C. Weichert, R. Kruse, *Acta Biomaterialia* **2014**, 10, 3225.
- [32] M. Böhl, K. Leichsenring, M. Ernst, A. E. Ehret, *Journal of the Mechanical Behavior of Biomedical Materials* **2016**, 63, 115.
- [33] S. C. Murtada, A. Arner, G. A. Holzapfel, *Journal of Theoretical Biology* **2012**, 297, 176.
- [34] S. Land, et al., *Proceedings of the Royal Society A: Mathematical, Physical and Engineering Sciences* **2015**, 471, 20150641.
- [35] S.-I. Murtada, M. Kroon, G. A. Holzapfel, *J. Mech. Phys. Solids* **2010**, 58, 2065.
- [36] O. Röhrle, J. B. Davidson, A. J. Pullan, *Frontiers in Physiology* **2012**, 3, 1.
- [37] T. Heidlauf, O. Röhrle, *Frontiers in Physiology* **2014**, 5, 1.
- [38] O. Röhrle, M. Sprenger, S. Schmitt, *Biomechanics and Modeling in Mechanobiology* **2017**, 16, 743.
- [39] C. Cherubini, S. Filippi, A. Gizzi, *Phys. Rev. E* **2012**, 85, 031915.
- [40] R. Ruiz-Baier, A. Gizzi, S. Rossi, C. Cherubini, A. Laadhari, S. Filippi, A. Quarteroni, *Mathematical Medicine and Biology* **2014**, 31, 259.
- [41] F. S. Costabal, F. A. Concha, D. E. Hurtado, S. Kuhl, *Comput. Methods Appl. Mech. Eng.* **2017**, 320, 352.
- [42] C. Cherubini, S. Filippi, A. Gizzi, R. Ruiz-Baier, *Journal of Theoretical Biology* **2017**, 430, 221.
- [43] G. S. Kassab, J. Guccione, *Frontiers in Physiology* **2018**, 9, 617.
- [44] K. M. Sanders, *Neurogastroenterology & Motility* **2008**, 20, 39.
- [45] K. M. Sanders, S. D. Koh, S. Ro, S. M. Ward, *Nat Rev Gastroenterol Hepatol* **2012**, 9, 633.
- [46] R. N. Miftahof, in *Proceedings of the V European Conference on Computational Fluid Dynamics ECCOMAS CFD 2010* (Eds: J. C. F. Pereira, A. Sequeira, J. M. C. Pereira), **2010**, p. 11.
- [47] R. N. Miftahof, H. G. Nam, *Mathematical Foundations and Biomechanics of the Digestive System*, Cambridge University Press **2010**.
- [48] A. Gizzi, A. Pandolfi, M. Vasta, *Mech. Mater.* **2016**, 92, 119.
- [49] M. Vasta, A. Gizzi, A. Pandolfi, *Probabilistic Engineering Mechanics* **2014**, 37, 170.
- [50] A. Pandolfi, A. Gizzi, M. Vasta, *J. Biomech.* **2016**, 49, 2436.
- [51] A. Pandolfi, A. Gizzi, M. Vasta, *Meccanica* **2017**, 52, 3399.
- [52] A. Altomare, A. Gizzi, M. P. L. Guarino, A. Loppini, A. Cocca, M. Dipaola, R. Alloni, S. Cicala, S. Filippi, *American Journal of Physiol Gastrointestine Liver Physiology* **2014**, 307, G77.
- [53] C. C. Mitchell, D. G. Schaeffer, *Bull. Math. Biol.* **2003**, 65, 767.
- [54] K. Djabella, M. Landau, M. Sorine, in *2007 46th IEEE Conference on Decision and Control*, Institute of Electrical & Electronics Engineers, **2007**, pp. 5186–5191.

- [55] S. Rossi, R. Ruiz-Baier, L. F. Pavarino, A. Quarteroni, *International Journal for Numerical Methods in Biomedical Engineering* **2012**, 28, 761.
- [56] F. H. Fenton, E. M. Cherry, *Scholarpedia* **2008**, 3, 1868.
- [57] J. Keener, J. Sneyd (Eds.), *Mathematical Physiology I: Cellular Physiology*, vol 8/1 of *Interdisciplinary Applied Mathematics*, Springer, New York **2009**.
- [58] A. Corrias, M. L. Buist, *Ann. Biomed. Eng.* **2007**, 35, 1595.
- [59] A. J. Pullan, L. K. Cheng, M. L. Buist, *Mathematically Modelling the Electrical Activity of the Heart: From Cell to Body Surface and Back Again*, World Scientific **2005**.
- [60] J. Keener, J. Sneyd (Eds.), *Mathematical Physiology II: Systems Physiology*, vol 8/2 of *Interdisciplinary Applied Mathematics*, Springer, New York **2009**.
- [61] A. Gizzi, C. Cherubini, S. Filippi, A. Pandolfi, *Communications in Computational Physics* **2015**, 17, 93.
- [62] K. M. Sanders, S. M. Ward, S. D. Koh, *Physiological Reviews* **2014**, 94, 859.
- [63] A. Quarteroni, T. Lassila, S. Rossi, R. Ruiz-Baier, *Computer Methods in Applied Mechanics and Engineering* **2017**, 314, 345.
- [64] J. Zhao, D. Liao, P. Chen, P. Kunwald, H. Gregersen, *J. Biomech.* **2008**, 41, 3441.
- [65] P. C. Franzone, L. F. Pavarino, S. Scacchi, *Frontiers in Physiology* **2018**, 9 (APR).
- [66] E. M. Cherry, F. H. Fenton, *Journal of Theoretical Biology* **2011**, 285, 164.
- [67] G. O'Grady, T. H. H. Wang, P. Du, T. Angeli, W. Lammers, L. K. Cheng, *Clinical and Experimental Pharmacology and Physiology* **2014**, 41, 854.
- [68] G. O'Grady, T. L. Abell, *Gastroenterology Clinics of North America* **2015**, 44, 169.
- [69] P. Du, G. O'Grady, L. K. Cheng, *Journal of Theoretical Biology* **2017**, 425, 72.
- [70] E. H. Livingston, E. P. Passaro, *Digestive Diseases and Sciences* **1990**, 35, 121.
- [71] A. Pal, K. Indreshkumar, W. Schwizer, B. Abrahamsson, M. Fried, J. G. Brasseur, *Proceedings of the Royal Society of London B: Biological Sciences* **2004**, 271, 2587.
- [72] H. Gregersen, G. Kassab, *Neurogastroenterology & Motility* **1996**, 8, 277.
- [73] R. K. Mittal, J. Liu, J. L. Puckett, V. Bhalla, V. Bhargava, N. Tipnis, G. Kassab, *Gastroenterology* **2005**, 128, 487.
- [74] G. O'Grady, P. Du, L. K. Cheng, J. U. Egbuji, W. J. E. P. Lammers, J. A. Windsor, A. J. Pullan, *American Journal of Physiology - Gastrointestinal and Liver Physiology* **2010**, 299, G585.
- [75] G. O'Grady, P. Du, N. Paskaranandavadi, T. R. Angeli, W. J. E. P. Lammers, S. J. Asirvatham, J. A. Windsor, G. Farrugia, A. J. Pullan, L. K. Cheng, *Neurogastroenterology and Motility* **2012**, 24, e299.
- [76] F. Ravelli, *Progress in Biophysics and Molecular Biology* **2003**, 82, 137.
- [77] A. Beyder, R. Lees-Green, G. Farrugia in *New Advances in Gastrointestinal Motility Research*, vol 10 of *Lecture Notes in Computational Vision and Biomechanics* (Eds: L. K. Cheng, A. J. Pullan, G. Farrugia), Springer, Netherlands **2013**, pp. 7–27.
- [78] S. Land, S.-J. Park-Holohan, N. P. Smith, C. G. dos Remedios, J. C. Kentish, S. A. Niederer, *Journal of Molecular and Cellular Cardiology* **2017**, 106, 68.
- [79] D. E. Hurtado, S. Castro, A. Gizzi, *Computer Methods in Applied Mechanics and Engineering* **2016**, 300, 70.
- [80] A. Gizzi, A. Loppini, R. Ruiz-Baier, A. Ippolito, A. Camassa, A. La Camera, E. Emmi, L. Di Perna, V. Garofalo, C. Cherubini, S. Filippi, *Chaos: An Interdisciplinary Journal of Nonlinear Science* **2017**, 27, 93919.
- [81] H. Gregersen, O. H. Gilja, T. Hausken, A. Heimdal, C. Gao, K. Matre, S. Ødegaard, A. Berstad, *American Journal of Physiology - Gastrointestinal and Liver Physiology* **2002**, 283, G368.
- [82] G. S. Kassab, J. A. Navia, *Magnetic Devices and Methods for Septal Occlusion*, **2015**, US Patent 9,198,646.
- [83] N. Paskaranandavadi, L. K. Cheng, P. Du, J. M. Rogers, G. O'Grady, *American Journal of Physiology - Gastrointestinal and Liver Physiology* **2017**, 313, G265.
- [84] T. H. H. Wang, P. Du, T. R. Angeli, N. Paskaranandavadi, J. C. Erickson, T. L. Abell, L. K. Cheng, G. O'Grady, *Neurogastroenterology & Motility* **2018**, 30, e13152.
- [85] J. M. Hoermann, C. Bertoglio, M. Kronbichler, M. R. Pfaller, R. Chabiniok, W. A. Wall, *International Journal for Numerical Methods in Biomedical Engineering* **2018**, 34, e2959.
- [86] D. E. Hurtado, G. Rojas, *Comput. Mech.* **2018**, 61, 485.
- [87] R. S. Oliveira, B. M. Rocha, D. Burgarelli, W. Meira, C. Constantinides, R. Weber dos Santos, *International Journal for Numerical Methods in Biomedical Engineering* **2018**, 34, e2913.
- [88] E. Bartocci, E. M. Cherry, J. Glimm, R. Grosu, S. A. Smolka, F. H. Fenton, in *Proceedings of the 9th International Conference on Computational Methods in Systems Biology - CMSB '11*, ACM Press, New York, New York, USA **2011**, p. 103. <http://dl.acm.org/citation.cfm?doid=2037509.2037525>.

- [89] A. Mena, J. M. Ferrero, J. F. Rodriguez Matas, *Comput. Phys. Commun.* **2015**, 196, 280.
- [90] R. C. Aydin, S. Brandstaeter, F. A. Breau, M. Steigenberger, R. P. Marcus, K. Nikolaou, M. Notohamiprodjo, C. J. Cyron, *Journal of the Mechanical Behavior of Biomedical Materials* **2017**, 74, 499.
- [91] A. Tomalka, M. Borsdorf, M. Böl, T. Siebert, *Frontiers in Physiology* **2017**, 8, 802.
- [92] R. N. Miftakhov, *Hydroelasticity of Shells* **1983**, 163.
- [93] R. N. Miftakhov, *Hydroelasticity of Shells* **1983**, 172.
- [94] R. N. Miftakhov, *Shell Interactions with Fluids* **1981**, 197.

How to cite this article: Brandstaeter S, Gizzi A, Fuchs SL, Gebauer AM, Aydin RC, Cyron CJ. Computational model of gastric motility with active-strain electromechanics. *Z Angew Math Mech.* 2018;98:2177–2197. <https://doi.org/10.1002/zamm.201800166>

APPENDIX: DERIVATION OF THE FIRST PIOLA KIRCHHOFF STRESS TENSOR FOR ACTIVE-STRAIN ELECTROMECHANICS

The first term on the right-hand side of (12) can be identified as the first Piola-Kirchhoff stresses that arise from the elastic deformation \mathbf{F}_e in the intermediate configuration Ω_a . We denote this tensor as \mathbf{P}_e . For the derivation of the second term, we switch to Einstein's index notation:

$$\begin{aligned} \left(\frac{\partial \mathbf{F}_e}{\partial \mathbf{F}} \right)_{ijkl} &= \frac{\partial (\mathbf{F} \mathbf{F}_a^{-1})_{ij}}{\partial F_{kl}} = \frac{\partial (F_{im} (\mathbf{F}_a^{-1})_{mj})}{\partial F_{kl}} = \left(\frac{\partial F_{im}}{\partial F_{kl}} \right) (\mathbf{F}_a^{-1})_{mj} + F_{im} \left(\frac{\partial (\mathbf{F}_a^{-1})_{mj}}{\partial F_{kl}} \right) \\ &= \delta_{ik} \delta_{ml} (\mathbf{F}_a^{-1})_{mj} + F_{im} \left(\frac{\partial (\mathbf{F}_a^{-1})_{mj}}{\partial F_{kl}} \right) = \delta_{ik} (\mathbf{F}_a^{-1})_{lj} + F_{im} \left(\frac{\partial (\mathbf{F}_a^{-1})_{mj}}{\partial F_{kl}} \right). \end{aligned}$$

The first Piola-Kirchhoff stress tensor now reads:

$$P_{kl} = \frac{\partial \Psi_e}{\partial (F_e)_{ij}} \left[\delta_{ik} (\mathbf{F}_a^{-1})_{lj} + F_{im} \left(\frac{\partial (\mathbf{F}_a^{-1})_{mj}}{\partial F_{kl}} \right) \right] = \frac{\partial \Psi_e}{\partial (F_e)_{kj}} (\mathbf{F}_a^{-1})_{lj} + \frac{\partial \Psi_e}{\partial (F_e)_{ij}} F_{im} \left(\frac{\partial (\mathbf{F}_a^{-1})_{mj}}{\partial F_{kl}} \right).$$

In tensor notation, the above equation reads:

$$\mathbf{P} = \frac{\partial \Psi_e}{\partial \mathbf{F}_e} \mathbf{F}_a^{-T} + \frac{\partial \Psi_e}{\partial \mathbf{F}_e} \left(\mathbf{F} \frac{\partial \mathbf{F}_a^{-1}}{\partial \mathbf{F}} \right).$$

Neglecting mechano-electrical feedback, the active deformation gradient \mathbf{F}_a does not depend on the the deformation \mathbf{F} , hence the derivative $\partial \mathbf{F}_a^{-1} / \partial \mathbf{F}$ vanishes and the first Piola-Kirchhoff stress tensor \mathbf{P} can be written as

$$\mathbf{P} = \frac{\partial \Psi_e}{\partial \mathbf{F}_e} \mathbf{F}_a^{-T}.$$

C

Global sensitivity analysis of a homogenized constrained mixture model of arterial growth and remodeling

Sebastian Brandstaeter, Sebastian L. Fuchs, Jonas Biehler, Roland C. Aydin,
Wolfgang A. Wall, Christian J. Cyron


published in

Journal of Elasticity, vol. 145, pp. 191–221, 2021. DOI: [10.1007/s10659-021-09833-9](https://doi.org/10.1007/s10659-021-09833-9).

Reprinted from [52], licensed under a Creative Commons Attribution 4.0 International License (<https://creativecommons.org/licenses/by/4.0/>).



Global Sensitivity Analysis of a Homogenized Constrained Mixture Model of Arterial Growth and Remodeling

Sebastian Brandstaeter^{1,2} · Sebastian L. Fuchs^{1,2} · Jonas Biehler¹ · Roland C. Aydin³ · Wolfgang A. Wall¹ · Christian J. Cyron^{2,3} 

This paper is dedicated to Professor Dr. Gerhard Holzapfel on the occasion of his sixtieth birthday

Received: 29 November 2020 / Accepted: 6 April 2021 / Published online: 20 May 2021
© The Author(s) 2021

Abstract

Growth and remodeling in arterial tissue have attracted considerable attention over the last decade. Mathematical models have been proposed, and computational studies with these have helped to understand the role of the different model parameters. So far it remains, however, poorly understood how much of the model output variability can be attributed to the individual input parameters and their interactions. To clarify this, we propose herein a global sensitivity analysis, based on Sobol indices, for a homogenized constrained mixture model of aortic growth and remodeling. In two representative examples, we found that 54–80% of the long term output variability resulted from only three model parameters. In our study, the two most influential parameters were the one characterizing the ability of the tissue to increase collagen production under increased stress and the one characterizing the collagen half-life time. The third most influential parameter was the one characterizing the strain-stiffening of collagen under large deformation. Our results suggest that in future computational studies it may - at least in scenarios similar to the ones studied herein - suffice to use population average values for the other parameters. Moreover, our results suggest that developing methods to measure the said three most influential parameters may be an important step towards reliable patient-specific predictions of the enlargement of abdominal aortic aneurysms in clinical practice.

As many young researchers, most of us first got to know Professor Holzapfel through his seminal book on nonlinear solid mechanics and subsequently through his similarly seminal work in the area of vascular biomechanics. We would like to thank Professor Holzapfel for the inspiration he has given by his work not only to us but in fact to numerous generations of doctoral students and postdoctoral researchers in biomechanics worldwide.

✉ C.J. Cyron
christian.cyron@hzg.de

¹ Institute for Computational Mechanics, Technical University of Munich, Boltzmannstrasse 15, 85748 Garching, Germany

² Institute of Continuum and Materials Mechanics, Hamburg University of Technology, Eissendorfer Str. 42, 21073 Hamburg, Germany

³ Institute of Material Systems Modeling, Helmholtz-Zentrum Geesthacht, Max-Planck-Strasse 1, 21502 Geesthacht, Germany

Keywords Homogenized constrained mixture · Growth and remodeling · Abdominal aortic aneurysm · Global sensitivity analysis

Mathematics Subject Classification 92C10 · 65C05 · 92C50

1 Introduction

Growth and remodeling of arteries has been researched extensively during the past 15 years. In particular their important role in diseases such as aneurysms, which belong to the most important causes of mortality and morbidity in industrialized countries, has attracted significant attention. Aneurysms are local pathological dilatations of blood vessels that often keep growing over years until the blood vessel ruptures. Understanding and predicting this process is important for planning surgical interventions and researching potential future therapies. In the early 2000s, Watton et al. [1] and Baek et al. [2] proposed the first computational models to understand the natural history and evolution of fusiform aneurysms. A few years later Kroon and Holzapfel studied for the first time growth and remodeling of saccular cerebral aneurysms and identified the “continuous turnover of collagen” as the “driving mechanism in aneurysmal growth” [3]. Together with the constrained mixture theory of growth and remodeling introduced by Humphrey and Rajagopal [4], [1–3] inspired a host of increasingly detailed studies of vascular growth and remodeling over the last decade, for example, [5–29]. While computational constrained mixture models of arterial growth and remodeling have substantially contributed to our understanding of this complex phenomenon, their clinical application, for example, for the computer-aided planning of treatments and surgeries, is still pending. A major difficulty in transferring these models from academic studies to clinical practice is the determination of patient-specific mechanobiological model parameters, which are required to make individualized predictions. It is naturally difficult and in particular potentially very expensive - if possible at all - to determine all these parameters with high accuracy. Therefore, it is important to understand which of these parameters have the most impact on the results of computational predictions. Knowing this, research can focus on the development of novel approaches to measure at least these parameters in a way that is on the one hand compatible with standard clinical workflows and acceptably cheap and on the other hand still sufficiently accurate for meaningful computer-aided predictions. To understand, which parameters in computational models of growth and remodeling are most important, [30, 31] proposed parametric studies where single parameters were varied in growth and remodeling model based on the constrained mixture theory introduced in [4]. While the studies presented in [30, 31] provided important insights, they also had limitations. Most importantly, they were limited to variations of single parameters, skipping thereby completely the in general important interactions between different parameters [32]. One notable exception was the study of Valentín and Humphrey [33] who investigated the combined influence of two parameters. Another more recent branch of research uses Bayesian methods [34–37], which are well-known from other areas of applied mechanics to be powerful tools for quantifying the effect of parameter uncertainties. However, what remains missing is a mathematically rigorous global sensitivity analysis ranking the importance of all the different parameters of computational models of growth and remodeling.

In this paper, we are presenting such an analysis for the homogenized constrained mixture models introduced in [38]. Our analysis uses the mathematically rigorous variance-based approach of Sobol and Saltelli [39–42]. This method decomposes the variance in the model’s output upon variation of the input parameters and determines the contribution of each input

parameter to the output's variance. Thereby, it allows us to understand not only the importance of single parameters of homogenized constrained mixture models but, for the first time, also the importance of combinations of input parameters. The resulting global and also quantitative understanding of parameter sensitivity allows us to make comprehensive, reliable and even quantitative statements about which parameters are most important in order to make reliable computational predictions. At the moment, most parameters of computational models of growth and remodeling are difficult to determine in a patient-specific way that fits into a standard clinical workflow. To overcome this problem systematically over the next years, one will have to develop step by step more and more methods to this end. The key question thereby is, the development of which methods should be prioritized in order to increase the predictive ability of computational models as fast and as much as possible. The global sensitivity analysis presented in this paper provides an important basis to make rational and well-founded decisions with respect to this question because it provides mathematically rigorous and quantitative statements about the importance of the different model parameters. We thus hope that this paper can help to guide the future biomedical research focused on vascular growth and remodeling.

This paper is organized as follows. In Sect. 2, we first introduce the concept of global sensitivity analysis and Sobol' indices. In Sect. 3, we briefly summarize the homogenized constrained mixture model introduced in [38]. In Sect. 4, we discuss the details of a global sensitivity analysis of this model. The results of this analysis are summarized in Sect. 5 and discussed in Sect. 6. Finally, in Sect. 7, we discuss the conclusions drawn from these results with respect to potential future research into methods for the clinical determination of mechanobiological parameters.

2 Sobol Indices: An Approach for Global Sensitivity Analysis

Many parameter studies use so-called local methods where only single parameters are varied at a time. However, this approach is not suitable for nonlinear models because it neglects the possibly important interactions between different parameters and tends to underestimate the input space due to the "curse of dimensionality". To overcome these limitations, global sensitivity analysis methods try to infer the global influence of model parameters on the model output by quantifying the amount of uncertainty in the model output caused by the individual parameters including their interactions with other parameters [32].

2.1 Definition and Interpretation of Sobol Indices

This section introduces variance-based global sensitivity measures for general, nonlinear models, which are often referred to as Sobol indices [39–44]. To keep the notation simple, we abstain in the following from a notational distinction between random variables and their realizations and trust that the difference is evident from the context. Thus, let $\mathbf{x} = \{x_1, x_2, \dots, x_n\} \in \Omega$ denote a continuous random vector whose components x_i are random variables. By $\mathbf{x}_{\sim i}$, we denote the random vector of all components except x_i , that is,

$$\mathbf{x}_{\sim i} = \{x_1, x_2, \dots, x_{i-1}, x_{i+1}, \dots, x_n\}. \quad (1)$$

The expected value of a function y of \mathbf{x} is denoted by

$$\mathbb{E}_{\mathbf{x}}[y(\mathbf{x})] = \int_{\Omega} y(\mathbf{x}) p_{\mathbf{x}}(\mathbf{x}) d\mathbf{x}, \quad (2)$$

where $p_{\mathbf{x}}(\mathbf{x})$ is the probability density function of \mathbf{x} . The corresponding variance follows as

$$\mathbb{V}_{\mathbf{x}}[y(\mathbf{x})] = \mathbb{E}_{\mathbf{x}}[(y(\mathbf{x}) - \mathbb{E}_{\mathbf{x}}[y(\mathbf{x})])^2] = \int_{\Omega} (f(\mathbf{x}) - \mathbb{E}_{\mathbf{x}}[f(\mathbf{x})])^2 p_{\mathbf{x}}(\mathbf{x}) d\mathbf{x}. \quad (3)$$

Let the model of interest be represented by an integrable function y with n mutually independent input parameters $\mathbf{x} = \{x_1, x_2, \dots, x_n\}$ and scalar output such that

$$y : K^n = [0, 1]^n \rightarrow \mathbb{R}, \quad \mathbf{x} \mapsto y(\mathbf{x}). \quad (4)$$

For the sake of readability, we commit a slight abuse of notation by not distinguishing between the function y and its value $y(\mathbf{x})$ in the following. Herein we assume, without loss of generality (cf. [42] or [45, Chap. 15]) that the model parameters are distributed uniformly within the n -dimensional unit hypercube K^n , that is, $x_i \sim U(0, 1)$, where $U(a, b)$ denotes the continuous uniform distribution on the interval $[a, b]$ with $-\infty < a < b < \infty$. Due to the mutual independence of the x_i , the joint probability density function is calculated as $p_{\mathbf{x}}(x_1, x_2, \dots, x_n) = \prod_{i=1}^n p_{x_i}(x_i) = 1$. One can show that, under the above assumptions, there exists a unique decomposition of y , often called analysis of variance (ANOVA) representation [39, 41] or high-dimensional model representation (HDMR) [45], such that

$$y(\mathbf{x}) = y_0 + \sum_{i=1}^n y_i + \sum_{i=1}^{n-1} \sum_{j>i}^n y_{ij} + \sum_{i=1}^{n-2} \sum_{j>i}^{n-1} \sum_{k>j}^n y_{ijk} + \dots + y_{12\dots n}, \quad (5)$$

where y_0 is constant and the components $y_{ijk\dots} = y_{ijk\dots}(x_i, x_j, x_k, \dots)$ are functions of as many (up to n) arguments $\{x_i, x_j, x_k, \dots\}$ as they exhibit subscripts. Using (5), we can decompose the total variance of y as

$$\mathbb{V}_{\mathbf{x}}[y] = \sum_{i=1}^n \mathbb{V}_{x_i}[y_i] + \sum_{i=1}^{n-1} \sum_{j>i}^n \mathbb{V}_{x_i x_j}[y_{ij}] + \sum_{i=1}^{n-2} \sum_{j>i}^{n-1} \sum_{k>j}^n \mathbb{V}_{x_i x_j x_k}[y_{ijk}] + \dots + \mathbb{V}_{\mathbf{x}}[y_{12\dots n}], \quad (6)$$

where $\mathbb{V}_{x_i x_j x_k \dots}[y_{ijk\dots}]$ are the variances of the summands in (5). Dividing (6) by $\mathbb{V}_{\mathbf{x}}[y]$ yields

$$\sum_{i=1}^n S_i + \sum_{i=1}^{n-1} \sum_{j>i}^n S_{ij} + \sum_{i=1}^{n-2} \sum_{j>i}^{n-1} \sum_{k>j}^n S_{ijk} + \dots + S_{12\dots n} = 1, \quad (7)$$

where the

$$S_{ijk\dots} = \frac{\mathbb{V}_{x_i x_j x_k \dots}[y_{ijk\dots}]}{\mathbb{V}_{\mathbf{x}}[y]} \quad (8)$$

define variance-based sensitivity measures, called Sobol indices. A Sobol index of order s (written with s subscripts) gives the fraction of the total variance of the model output that can be attributed to the interaction between the s different input parameters x_i, x_j, x_k, \dots alone. In general, the computation of all Sobol indices of a model is very expensive. For this reason, in practice one often computes only the first order sensitivity indices S_i and the so-called total sensitivity indices S_i^T . The latter is defined as the sum of all Sobol indices

where parameter x_i is involved:

$$S_i^T = S_i + \sum_{\substack{j=1 \\ j \neq i}}^n S_{ij} + \sum_{\substack{j=1 \\ j \neq i}}^n \sum_{\substack{k>j \\ k \neq i}}^n S_{ijk} + \cdots + S_{i2\dots n}. \quad (9)$$

One can prove [39–42] that the first order sensitivity indices and total sensitivity indices can be computed equivalently to the definitions (8) and (9) as

$$S_i = \frac{\mathbb{V}_{x_i} [\mathbb{E}_{\mathbf{x}_{\sim i}} [y|x_i]]}{\mathbb{V}_x [y]}, \quad (10)$$

$$S_i^T = 1 - \frac{\mathbb{V}_{\mathbf{x}_{\sim i}} [\mathbb{E}_{x_i} [y|\mathbf{x}_{\sim i}]]}{\mathbb{V}_x [y]} = \frac{\mathbb{E}_{\mathbf{x}_{\sim i}} [\mathbb{V}_{x_i} [y|\mathbf{x}_{\sim i}]]}{\mathbb{V}_x [y]}, \quad (11)$$

where $\mathbb{E}_{\mathbf{x}_{\sim i}} [y|x_i]$ and $\mathbb{E}_{x_i} [y|\mathbf{x}_{\sim i}]$ are the expected values given the component x_i respectively the vector $\mathbf{x}_{\sim i}$. The latter two equations are often used for the efficient computation of Sobol indices (see [Appendix](#)).

The first order sensitivity index S_i is often also called the main effect of parameter x_i . It describes the fraction of the variance of y that can directly be linked to an uncertainty in x_i alone. In other words, it describes by which fraction the variance of y would reduce if the component x_i were known exactly. The total sensitivity index S_i^T is also called the total effect of parameter x_i . It describes the expected fraction of the variance of the output y that would remain if all parameters except for x_i were known exactly. It is a measure of the combined influence of x_i alone (i.e., its first order effect) together with all higher order interaction terms where x_i is involved.

While the S_i quantify the influence of each parameter alone on the model output variance, the S_i^T additionally quantify the influence of the interactions into which each parameter is involved. In practice, computing these two types of indices and omitting the other higher order indices defined above has been found to be a good trade-off between computational cost and insight into the characteristic properties of the model of interest [43]. For example, the S_i and S_i^T can be used for the following analyses.

Linearity analysis: if $\sum_{i=1}^n S_i$ is close to one, the model is largely linear, whereas if this sum is close to zero, the model is dominated by nonlinear interaction terms. Similarly, on the individual parameter level, the difference $S_i^T - S_i$ gives the amount of variance of y due to all interactions where parameter x_i is involved.

Parameter priority analysis: let us assume, we seek to reduce the uncertainty of our model as much as we can by measuring one of the input parameters exactly. Then the above delineated theory tells us that we have to focus on the parameter with the highest first order sensitivity index S_i .

Parameter fixation: to simplify the execution of computations, it is often helpful to choose reasonable ad-hoc values for a couple of parameters without spending too much effort on measurements or analyses of their exact value. Such simplifications are acceptable, however, only if the effect of where exactly a parameter is fixed within a certain reasonable range can be trusted to be small. As pointed out by [43] this is the case for parameters with $S_i^T \approx 0$.

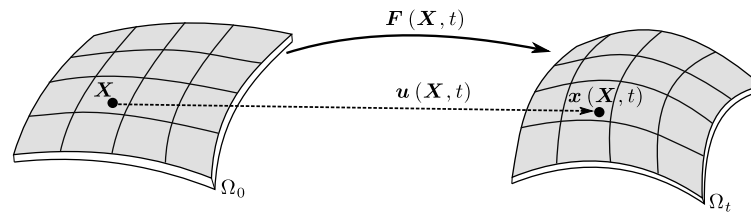


Fig. 1 Membrane subject to a large deformation: a displacement field \mathbf{u} translates at each time t each material point \mathbf{X} in some reference configuration Ω_0 to a current position \mathbf{x} in the current configuration Ω_t (image created by Sebastian L. Fuchs and licensed under the Creative Commons Attribution 4.0 International License, <https://creativecommons.org/licenses/by/4.0/>)

For practical purposes it is important to choose a smart strategy to compute the sensitivity indices because brute-force approaches quickly become prohibitively expensive as the number of model input parameters increases. The [Appendix](#) briefly summarizes such a smart strategy that enables the evaluation of a full set of first order and total sensitivity indices at the cost of just $N_{\text{tot}} = N(n + 2)$ model evaluations, where N is the number of Monte Carlo sample points used for integration and n the number of model input parameters [42, 46].

3 Homogenized Constrained Mixture Model of Vascular Growth and Remodeling

3.1 Continuum Mechanical Framework

In this section, we briefly summarize the concept of homogenized constrained mixture models of vascular growth and remodeling as developed in [38, 47, 48]. Thereby, we focus on the simple (but for this paper sufficient) special case that the blood vessel is modeled as a thin membrane. The deformation of this membrane is modeled on the basis of the theory of nonlinear continuum mechanics [49]. Thereby we model the artery as a continuum with some reference configuration Ω_0 . Mechanical loading as well as growth and remodeling can result in a deformation of the artery over time t into some current configuration Ω_t . This deformation translates each material point \mathbf{X} in the reference configuration to at time t to a current position

$$\mathbf{x}(\mathbf{X}, t) = \mathbf{X} + \mathbf{u}(\mathbf{X}, t), \quad (12)$$

where \mathbf{u} is the so-called displacement field (Fig. 1). A key quantity to describe this deformation within the theory of nonlinear continuum mechanics is the deformation gradient

$$\mathbf{F} = \frac{\partial \mathbf{x}}{\partial \mathbf{X}}. \quad (13)$$

Constrained mixture models assume that a mechanical body consists in general of m different constituents, distinguished in the following by m different superscripts $i \in I$ gathered in an index set I . These different constituents share each differential volume element. They form a compound and thus deform together. However, the single constituents may exhibit different stress-free configurations [4]. In the theory of nonlinear continuum mechanics this concept can be modeled as follows. As the constituents deform together, they all exhibit

the same deformation gradient \mathbf{F} . However, for the different constituents it is in general multiplicatively decomposed into different elastic parts \mathbf{F}_e^i and inelastic parts \mathbf{F}_{gr}^i :

$$\mathbf{F} = \mathbf{F}_e^i \mathbf{F}_{gr}^i. \quad (14)$$

The inelastic part changes only by growth and remodeling of the respective constituent. For each constituent, \mathbf{F} and \mathbf{F}_{gr}^i define its respective state of elastic deformation and thus its strain energy $\Psi^i(\mathbf{F}_e^i)$. The total strain energy of the constrained mixture is assumed to be the sum of the contributions of the individual constituents:

$$\Psi = \sum_{i \in I} \Psi^i = \sum_{i \in I} \rho_0^i W^i. \quad (15)$$

Here Ψ^i denotes a strain energy per unit (referential) volume of the i -th constituent, W^i its strain energy per unit mass, and ρ_0^i its (referential) mass density. The mechanical stress in the continuum can be defined by the 1st Piola Kirchhoff stress

$$\mathbf{P} = \frac{\partial \Psi}{\partial \mathbf{F}}, \quad (16)$$

where the partial derivative with respect to \mathbf{F} should be understood in a way that all \mathbf{F}_{gr}^i are kept constant so that only the \mathbf{F}_e^i and thus also \mathbf{F} may vary. Growth and remodeling in vascular tissue occurs on very long time scales so that inertia can be neglected. As typically also body forces such as gravitation are negligible in vascular tissue compared to the mechanical loading from blood pressure, the balance of linear momentum reduces to

$$\operatorname{div} \mathbf{P}(\mathbf{F}) = \mathbf{0}. \quad (17)$$

Solving this equation renders at each point in time and space the a priori unknown deformation. This is possible with standard methods such as a finite element discretization of the blood vessel geometry as long as the inelastic parts \mathbf{F}_{gr}^i of the deformation gradient are known. These can be computed by the mathematical model of growth and remodeling as pointed out below in Sect. 3.3.

3.2 Constitutive Equations

Following the lines of [50] and subsequently in the context of growth and remodeling, for example [30, 31, 38], we assume herein that vascular tissue can be modeled as a constrained mixture of elastin and a number of collagen and smooth muscle fiber families.

For elastin, we use a superscript $i = el$ and assume a Neo-Hookean strain energy per unit mass

$$W^{el} = \frac{\mu}{2} [\operatorname{tr}(\mathbf{F}_e^{elT} \mathbf{F}_e^{el}) - 3], \quad (18)$$

with the trace operator $\operatorname{tr}(\cdot)$ and a material parameter μ .

Smooth muscle and collagen are modeled as uniaxial fiber families aligned in the reference direction with some unit vector \mathbf{a}_0^i . Unlike in [30, 31, 38], for simplicity we do not distinguish herein between collagen and smooth muscle and rather assume that the fiber

families in our model describe a mixture of both together. Their elasticity is governed by a Fung exponential function, which for the i -th constituent takes on the form

$$W^i = \frac{k_1}{2k_2} \left(\exp \left[k_2 (\mathbf{C}_e^i : (\mathbf{a}_{gr}^i \otimes \mathbf{a}_{gr}^i) - 1)^2 \right] - 1 \right). \quad (19)$$

Here \otimes denotes a dyadic tensor product, the colon a double contraction product, $\mathbf{C}_e^i = \mathbf{F}_e^{iT} \mathbf{F}_e^i$ is the elastic right Cauchy-Green tensor, and $\mathbf{a}_{gr}^i = \mathbf{F}_{gr}^i \mathbf{a}_0^i / \|\mathbf{F}_{gr}^i \mathbf{a}_0^i\|$. Note that herein we assume that the two material parameters k_1 and k_2 of the Fung exponential function are identical for all the fiber families in our model.

Vascular tissue can often be modeled as an incompressible material. Specifically when blood vessels are modeled as membranes as we are doing it herein, this constitutive assumption can easily be implemented by requiring that the out-of-plane component of \mathbf{F} always equals the inverse of the product of the two principle stretches in in-plane direction. Doing so, the related elasticity problem can be solved by a discretization with two-dimensional membrane finite elements whose thickness parameter is simply always adjusted such that it preserves the tissue volume under elastic deformation, see also [30, 31, 38].

Remark 1 Note that herein we neglect for simplicity active smooth muscle tension because we primarily aim at aortic aneurysms. Unlike cerebral vessels, the aorta is an elastic rather than a muscular artery so that smooth muscle tension can be assumed to play only a minor role there compared to passive elasticity.

3.3 Growth and Remodeling

Living tissues are subject to a continuous mass turnover during which extant collagen and smooth muscle tissue is degraded and new such tissue is deposited. In mathematical models of growth and remodeling, it is often assumed that deposition and degradation balance in case the tissue is in a so-called homeostatic state. The exact definition of the homeostatic state remains controversial. For simplicity most mathematical models define it as a preferred (homeostatic) stress or strain of the collagen and smooth muscle tissue. Herein, we follow this approach and assume that no growth and remodeling takes place if the absolute value of the Cauchy stress σ^i in collagen and smooth muscle fibers equals a preferred value σ_h . Deviations from this preferred stress value are assumed to have two consequences.

First, they result in a net mass production, which is assumed to be governed for each constituent subject to growth and remodeling by the evolution equation

$$\dot{\rho}_0^i(t) = \rho_0^i(t) \frac{\bar{k}_\sigma}{T} \frac{\sigma^i - \sigma_h}{\sigma_h}, \quad (20)$$

where \bar{k}_σ is a dimensionless gain parameter for mass deposition and T represents the average life time of fibers during the continuous turnover process of deposition and degradation in the tissue. It is worth mentioning that the turnover time T corresponds to a half-life time of $\ln(2)T$. This simple evolution equation assumes that the production of collagen and smooth muscle is directly proportional to the amount of extant tissue, which appears reasonable, because production and degradation are mainly driven by cells, whose number can be assumed to scale in living tissues under typical conditions roughly linearly with the amount of tissue. Moreover, (20) assumes that the net mass production scales linearly with the deviation of the current stress from the homeostatic value, which can always be considered a straightforward first order approximation of reality, following directly from

the rational of Taylor expansion around a homeostatic state with zero net mass production. In a nonlinear continuum mechanical membrane model of incompressible vascular tissue as assumed herein, net mass production and degradation can directly be included via an inelastic net change of the membrane thickness by a factor

$$\lambda_g(t) = \frac{\sum_{i \in I} \rho_0^i(t)}{\sum_{i \in I} \rho_0^i(t=0)}, \quad (21)$$

where the denominator is equal to the constant current mass density $\rho = \sum_{i \in I} \rho_0^i(t=0)$. For reasons discussed in [38], in membrane models of vascular growth and remodeling $\lambda_g(t)$ is typically assumed to govern the inelastic deformation due to changes of mass of all constituents alike.

The second result of a deviation between the current and the homeostatic stress in collagen and smooth muscle tissue is remodeling. Remodeling can be understood as a reorganization of the tissue microstructure, which results in an inelastic deformation of the tissue on the macroscale, in many respects similar (though not exactly identical [51]) to a viscoelastic deformation. As discussed in [38], for uniaxial fiber families as used herein to model collagen and smooth muscle this inelastic deformation can be captured by an inelastic part λ_r^i of the total fiber stretch λ^i along the fiber axis, and the evolution equation for this inelastic fiber stretch can be shown to be

$$\dot{\lambda}_r^i = \left[\frac{\dot{\rho}_0^i(t)}{\rho_0^i} + \frac{1}{T} \right] \frac{\lambda_r^i}{\lambda_e^i} \left[\frac{\partial \Psi^i}{\partial \lambda_e^i} + \lambda_e^i \frac{\partial^2 \Psi^i}{(\partial \lambda_e^i)^2} \right]^{-1} (\sigma^i - \sigma_h). \quad (22)$$

In (22) it is assumed that fibers are aligned in the in-plane direction of the membrane representing the vessel wall and that growth, that is, the above λ_g results in a nonlinear deformation only in the referential out-of-plane direction \mathbf{a}_0^\perp so that the in-plane fiber stretch $\lambda^i = \lambda_e^i \lambda_r^i$ can always be multiplicatively decomposed into an inelastic remodeling part λ_r^i and an elastic part λ_e^i . With these assumptions (20), (21) and (22) together define the temporal evolution of the inelastic part of the deformation gradient, which itself can be computed at each point in time from

$$\mathbf{F}_{gr}^i = \frac{\lambda_g}{\sqrt{\lambda_r^i}} \mathbf{a}_0^\perp \otimes \mathbf{a}_0^\perp + \lambda_r^i \mathbf{a}_0^i \otimes \mathbf{a}_0^i + \frac{1}{\sqrt{\lambda_r^i}} (\mathbf{I} - \mathbf{a}_0^i \otimes \mathbf{a}_0^i - \mathbf{a}_0^\perp \otimes \mathbf{a}_0^\perp). \quad (23)$$

The first term on the right-hand side captures the thickening in out-of-plane direction by net mass deposition and the potential simultaneous transverse contraction that may result in case of an inelastic fiber remodeling stretch due to the assumption of incompressibility. The second term captures the inelastic fiber remodeling stretch, and the third term the resulting in-plane transverse contraction.

The algebraic and differential equations (12) through (23) form a closed system that defines at each point in time and space the deformation of vascular tissue due to growth and remodeling if the material parameters and the parameters characterizing the vascular geometry are known. Both types of parameters form the set of input parameters to our model of growth and remodeling. It is the objective of this paper to analyze the sensitivity of the output of our model to variations of these input parameters. Details of this sensitivity analysis are discussed in the subsequent section.

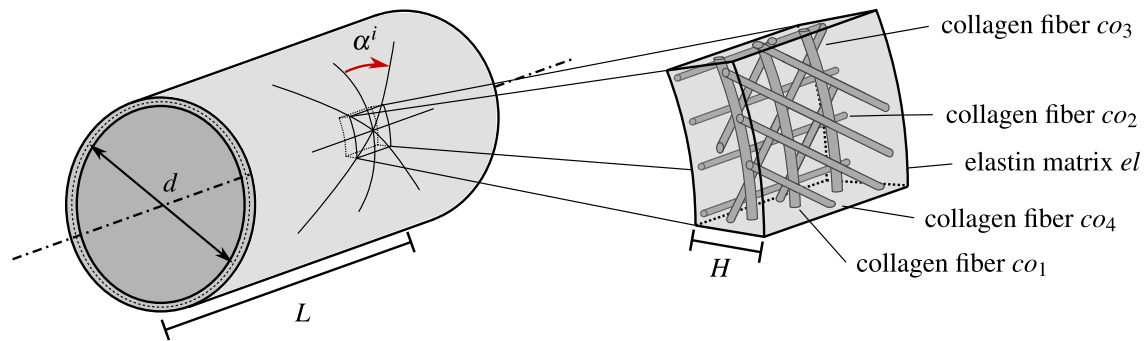


Fig. 2 Illustration of idealized thin-walled cylindrical model aorta of length L , diameter d and wall thickness H . The inlay depicts the constituents of the constrained mixture forming the wall and consisting of four collagen fiber families $co_1 - co_4$ embedded in an elastin matrix el . The fiber directions are uniquely defined with respect to the circumferential direction by the angle α^i . (image created by Sebastian L. Fuchs and licensed under the Creative Commons Attribution 4.0 International License, <https://creativecommons.org/licenses/by/4.0/>)

4 Global Sensitivity Analysis of Arterial Growth and Remodeling

In this section, we discuss how the global sensitivity analysis framework from Sect. 2 can be applied to the homogenized constrained mixture model of growth and remodeling from Sect. 3. Thereby we focus on a generic, idealized model of the abdominal aorta described in the following subsection.

4.1 Idealized Model of Abdominal Aorta

Geometry: we study an idealized abdominal aorta represented by a thin-walled cylinder of diameter $d = 2$ cm, length $L = 18$ cm and wall thickness H . Dirichlet boundary conditions are imposed at both ends of the cylinder mimicking the support of the aorta by surrounding tissue and branching vessels such as the renal arteries. Our model aorta is subject to an internal mean blood pressure $p = 100$ mmHg. The vessel wall is modeled as a constrained mixture of $m = 5$ constituents, which are an elastin matrix and four fiber families modeling the collagen and smooth muscle fibers. Hence, our index set to distinguish between the different constituents is $I = \{el, co_1, co_2, co_3, co_4\}$, where index el refers to elastin and the other four indices to the four collagen and smooth muscle fiber families. The referential unit direction vector \mathbf{a}_0^i of these fiber families can be uniquely defined by the angle α^i between them and the circumferential direction of the cylinder. We assume that one fiber family is oriented in circumferential and axial direction, respectively. Moreover, we assume that there exist two diagonal fiber families forming an angle of $\pm 45^\circ$ with the circumferential direction. This setting is illustrated in Fig. 2. Note that by variations of the mass densities assigned to the different fiber families one can resemble at least in the sense of a good approximation the effect of a great variety of different fiber orientation distributions, which endows our study with a sufficient generality.

Constituent mass in constrained mixture: the mass of the different constituents in the constrained mixture at any point in time is defined by their referential mass density $\rho_0^i(t)$. In our discussion below, it is convenient to express it in a normalized form in terms of a mass fraction

$$\varphi^i(t) = \frac{\rho_0^i(t)}{\sum_{i \in I} \rho_0^i(t)}. \quad (24)$$

The mass fractions of the different constituents satisfy a partition of unity property. For simplicity, we assume herein that both the mass fractions of the circumferential and axial fiber families and the mass fractions of the two diagonal fiber families are equal, respectively. The partition of the total fiber content between these two sets of fiber families remains, however, a free parameter. Overall, this reduces the number of free input parameters in the model and thus the computational cost of a global sensitivity analysis without compromising too much the generality. We formalize the above assumptions by first introducing the initial mass fraction of elastin $\varphi_{t_0}^{el} = \varphi^{el}(t = 0)$. In the following, the index t_0 shall always refer to (initial) quantities at $t = 0$. Next, the initial mass fraction of all four fiber families together is $\varphi_{t_0}^{co} = 1 - \varphi_{t_0}^{el}$. Finally, we introduce the initial fraction of total fiber content attributed to one diagonal fiber family $\beta_{t_0} \in [0, 0.5]$. In the extreme case of $\beta_{t_0} = 0.5$ all fiber mass is initially oriented in diagonal direction. For soft tissue one often assumes as a reasonable approximation a constant spatial mass density $\rho = 1050 \text{ kg/m}^3$ of the tissue as a whole. Under this assumption, the initial referential mass density of elastin is $\varphi_{t_0}^{el} \rho$, the one of the diagonal fiber families take on the value $\beta_{t_0} (1 - \varphi_{t_0}^{el}) \rho$ and the ones of the circumferential and axial fiber families the value $(1 - \beta_{t_0}) (1 - \varphi_{t_0}^{el}) \rho$. In other words, with respect to referential mass densities our model has two independent input parameters, which are $\varphi_{t_0}^{el}$ and β_{t_0} .

Initial configuration: we assume that our model aorta is in a homeostatic configuration at $t < 0$, that is, no growth and remodeling of the fiber families takes place until $t = 0$ because the Cauchy stress of all fibers equals the homeostatic value. In our simulations, we establish such an initial configuration as follows. First, the homeostatic stress σ_h of the fiber families is prescribed as an independent input parameter. Second, the balance of linear momentum in the circumferential direction is used to eliminate the model parameter H , which is uniquely determined by this balance equation and the other input parameters of our model.

Elastin degradation and prestretch: during adulthood, no deposition of load-bearing elastin takes place [47]. Rather it is degraded with half-life time of a few decades. Therefore, (20) does not apply to elastin, but the elastin referential mass density is rather assumed to be governed by an evolution equation of the type

$$\rho_0^{el}(t) = [1 - D(t)] \rho_0^{el}(0), \quad (25)$$

where $D(t)$ describes a time-dependent damage parameter between zero and one that can be used to model damage and loss of elastin and that is specified in more detail below. As elastin is not subject to growth and remodeling according to (20), its elastic prestretch in the initial (homeostatic) configuration at time $t = 0$ is not defined by σ_h so that we have to define it independently. While there is some evidence that axial and circumferential prestretches of elastin are different in general [18, 52], their values are typically found to be very similar in healthy blood vessels (see also [30, 53]). In this study, we thus assume both of them to be defined by some (in principle independent) model input parameter λ_{pre} .

The above paragraphs define an initial configuration resembling a healthy blood vessel. We will use this configuration as a starting point for two case studies of arterial growth and remodeling.

Case 1: Hypertension. In this example, we study the growth and remodeling response of our idealized aorta to hypertension, that is, a persistent increase of mean blood pressure p inside the vessel. For this purpose, we track the radial expansion of the model aorta over a

period of 15 years. As already in previous work [12, 13], we assume hypertension to arise in the following way: during the first year, the mean blood pressure increases linearly from the reference value p to an elevated level of $\hat{p} = 120$ mmHg. The pressure remains at this elevated level for the rest of the simulated time. For simplicity, we do not consider any damage to the elastin matrix in the context of hypertension, i.e., $D(t) = 0$.

Case 2: Idealized fusiform abdominal aortic aneurysm (AAA). Spontaneous damage to the elastin matrix has previously been hypothesized to trigger the development of aneurysms [13, 26, 30, 38, 53]. We adhere to this approach and apply the following damage to the elastin matrix of the model aorta:

$$D(t) = H(t) \exp \left[-0.5 \left(\frac{X_3}{L_{dam}} \right)^2 \right]. \quad (26)$$

We use a coordinate system whose center coincides with the center of the cylinder representing our aorta and whose X_3 -axis is aligned with its rotational symmetry axis. The term on the right-hand side describes an abrupt, spatially distributed damage to the elastin matrix with spread parameter L_{dam} . $H(t)$ denotes the Heaviside function. Typically AAAs are accompanied with significant reduction in the elastin content of the tissue over time often until complete depletion [54–57]. Here, we model this degradation process with a simplified approach by instantly removing the complete elastin content at the center. The geometrical shape of the elastin damage has a large influence on the evolving aneurysm shape [17, 19, 25]. However, we limit our analysis to L_{dam} and fix the shape as defined by (26) in order to keep the number of overall parameters for the global sensitivity analysis feasible. Again, we track in our simulations the radial expansion over a period of 15 years. The mean blood pressure inside the vessel remains constant at the initial value p .

4.2 Sensitivity Analysis Setup

4.2.1 Output

Naturally, the growth and remodeling response of the two cases specified in the previous section depends on the choice of model parameters. It is our main goal to quantify the sensitivity of the model output to the model input parameters for both cases. Sobol's method for global sensitivity analysis as introduced in Sect. 2 is defined for models with scalar outputs only. By contrast, the solution of the homogenized constrained mixture model of Sect. 3 results in a vectorial displacement field. To resolve this mismatch, we define herein as our model output the maximum current diameter d_{max} of our aorta over time. We define

$$d_{max}(t) = \begin{cases} d(t), & \text{if } d(t) < 8 \text{ cm} \\ 8 \text{ cm}, & \text{else} \end{cases}. \quad (27)$$

Here the limit value of $d_{max} = 8$ cm is assumed to represent the diameter where the aneurysm ruptures. This choice is motivated by statistical data showing that unruptured AAAs with a diameter larger than 8 cm are extremely rare [58]. Mapping all diameters greater or equal to 8 cm to the same diameter value of 8 cm is thus reasonable because all aneurysms with such a large diameter indeed represent the same model outcome, that is, a ruptured aneurysm. Of course, the rupture criterion applied here is very simplistic. However, it appears sufficient for the purpose of this paper which does not aim at quantifying the exact moment of rupture for a specific aneurysm but rather the impact of the different model parameters on growth and remodeling in arteries in general.

Table 1 Parameters with fixed values for the model cases of Sect. 4.1

Parameter		Value
initial diameter	d	2 cm
length	L	18 cm
mean blood pressure	p	100 mmHg
current mass density	ρ	$1050 \frac{\text{kg}}{\text{m}^3}$
collagen fiber angles	α^i	$0^\circ, 90^\circ, \pm 45^\circ$
<i>hypertension:</i>		
mean high blood pressure	\hat{p}	120 mmHg

4.2.2 Known Input Parameters

In our sensitivity analysis, we do not include all the model parameters because some can be assumed to be known in clinical practice and others can be assumed a priori to play such a minor role that they need not be included in our study. Indeed, d and L can be measured in clinical practice by medical imaging, and p and \hat{p} by standard blood pressure measurements. On the other hand, the mass density ρ obviously has nearly no impact as we model arteries as thin membranes and define their strain energy per unit fiber mass. Finally, also our choice of α^i does not significantly determine the model as long as the mass fractions of the different fiber families are allowed to vary freely. Therefore, we fix all these parameters according to Table 1 and do not include them in our sensitivity analysis.

4.2.3 Unknown Input Parameters

Fixing some parameters according to Table 1, there remain nine parameters in *case 1* (*hypertension*) and 10 parameters in *case 2* (*idealized AAA*). These are in both cases the homeostatic Cauchy fiber stress σ_h , the turnover time T , the gain parameter \bar{k}_σ , the stiffness parameters μ , k_1 and k_2 , the initial mass fraction of elastin $\varphi_{t_0}^{el}$, the initial fraction of the fiber mass attributed to the diagonal fiber families β_{t_0} and the prestretch of elastin λ_{pre} (equal in axial and circumferential direction). In *case 2* (*idealized AAA*), we additionally study the spatial damage spread L_{dam} .

Remark 2 Due to the assumption of an initial homeostatic configuration (see Sect. 4.1) and the definition of stress (16), the choice of the collagen material parameters k_1 , k_2 and the homeostatic Cauchy fiber stress σ_h as independent input parameters implies that the deposition stretch of collagen becomes a dependent parameter that is varied implicitly with these three parameters.

These parameters can typically not be measured in clinical practice at the moment and yet it cannot be excluded that they have a considerable impact on the model output. However, while patient-specific measurements of these parameters in vivo are not possible, we have information from various experimental and clinical studies, for example, from mechanical testing of tissue samples ex vivo. Therefore, we can at least define a reasonable range for the above parameters within which they can be assumed to vary. In the following, we will do so for all the above parameters and assume for simplicity (and typically lacking more specific information) a uniform distribution of the parameters within the defined bounds in our sensitivity analysis. The derived distributions are summarized in Table 2.

Table 2 Probability distributions of uncertain (free) input parameters as derived in Sect. 4.2.3. All parameters are assumed to be distributed uniformly within the given bounds. The last column collects the literature references on which our estimates rely

Parameter		Distribution	Unit	References
<i>elastin:</i>				
constitutive parameter	μ	$U(40, 80)$	$\frac{\text{J}}{\text{kg}}$	[18, 53, 68, 73, 75, 77]
initial volume fraction	φ_{i0}^{el}	$U(0.2, 0.3)$	-	[53, 59, 60]
prestretch	λ_{pre}	$U(1.2, 1.4)$	-	[18, 53, 65–68]
spatial spread of damage (case 2)	L_{dam}	$U(0.5, 2)$	cm	
<i>collagen:</i>				
constitutive parameter	k_1	$U(450, 600)$	$\frac{\text{J}}{\text{kg}}$	[30, 53, 68]
constitutive parameter	k_2	$U(7, 30)$	-	[30, 53, 68]
initial fraction diagonal fibers	β_{i0}	$U(0.0, 0.5)$	-	
homeostatic stress	σ_h	$U(125, 250)$	kPa	[47, 92, 93]
turnover time	T	$U(25, 140)$	d	[86–89]
gain parameter (case 1)	\bar{k}_σ	$U(0.12, 0.42)$	-	[12]
gain parameter (case 2)	\bar{k}_σ	$U(0.05, 0.150)$	-	[12]

Elasticity and mass fraction of elastin: The elastin content in healthy aortic tissue has been investigated in several studies [53, 59, 60]. In these studies, consistent values between 0.227 ± 0.057 [59] and 0.224 ± 0.031 [60] have been reported. Based on these findings, we set the bounds for the initial mass fraction of elastin φ_{i0}^{el} to $[0.2, 0.3]$. Elastin is predominantly deposited during early life [61] and has a very long mean life time of approximately 101 y, cf. Table 1, [62]. During normal biological growth, elastin therefore undergoes significant mechanical deformation which has been hypothesized to result in a considerable level of prestretch in the healthy aorta [63, 64]. Mean values reported in the literature are between 1.18 and 1.37 [18, 53, 65–68]. We follow these studies and assume that the prestretch of elastin λ_{pre} varies in the range $[1.2, 1.4]$. Physiological ranges of mechanical wall properties of arterial tissue in health and disease have been studied extensively in the literature [57, 69–76]. However, the quantitative comparison of material parameters derived from different experimental studies is a challenging task. One reason for this is the fact that often the experimental data is fitted to different constitutive models. A general method to solve this problem is beyond the scope of this paper. As a simplistic solution, we tried to relate at least reported values for closely related constitutive models in a reasonable way to each other. For example, we made the parameter values from homogeneous models of the arterial wall comparable to the values reported for constrained mixture models by correcting them by a factor accounting for the mass fractions of the different constituents that can typically be assumed (see also [77]). Pooling in such a way the data reported in [18, 53, 68, 73, 75, 77] - under the assumption of ρ as in Table 1 and $\varphi^{el} = 0.25$ - we were able to define for the material parameter μ of elastin a range 40–80 $\frac{\text{J}}{\text{kg}}$. For the spatial spread parameter L_{dam} , we choose 0.5–2 cm to mimic both localized as well as considerably spread elastin damages.

Elasticity and mass fraction of collagen: A quantitative comparison of the material parameters k_1 and k_2 for collagen from different sources is even more challenging than for the parameter μ of elastin. For modeling the constitutive behavior of collagen generally includes also several other structural parameters [78] whose choice may then also affect the values of k_1 and k_2 reported. These other parameters are, for example, the number of fiber families

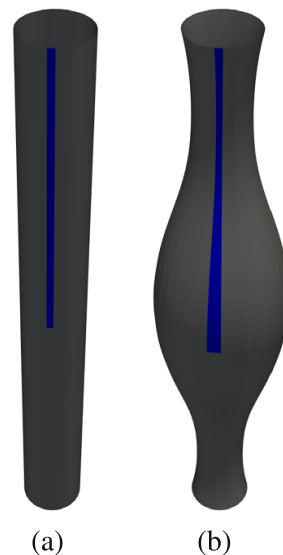


Fig. 3 Exemplary simulation result for one sample of *case 2 (idealized AAA)*. **(a)** shows the reference configuration and **(b)** the deformed configuration with $d_{max} = 4$ cm after 15 years. The aneurysmatic dilatation of the vessel is clearly visible. The reduced computational domain, exploiting the symmetries of the problem, is depicted in blue

and their orientation or the fiber dispersion. Naturally, structural parameters and material parameters co-depend nonlinearly rendering approximate conversions, as suggested for the elastin case above, almost impossible [76]. Therefore, we had to limit our focus on a choice of papers using very similar constitutive models [30, 53, 68]. From these, we derive the parameter range 450–600 $\frac{\text{J}}{\text{kg}}$ for k_1 and 7–30 for k_2 . Research concerning the structural parameters of collagen in arterial tissue, like fiber orientation and dispersion, is a vibrant field [57, 71, 79–85]. In particular is known that fiber orientation and dispersion may vary considerably in health and disease. To ensure a sufficient scope of our analysis, we thus allowed the initial fraction of collagen and smooth muscle fibers in the diagonal direction to vary in the theoretically maximal range, that is, $\beta_{t_0} \in [0-0.5]$.

Growth and remodeling: the half-life time of collagen is in the range of 60–70 d for healthy aortic tissue [86, 87]. It can however change drastically due to a change of mechanical loading or during disease [86, 88, 89]. Therefore, we consider in our study an extended range of 25–140 d for the turnover time T . Note, that there is a linear dependence between half-life and turnover time by a factor of $\ln 2$. The exact nature of the homeostatic state of soft tissue remains controversial to date [47, 89–91]. Thus only little information is available about a reasonable range for σ_h . The studies of [92] and [93] suggest for the homeostatic stress of arterial tissue a range of 150–300 kPa. [47] derived a homeostatic stress range of around 200–300 kPa from theoretical considerations. Motivated by these studies we assume herein for the collagen and smooth muscle fibers alone a range $\sigma_h \in [125-250 \text{ kPa}]$.

Experimental data on the gain parameter \bar{k}_σ is very limited. Based on the concept of mechanobiological stability, [11, 12] estimated typical values in health and disease. Following these considerations, we assume herein for *case 1 (hypertension)* $\bar{k}_\sigma \in [0.12-0.42]$ and for *case 2 (idealized AAA)* $\bar{k}_\sigma \in [0.05-0.15]$.

4.3 Implementation and Discretization

The homogenized constrained mixture model for thin-walled (membranous) anisotropic volumetric growth described in Sect. 3 was implemented in our in-house research code BACI

(written in C++) [94]. An explicit time integration scheme is used to solve the evolution equations at each time step (see, for example, Appendix 3 of [13]).

We note that the two cases introduced in Sect. 4.1 exhibit both a reflection symmetry with respect to the cross-sectional plane in the center of the vessel and a rotational symmetry around the cylinder axis. To reduce the computational cost, we exploited these symmetries. That is, we simulated only half of the cylinder in axial direction and only a wedge with an opening angle of 11.25° in circumferential direction. The application of suitable Dirichlet boundary conditions enforcing the respective symmetries enables this reduction. Figure 3 illustrates the reduced computational domain in comparison with the full domain for one exemplary simulation of *case 2 (idealized AAA)*. We discretized the computational domain with 50 standard quadrilateral nonlinear membrane finite elements in axial direction and one in circumferential direction. Within each finite element, the direction vectors of the fiber families were assumed to be constant. In all simulations, we used a timestep size of 10 d.

The implementation of the algorithm to compute the Sobol indices according to Sect. 2.1 has been adapted from the open-source project SALib [95]. The adapted code was included in the QUEENS code project (written in Python). QUEENS is a general purpose framework for large scale uncertainty quantification and simulation analytics of complex computational models [96]. For each sensitivity analysis, we use $N = 6000$ Monte Carlo samples which results in a total of 66000 model evaluations for *case 1 (hypertension)* and 72000 for *case 2 (idealized AAA)*. These can be split into 12000 independent – drawn from the distributions defined in Table 2 – plus 54000 or 60000 cross-sampled samples, respectively (cf., Appendix).

5 Results

5.1 Probability Distributions of Model Output

Figure 4 shows the probability density functions (PDFs) of the maximum current diameter d_{max} for both *case 1 (hypertension)* and *case 2 (idealized AAA)* for three points in time illustrating their evolution in time. The densities are approximated by kernel density estimation (KDE) with Epanechnikov kernels based on the 12000 independent samples of each case study.

In *case 1 (hypertension)*, the increase in mean blood pressure of 20 mmHg generally leads to minor dilatation of the vessel that largely stabilizes after around 10 years. By contrast, the elastin damage in *case 2 (idealized AAA)* typically entails a substantial dilatation, which surpasses the dilatation threshold of 3 cm - the clinical criterion for an aneurysm - in more than 18% of cases. A considerable number of simulated aneurysms does not stabilize even after a decade but rather keeps enlarging, which in reality typically results in rupture at some point, if not treated clinically. In total 3.83% of the 72000 simulations performed for *case 2 (idealized AAA)* numerically failed within the simulated 15 years. A detailed analysis revealed that this phenomenon was exclusively linked to buckling close to the clamped ends of the cylinder. In accordance with the remarks in Sect. 4.1, the missing results of the numerically failed simulations were mapped to $d_{max} = 8$ cm because in these simulations we also observed an excessive volume of the aneurysm, which is in practice typically associated with excessive stresses and thus rupture.

5.2 Sensitivity Analysis

In this section, we present the evolution of the first order and total sensitivity indices of the maximum current diameter d_{max} for each free input parameter over a period of 15 years.

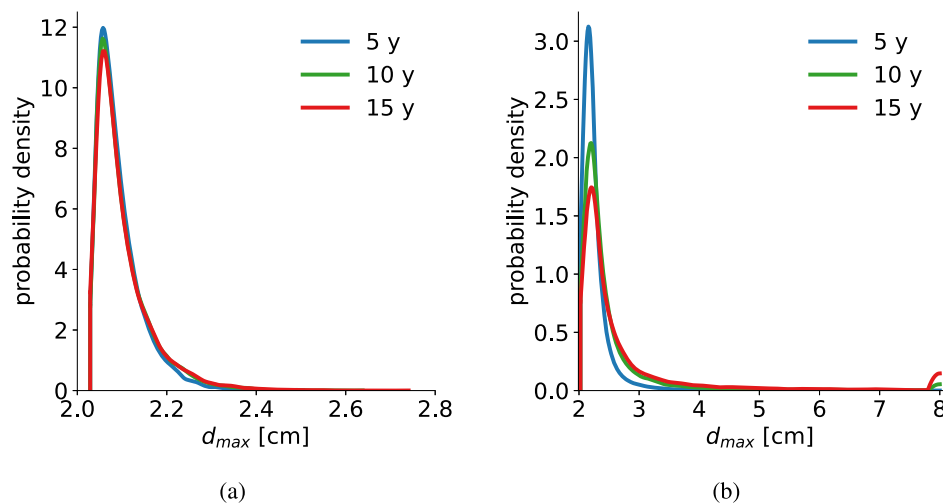


Fig. 4 Probability density of the maximum diameter d_{max} for different points in time in (a) case 1 (hypertension) and (b) case 2 (idealized AAA)

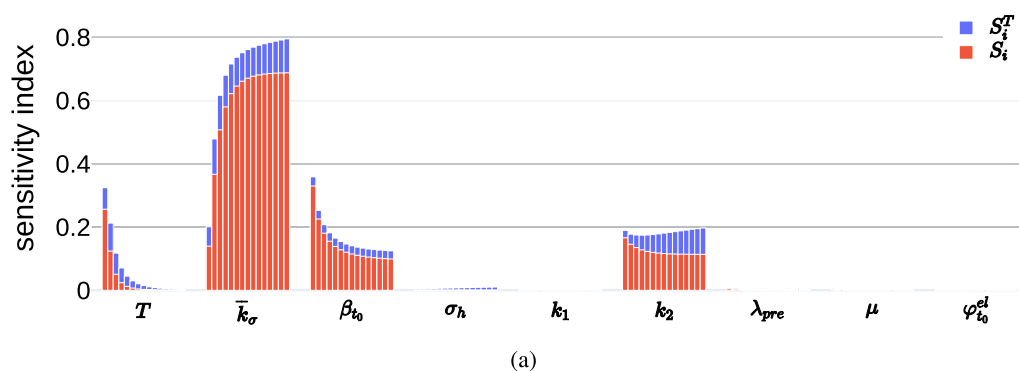


Fig. 5 Evolution of first order and total Sobol indices for the maximum current diameter d_{max} over a period of 15 years for case 1 (hypertension). For each parameter 15 bars are shown: from left to right, each bar corresponds to an annual pair of first order (orange) and total (blue) indices, such that the left-most bar represents the indices after one year and the right-most the ones after 15 years

Case 1 (hypertension): Fig. 5 shows the evolution of the Sobol indices for the nine free input parameters. Values of the indices for selected years are collectively shown in Table 3. Only four parameters have noticeable total indices. These are the turnover time of collagen T , the gain parameter \bar{k}_σ , the initial fraction of total fiber content attributed to each diagonal fiber family β_{t_0} and the collagen material parameter k_2 . These four parameters can be further separated where k_2 , β_{t_0} , and \bar{k}_σ sustain considerably larger, long-term total indices compared to T . The total indices of the remaining five parameters are all below 0.01 and many are practically zero. Therefore, their influence on the variability of d_{max} appears to be negligible compared to the other four parameters. As explained in Sect. 2.1, these five parameters are prime candidates for parameter fixation.

The four indices of considerable magnitude change drastically over time. The turnover time of collagen T influences d_{max} only during the first years. Its total index quickly decreases from 0.325 to 0.045 within the first five years. After 10 years, T has become negligible. With a total index of 0.359, β_{t_0} is the most influential parameter after the first year. However, its total index decreases almost exponentially and seems to stabilize at approximately 0.125 after 15 years. With this value β_{t_0} remains the third most influential parameter. The difference between first order and total indices of β_{t_0} is very small and increases only

Table 3 First order and total Sobol indices in *case 1 (hypertension)* for selected years. The last row shows the sum of first order indices $\sum_{i=1}^n S_i$, a measure for the linearity of the model (cf., Sect. 2.1). The amount of interactions of parameter i is given by $S_i^T - S_i$. In each total index column, the four highest values are highlighted in bold letters

Parameter	1 year		5 year		10 year		15 year	
	S_i	S_i^T	S_i	S_i^T	S_i	S_i^T	S_i	S_i^T
μ	0.003	0.006	0.001	0.002	0.001	0.002	0.001	0.001
$\varphi_{t_0}^{el}$	0.003	0.004	0.001	0.001	0.001	0.001	0.001	0.001
λ_{pre}	0.005	0.008	0.003	0.006	0.002	0.006	0.002	0.006
k_1	0.000	0.002	0.000	0.002	0.000	0.002	0.000	0.002
k_2	0.166	0.189	0.123	0.175	0.115	0.186	0.114	0.197
β_{t_0}	0.330	0.359	0.139	0.165	0.108	0.133	0.099	0.125
σ_h	0.000	0.004	0.001	0.006	0.001	0.009	0.001	0.010
T	0.256	0.325	0.013	0.045	0.001	0.009	0.001	0.003
\bar{k}_σ	0.140	0.201	0.622	0.716	0.681	0.775	0.688	0.795
sum:	0.904		0.902		0.910		0.906	

minimally to a maximum of 0.026 at 15 years indicating that interactions of β_{t_0} with other parameters are minor. The second most influential parameter is the material parameter k_2 . For k_2 the total index drops from 0.189 after the first years to a value of 0.175 before it rises to 0.197 after 15 years again. In the later years, the first order index of k_2 remains constant such that the influence of the interaction of k_2 with the other parameters increases over time. Figure 5 clearly shows that the gain parameter \bar{k}_σ is by far the most influential parameter except for the first year. From an initial value of 0.201, its total index rises to 0.716 within 5 years. It peaks at 0.795 after 15 years. The evolution of the total index of \bar{k}_σ over time suggests that it converges to a value close to this. With a value of 0.688 for the first order index of the gain parameter \bar{k}_σ at 15 years, an overwhelming amount of the total variance of d_{max} after 15 years can be explained by the uncertainty in \bar{k}_σ alone. From five through 15 years, the interaction terms of \bar{k}_σ account for 10% of the output variance which is approximately equal to the overall amount of interactions (compare to $1 - \sum_{i=1}^n S_i$). The majority of interactions occur between \bar{k}_σ and k_2 alone. Ultimately, this reveals, however, that \bar{k}_σ is the cornerstone of the relevant interactions between all parameters.

The sum of all first order indices is shown in the last row of Table 3. At all times, it is $\sum_{i=1}^n S_i > 0.902$, which is close to the theoretical limit of 1.0 indicating that the variability in the model output is dominated by linear terms while interaction between the parameters seem to play a minor role.

Case 2 (idealized fusiform abdominal aortic aneurysm): in the sensitivity analysis of the radial expansion of the idealized AAA, we investigated the influence of 10 parameters on the variability of the model output d_{max} . Table 4 summarizes the values of Sobol indices for four selected points in time, namely after one, five, 10, and 15 years. Figure 6 shows the evolution of the sensitivity indices in time over a period of 15 years evaluated annually. The collagen material parameter k_2 , turnover time T and gain parameter \bar{k}_σ all have considerably higher total indices compared to the rest of the parameters. While, some of the less-influential parameters have non-zero total indices of up to 0.149 (β_{t_0}) in the first year, their total indices decrease over time; in many cases until they are almost zero. Interestingly, most of the less

Table 4 First order and total Sobol indices in *case 2 (idealized AAA)* for selected years. The last row shows the sum of first order indices $\sum_{i=1}^n S_i$, a measure for the linearity of the model (cf., Sect. 2.1). The amount of interactions of parameter i is given by $S_i^T - S_i$. In each total index column, the four highest values are highlighted in bold letters

Parameter	1 year		5 year		10 year		15 year	
	S_i	S_i^T	S_i	S_i^T	S_i	S_i^T	S_i	S_i^T
μ	0.074	0.098	0.021	0.045	0.006	0.021	0.006	0.016
$\varphi_{t_0}^{el}$	0.047	0.062	0.012	0.027	0.003	0.013	0.004	0.010
λ_{pre}	0.052	0.068	0.016	0.033	0.008	0.019	0.008	0.016
k_1	0.000	0.001	0.000	0.005	0.000	0.005	0.000	0.005
k_2	0.087	0.137	0.087	0.339	0.088	0.375	0.103	0.334
β_{t_0}	0.115	0.149	0.035	0.069	0.009	0.031	0.006	0.024
σ_h	0.053	0.066	0.008	0.014	0.002	0.009	0.002	0.008
T	0.360	0.484	0.187	0.617	0.132	0.524	0.117	0.420
\bar{k}_σ	0.030	0.062	0.182	0.508	0.221	0.636	0.323	0.693
L_{dam}	0.036	0.058	0.021	0.062	0.010	0.034	0.011	0.029
<i>sum:</i>	0.853		0.568		0.479		0.579	

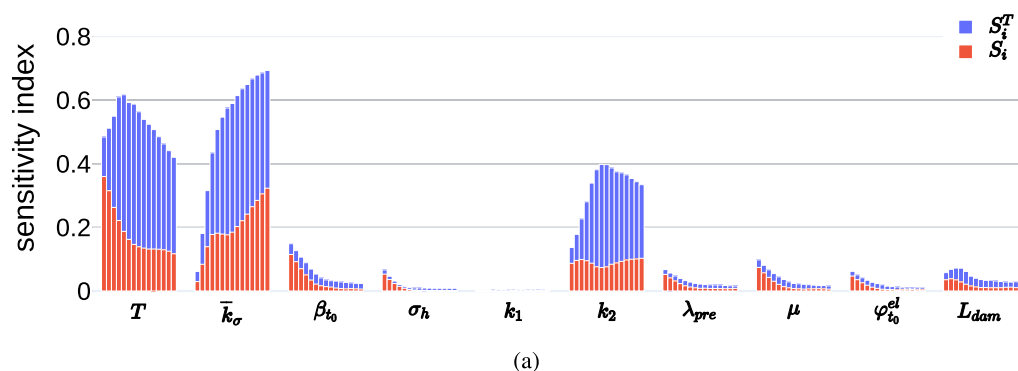


Fig. 6 Evolution of first order and total Sobol indices for the maximum current diameter d_{max} over a period of 15 years for *case 2 (idealized AAA)*. For each parameter 15 bars are shown: from left to right, each bar corresponds to an annual pair of first order (orange) and total (blue) indices, such that the left-most bar represents the indices after one year and the right-most the ones after 15 years

influential parameters are related to the elasticity of the tissue with the notable exception of k_2 . Generally, the sum of first order indices decreases from 0.853 to 0.579 after 15 years showing that the importance of interactions increases substantially over time.

In the first years, the variability of the model output is dominated by T as indicated by the comparably large total index of 0.484. The total index of T evolves markedly over time. Overall, it decreases slightly. A minimal value of 0.420 makes T the second most influential parameter at 15 years. By contrast, the first order index of T decreases from 0.360 to 0.117 indicating that T is increasingly involved in higher order interactions. The total index of the material parameter k_2 rises over time from 0.137 to a final value of 0.334 at 15 years. Within 2 years, k_2 becomes and stays the third most influential parameter. However, the first order index of k_2 remains almost constant between 0.074–0.102 indicating that a rise of higher order interactions is responsible for the increase of the total order index. The gain parameter \bar{k}_σ quickly becomes the most influential parameter. Initially, its total index is very small

(0.062) but it rapidly grows to a maximum value of 0.693 at 15 years. While its first order index follows this trend, the difference between the two increases considerably over time. With values between 0.415 at 10 years and 0.370 at 15 years, \bar{k}_σ has the highest amount of interactions in the last five year period. In fact, these values are close to the total interaction values indicating that \bar{k}_σ is involved in nearly all interactions.

Interestingly, interactions seem to occur almost exclusively between the three most influential parameters (k_2 , T and \bar{k}_σ). Generally, higher order interactions between parameters play a significant role in explaining output variability, in particular in later years, as indicated by the large total interaction value $1 - \sum_{i=1}^n S_i$ in this period.

5.3 Input-Output Relations

The results of the sensitivity analysis in Sect. 5.2 reveal that in particular in *case 2 (idealized AAA)* there remains a substantial fraction of output variability that can only be explained by interactions between the input parameters. Sensitivity analysis can identify *which* parameters influence the model output but it is beyond its scope to identify *how* the parameters influence the model output. In general, such an analysis is a very complex task in particular when studying the nature of nonlinear interactions between the parameters. In this section, we use the model evaluations carried out during the sensitivity analysis to partially answer this question. We do so by studying so-called parallel coordinate plots for *case 2 (idealized AAA)* as depicted in Fig. 7.

Remark 3 For an interactive experience of this section, the reader may refer to the electronic supplementary material. It provides an interactive version of the parallel coordinate plot discussed in this section in a standalone HTML file. The user can constrain arbitrary combinations of parameter and output ranges. Additionally the order of coordinates can be adjusted. The figure was created with the visualization software plotly [98]. Image created by Sebastian Brandstaeter and licensed under the Creative Commons Attribution 4.0 International License, <https://creativecommons.org/licenses/by/4.0/>.

In Fig. 7a, all 12000 independent samples evaluated are shown together with the corresponding model outputs: each line connects the respective parameter values with their output. The color additionally illustrates the value of the model output. The parameters are arranged by ascending total index after 15 years from left to right. The objective is to study whether specific parameter combinations can be identified as mainly responsible for certain output ranges. From the orange to dark red lines in Fig. 7a, we see that the unifying property of samples that lead to very large model outputs $d_{max} \geq 6$ cm is a combination of relatively small turnover time $T < 100$ d and most prominently small gain parameter $\bar{k}_\sigma < 0.1$. At the same time, very large values of $k_2 > 26$ inhibit extreme radial expansions. This is also highlighted by Fig. 7b which shows all samples that lead to aneurysmatic dilatations with $d_{max} \geq 3$ cm. Figure 7b shows for example that also large T can lead to aneurysms but only in combination with very small \bar{k}_σ and small k_2 . Albeit not shown here, the same is true for large values of k_2 which may lead to aneurysms but only in combination with very small T and \bar{k}_σ . Indeed, these three parameters have the highest total sensitivity indices with the largest fraction of interactions $S_i^T - S_i$ (see Table 4). The other parameters do not show a clear trend as indicated by the random arrangement of lines on the left side of Fig. 7a. Although less visible from Fig. 7a, it is truly the interaction between T and \bar{k}_σ that leads to elevated d_{max} . Choosing a small value for only one of these two parameters generally does not yet produce a large, aneurysmatic dilatation. Figure 7c illustrates this by restricting the

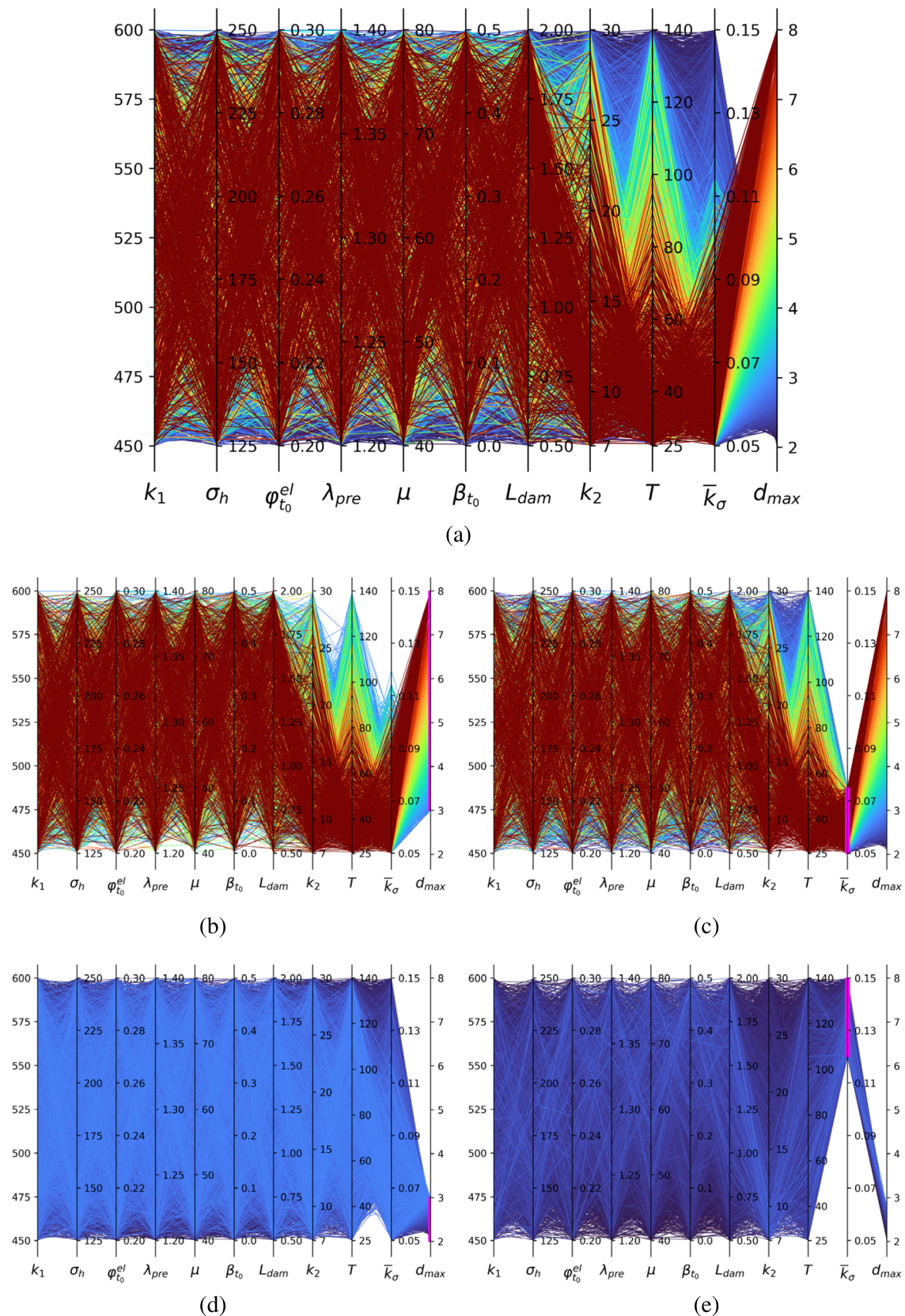


Fig. 7 Parallel coordinate plot of parameter samples and model output d_{max} after 15 years for case 2 (*idealized AAA*). Units for the parameters are as defined in Table 2. d_{max} is given in cm. The colorbar relates to d_{max} and applies to all figures. Coordinates are arranged according to increasing total index from left to right. (a) shows all 12000 independent samples. The smaller figures extract a subset of samples as indicated by the magenta colored areas; (b) shows all samples that lead to $d_{max} \geq 3$ cm, i.e., all samples that can be classified as aneurysms [97]; (c) shows only samples with $\bar{k}_\sigma \leq 0.075$; (d) depicts $d_{max} < 3$ cm; (e) limits the samples to $\bar{k}_\sigma \geq 0.12$

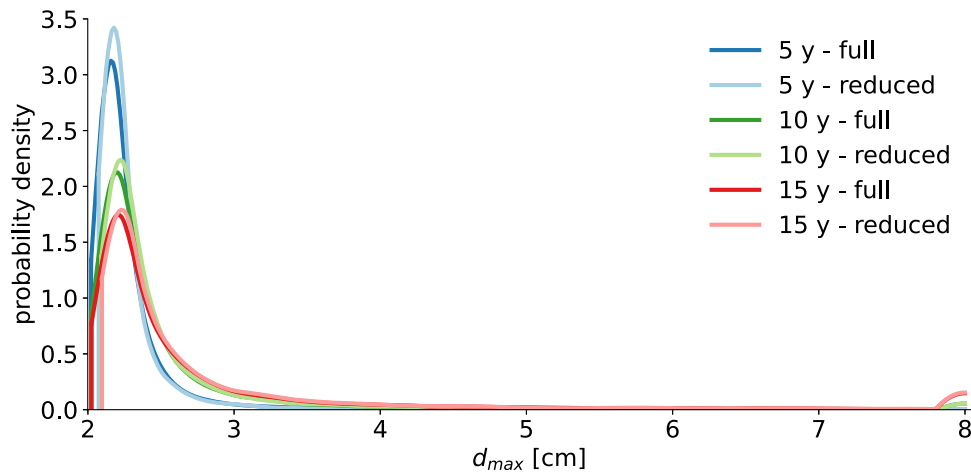


Fig. 8 Comparison of the PDFs of the maximum current diameter d_{max} for case 2 (idealized AAA) for different points in time resulting from varying numbers of uncertain parameters. The dark lines show the reference solution with all 10 parameters (cf., Fig. 4b). The pale lines show the distributions resulting if all parameters except the three most influential ones (collagen material parameter k_2 , turnover time T and gain parameter \bar{k}_σ) were fixed at their mean values. The good agreement between the distributions confirms the results of the sensitivity analysis: a restriction of the uncertainty problem to only the three most influential input parameters suffices for a good approximation of the output uncertainty

range of \bar{k}_σ to $\bar{k}_\sigma \leq 0.075$. We find that, on the one hand, small \bar{k}_σ can result in almost the full range of model output, which means that small \bar{k}_σ is a necessary condition for large d_{max} but not sufficient. On the other hand, large values of $\bar{k}_\sigma \geq 0.12$ alone guarantee smaller radial expansions. Figure 7e shows that $d_{max} < 3$ cm for $\bar{k}_\sigma \geq 0.12$ irrespective of the other parameters. The reverse statement is, however, not necessarily true. Figure 7d shows all samples with $d_{max} < 3$ cm indicating again that also small \bar{k}_σ can lead to non-aneurysmatic dilatations if the other parameter values are favorable. The missing lines between small \bar{k}_σ and small T illustrate again that the combination of these always result in aneurysmatic radial expansion.

5.4 Validation of Parameter Fixation

As described in Sect. 2.1, the parameter fixation paradigm suggests that parameters with $S_i^T \approx 0$ can be fixed anywhere within the range studied without significantly affecting the model output. Thereby, the complexity of the uncertainty quantification problem can be reduced substantially. In this section, we compare the PDFs of the maximum current diameter for case 2 (idealized AAA) resulting from a parameter fixation, with the fully resolved results as presented in Sect. 5.1. Specifically, we fixed all parameters that were identified with negligible total indices to the mean value of their respective probability distributions defined in Table 2. We then evaluated the model for 12000 independent samples from the distributions of the remaining 3 parameters, that is, collagen material parameter k_2 , collagen turnover time T and gain parameter \bar{k}_σ . Figure 8 shows the KDE of the resulting distributions of the maximum current diameter d_{max} after 5, 10 and 15 years compared to the fully resolved ones with 10 uncertain parameters. As predicted by the sensitivity analysis, the distributions of the reduced uncertainty model are indeed very good approximations of the full model in particular after 10 and 15 years. The densities depicted in Fig. 8 agree very well. Both the mean values and the variances are almost identical. Due to the quasi-random nature of the Sobol sequences used to draw the samples (cf., Appendix), we were able to directly relate the samples of the full model with the ones from the reduced model. This enabled

the computation of the mean relative error of $d_{max}(t = 15 \text{ y})$ caused by the fixation of the non-influential parameters at their mean values. This mean relative error was computed as 6.54%. Overall, these results justify the fixation of the 7 non-influential parameters with small total indices as predicted by the parameter fixation paradigm.

6 Discussion

The choice of our examples allows a systematic interpretation of our results. Both in *case 1* (*hypertension*) and *case 2* (*idealized AAA*), an inelastic deformation by growth and remodeling is triggered by some perturbation. However, while in *case 1* our system quickly converges to a new steady state after an initial period of growth and remodeling, in *case 2*, a continued, unbounded enlargement of the vessel is observed in many cases. That is, in *case 1*, we study a mechanobiologically stable system in the sense of [11, 12], whereas in *case 2*, we study a potentially mechanobiologically unstable system.

In both cases, the turnover time T determines the time scale of growth and remodeling. Therefore, it substantially affects the model output in both cases directly after the perturbation when the system is subject to highly dynamic growth and remodeling. In *case 2*, this remains so for the whole simulated period at least for mechanobiologically unstable vessels, which are subject to a continued process of growth and remodeling and which, as a subclass of the vessels studied in *case 2*, have a large impact on the overall variance of the model due to their unbounded enlargement. By contrast, in *case 1* the influence of T quickly declines over time. Because after a while all the vessel attain a new stable mechanobiological equilibrium configuration, which depends on \bar{k}_σ but only to a minor extent on T . The latter can be seen from combining Eq. (79) and Eq. (82) in [11]. This reveals that in mechanobiologically stable blood vessels the residual deformation, that remains in the long term after a perturbation, depends only to a relatively small extent on the turnover time T (for parameter values typical for the aorta). In short, T is typically a parameter of high impact on the model output as long as a blood vessel is subject to an ongoing growth and remodeling dynamics. Therefore, it can be expected to be of particular importance for clinical predictions of aneurysmal enlargement.

The two only elastic parameters of major importance for the model output in our study are β_{i_0} and k_2 . The former describes the orientation of the collagen fibers in the vessel wall. In both examples, it was found to be of major importance directly after the perturbation of the systems. In this very early stage, elastic deformation is still much larger than inelastic deformation due to growth and remodeling. Therefore, it is not surprising that the orientation of the collagen fibers, which substantially affects the elastic properties of the vessel wall, has a large impact on the model output. However, the larger the ratio between inelastic and elastic deformation of the vessel, the less important becomes β_{i_0} . In *case 1*, it can always retain some importance because the overall deformation due to growth and remodeling remains small. However, in mechanobiologically unstable systems such as the one studied in *case 2*, the substantial inelastic deformation due to growth and remodeling soon makes the impact of β_{i_0} negligible. This indicates that β_{i_0} is an important parameter for the elastic deformation of the system but not for its growth and remodeling dynamics. The latter is affected only by one elastic parameter, k_2 , which determines the strain-stiffening of the tissue. Large k_2 are associated with substantial strain-stiffening, which apparently can effectively reduce the inelastic deformation due to growth and remodeling.

Both in the early and late stage of *case 1* and *case 2*, \bar{k}_σ plays a dominant role. Again, this is coherent with the theory of mechanobiological stability [11, 12], which reveals that this

parameter has not only a major impact on the rates of inelastic deformation during growth and remodeling but also on the steady state itself that is reached in mechanobiologically stable systems in the long term.

7 Conclusions

We presented a variance-based global sensitivity analysis for the homogenized constrained mixture model of arterial growth and remodeling in two case studies. In *case 1 (hypertension)*, we investigated the adaptation of an idealized vessel to an elevated mean blood pressure level. In *case 2 (idealized AAA)*, we considered radial expansion of an idealized vessel induced by spontaneous damage to the elastin component. For each case, we studied how the uncertainty in the model input parameters contributes to the uncertainty in the chosen model output, that is, the maximum current diameter of the vessel.

A striking difference between *case 1* and *case 2* is the fact that in the latter, interactions between the parameters were observed to play a much larger role. This underlines the necessity for global sensitivity analysis and suggests that previous simple parameter studies where only one parameter at a time was varied [30, 33, 53] could reveal in principle only a limited part of the parameter sensitivities.

As discussed in Sect. 6, the results of our simulations can be interpreted in a systematic way. In the cases studied herein, only three model parameters were found to have a major impact on the inelastic deformation of the blood vessel due to growth and remodeling. These parameters were \bar{k}_σ , T and k_2 . While \bar{k}_σ can be identified with the ability of the tissue to increase collagen production as stress in the vessel wall increases, T is the average life time of collagen fibers, directly linked to their half-life time. The elastic parameter k_2 describes the strain stiffening of the collagen tissue.

Our results may have important implications both for future computational studies and for the directions that appear promising in clinical research.

For future computational studies of growth and remodeling, they mean that it can be acceptable to fix many of the parameters to values close to the population mean reported by the literature without bothering about case- or patient-specific values. This can substantially simplify the design of future computational studies and save resources in parameter studies.

It remains an important goal of clinical research to predict which enlargement can be expected for specific aneurysms. Our global sensitivity analysis clearly suggests that significant progress could be made if ways are found to measure or at least estimate the ability of the vascular tissue to produce collagen and ideally also the collagen half-life time. At the moment there are no clinical imaging protocols available to measure both. Our study suggests that developing such protocols, for example on the basis of functional magnetic resonance tomography, might be one of the most effective steps that could be taken to improve our ability to predict the future enlargement of aneurysms. Additionally, model predictive capabilities might be enhanced by improving the measurement of collagen material properties under large deformation, which, however, may be non-trivial in a non-invasive manner.

While this seems to indicate a promising direction of future research, also some limitations of the presented study should be mentioned. First, only scalar output quantities can be investigated with the variance-based method chosen herein. Hence, we focused on the maximal diameter as the single output quantity of interest. However, input parameters that have little effect on one output quantity might be very important for another one. To overcome this limitation of our study one may combine in the future multiple scalar outputs as suggested in [44] or use more sophisticated methods as suggested in [99–101]. Next, it

is important to underline that our study is based on simplified physical model assumptions neglecting the influence of blood flow and associated wall shear stresses. For larger, elastic arteries such as the aorta considered herein, also several other groups have apparently considered this simplification acceptable [6, 19, 30, 53, 67]. However, at least for smaller arteries such as cerebral arteries blood flow and wall shear stress are frequently discussed as key quantities [5, 24, 102, 103]. In the future, more detailed work should therefore aim at including also such effects. It should also be noted that in clinical practice many larger AAAs contain intraluminal thrombi, which were not considered herein. Their effect on aneurysmal expansion is, however, often not thought to be primarily a mechanical one [104–106] but rather a biochemical one [21, 29, 56]. That is, it should translate into changes of the parameter T and \bar{k}_σ in our model and is thus at least implicitly covered by this study to some extent. Nevertheless, an extended sensitivity analysis on the basis of a model including the intraluminal thrombus explicitly would be required to make strong statements about its role.

Finally, we note that, as is the nature of global sensitivity analysis, our study focused on but one computational model of vascular growth and remodeling, the homogenized constrained mixture model. Therefore, additional research is needed to corroborate the results of our study and to ensure that the conclusions drawn here are not artifacts of a specific model but are in fact revealing important aspects of the real physiology.

Appendix: Algorithm for the Computation of First and Total Order Indices

The computation of an estimate for the first order and total order Sobol indices can be carried out by the following algorithm which is similar to the one presented in [44]:

1. Generate two sampling matrices \mathbf{A} and \mathbf{B} which each have dimension $N \times n$ such that each row in \mathbf{A} and \mathbf{B} corresponds to a realization of \mathbf{x} :

$$\mathbf{A} = \begin{bmatrix} a_1^1 & \dots & a_i^1 & \dots & a_n^1 \\ & & \vdots & & \\ a_1^N & \dots & a_i^N & \dots & a_n^N \end{bmatrix}, \quad \mathbf{B} = \begin{bmatrix} b_1^1 & \dots & b_i^1 & \dots & b_n^1 \\ & & \vdots & & \\ b_1^N & \dots & b_i^N & \dots & b_n^N \end{bmatrix}. \quad (28)$$

In other words, the a_i^j and b_i^j are independently drawn samples from $U(0, 1)$. In practice, instead of using pseudo-random numbers one uses quasi-random samples from low-discrepancy sequences such as the Sobol sequence for improved performance [107–109]. In the following, we denote the j -th row of \mathbf{A} and \mathbf{B} by \mathbf{a}_j and \mathbf{b}_j , respectively.

2. Based on \mathbf{A} and \mathbf{B} compute n cross-sampling matrices $\mathbf{A}_B^{(i)}$ in the following manner: every column of $\mathbf{A}_B^{(i)}$ is from \mathbf{A} except for the i -th column which is replaced by the i -th column of \mathbf{B} ,

$$\mathbf{A}_B^{(i)} = \begin{bmatrix} a_1^1 & \dots & b_i^1 & \dots & a_n^1 \\ & & \vdots & & \\ a_1^N & \dots & b_i^N & \dots & a_n^N \end{bmatrix}. \quad (29)$$

3. Evaluate the model $y(\mathbf{x})$ at every row of the $(n+2)$ matrices $\{\mathbf{A}, \mathbf{B}, \mathbf{A}_B^{(1)}, \mathbf{A}_B^{(2)}, \dots, \mathbf{A}_B^{(n)}\}$. This results in a total of $N_{\text{tot}} = N(n+2)$ model evaluations. In the following, we denote by $y(\mathbf{A})$ a vector whose j -th component is $y(\mathbf{a}_j)$, that is y evaluated at the j -th row

of \mathbf{A} . Likewise, we define the vectors $y(\mathbf{B})$ and $y(\mathbf{A}_B^{(i)})$. Note that keeping the ordering between the sampling matrices and the result vectors is essential. For ease of notation, we introduce the vector $y(\mathbf{C}) \in \mathbb{R}^{2N}$ denoting the concatenated vectors of $y(\mathbf{A})$, $y(\mathbf{B})$, that is

$$y(\mathbf{C}) = \begin{bmatrix} y(\mathbf{A}) \\ y(\mathbf{B}) \end{bmatrix}. \quad (30)$$

4. Based on the above model evaluations the following estimators for the first-order and total-order sensitivity indices can be computed:

$$S_i \approx \frac{\frac{1}{N} \sum_{j=1}^N y(\mathbf{B})_j \left(y(\mathbf{A}_B^{(i)})_j - y(\mathbf{A})_j \right)}{V_x[y]} \quad (31)$$

and

$$S_i^T \approx \frac{\frac{1}{2N} \sum_{j=1}^N \left(y(\mathbf{A}_B^{(i)})_j - y(\mathbf{A})_j \right)^2}{V_x[y]}, \quad (32)$$

where the total variance of y is estimated with

$$V_x[y] \approx V_x[y] = \frac{1}{2N} \sum_{j=1}^{2N} y(\mathbf{C})_j y(\mathbf{C})_j - \left(\frac{1}{2N} \sum_{j=1}^{2N} y(\mathbf{C})_j \right)^2. \quad (33)$$

Supplementary Information The online version contains supplementary material available at <https://doi.org/10.1007/s10659-021-09833-9>.

Acknowledgements We thank Professor Dr. Ray Ogden for inviting this paper. Funded by the Deutsche Forschungsgemeinschaft (DFG, German Research Foundation) - Projektnummer 257981274, Projektnummer 386349077. The authors also gratefully acknowledge financial support by the International Graduate School of Science and Engineering (IGSSE) of Technical University of Munich, Germany. The software QUEENS was provided by the courtesy of AdCo Engineering^{GW} GmbH, which is gratefully acknowledged. We would like to thank Jonas Nitzler for his invaluable contributions to the software infrastructure necessary for this study, and Jonas Nitzler and Maximilian Rixner for many inspiring discussions on statistics in general and on global sensitivity analysis in particular.

Funding Note Open Access funding enabled and organized by Projekt DEAL.

Open Access This article is licensed under a Creative Commons Attribution 4.0 International License, which permits use, sharing, adaptation, distribution and reproduction in any medium or format, as long as you give appropriate credit to the original author(s) and the source, provide a link to the Creative Commons licence, and indicate if changes were made. The images or other third party material in this article are included in the article's Creative Commons licence, unless indicated otherwise in a credit line to the material. If material is not included in the article's Creative Commons licence and your intended use is not permitted by statutory regulation or exceeds the permitted use, you will need to obtain permission directly from the copyright holder. To view a copy of this licence, visit <http://creativecommons.org/licenses/by/4.0/>.

References

1. Watton, P.N., Hill, N.A., Heil, M.: A mathematical model for the growth of the abdominal aortic aneurysm. *Biomech. Model. Mechanobiol.* **3**(2), 98–113 (2004). <https://doi.org/10.1007/s10237-004-0052-9>

2. Baek, S., Rajagopal, K.R., Humphrey, J.D.: A theoretical model of enlarging intracranial fusiform aneurysms. *J. Biomech. Eng.* **128**(1), 142–149 (2006). <https://doi.org/10.1115/1.2132374>
3. Kroon, M., Holzapfel, G.A.: A model for saccular cerebral aneurysm growth by collagen fibre remodelling. *J. Theor. Biol.* **247**(4), 775–787 (2007). <https://doi.org/10.1016/j.jtbi.2007.03.009>
4. Humphrey, J.D., Rajagopal, K.R.: A constrained mixture model for growth and remodeling of soft tissue. *Math. Models Methods Appl. Sci.* **12**(3), 407–430 (2002). <https://doi.org/10.1142/S0218202502001714>
5. Watton, P., Ventikos, Y.: Modelling evolution of saccular cerebral aneurysms. *J. Strain Anal. Eng. Des.* **44**(5), 375–389 (2009). <https://doi.org/10.1243/03093247JSA492>
6. Grytsan, A., Eriksson, T.S., Watton, P.N., Gasser, T.C.: Growth description for vessel wall adaptation: a thick-walled mixture model of abdominal aortic aneurysm evolution. *Materials* **10**(9), 1–19 (2017). <https://doi.org/10.3390/ma10090994>
7. Watton, P.N., Hill, N.A.: Evolving mechanical properties of a model of abdominal aortic aneurysm. *Biomech. Model. Mechanobiol.* **8**(1), 25–42 (2009). <https://doi.org/10.1007/s10237-007-0115-9>
8. Watton, P.N., Raberger, N.B., Holzapfel, G.A., Ventikos, Y.: Coupling the hemodynamic environment to the evolution of cerebral aneurysms: computational framework and numerical examples. *J. Biomech. Eng.* **131**(10), 1–14 (2009). <https://doi.org/10.1115/1.3192141>
9. Kroon, M., Holzapfel, G.A.: A theoretical model for fibroblast-controlled growth of saccular cerebral aneurysms. *J. Theor. Biol.* **257**(1), 73–83 (2009). <https://doi.org/10.1016/j.jtbi.2008.10.021>
10. Kroon, M., Holzapfel, G.A.: Modeling of saccular aneurysm growth in a human middle cerebral artery. *J. Biomech. Eng.* **130**(5), 1–10 (2008). <https://doi.org/10.1115/1.2965597>
11. Cyron, C.J., Humphrey, J.D.: Vascular homeostasis and the concept of mechanobiological stability. *Int. J. Eng. Sci.* **85**, 203–223 (2014). <https://doi.org/10.1016/j.ijengsci.2014.08.003>
12. Cyron, C.J., Wilson, J.S., Humphrey, J.D.: Mechanobiological stability: a new paradigm to understand the enlargement of aneurysms? *J. R. Soc. Interface* **11**(100), 20140680 (2014). <https://doi.org/10.1098/rsif.2014.0680>
13. Braeu, F.A., Seitz, A., Aydin, R.C., Cyron, C.J.: Homogenized constrained mixture models for anisotropic volumetric growth and remodeling. *Biomech. Model. Mechanobiol.* **16**(3), 889–906 (2017). <https://doi.org/10.1007/s10237-016-0859-1>
14. Watton, P.N., Selimovic, A., Raberger, N.B., Huang, P., Holzapfel, G.A., Ventikos, Y.: Modelling evolution and the evolving mechanical environment of saccular cerebral aneurysms. *Biomech. Model. Mechanobiol.* **10**(1), 109–132 (2011). <https://doi.org/10.1007/s10237-010-0221-y>
15. Figueroa, C.A., Baek, S., Taylor, C.A., Humphrey, J.D.: A computational framework for fluid–solid-growth modeling in cardiovascular simulations. *Comput. Methods Appl. Mech. Eng.* **198**(45–46), 3583–3602 (2009). <https://doi.org/10.1016/j.cma.2008.09.013>
16. Sheidaei, A., Hunley, S.C., Zeinali-Davarani, S., Raguin, L.G., Baek, S.: Simulation of abdominal aortic aneurysm growth with updating hemodynamic loads using a realistic geometry. *Med. Eng. Phys.* **33**(1), 80–88 (2011). <https://doi.org/10.1016/j.medengphy.2010.09.012>
17. Zeinali-Davarani, S., Baek, S.: Medical image-based simulation of abdominal aortic aneurysm growth. *Mech. Res. Commun.* **42**, 107–117 (2012). <https://doi.org/10.1016/j.mechrescom.2012.01.008>
18. SeyedSalehi, S., Zhang, L., Choi, J., Baek, S.: Prior distributions of material parameters for Bayesian calibration of growth and remodeling computational model of abdominal aortic wall. *J. Biomech. Eng.* **137**(10), 1–13 (2015). <https://doi.org/10.1115/1.4031116>
19. Farsad, M., Zeinali-Davarani, S., Choi, J., Baek, S.: Computational growth and remodeling of abdominal aortic aneurysms constrained by the spine. *J. Biomech. Eng.* **137**(9), 1–12 (2015). <https://doi.org/10.1115/1.4031019>
20. Do, H.N., Ijaz, A., Gharahi, H., Zambrano, B., Choi, J., Lee, W., Baek, S.: Prediction of abdominal aortic aneurysm growth using dynamical Gaussian process implicit surface. *IEEE Trans. Biomed. Eng.* **66**(3), 609–622 (2019). <https://doi.org/10.1109/TBME.2018.2852306>
21. Virag, L., Wilson, J.S., Humphrey, J.D., Karšaj, I.: A computational model of biochemomechanical effects of intraluminal thrombus on the enlargement of abdominal aortic aneurysms. *Ann. Biomed. Eng.* **43**(12), 2852–2867 (2015). <https://doi.org/10.1007/s10439-015-1354-z>
22. Stevens, R.R., Grytsan, A., Biasetti, J., Roy, J., Liljeqvist, M.L., Gasser, T.C.: Biomechanical changes during abdominal aortic aneurysm growth. *PLoS ONE* **12**(11), 1–16 (2017). <https://doi.org/10.1371/journal.pone.0187421>
23. Karšaj, I., Sorić, J., Humphrey, J.D.: A 3-D framework for arterial growth and remodeling in response to altered hemodynamics. *Int. J. Eng. Sci.* **48**(11), 1357–1372 (2010). <https://doi.org/10.1016/j.ijengsci.2010.06.033>
24. Karšaj, I., Humphrey, J.D.: A multilayered wall model of arterial growth and remodeling. *Mech. Mater.* **44**, 110–119 (2012). <https://doi.org/10.1016/j.mechmat.2011.05.006>

25. Horvat, N., Virag, L., Holzapfel, G.A., Sorić, J., Karšaj, I.: A finite element implementation of a growth and remodeling model for soft biological tissues: verification and application to abdominal aortic aneurysms. *Comput. Methods Appl. Mech. Eng.* **352**, 586–605 (2019). <https://doi.org/10.1016/j.cma.2019.04.041>
26. Mousavi, S.J., Farzaneh, S., Avril, S.: Patient-specific predictions of aneurysm growth and remodeling in the ascending thoracic aorta using the homogenized constrained mixture model. *Biomech. Model. Mechanobiol.* **18**(6), 1895–1913 (2019). <https://doi.org/10.1007/s10237-019-01184-8>
27. Laubrie, J.D., Mousavi, J.S., Avril, S.: A new finite-element shell model for arterial growth and remodeling after stent implantation. *Int. J. Numer. Methods Biomed. Eng.* **36**(1), 1–19 (2020). <https://doi.org/10.1002/cnm.3282>
28. Wilson, J.S., Bersi, M.R., Li, G., Humphrey, J.D.: Correlation of wall microstructure and heterogeneous distributions of strain in evolving murine abdominal aortic aneurysms. *Cardiovasc. Eng. Technol.* **8**(2), 193–204 (2017). <https://doi.org/10.1007/s13239-017-0301-6>
29. Virag, L., Wilson, J.S., Humphrey, J.D., Karšaj, I.: Potential biomechanical roles of risk factors in the evolution of thrombus-laden abdominal aortic aneurysms. *Int. J. Numer. Methods Biomed. Eng.* **33**(12), 1–18 (2017). <https://doi.org/10.1002/cnm.2893>
30. Wilson, J.S., Baek, S., Humphrey, J.D.: Parametric study of effects of collagen turnover on the natural history of abdominal aortic aneurysms. *Proc. R. Soc. A, Math. Phys. Eng. Sci.* **469**(2150), 20120556 (2013). <https://doi.org/10.1098/rspa.2012.0556>
31. Wilson, J.S., Humphrey, J.D.: Evolving anisotropy and degree of elastolytic insult in abdominal aortic aneurysms: potential clinical relevance? *J. Biomech.* **47**(12), 2995–3002 (2014). <https://doi.org/10.1016/j.jbiomech.2014.07.003>
32. Saltelli, A., Aleksankina, K., Becker, W., Fennell, P., Ferretti, F., Holst, N., Li, S., Wu, Q.: Why so many published sensitivity analyses are false: a systematic review of sensitivity analysis practices. *Environ. Model. Softw.* **114**, 29–39 (2019). <https://doi.org/10.1016/j.envsoft.2019.01.012>
33. Valentín, A., Humphrey, J.D.: Parameter sensitivity study of a constrained mixture model of arterial growth and remodeling. *J. Biomech. Eng.* **131**(10), 1–11 (2009). <https://doi.org/10.1115/1.3192144>
34. Biehler, J., Gee, M.W., Wall, W.A.: Towards efficient uncertainty quantification in complex and large-scale biomechanical problems based on a Bayesian multi-fidelity scheme. *Biomech. Model. Mechanobiol.* **14**(3), 489–513 (2015). <https://doi.org/10.1007/s10237-014-0618-0>
35. Biehler, J., Kehl, S., Gee, M.W., Schmies, F., Pelisek, J., Maier, A., Reeps, C., Eckstein, H.H., Wall, W.A.: Probabilistic noninvasive prediction of wall properties of abdominal aortic aneurysms using Bayesian regression. *Biomech. Model. Mechanobiol.* **16**(1), 45–61 (2017). <https://doi.org/10.1007/s10237-016-0801-6>
36. Zhang, L., Jiang, Z., Choi, J., Lim, C.Y., Maiti, T., Baek, S.: Patient-specific prediction of abdominal aortic aneurysm expansion using Bayesian calibration. *IEEE J. Biomed. Health Inform.* **23**(6), 2537–2550 (2019). <https://doi.org/10.1109/JBHI.2019.2896034>
37. Nitzler, J., Biehler, J., Fehn, N., Koutsourelakis, P.S., Wall, W.A.: A generalized probabilistic learning approach for multi-fidelity uncertainty propagation in complex physical simulations (2020). [arXiv: 2001.02892](https://arxiv.org/abs/2001.02892)
38. Cyron, C.J., Aydin, R.C., Humphrey, J.D.: A homogenized constrained mixture (and mechanical analog) model for growth and remodeling of soft tissue. *Biomech. Model. Mechanobiol.* **15**(6), 1389–1403 (2016). <https://doi.org/10.1007/s10237-016-0770-9>
39. Sobol, I.M.: Sensitivity estimates for nonlinear mathematical models. *Math. Model. Comput. Exp.* **1**(4), 407–414 (1993).
40. Homma, T., Saltelli, A.: Importance measures in global sensitivity analysis of nonlinear models. *Reliab. Eng. Syst. Saf.* **52**(1), 1–17 (1996). [https://doi.org/10.1016/0951-8320\(96\)00002-6](https://doi.org/10.1016/0951-8320(96)00002-6)
41. Sobol, I.M.: Global sensitivity indices for nonlinear mathematical models and their Monte Carlo estimates. *Math. Comput. Simul.* **55**(1–3), 271–280 (2001). [https://doi.org/10.1016/S0378-4754\(00\)00270-6](https://doi.org/10.1016/S0378-4754(00)00270-6)
42. Saltelli, A., Annoni, P., Azzini, I., Campolongo, F., Ratto, M., Tarantola, S.: Variance based sensitivity analysis of model output. Design and estimator for the total sensitivity index. *Comput. Phys. Commun.* **181**(2), 259–270 (2010). <https://doi.org/10.1016/j.cpc.2009.09.018>
43. Saltelli, A., Ratto, M., Andres, T., Campolongo, F., Cariboni, J., Gatelli, D., Saisana, M., Tarantola, S.: Global Sensitivity Analysis. The Primer. Wiley, Chichester (2008). <https://doi.org/10.1002/9780470725184>
44. Wentworth, M.T., Smith, R.C., Banks, H.T.: Parameter selection and verification techniques based on global sensitivity analysis illustrated for an HIV model. *SIAM-ASA J. Uncertain. Quantificat.* **4**(1), 266–297 (2016). <https://doi.org/10.1137/15M1008245>
45. Smith, R.C.: Uncertainty Quantification: Theory, Implementation, and Applications. SIAM, Philadelphia (2014)

46. Saltelli, A.: Making best use of model evaluations to compute sensitivity indices. *Comput. Phys. Commun.* **145**(2), 280–297 (2002). [https://doi.org/10.1016/S0010-4655\(02\)00280-1](https://doi.org/10.1016/S0010-4655(02)00280-1)
47. Cyron, C.J., Humphrey, J.D.: Growth and remodeling of load-bearing biological soft tissues. *Meccanica* **52**(3), 645–664 (2017). <https://doi.org/10.1007/s11012-016-0472-5>
48. Braeu, F.A.: Three-dimensional Homogenized Constrained Mixture Model of Anisotropic Vascular Growth and Remodeling. Phd thesis, Technical University of Munich (2019)
49. Holzapfel, G.A.: *Nonlinear Solid Mechanics: A Continuum Approach for Engineering*. Wiley, New York (2000)
50. Holzapfel, G.A., Gasser, T.C., Ogden, R.W.: A new constitutive framework for arterial wall mechanics and a comparative study of material models. *J. Elast.* **61**(1–3), 1–48 (2000). <https://doi.org/10.1023/A:1010835316564>
51. Cyron, C.J., Aydin, R.C.: Mechanobiological free energy: a variational approach to tensional homeostasis in tissue equivalents. *Z. Angew. Math. Mech.* **97**(9), 1011–1019 (2017). <https://doi.org/10.1002/zamm.201600126>
52. Bellini, C., Ferruzzi, J., Roccabianca, S., Di Martino, E.S., Humphrey, J.D.: A microstructurally motivated model of arterial wall mechanics with mechanobiological implications. *Ann. Biomed. Eng.* **42**(3), 488–502 (2014). <https://doi.org/10.1007/s10439-013-0928-x>
53. Wilson, J.S., Baek, S., Humphrey, J.D.: Importance of initial aortic properties on the evolving regional anisotropy, stiffness and wall thickness of human abdominal aortic aneurysms. *J. R. Soc. Interface* **9**(74), 2047–2058 (2012). <https://doi.org/10.1098/rsif.2012.0097>
54. Rizzo, R.J., McCarthy, W.J., Dixit, S.N., Lilly, M.P., Shively, V.P., Flinn, W.R., Yao, J.S.: Collagen types and matrix protein content in human abdominal aortic aneurysms. *J. Vasc. Surg.* **10**(4), 365–373 (1989). [https://doi.org/10.1016/0741-5214\(89\)90409-6](https://doi.org/10.1016/0741-5214(89)90409-6)
55. Baxter, B.T., McGee, G.S., Shively, V.P., Drummond, I.A.S., Dixit, S.N., Yamauchi, M.N., Pearce, W.H.: Elastin content, cross-links, and mRNA in normal and aneurysmal human aorta. *J. Vasc. Surg.* **16**(2), a36429 (1992). <https://doi.org/10.1067/mva.1992.36429>
56. Tong, J., Cohnert, T., Holzapfel, G.A.: Diameter-related variations of geometrical, mechanical, and mass fraction data in the anterior portion of abdominal aortic aneurysms. *Eur. J. Vasc. Endovasc. Surg.* **49**(3), 262–270 (2015). <https://doi.org/10.1016/j.ejvs.2014.12.009>
57. Niestrawska, J.A., Regitnig, P., Viertler, C., Cohnert, T.U., Babu, A.R., Holzapfel, G.A.: The role of tissue remodeling in mechanics and pathogenesis of abdominal aortic aneurysms. *Acta Biomater.* **88**, 149–161 (2019). <https://doi.org/10.1016/j.actbio.2019.01.070>
58. Li, X., Zhao, G., Zhang, J., Duan, Z., Xin, S.: Prevalence and trends of the abdominal aortic aneurysms epidemic in general population—a meta-analysis. *PLoS ONE* **8**(12), 1–11 (2013). <https://doi.org/10.1371/journal.pone.0081260>
59. He, C.M., Roach, M.R.: The composition and mechanical properties of abdominal aortic aneurysms. *J. Vasc. Surg.* **20**(1), 6–13 (1994). [https://doi.org/10.1016/0741-5214\(94\)90169-4](https://doi.org/10.1016/0741-5214(94)90169-4)
60. Sobolewski, K., Wolańska, M., Bańkowski, E., Gacko, M., Głowiński, S.: Collagen, elastin and glycosaminoglycans in aortic aneurysms. *Acta Biochim. Pol.* **42**(3), 301–307 (1995)
61. Davis, E.C.: Elastic lamina growth in the developing mouse aorta. *J. Histochem. Cytochem.* **43**(11), 1115–1123 (1995). <https://doi.org/10.1177/43.11.7560894>
62. Ghorpade, A., Baxter, B.T.: Biochemistry and molecular regulation of matrix macromolecules in abdominal aortic aneurysms. *Ann. N.Y. Acad. Sci.* **800**(1), 138–150 (1996). <https://doi.org/10.1111/j.1749-6632.1996.tb33305.x>
63. Dobrin, P.B., Schwarcz, T.H., Mrkvicka, R.: Longitudinal retractive force in pressurized dog and human arteries. *J. Surg. Res.* **48**(2), 116–120 (1990). [https://doi.org/10.1016/0022-4804\(90\)90202-D](https://doi.org/10.1016/0022-4804(90)90202-D)
64. Cardamone, L., Valentín, A., Eberth, J.F., Humphrey, J.D.: Origin of axial prestretch and residual stress in arteries. *Biomech. Model. Mechanobiol.* **8**(6), 431–446 (2009). <https://doi.org/10.1007/s10237-008-0146-x>
65. Holzapfel, G.A., Ogden, R.W.: Modelling the layer-specific three-dimensional residual stresses in arteries, with an application to the human aorta. *J. R. Soc. Interface* **7**(46), 787–799 (2010). <https://doi.org/10.1098/rsif.2009.0357>
66. Zeinali-Davarani, S., Raguin, L.: An inverse optimization approach toward testing different hypotheses of vascular homeostasis using image-based models. *Int. J. Struct. Chang. Solids* **3**(2), 33–45 (2011)
67. Zeinali-Davarani, S., Sheidaei, A., Baek, S.: A finite element model of stress-mediated vascular adaptation: application to abdominal aortic aneurysms. *Comput. Methods Biomech. Biomed. Eng.* **14**(9), 803–817 (2011). <https://doi.org/10.1080/10255842.2010.495344>
68. Roccabianca, S., Figueroa, C.A., Tellides, G., Humphrey, J.D.: Quantification of regional differences in aortic stiffness in the aging human. *J. Mech. Behav. Biomed. Mater.* **29**, 618–634 (2014). <https://doi.org/10.1016/j.jmbbm.2013.01.026>

69. Vande Geest, J.P., Sacks, M.S., Vorp, D.A.: Age dependency of the biaxial biomechanical behavior of human abdominal aorta. *J. Biomech. Eng.* **126**(6), 815–822 (2004). <https://doi.org/10.1115/1.1824121>
70. Vande Geest, J.P., Sacks, M.S., Vorp, D.A.: The effects of aneurysm on the biaxial mechanical behavior of human abdominal aorta. *J. Biomech.* **39**(7), 1324–1334 (2006). <https://doi.org/10.1016/j.jbiomech.2005.03.003>
71. Schriebl, A.J., Zeindlinger, G., Pierce, D.M., Regitnig, P., Holzapfel, G.A.: Determination of the layer-specific distributed collagen fibre orientations in human thoracic and abdominal aortas and common iliac arteries. *J. R. Soc. Interface* **9**(71), 1275–1286 (2012). <https://doi.org/10.1098/rsif.2011.0727>
72. Sommer, G., Holzapfel, G.A.: 3D constitutive modeling of the biaxial mechanical response of intact and layer-dissected human carotid arteries. *J. Mech. Behav. Biomed. Mater.* **5**(1), 116–128 (2012). <https://doi.org/10.1016/j.jmbbm.2011.08.013>
73. Weisbecker, H., Pierce, D.M., Regitnig, P., Holzapfel, G.A.: Layer-specific damage experiments and modeling of human thoracic and abdominal aortas with non-atherosclerotic intimal thickening. *J. Mech. Behav. Biomed. Mater.* **12**, 93–106 (2012). <https://doi.org/10.1016/j.jmbbm.2012.03.012>
74. Reeps, C., Maier, A., Pelisek, J., Härtl, F., Grabher-Meier, V., Wall, W.A., Essler, M., Eckstein, H.H., Gee, M.W.: Measuring and modeling patient-specific distributions of material properties in abdominal aortic aneurysm wall. *Biomech. Model. Mechanobiol.* **12**(4), 717–733 (2013). <https://doi.org/10.1007/s10237-012-0436-1>
75. Niestrawska, J.A., Viertler, C., Regitnig, P., Cohnert, T.U., Sommer, G., Holzapfel, G.A.: Microstructure and mechanics of healthy and aneurysmatic abdominal aortas: experimental analysis and modelling. *J. R. Soc. Interface* **13**(124), 20160620 (2016). <https://doi.org/10.1098/rsif.2016.0620>
76. Jadidi, M., Habibnezhad, M., Anttila, E., Maleckis, K., Desyatova, A., MacTaggart, J., Kamenskiy, A.: Mechanical and structural changes in human thoracic aortas with age. *Acta Biomater.* **103**, 172–188 (2020). <https://doi.org/10.1016/j.actbio.2019.12.024>
77. Ferruzzi, J., Vorp, D.A., Humphrey, J.D.: On constitutive descriptors of the biaxial mechanical behaviour of human abdominal aorta and aneurysms. *J. R. Soc. Interface* **8**(56), 435–450 (2011). <https://doi.org/10.1098/rsif.2010.0299>
78. Holzapfel, G.A., Ogden, R.W.: An arterial constitutive model accounting for collagen content and cross-linking. *J. Mech. Phys. Solids* **136**, 103682 (2020). <https://doi.org/10.1016/j.jmps.2019.103682>
79. Gasser, T.C., Ogden, R.W., Holzapfel, G.A.: Hyperelastic modelling of arterial layers with distributed collagen fibre orientations. *J. R. Soc. Interface* **3**(6), 15–35 (2006). <https://doi.org/10.1098/rsif.2005.0073>
80. Tsamis, A., Krawiec, J.T., Vorp, D.A.: Elastin and collagen fibre microstructure of the human aorta in ageing and disease: a review. *J. R. Soc. Interface* **10**(83), 20121004 (2013). <https://doi.org/10.1098/rsif.2012.1004>
81. Holzapfel, G.A., Niestrawska, J.A., Ogden, R.W., Reinisch, A.J., Schriebl, A.J.: Modelling non-symmetric collagen fibre dispersion in arterial walls. *J. R. Soc. Interface* **12**(106), 20150188 (2015). <https://doi.org/10.1098/rsif.2015.0188>
82. Cyron, C.J., Humphrey, J.D.: Preferred fiber orientations in healthy arteries and veins understood from netting analysis. *Math. Mech. Solids* **20**(6), 680–696 (2015). <https://doi.org/10.1177/1081286514551495>
83. Niestrawska, J.A., Haspinger, D.Ch., Holzapfel, G.A.: The influence of fiber dispersion on the mechanical response of aortic tissues in health and disease: a computational study. *Comput. Methods Biomech. Biomed. Eng.* **21**(2), 99–112 (2018). <https://doi.org/10.1080/10255842.2017.1418862>
84. Holzapfel, G.A., Ogden, R.W., Sherifova, S.: On fibre dispersion modelling of soft biological tissues: a review. *Proc. R. Soc. A, Math. Phys. Eng. Sci.* **475**(2224), 20180736 (2019). <https://doi.org/10.1098/rspa.2018.0736>
85. Gasser, T.C.: Modeling the structural and mechanical properties of the normal and aneurysmatic aortic wall. In: Zhang, Y. (ed.) *Multi-Scale Extracellular Matrix Mechanics and Mechanobiology, Studies in Mechanobiology, Tissue Engineering and Biomaterials*, vol. 23, pp. 55–82. Springer, Cham (2020). <https://doi.org/10.1007/978-3-030-20182-1>
86. Nissen, R., Cardinale, G.J., Udenfriend, S.: Increased turnover of arterial collagen in hypertensive rats. *Proc. Natl. Acad. Sci. USA* **75**(1), 451–453 (1978). <https://doi.org/10.1073/pnas.75.1.451>
87. Humphrey, J.D.: *Cardiovascular Solid Mechanics*. Springer, New York (2002). <https://doi.org/10.1007/978-0-387-21576-1>
88. Gineyts, E., Cloos, P.A., Borel, O., Grimaud, L., Delmas, P.D., Garnerio, P.: Racemization and isomerization of type I collagen C-telopeptides in human bone and soft tissues: assessment of tissue turnover. *Biochem. J.* **345**(3), 481–485 (2000). <https://doi.org/10.1042/0264-6021:3450481>
89. Humphrey, J.D., Dufresne, E.R., Schwartz, M.A.: Mechanotransduction and extracellular matrix homeostasis. *Nat. Rev. Mol. Cell Biol.* **15**(12), 802–812 (2014). <https://doi.org/10.1038/nrm3896>

90. Eichinger, J.F., Paukner, D., Szafron, J.M., Aydin, R.C., Humphrey, J.D., Cyron, C.J.: Computer-controlled biaxial bioreactor for investigating cell-mediated homeostasis in tissue equivalents. *J. Biomech. Eng.* **142**(7), 1–8 (2020). <https://doi.org/10.1115/1.4046201>
91. Eichinger, J.F., Haeusel, L.J., Paukner, D., Aydin, R., Humphrey, J.D., Cyron, C.J.: Mechanical homeostasis in tissue equivalents: a review. *Biomech. Model. Mechanobiol.* (2021). <https://doi.org/10.1007/s10237-021-01433-9>
92. Wolinsky, H.: Long-term effects of hypertension on the rat aortic wall and their relation to concurrent aging changes: morphological and chemical studies. *Circ. Res.* **30**(3), 301–309 (1972). <https://doi.org/10.1161/01.RES.30.3.301>
93. Matsumoto, T., Hayashi, K.: *Response of Arterial Wall to Hypertension and Residual Stress* pp. 93–119. Springer, Tokyo (1996)
94. BACI: A Comprehensive Multi-Physics Simulation Framework (2020). <https://baci.pages.gitlab.lrz.de/website>
95. Herman, J., Usher, W.: SALib: an open-source Python library for sensitivity analysis. *J. Open Sour. Softw.* **2**(9), 97 (2017). <https://doi.org/10.21105/joss.00097>
96. Biehler, J., Nitzler, J., Brandstaeter, S., Wall, W.A., Gravemeier, V.: QUEENS – a Software Platform for Uncertainty Quantification, Physics-Informed Machine Learning, Bayesian Optimization, Inverse Problems and Simulation Analytics: User Guide (2020). AdCo Engineering GW GmbH
97. Chaikof, E.L., Dalman, R.L., Eskandari, M.K., Jackson, B.M., Lee, W.A., Mansour, M.A., Mastracci, T.M., Mell, M., Murad, M.H., Nguyen, L.L., Oderich, G.S., Patel, M.S., Schermerhorn, M.L., Starnes, B.W.: The society for vascular surgery practice guidelines on the care of patients with an abdominal aortic aneurysm. *J. Vasc. Surg.* **67**(1), 2–77.e2 (2018). <https://doi.org/10.1016/j.jvs.2017.10.044>
98. Plotly Technologies Inc.: Collaborative data science, Montreal, QC (2015). <https://plot.ly>
99. Gamboa, F., Janon, A., Klein, T., Lagnoux, A.: Sensitivity indices for multivariate outputs. *C. R. Math.* **351**(7–8), 307–310 (2013). <https://doi.org/10.1016/j.crma.2013.04.016>
100. Campbell, K., McKay, M.D., Williams, B.J.: Sensitivity analysis when model outputs are functions. *Reliab. Eng. Syst. Saf.* **91**(10–11), 1468–1472 (2006). <https://doi.org/10.1016/j.res.2005.11.049>
101. Sumner, T., Shephard, E., Bogle, I.D.: A methodology for global-sensitivity analysis of time-dependent outputs in systems biology modelling. *J. R. Soc. Interface* **9**(74), 2156–2166 (2012). <https://doi.org/10.1098/rsif.2011.0891>
102. Cebal, J.R., Castro, M.A., Burgess, J.E., Pergolizzi, R.S., Sheridan, M.J., Putman, C.M.: Characterization of cerebral aneurysms for assessing risk of rupture by using patient-specific computational hemodynamics models. *Am. J. Neuroradiol.* **26**(10), 2550–2559 (2005). [https://doi.org/10.1016/s0098-1672\(08\)70473-9](https://doi.org/10.1016/s0098-1672(08)70473-9)
103. Sforza, D.M., Kono, K., Tateshima, S., Viñuela, F., Putman, C., Cebal, J.R.: Hemodynamics in growing and stable cerebral aneurysms. *J. Neurointerv. Surg.* **8**(4), 407–412 (2016). <https://doi.org/10.1136/neurintsurg-2014-011339>
104. Gasser, T., Görgülü, G., Folkesson, M., Swedenborg, J.: Failure properties of intraluminal thrombus in abdominal aortic aneurysm under static and pulsating mechanical loads. *J. Vasc. Surg.* **48**(1), 179–188 (2008). <https://doi.org/10.1016/j.jvs.2008.01.036>
105. Riveros, F., Martufi, G., Gasser, T.C., Rodriguez-Matas, J.F.: On the impact of intraluminal thrombus mechanical behavior in AAA passive mechanics. *Ann. Biomed. Eng.* **43**(9), 2253–2264 (2015). <https://doi.org/10.1007/s10439-015-1267-x>
106. Martufi, G., Satriano, A., Moore, R.D., Vorp, D.A., Di Martino, E.S.: Local quantification of wall thickness and intraluminal thrombus offer insight into the mechanical properties of the aneurysmal aorta. *Ann. Biomed. Eng.* **43**(8), 1759–1771 (2015). <https://doi.org/10.1007/s10439-014-1222-2>
107. Joe, S., Kuo, F.Y.: Constructing Sobol’ sequences with better two-dimensional projections. *SIAM J. Sci. Comput.* **30**(5), 2635–2654 (2007). <https://doi.org/10.1137/070709359>
108. Sobol’, I.M., Asotsky, D., Kreinin, A., Kucherenko, S.: Construction and comparison of high-dimensional Sobol’ generators. *Wilmott* **2011**(56), 64–79 (2011). <https://doi.org/10.1002/wilm.10056>
109. Kucherenko, S., Albrecht, D., Saltelli, A.: Exploring multi-dimensional spaces: a Comparison of Latin Hypercube and Quasi Monte Carlo Sampling Techniques (2015). <http://arxiv.org/abs/1505.02350>. [arXiv:1505.02350](https://arxiv.org/abs/1505.02350)

Verzeichnis der betreuten Studienarbeiten

Im Rahmen dieser Dissertation entstanden am Lehrstuhl für Numerische Mechanik (LNM) in den Jahren von 2016 bis 2021 unter wesentlicher wissenschaftlicher, fachlicher und inhaltlicher Anleitung des Autors die im Folgenden aufgeführten studentischen Arbeiten. Der Autor dankt allen Studierenden für ihr Engagement bei der Unterstützung seiner wissenschaftlichen Arbeit.

Studierender	Studienarbeit
Maximilian Steigenberger	<i>Identification of the Mechanical Properties of the Gastric Wall by Inverse Analysis of Biaxial Tensile Tests</i> , Masterarbeit, 2017
Alvaro Ramos Rubio	<i>Development of an Extended Gastric Electrophysiology Model</i> , Masterarbeit, 2017
Natalia Moreno-Arrones Fuentes	<i>Experimental and Computational Analysis of the Constitutive Properties of the Stomach</i> , Masterarbeit, 2017
Amadeus Gebauer	<i>Computational Modeling of Gastric Electromechanics</i> , Semesterarbeit, 2018, eingeflossen in Paper B , [51]
Fabiola Rienäcker	<i>Inverse Analysis of Biaxial Tensile Experiments for Soft Biological Tissue based on a Finite Element Model</i> , Semesterarbeit, 2018
Fabiola Rienäcker	<i>A Human Gastric Electromechanics Model with Realistic Geometry</i> , Masterarbeit, 2019
Lisa Kühn	<i>An electromechanics material model for the simulation of human gastric tissue</i> , Semesterarbeit, 2020
Andrea Bonifacio	<i>Computational modeling of patient-specific gastric electromechanics</i> , Masterarbeit, 2021, in Kooperation mit Prof. Alessio Gizzi, Università Campus Bio-Medico di Roma